BioRisk 18: 1–16 (2022)
doi: 10.3897/biorisk.18.76114
https://biorisk.pensoft.net

RESEARCH ARTICLE

A peer-reviewed open-access journal
BioRisk

Relocation and formation of new local population of *Viola pumila* Chaix – an endangered species in Europe and identification of measures for improvement of its habitat

Maria Zh. Kaschieva[1], Nikolay P. Nedyalkov[1]

1 *University of Shumen Konstantin Preslavski, Faculty of Natural Sciences, 115 Universitetska Str., 9700 Shumen, Bulgaria*

Corresponding author: Maria Zh. Kaschieva (m.kaschieva@shu.bg)

Academic editor: Josef Settele | Received 4 October 2021 | Accepted 30 December 2021 | Published 27 April 2022

Citation: Kaschieva MZ, Nedyalkov NP (2022) Relocation and formation of new local population of *Viola pumila* Chaix – an endangered species in Europe and identification of measures for improvement of its habitat. BioRisk 18: 1–16. https://doi.org/10.3897/biorisk.18.76114

Abstract

The meadow violet (*Viola pumila* Chaix) is an endangered species which is regionally extinct in many European countries. This is a stenobiontic species with a very limited distribution in Bulgaria. Only a few populations have been detected, and they consist of several tens to several hundreds of specimens. The meadow violet has limited reproductive abilities and weak competitiveness. The species is exposed to various anthropogenic threats, as the most significant of them are related to ploughing, conversion of the mesophilic meadows into arable lands, changes in the water regime of the habitats, the expansion of highly competitive species from the group of tufted cereal grasses and infrastructure construction. To date, information concerning the relocation of rare and endangered plant species in Bulgaria is rather scarce. In the present study we provide a protocol on our activities during a successful establishment of a new locality as part of our effort to successfully relocate one particular population of the meadow violet. The observations made after the relocation of the species over a two-year period (2020 and 2021) provided data on the successful relocation, and the creation of a new locality for the species. We discuss the conservation measures needed for this rare and endangered species, and efforts to increase its population, as well as the measures needed for effective management of the habitats of *V. pumila* (mainly 6510 "Lowland hay meadows").

Keywords

Biological restoration, conservation measures, eco-management, grassland habitat, plant ecology, *Viola pumila* Chaix

Introduction

The extinction of plant species is a well-recognized global problem. In the last 250 years about 571 plant species have become extinct (Humphreys et al. 2019) and that means that two or three plant species have been lost every year. The extinction of one particular plant species may directly impact other related organisms and even entire ecosystems (GBIF 2021). In recent decades, some plant species registered a dramatic decline in their population numbers. Several taxonomically closely related species of the genus *Viola* L. fall into this category: *V. elatior* Fr., *V. pumila* Chaix and *V. persicifolia* Roth (= *V. stagnina* Kit.). These species are among the most endangered plants in Central Europe (Eckstein et al. 2006; Holzel 2003). Due to the loss of suitable habitats or changes in their hydrological regime, these species have become extremely rare (Korneck et al. 1996) and are the subject of restoration programs in several European countries (Pullin and Woodell 1987). The meadow violet is suffering a severe decline in Europe. Reports attest to a diminishing number of this species (Eckstein et al. 2006) and this is the reason why the species is included in the red lists of several European countries: Switzerland (Info flora); Czech Republic (Grulich 2012); Italy (Buldrini and Dallai 2011) and also Bulgaria (Petrova and Vladimirov 2009).

V. pumila is a hemicryptophyt, in which the regenerative buds are located below the soil surface. The species is a representative of the spring ephemeroids and begins its growth in the early spring. It develops in a short time, but only by favorable soil moisture and scant competition for light by the syntopic species. According to Eckstein et al. (2006), *V. pumila* has a special type of life cycle and reproduction. The mechanisms of distribution of the species were not well studied. Pollination takes place in the flowers, but that mechanism has not been understood to date. Most likely, the species is a self-pollination (cleistogamic) plant, which is characteristic of members of the Violaceae family. This violet is a myrmecochor plant – ants are partially responsible for dispersal of the seeds, which is indicated by the presence of elaismosom in the seeds. During cracking, the seed boxes shoot the seeds at a distance of up to 1.19 m. In the soil, the scattered seeds are located in the 5 cm soil layer, where they undergo a period of stratification before beginning their active life cycle. The end of the growing season of *V. pumila* is in autumn, when the above ground parts of the plant dry out and the plant prepares for overwintering.

V. pumila has a Eurasian-continental distribution in the temperate climate zone (Buldrini et al. 2013). Populations of the species have been registered in Western Europe (Aeschiman and Burdet 1994), Central Europe (Danihelka et al. 2009) as well as in Eastern Europe (Gejdeman 1986). In Bulgaria, the species was considered extinct for a prolonged period, however, in the 1990s, the species was rediscovered by Andreev (1993). There were six known localities of the species, however two of them have disappeared in recent years (Apostolova and Meshinev 2015). In Bulgaria, the species can be found at altitudes between 500 and 1000 a.s.l. Currently, the largest populations are located around the villages of Kokalyane and Tsraklevtsi, as well as in the vicinity of Aldomirovsko and the Dragoman marshes (Apostolova and Meshinev 2015).

In the case of our study, a population of the meadow violet was threatened with direct annihilation during the construction of a motorway. The situation demanded fast and precise actions for localization of a possible new habitat, selection of relocation tactics and procedures for transporting and planting the violets, as well as developing a plan for sustaining the new local populations. Our activities resulted in a successful relocation of one particular population of *V. pumila*. To our knowledge this is the first successful establishment of a new locality following the relocation of an endangered plant species on the territory of Bulgaria. We discuss the necessary conservation measures for the habitat of *V. pumila* (mainly 6510 "Lowland hay meadows").

Materials and methods

The most complete morphological description of the species *V. pumila* was provided by Eckstein et al. (2006) and from Buldrini and Dallai (2011). The species is a perennial herbaceous plant, with a rhizome up to 30 cm long and a root thickness of 0.5 to 1 cm. The stem is erected, with a height of between 5 and 20 cm. The leaves have 0.3 to 0.6 mm long hairs; the leaf length is 2–6 cm and their width is 1–2 cm; the edges are shallowly serrated. The flower stalks are 5–10 cm long, the petals are purple at the beginning of flowering and later they become pale purple to whitish, with cilia at the base and 3–5 dark longitudinal lines. The fruit box is elongated, with yellow to brown coloration with a 10 mm length and width of 6–7 mm. One box may contain 24 seeds which are brownish and about 1 mm in length. Flowering occurs in the period April–May, and fruit formation and fruiting is in the period May–June (Table 1).

In the late spring of 2019 we provided the first on spot field survey for identification of the exact position and ranges of the population of meadow violet, as well as the number of the plants that had to be relocated. We inspected the terrains along the road Sofia-Kalotina between the km. 21 and km. 22. The field study was performed by the use of the transect method. The transects were repeated three times in three days by three qualified experts with the necessary experience. The species identification was performed according to Delipavlov 1979, Delipavlov et al. (2011).

Table 1. Phenological peculiarities in *V. pumila.*

	Period of the year	Developmental phase
1.	Beginning of April	Appearance of the first aboveground stalks
2.	Middle of April to the end of the month	Buttonization phase – forming of the flower buds
3.	End of April – beginning of May	Beginning of blooming
4.	First half of May	Mass blooming
5.	Second half of May	End of the blooming phase
6.	End of May to the middle of June	Gradual ripening and cracking of the seed boxes
7.	Middle of June	End of mass dissemination
8.	October	The aboveground parts dry out and the plant prepares to overwinter

* Depending on the specific meteorological conditions during the year, the phenophases during which *V. pumila* passes, may occur at different times

In the processing of the digital data for the identification of the most suitable sites for relocation, the layer with the distribution of the natural habitat within the Natura 2000 site SCI BG0000322 Dragoman (in "shape" format) was intersected with the layer containing the boundaries of the national protected area "Aldomirovsko Blato" and the layer of the municipal property in the protected area. The data processing and statistical analyzes were performed with the standard tools of ArcGIS 10 and the corresponding extensions of the used software.

Two satellite images from the Sentinel-2A L2A satellite (https://apps.sentinel-hub.com/eo-browser/) were used to determine the boundaries of the fire that occurred in 2019. In accordance with the period of the fire, the images used were selected respectively before the fire (September 21, 2019) and immediately after its end (October 26, 2019). Standard Arc GIS 10 tools were used for drawing the boundaries of the burned area, as well as for the map visualization.

The violets were manipulated in the morning or late afternoon, when the intensity of sunshine is not very high and the temperatures are lower. With the use of suitable tools the plants were dug up along with the adjacent soil around their rhizomes (in a radius of 25 cm. from its center). The plants were then immediately placed in vegetation containers with a depth of 30 cm and some water was added (Fig. 1). The specimens were covered with a transparent foil to preserve the soil moisture and the freshness of the plants. In this form, the violets were transported to their new locality. The specimens were planted in pre-prepared and moistened pits – 3 holes of the size of the

Figure 1. Technology for the relocation **a** identification of the plant **b** extraction of a rhizome **c** replacement of the rhizomes in container **d** preparation of the rhizomes for transportation.

Figure 2. Implementation of the Action plan for permanent relocation of the species to a suitable habitat: **a** preparation of the relocation pits **b** planting of the rhizoms **c** stuffing of the soil around the newly planted rhizome.

rhizomes in a raw in 10 m distance, to ensure enough space for the root system. The rhizomes were carefully positioned in the pits and the soil was compacted afterwards for reduction of the soil air (Fig. 2). We then watered the plants with 60 cl to prevent further water stress, as well as for faster adaptation.

After planting the violets in the new location, special care was taken in situ until their full adaptation (3–6 months) and subsequent two-years monitoring was carried out. During this period, the following activities were performed: watering (monthly); mowing around the localities in periods of three months; monitoring of the seed dispersal; observation of the flowering of the specimens during the next vegetation cycle; monitoring for pressures (fire, pollution, ploughing). All of our activities were coordinated with the competent authorities.

Results

The population of *V. pumila*, which was the focus of the present study, was endangered by a large linear infrastructure project. The project envisages the enlargement of an existing road section in the Sofia-Kalotina direction and its restructuring in "Europe Motorway". To protect the specimens, it was necessary to relocate the plants away from the route of the future motorway (Fig. 3), to create a new locality and to identify appropriate measures for its new habitats.

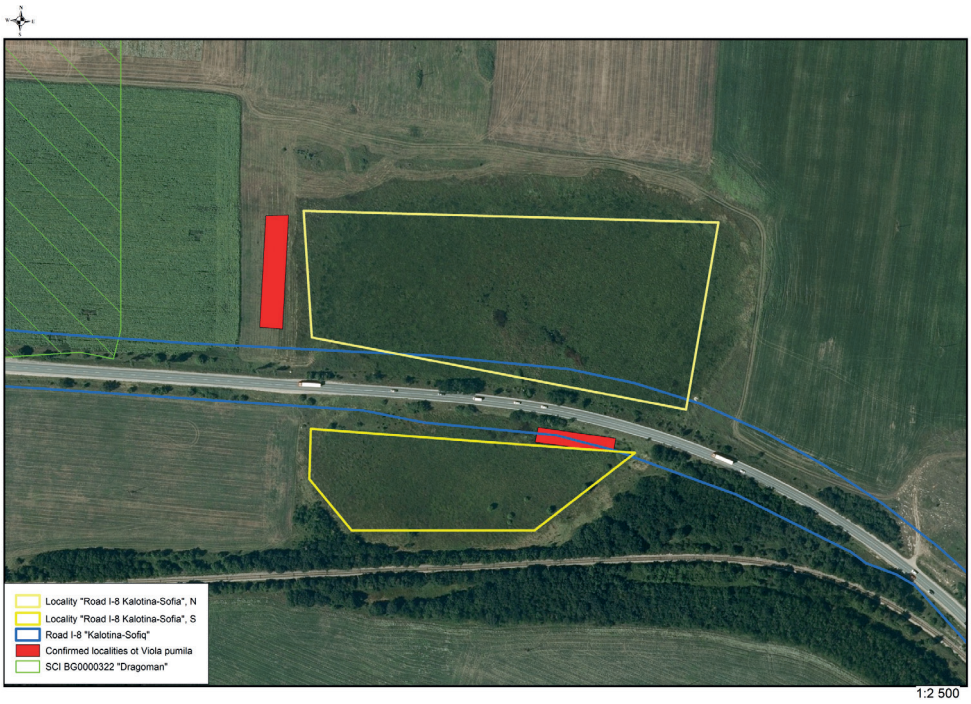

Figure 3. Plan for reconstruction of the existing road as part of Europe Motorway and position of two localities of *V. pumila*.

During our field surveys we identified a total of 50 individuals of *V. pumila* formed in 8 tufts. The other species detected around the violets were: *Alopecurus pratensis*, *Deschampsia cespitosa*, *Lysimachia vulgaris*, *Molinia caerulea* and *Potentilla reptans*.

The identification of a suitable new location was performed with the idea that it had to be identical to the current habitat of the plants. The new habitat had to possess similar physical characteristics, species composition, soil-climatic conditions and the water regime had to be similar to those of the original habitat. Several possible variants of suitable terrains were considered for creating the new habitat for the violets.

As a result of the analysis of all collected data, we calculated that possible sites for relocation of the species were the following four areas from the territory of the village of Aldomirovtsi: land properties with the following numbers 00223.257.32, 00223.257.62, 00223.257.68 and 00223.257.186. These terrains were municipal property and were managed by the municipality of Slivnitsa. All four land properties fall within the boundaries of the Aldomirovsko Blato protected area. The area was declared for the purpose of preserving the natural habitats of protected and rare species of waterfowl and 40 species of higher plants. The land properties also fall within the boundaries of a Natura 2000 site (SCI BG0000322 Dragoman). Another land property was identified as a possible variant – 00223.257.294 from the territory of the village of Aldomirovtsi. In this sector is located one of the most numerous populations of *V. pumila* in the country. However, the crucial disadvantage of this land was that it is private property and falls outside the boundaries of the Aldomirovsko Blato protected area.

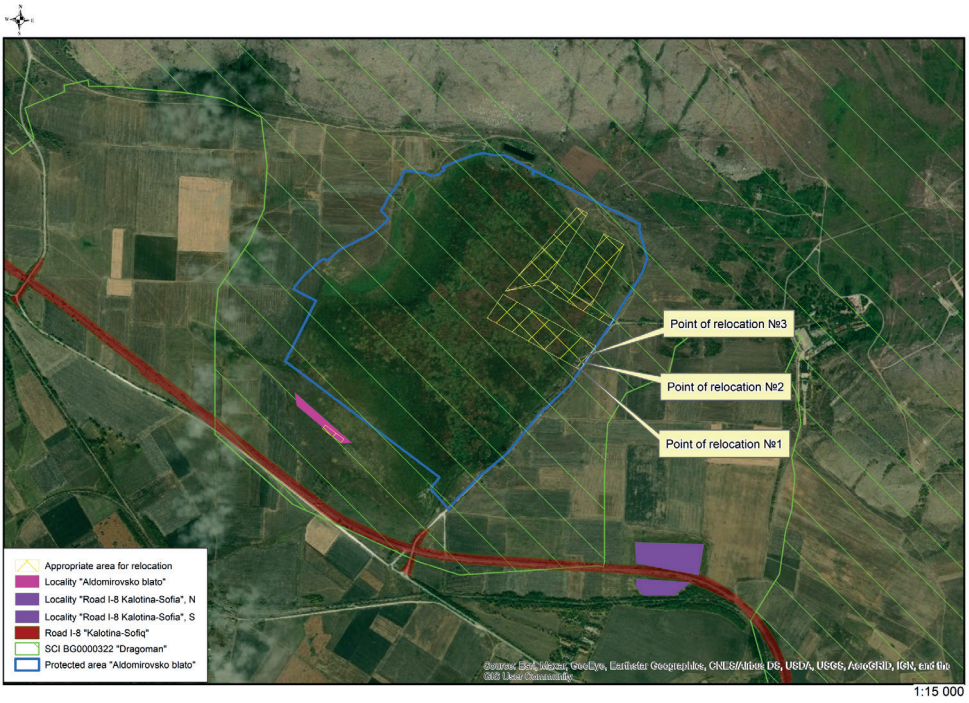

Figure 4. Sites of relocation of *V. pumila*.

After geodetic and ecological field surveys were performed, we selected as the most suitable property for the relocation of *V. pumila* – 00223.257.68 from the territory of the Aldomirovtsi village (Fig. 4). That terrain met the requirements of the meadow violet concerning the conditions of the soil, the vegetation and the water regime. We selected floodplain meadows, which were moist as water was retained above the soil surface in the local depressions. The soil in the habitat was of "meadow-swamp" type. It was covered by hydrophilic, mesophilic and xeromesophilic grass communities.

Part of the selected terrain was occupied by natural habitat 3150 "Natural eutrophic lakes with Magnopotamion or Hydrocharition", and another part by natural habitat 6510 "Lowland hay meadows" (Fig. 5). Because we worked with a very rare plant species with few remaining localities in the country, as well as because of the small population subject for relocation (only 50 specimens), we decided not to divide the individuals and provide experiments to grow them in different conditions. We identified the most optimal suited location and planted all specimens together.

The other three potential land properties from the territory of the Aldomirovtsi village were occupied only by a natural habitat "3150 Natural eutrophic lakes with Magnopotamion or Hydrocharition" and were flooded almost all year round. On that basis, we assessed them less suitable for the relocation of the violets.

A key step in the initial phase of our efforts was the coordination of our actions with the local municipality. The new habitat was in a municipal property, which allowed for regular grooming of the terrain and monitoring of the plants. With the next

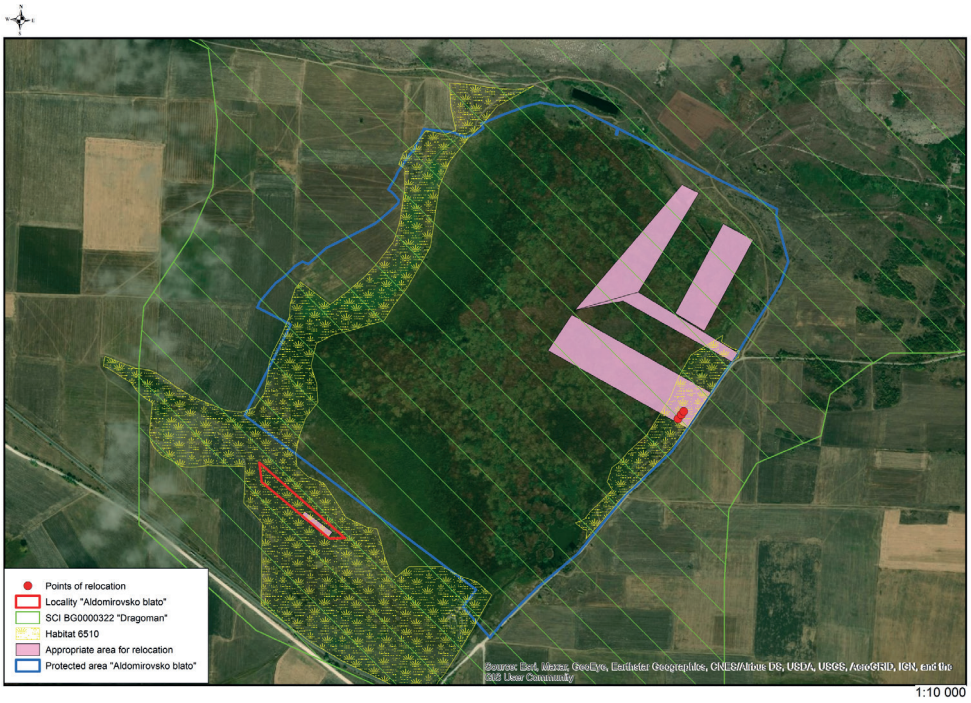

Figure 5. Location of the new habitats of *V. pumila* in natural habitat 6510 Lowland hay meadows.

step we prepared an Action plan for all activities. The plan and the technology for the permanent relocation of the species were reconciled by the relevant competent authorities and implemented in full scale.

The relocation of the *V. pumila* specimens was accomplished before the end of the vegetation period – in our case before the full rupture of the seed boxes (Table 1). We aimed the rupture of the seed boxes and the dissemination to occur on the spot of the new location in order to improve the chance of successful seed generation and development of the next vegetation (see Volis 2019). According to Eckstein et al. (2006), the vegetation period of the species ends in the October – November period when the upper sections of the plant die out and the violets prepare for overwintering.

After the establishment of the new locality, we performed in situ care until the complete adaptation of the plants. This included watering and mowing around all of the three new micro- localities. In the first month after the relocation (June), regular watering was carried out (every 3 days), and during the next two months (July and August) – every 7 days. Mowing was carried out on an area of 4 square meters around each of the micro-localities in the middle of July. The two-year follow-up monitoring of the new sites and adjacent areas of habitat 6510 "Lowland hay meadows" showed success in preserving the relocated specimens and also their successful reproduction (Fig. 6)

In October 2019, a large-area fire was detected within the Natura 2000 site SCI BG0000322 Dragoman and it reached the territory of the new locality of *V. pumila* (Fig. 7 and Fig. 8). None of the three plots with relocated plants was affected by that fire.

Figure 6. Condition of the relocated plants: **a** successful replanting **b** rupture of the seed boxes **c** dissemination.

Volis (2019) described two main successive stages that plant species go through after reintroduction to a new location. The first stage begins with the flowering of a mature (relocated) plant. The second involves the establishment of an entirely new reproductive individual at the site of transmission (reintroduction). The second stage consists of smaller phases associated with the appearance of reproductive organs, feeding flowers and seeds, scattering the seeds in places, with conditions for germination and survival of the young plants. In *V. pumila* we detected flowering in a mature adult in the year after reintroduction – the first stage indicated by Volis was successfully completed. The implementation of the second stage began in the year of relocation (2019) with the scattering of seeds from the seed boxes of the transferred adults. The full completion of the second stage required more time due to the specific features of the species *V. pumila*. The fact that there are flowers from adults a year after reintroduction, (Fig. 9), as well as cracked seed boxes in the year of reintroduction (Fig. 6b), gives us hope for the successful completion of the second stage.

In the early summer of 2021 (early July) we started the monitoring of the new locality of the violets in the second year after relocation. We identified new juvenile specimens with different heights from 2 to 7 cm, which were in the vegetation phase between the first and third pair of true leaves (Fig. 10). They all sprouted after the plants were relocated. All of the young plants were found at relocation points 2 and 3 (Fig. 4) – in point 2 there were found seven young specimens, and in point 3 there were two young specimens. The young plants were located outside the main tuft.

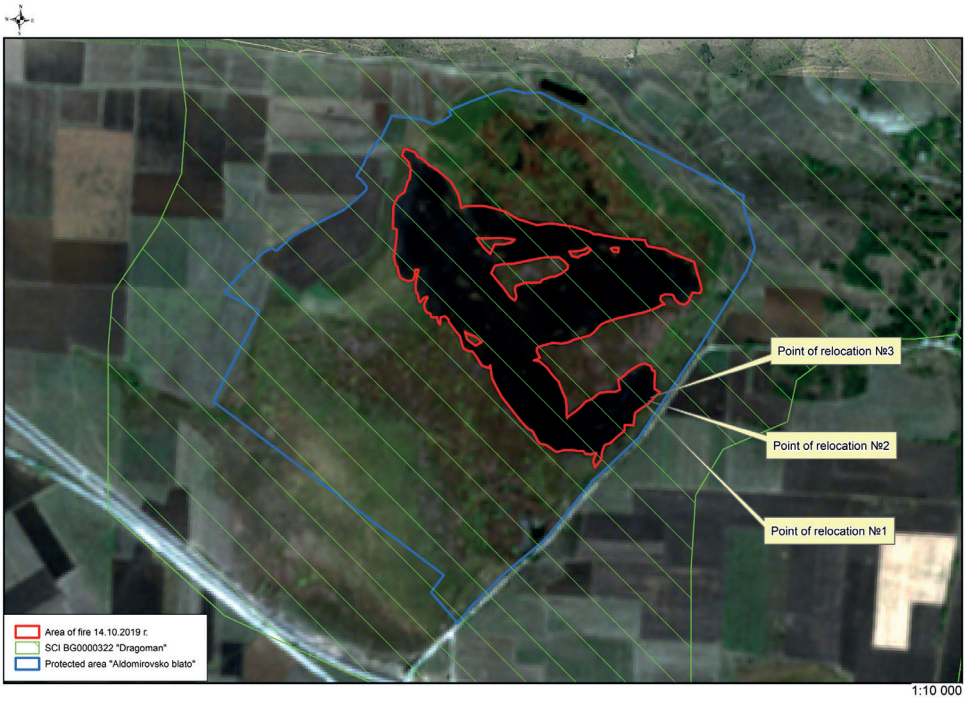

Figure 7. Map of the fire in the area of the new locality of *V. pumila*.

Figure 8. Pictures of the three working polygons of the new locality which are not affected by the fire: **a** picture of polygon number 1 represented on Figure 07 **b** picture of polygon number 2 represented on Figure 07 **c** picture of polygon number 3 represented on Figure 7.

Figure 9. Photograph of blooming (late phase) in *V. pumila* detected in the spring after the fire.

Figure 10. New young plants obtained from seeds of different heights and vegetation phases.

Discussion

The cycle of regeneration of the species at the new location (including transfer from the original location to the new one) included several successive stages. The process started with the planting of the mature adult specimens in a new location and ended with the establishment of a new reproductive local population. Intermediate phases in the establishment of that new locality included: production of living pollen, building of knots, development of seeds, dissemination and growing of a viable young plant (Volis 2019). With the discovery of juvenile (young) specimens of *V. pumila* at the site of relocation, it can be considered that the second (final, concluding) phase described by Volis (2019) has been successfully completed.

The newly established localities of *V. pumila* were saved from the fire in 2019 (see results) due to the special algorithm of the cultivation of the relocated plants and, especially, measures related to mowing the habitat.

The fires are often related to the functioning of the entire ecosystems. They can start spontaneously or may have anthropogenic origins. The fires impact the biodiversity and may change the structure of the ecosystems and the landscape (Whelan 2009, Argañaraz et al. 2015). In 2000, a bulletin was published for Australia, which determined the impact of fires on wetland flora (similar to that of the habitat of *V. pumila*). According to Allen (2000), the plants can survive the effects of fires by regenerating dormant buds from stems or roots, while fire can cause the germination of seeds of some plants stored in the soil. If a fire occurs during an inappropriate growing season, it would result in the loss of stocks of seeds or mature plants. The strength and intensity of the fire depends on the season of occurrence, which affects the plant communities inhabiting the wetlands. Fires in this type of habitat may destroy a significant part of the existing dry biomass, which is above the water level, as well as nearby terrains with mesophilic vegetation. It should be noted that due to the cares taken during the first year of reintroduction (cleaning of the area and mowing around the nests with the reintroduced plants) the fire's boundaries (demonstrated on Fig. 7) did not affect the violets, but all of the vegetation in the vicinity was burned out (Fig. 8 a,b,c). We can conclude that taking proper measures for the plants in the first year of their relocation is key to both their successful adaptation and the prevention of damage.

We selected to relocate the saved plants in one particular habitat of type 6510 "Lowland hay meadows", which has good representativeness and degree of conservation in SCI BG0000322 Dragoman.

However, at biogeographical level, the habitat 6510 is not in good condition due to anthropogenic threats (Eionet CDR 2020). In the RUHD (2015) for Bulgaria, no habitats were reported to be in "Unfavorable – Bad" condition. According to the second report for Republic of Bulgaria concerning the period 2013–2018 (RUHD 2020a), for the Continental Biogeographic Region (CON) the assessment of the conservation status of three grassland habitats was "Unfavourable – Bad" (U2) and one of these habitat was habitat 6510 "Lowland hay meadows". Because of the poor assessment of the condition of the habitat 6510 "Lowland hay meadows" in RUHD

(2020b), concerning the parameters "Future perspectives", the conservation measures have to be focused on the reduction of the pressures and the threats.

According to Apostolova and Meshinev (2015) the most important threats for the habitats of *V. pumila* are related to the conversion of mesophilic meadows into arable land through habitat drainage. As necessary measures, the authors pointed out the maintenance of the haymakingregime in the sites and maintaining a moderate degree of disturbance within populations. Tzonev and Gusev (2020) identified the following main threats to habitat 6510 "Lowland hay meadows": the abandonment of haymaking, overgrazing, the ploughing for arable land, and changes in the water regimes. The measures they offer for the conservation of the habitat are related to the restoration of the haymaking use, change of the mowing terms and the reduction of the grazing intensity. Brzank et al. (2019) reported that the mowing delay or sporadic mowing lead rapidly to significant changes in species composition in the habitat. The drying of marshy soils leads to fast mineralization, carbon dioxide and nitrogen release, encroachment of nitrophilous plants, and the disappearance of peat earth layer. According to Martin et al (2018), pressures such as agricultural intensification, abandonment, lack of mowing and the application of natural fertilizers (such as slurry) are the largest threats to the conservation of the habitat 6510

"Lowland hay meadows". As appropriate conservation measures, the authors propose implementation of management plans and targeted agri-environment schemes, and engagement with landowners and other stakeholders.

Our results indicate that the most important conservation measures which are essential for the management and protection of habitat 6510 "Lowland hay meadows" in the CON Biogeographical Region (incl. the Natura 2000 site SCI BG0000322 Dragoman) are as follows: i) regulation of the haymaking regime of the meadows; ii) regulation of grazing of farm animals; iii) conversion of abandoned arable land into meadows; iv) restoration of the water regime of the meadows where it was disturbed; v) creation and implementation of incentives and compensatory mechanisms for the owners of private lands in which the habitat is distributed; vi) fire prevention; vii) surveillance of the status of the meadows and data collection on the structure and function of the habitat in the particular Natura 2000 sites; viii) updating of the information in the Standard Data Forms (SDFs) of Natura 2000 sites; ix) raising the awareness of the stakeholders by conducting regular information campaigns aimed at the local public, as well as by providing publicly available up-to-date information by the competent authorities, and scientific and environmental non-governmental organizations.

Conclusions

The successful relocation and the creation of new habitats for rare and endangered plant species can be achieved by adhering to a certain algorithm of actions. By setting the site specific conservation objectives (Commission note, 2012) and the necessary conservation measures for habitat 6510 "Lowland hay meadows" in SCI BG0000322

"Dragoman", the original and the new localities of *V. pumila* should be taken into consideration. The determination of the site specific conservation measures in SCI BG0000322 "Dragoman" and the territories where they will be applied (the specific landfills / properties) should be implemented with the active participation of the relevant stakeholders (Commission note 2013). The management plans for Natura 2000 sites could represent an appropriate tool for this (NEC 2019). The availability of reliable up-to-date information on the distribution and condition of *V. pumila* and its habitats is crucial in order to implement proper management and conservation policy.

Author's contribution

MK and NN provided the field surveys, all of the relocation activities and the monitoring of the condition of the plants. MK issued the time tables, NN organized the coordination with the competent authorities and the government institutions. Both authors wrote the manuscript, prepared the maps and designed the figures.

Acknowledgements

We thank the scientific staff of Shumen University (Shumen, Bulgaria) for their support. Konstantin Preslavsky University of Shumen, Project No. RD-08-109 / 02. 02.2021.

References

Aeschiman D, Burdet HM (1994) Flore de la Suisse et desterritoires limitrophes. Le noveau Binz, second ed. Editiondu Griffon, Neuchatel, 603 pp.

Allen M (2000) Water notes for wetlands management. Wetlands and fire. Water notes. Water and Rivers Commission, Government of western Australia. Advisory notes for land managers on river and wetland restoration, Australia. https://water.wa.gov.au/__data/assets/pdf_file/0019/3349/11412.pdf

Andreev N (1993) Materials and critical notes on the flora of Bulgaria. Hist. Nat. Bulg. 4: 29–37.

Apostolova I, Meshinev T (2015): *Viola pumila* Chaix. In: Peev D (Ed.) Red list of Republic of Bulgaria (1) Plants and fungi. BAS and MoEW, Sofia, 652. http://e-ecodb.bas.bg/rdb/bg/vol1/

Argañaraz JP, Pizarro GG, Zak M, Bellis LM (2015) Fire Regime in Córdoba. Fire Ecology 11: 55–73. https://doi.org/10.4996/fireecology.1101055

Brzank M, Piekut K, Dąbrowski P, Pawluśkiewicz B (2019) The succession and regression of plant species on lowland hay meadows in Poland. Polish Journal of Environmental Studies 28(3): 1567–1577. https://doi.org/10.15244/pjoes/85302

Buldrini F, Dallai D (2011) *Viola pumila* Chaix, Schede per una Lista Rossa della Flora vascolare e crittogamica Italiana. Informatore Botanico Italiano 43: 381–458. https://www.societabotanicaitaliana.it/sbi//IBI%2043%20(2)%202011/381-458%20-%20Schede%20per%20una%20Lista%20Rossa%20della%20Flora%20vascolare%20e%20crittogamica%20Italiana.pdf

Buldrini F, Conte L, Dallai D, Ferrari C (2013) Genetic diversity of the rare and endangered meadow violet (*Viola pumila* Chaix) at the southern margin of its range, Plant Biosystems. Official Journal of the Societa Botanica Italiana. 147: 563–572. https://doi.org/10.1080/11263504.2012.754383

Commission note (2012) Setting conservation objectives for Natura 2000 sites, 1–8. https://ec.europa.eu/environment/nature/natura2000/management/docs/commission_note/commission_note2_EN.pdf

Commission note (2013) Establishing conservation measures for Natura 2000 sites, 1–9. https://ec.europa.eu/environment/nature/natura2000/management/docs/commission_note/co mNote%20conservation%20measures_EN.pdf

Danihelka J, Niklfeld H, Šípošová H (2009) *Viola elatior*, *V. pumila* and *V. stagnina* in Austria, Czechia and Slovakia: A story of decline. Preslia 81: 151–171. https://www.cabdirect.org/cabdirect/abstract/20103074757

Delipavlov D (1979) *Viola* sp. In: Yordanov D (Ed.) Flora of Bulgaria (7). BAS, Sofia, 529.

Delipavlov D, Tcheshmedjiev I, Popova M, Terziiski D, Kovachev I (2011) Key to the plants in Bulgaria. Academic Publishing House of the Agricultural University, Plovdiv.

Eckstein RL, Hölzel N, Danihelka J (2006) Biological Flora of Central Europe: *Viola elatior*, *V. pumila* and *V. stagnina*. Perspectives in Plant Ecology, Evolution and Systematics 8(1): 45–66. https://doi.org/10.1016/j.ppees.2006.01.001

Eionet CDR (Central Data Repository) (2020) European Environment Agency BG_habitats_report_2013–2018-Redelivery 2020. https://cdr.eionet.europa.eu/bg/eu/art17/envxhyhkg/

GBIF (2021) Occurrence Download. https://doi.org/10.15468/dl.7rag2h

Gejdeman TS (1986) Higher plants of Moldova SSR, 3rd ed. Kisinev, 576 pp.

Grulich V (2012) Red List of vascular plants of the Czech Republic. Preslia 84: 631–645. https://www.ms-cbs.cz/_publikace/P123Grulich.pdf

Holzel N (2003) Re-assessing the ecology of rare flood-meadow violets (*V. elatior*, *V. pumila*, *V. persicifolia*) with large phytosociological data sets. Folia Geobotanica 38(3): 281–298. https://link.springer.com/article/10.1007/BF02803200. https://doi.org/10.1007/BF02803200

Humphreys AM, Govaerts R, Ficinski SZ, Lughadha EN, Vorontsova MS (2019) Global dataset shows geography and life form predict modern plant extinction and rediscovery. Nature Ecology & Evolution 3(7): 1043–1047. https://doi.org/10.1038/s41559-019-0906-2

Info Flora (2021) Info Flora. https://www.infoflora.ch/en/flora/viola-pumila.html

Korneck D, Schnittler M, Vollmer JR (1996) Liste der Farn- und Blütenpflanzen (Pteridophyta et Spermatophyta). Deutschlands. Schriftenr. Vegetationsk. 28: 21–187. [Bonn-Bad Godesberg.]

Natura (2000) site SCI BG0000322 Dragoman http://natura2000.moew.government.bg/PublicDownloads/Auto/PS_SCI/BG0000322/BG0000322_PS_16_1.pdf

Martin JR, O'Neill FH, Daly OH (2018) The monitoring and assessment of three EU Habitats Directive Annex I grassland habitats. Irish Wildlife Manuals, No. 102. National Parks and Wildlife Service, Department of Culture, Heritage and the Gaeltacht, Ireland.

NEC (2019) Managing Natura 2000 sites – The provisions of Article 6 of the 'Habitats' Directive 92/43/EEC. https://eur-lex.europa.eu/legal-content/EN/TXT/?qid=1548663172672&uri=CELEX:52019 XC0125(07)

Petrova A, Vladimirov V (Eds.) (2009) Red List of Bulgarian vascular plants. Phytologia Balcanica 15: 63–94. http://www.bio.bas.bg/~phytolbalcan/PDF/15_1/15_1_08_Petrova_&_Vladimirov.pdf

Pullin AS, Woodell SRJ (1987) Response of the fen violet, *Viola persicifolia* Schreber, to different management regimes at Woodwalton Fen National Nature Reserve, Cambridgeshire, England. Biological Conservation 41(3): 203–217. https://doi.org/10.1016/0006-3207(87)90103-0

RUHD (2015) Reporting of the Republic of Bulgaria under Art. 17 of Habitat Directive. State of nature in the EU Results from reporting under the nature directives 2007–2012. https://www.eea.europa.eu/publications/state-of-nature-in-the-eu

RUHD (2020a) Reporting of the Republic of Bulgaria under Art. 17 of Habitat Directive. State of nature in the EU Results from reporting under the nature directives 2013–2018. https://www.eea.europa.eu/publications/state-of-nature-in-the-eu-2020

RUHD (2020b) Reporting of the Republic of Bulgaria under Art. 17 of Habitat Directive for the period 2013–2018, habitat 6510 CON "Lowland hay meadows". https://cdr.eionet.europa.eu/Converters/run_conversion?file=bg/eu/art17/envxhyhkg/BG_ha bitats_reports-20190828-114556.xml&conv=589&source=remote#6510CON

Tzonev R, Gusev Ch (2020) Guide for identification and effective management of grassland habitats (pastures, meadows and permanent grasslands) – object of protection and economic use in Bulgaria. Bulgarian Society for the Protection of Birds, Nature Conservation Series, 34, Sofia.

Volis S (2019) Conservation-oriented restoration – a two for one method to restore both threatened species and their habitats. Plant Diversity 41(2): 50–58. https://doi.org/10.1016/j.pld.2019.01.002

Whelan RJ (2009) The Ecology Of Fire – Developments Since 1995 And Outstanding Questions. Proceedings of the Royal Society of Queensland 115: 59–68. https://ro.uow.edu.au/scipapers/367/

BioRisk 18: 17–34 (2022)
doi: 10.3897/biorisk.18.78548
https://biorisk.pensoft.net

REVIEW ARTICLE

A peer-reviewed open-access journal
BioRisk

Studies on the Bulgarian members of the family Chenopodiaceae *s. stricto*: a review

Vanya Stoyanova Boneva[1], Nadezhda Traycheva Petkova[2]

1 *Department of Biology and Aquaculture, Faculty of Agriculture, Trakia University, 6000, Stara Zagora, Bulgaria* **2** *Department of Organic Chemistry and Inorganic Chemistry, Technological Faculty, University of Food Technologies, 4002, Plovdiv, Bulgaria*

Corresponding author: Vanya Stoyanova Boneva (vannboneva@gmail.com)

Academic editor: Josef Settele | Received 27 November 2021 | Accepted 7 March 2022 | Published 27 April 2022

Citation: Boneva VS, Petkova NT (2022) Studies on the Bulgarian members of the family Chenopodiaceae *s. stricto*: a review. BioRisk 18: 17–34. https://doi.org/10.3897/biorisk.18.78548

Abstract

The Bulgarian members of Chenopodiaceae are mainly ruderal and weed species; another part are halophytes. Over the last two decades, phylogenetic molecular studies have led to a number of taxonomic changes in the above mentioned family. Changes have also occurred in one of the largest genera – *Chenopodium*. The aim of the present study is to review the research on Bulgarian members of the Chenopodiaceae family. The data available in the literature on the taxonomic composition, chorology, morphological features and karyological variability of the species from their Bulgarian populations has been studied. A review of the phytochemical studies of Chenopodiaceae plants from their Bulgarian populations has been made. The systematized data is presented in chronological order, which allows for tracing the current level of study on the family in Bulgaria and opportunities for new research.

Keywords

Bulgaria, Chenopodiaceae, chorology, karyology, morphology, phytochemical investigations

Introduction

The family Chenopodiaceae is relatively large and worldwide it numbers about 1600 species belonging to more than 100 genera, spread more widely in the moderate and subtropical regions (Kühn et al. 1993; Kadereit et al. 2003).

The greater part of the Bulgarian members of the family belongs to the group of the highly movable ruderal plants and weeds with habitats in the central and

southern part of the continent but having successfully spread in Bulgaria's thermal zone and in the western parts of its territory (Stefanov 1943). Their wide distribution is related to the ability of most species to grow under extreme conditions such as high air and soil temperature (Ilyin 1936). Some of the species are North American, North African or Australian and have spread over the territory of the country due to human activity. The last part is the number of species belonging to the Mediterranean and Boreal floral element, as well as those distributed on most of the continents. Another part of the Bulgarian members of the family are halophytes inhabiting the periodically flooded, muddy and sandy terrains on the periphery of the hyperhaline and, less frequently, the brackish Black Sea lakes. They form the communities of the annual halophytes in the Black Sea salt lakes (Tzonev and Gussev 2015). The globalization we have witnessed over the last two decades has led to the penetration of many foreign species, and molecular research has led to new taxonomic changes and decisions in the family.

The objective of the present study is to review the chorological, morphological, karyological, and phytochemical studies regarding the Bulgarian members of the family Chenopodiaceae.

Data about the taxonomic composition and distribution of the bulgarian members of the family Chenopodiaceae

Available literature from the last decades of the 19th century

The first data about the distribution of the Bulgarian members of the family Chenopodiaceae was published in the 19th century by: Bornmüller (1888), Georgiev (1889), Yavashev (1890), Toshev (1895), and Urumov (1897). The information there occurring has been summarized by Velenovský (1891, 1898) in the two editions of his Flora bulgarica.

The 1st edn. of Flora bulgarica (Velenovský 1891) listed 28 Chenopodiaceae species belonging to 9 genera. Concerning *Chenopodium*, the following 12 species were reported: *C. bonus-henricus* L., *C. rubrum* L., *C. glaucum* L., *C. polyspermum* L. *C. hybridum* L., *C. murale* L., *C. urbicum* L., *C. album* L., *C. ficifolium* Sm., *C. opulifolium* Schrad., *C. vulvaria* L., *C. botrys* L. For *Atriplex* 4 representatives were reported, i.e. *A. rosea* L., *A. laciniata* L., *A. patula* L., and *A. hastata* L. The genus *Kochia* is represented by 4 species in Velenovský's work: *K. scoparia* Schrad., *K. prostrata* Schrad., *K. arenaria* Roth., and *K. sedoides* Schrad. Two species of *Camphorosma* (*C. monspeliaca* L. and *C. ovata* WK.) and two of *Suaeda* (*S. maritima* Dumort. and *S. altissima* Pall.) were recognized. Finally, just one species was given for four genera: *Beta trygina* B. K, *Blitum virgatum* L., *Salicornia herbacea* L, *Salsola kali* L.

In the 2nd edn. of Flora bulgarica Supplementum (Velenovský 1898) new information concerning the distribution has been included regarding: 6 species from genus *Chenopodium* – *C. bonus-henricus*, *C. hybridum*, *C. urbicum*, *C. botrys*, *C. vulvaria*, *C. album*; 3 species belonging to genus *Atriplex* – *A. rosea*, *A. patula*, *A. tatarica*;

2 species from genus *Beta* – *B. trygina*, *B. maritima* and 1 species from each of genus *Blitum* (*B. virgatum*), *Kochia* (*K. scoparia*), *Suaeda* (*S. heterophylla*), *Salsola* (*S. kali*).

Therefore, a total of 32 Chenopodiaceae species were reported for Bulgaria in the 19th century, including data about the distribution in the country.

Available literature from the 20th century

In the first two decades of the 20th century the main source of information about the Bulgarian Chenopodiaceae species was works by Urumov (1901, 1904, 1905, 1906, 1908a, 1908b, 1908c, 1909, 1913, 1917, 1923), Kovachev (1903), Davidov (1904, 1905), Neichev (1905), Petkov (1907), Stranski (1921), and Yordanov (1923–1924).

The gathered chorological information was summarized in the 1st edn. of Flora of Bulgaria (Stoyanov and Stefanov 1924), where family Chenopodiaceae is presented by 44 species and 13 genera. Cyclolobae C. A. Mey. comprises members of the following genera: *Atriplex* (7), *Bassia* (2), *Beta* (2), *Camphorosma* (3), *Chenopodium* (12), *Corispermum* (3), *Kochia* (3), *Polycnemum* (3 species), *Salicornia* (1), *Spinacia* (1). Spirolobae comprises 3 genera – *Petrosimonia* (1), *Salsola* (3), *Suaeda* (3).

In the period prior to the publication of the 2nd edn. of Flora of Bulgaria (Stoyanov and Stefanov 1933), data about the Chenopodiaceae plants was published mainly by Urumov (1926, 1928, 1929a, 1929b, 1930).

The 2nd edn. of the Flora of Bulgaria (Stoyanov and Stefanov 1933) reports 39 Chenopodiaceae species (13 genera): *Atriplex* (7), *Bassia* (2), *Beta* (2), *Camphorosma* (2), *Chenopodium* (12), *Corispermum* (3), *Kochia* (3), *Petrosimonia* (1), *Polycnemum* (3 species), *Salicornia* (1), *Salsola* (2), *Spinacia* (1), *Suaeda* (2).

From the members of the family included in the 1st edn. of Flora of Bulgaria 5 of the species were removed: *Camphorosma ruthenicum* M.B., *Corispermum canescens* Kit., *Corispermum orientale* Lam., *Salsola toseffi* Urumov, and *Suaeda heterophylla* Bunge.

Later chorological data about the species in the family was published by Rechinger (1933), Urumov (1935), and Baev (1947) which were included in the 3rd edn. of the Flora of Bulgaria (Stoyanov and Stefanov 1948). Forty one species of Chenopodiaceae are mentioned, belonging to 13 genera: *Atriplex* (7), *Bassia* (2), *Beta* (2), *Camphorosma* (2), *Chenopodium* (13), *Corispermum* (2), *Kochia* (3), *Petrosimonia* (1), *Polycnemum* (3), *Salicornia* (1), *Salsola* (2), *Spinacia* (1), *Suaeda* (2). In the same edition 2 new species of Bulgarian flora are included in family Chenopodiaceae – *Chenopodium opulifolium* Schrad. and *Corispermum hyssopifolium* L. *C. opulifolium* was mentioned as a ruderal plant widely spread in the country, while the second one was discovered in an area on the sands of the Danubian islands from the Belene group (isle of Milka and isle of Persina).

In subsequent years new data about the distribution and the ecology of Chenopodiaceae was found in works by Stoyanov et al. (1954), Kiryakov et al. (1951), and Kolev (1956, 1959).

The next edition (4th) of Flora of Bulgaria (Stoyanov et al. 1966) the author reported one new genus and species for Bulgaria, i.e. *Ceratocarpus arenarius*.

The most exhaustive information about the family Chenopodiaceae in our country was given by Yordanov et al. (1966) in Flora of the People's Republic of Bulgaria. A total of 48 Chenopodiaceae species were reported, belonging to 15 genera: *Atriplex* (7), *Bassia* (2), *Beta* (2), *Camphorosma* (2), *Ceratocarpus* (1), *Chenopodium* (15), *Corispermum* (2), *Halimione* (2), *Kochia* (3), *Petrosimonia* (1), *Polycnemum* (3), *Salicornia* (2), *Salsola* (2), *Spinacia* (1), *Suaeda* (3). Members of the family are 4 cultivated species as well as *Atriplex hortensis*, *Spinacia oleracea*, *Beta vulgaris*, *Kochia scoparia*. *Chenopodium ambrosioides* was published as new species for the country and it was reported for the first time for the sands near Varna and the experimental field in Ovcha kupel.

Following the publication of Flora of the People's Republic of Bulgaria floristic reports have been presented supplementing the data about the family Chenopodiaceae in Bulgarian flora (Delipavlov and Dimitrov 1973; Panov 1975, 1987; Delipavlov and Cheshmedzhiev 1984; Cheshmedzhiev 1988; Meshinev et al. 1994).

Summarized studies about the family during that period are presented in the Field Guide to the vascular plants in Bulgaria (Andreev 1992), where Chenopodiaceae is represented by 48 species (14), as follows: *Atriplex* (8), *Bassia* (2), *Beta* (2), *Camphorosma* (2), *Ceratocarpus* (1), *Chenopodium* (16), *Corispermum* (2), *Halimione* (2), *Kochia* (2), *Petrosimonia* (1), *Polycnemum* (3), *Salicornia* (2), *Salsola* (2), *Suaeda* (3).

It is noted that *Bassia sedoides* distribution in Bulgaria has not been confirmed by Andreev (1992). The publication does not mention any cultivated species. Concerning the genus *Chenopodium*, a new record from the Northern Black Sea coast has been reported, i.e. *Chenopodium chenopodioides* (L.) Aellen. (= *C. botryoides* Sm.; see e.g., Iamonico 2014). Among the representatives of genus *Atriplex* two new species have been added to the national flora, i.e. *A. micrantha* (= *A. heterosperma*) and *A. halimus*. The first species is indicated as in doubt, whereas *A. halimus* has been reported for the Northern Black Sea coast. Philipova-Marinova et al. (1997) indicated *C. botryoides* as new for the country from the territory of Shabla Lake.

The summarized data from the studies about the Bulgarian members of the family Chenopodiaceae in the 20th century showed that the species diversity of the family comprised 48 species belonging to 14 genera.

Available literature from the new millennium

Chorological studies of the members of Chenopodiaceae from the end of the 20th century and the beginning of the 21st century have been published by Delipavlov and Cheshmedzhiev (2011). Fifty species have been listed for the family (15), as follows: *Atriplex* (8), *Bassia* (1), *Beta* (2), *Camphorosma* (2), *Ceratocarpus* (1), *Chenopodium* (17), *Corispermum* (2), *Halimione* (2), *Kochia* (3), *Petrosimonia* (1), *Polycnemum* (3), *Salicornia* (2), *Salsola* (2), *Spinacia* (1), *Suaeda* (3). The composition of the genus *Chenopodium* comprises the 16 species indicated by Andreev (1992) and 1 of the species published by Panov (1987) – *C. acuminatum* – confirmed for the Northern Black Sea coast. *Bassia sedoides* has been excluded from the genus *Bassia*. Four cultivated species were reported - *Atriplex hortensis*, *Spinacia oleracea*, *Beta vulgaris*, *Kochia scoparia*.

Conspectus of the Bulgarian vascular flora by Assyov and Petrova (2006) registered 50 species of Chenopodiaceae belonging to 13 genera: *Atriplex* (9), *Bassia* (1), *Beta* (2), *Camphorosma* (2), *Chenopodium* (18 species), *Corispermum* (2), *Halimione* (2), *Kochia* (3), *Petrosimonia* (1), *Polycnemum* (3), *Salicornia* (2), *Salsola* (2), *Suaeda* (3). The composition of genus *Chenopodium* included 1 new species for the country, *C. schraderianum* Schult.

Five Chenopodiaceae species are protected by the Biological Diversity Act (2007): *Bassia hirsuta*, *Halimione pedunculata*, *H. portulacoides*, *Petrosimonia brachiata*, and *Suaeda heterophylla*. The Red Data Book of the Republic of Bulgaria (Peev et al.2015) includes 4 species, i.e. *B. hirsuta*, *Corispermum marschalii*, *P. brachiata*, and *S. heterophylla*. *B. hirsuta* and *C. marschalii* have been referred to the IUCN category EN (endangered), whereas *P. brachiata* and *S. heterophylla* are assessed as CE (critically endangered). *B. hirsuta*, *P. brachiata* and *S. heterophylla* are part of the communities of annual halophytes in the salty lakes along the Black Sea coast. The annual halophyte communities are among the protected natural habitats pursuant to Directive 92/43/EEC (1992). The habitat is included in Annex 1 of Biological Diversity Act (2007) and in the Red Data Book of the Republic of Bulgaria by Tzonev and Gussev (2015) in the category "endangered" habitat. The data about *B. hirsuta*, *P. brachiata*, and *S. heterophylla* populations are found in some works concerning the Black Sea coast vegetation and in the protected area management plans of Burgas wetlands (Michev et al. 2003; Grozeva et al. 2004; Grozeva 2004, 2005; Tzonev et al. 2008; Stoyanov 2009; Todorova et al. 2014).

In the last decade the genus *Chenopodium* has been subject to a number of studies resulting in changes in the species composition of both the genus and the family Chenopodiaceae. Grozeva (2007a) reported a new species for the country *Chenopodium pumilio*. Based on a taxonomic revision Grozeva (2009) suggested *Chenopodium acuminatum* to be deleted from the members of the Bulgarian flora as incorrectly identified. This change was later recorded by Assyov et al. (2012).

Six new species and one subspecies from the genus *Chenopodium* (*C. strictum* Roth, *C. striatiforme* Murr, *C. album* subsp. *pedunculare* (Bertol.) Arcang., *C. pratericola* Rydb., *C. probstii* Aellen, and *C. missouriense* Aellen) have been reported for the Bulgarian flora by Grozeva (2009, 2010a, 2010b, 2012a, 2012b).

The changes that had occurred in the taxonomic composition of Chenopodiaceae have been recorded in the 4th edn. of Conspectus of Bulgarian vascular flora (Assyov et al. 2012), where 56 species (14 genera) are listed as follows: *Atriplex* (9), *Bassia* (1), *Beta* (2), *Camphorosma* (2), *Ceratocarpus* (1), *Chenopodium* (23), *Corispermum* (2), *Kochia* (3), *Petrosimonia* (1), *Polycnemum* (3 species), *Salicornia* (2), *Salsola* (3), *Spinacia* (1), *Suaeda* (3).

The Euro+Med Plant Base (Uotila 2011) reported 53 species and 19 genera for Bulgaria: *Atriplex* (8), *Bassia* (4), *Beta* (2), *Blitum* (2), *Camphorosma* (2), *Ceratocarpus* (1), *Chenopodiastrum* (2), *Chenopodium* (6), *Corispermum* (2), *Dysphania* (4), *Halimione* (2), *Lipandra* (1), *Oxybasis* (4), *Petrosimonia* (1), *Polycnemum* (3 species), *Salicornia* (2), *Salsola* (2), *Spinacia* (1), *Suaeda* (3). The differences in the composition of genus

Chenopodium between Conspectus of Bulgarian vascular flora (Assyov et al. 2012) and The Euro+Med Plant Base (Uotila 2011) are because Euro+Med Plant Base (Uotila 2011) gives the composition of *Chenopodium s. str.*, including the genera *Blitum*, *Chenopodiastrum*, *Dysphania*, *Lipandra*, *Oxybasis*, while Conspectus of Bulgarian vascular flora (Assyov et al. 2012) presents *Chenopodium s. lat*.

From data by Grozeva (2018b) the family Chenopodiaceae is represented in Bulgarian flora by 51 species and 2 subspecies [*Chenopodium strictum* subsp. *striatiforme* (Murr) Uotila and *C. album* subsp. *pedunculare* (Bertol.) Arcang.] and the author does not include the cultivated species *Beta vulgaris* and *Spinacia oleracea* in the species composition.

The summarized data about the taxonomic composition of family Chenopodiaceae is presented in Table 1.

Morphological studies on members of Chenopodiaceae in Bulgar-ia

Detailed studies on the morphology of Chenopodiaceae in Bulgaria were conducted, mainly on *Chenopodium s. lat.* In particular, the following species were investigated: *Chenopodium album* and *Dysphania botrys* from 18 populations (Grozeva and Cvetanova 2008), *Blitum bonus-henricus* from 10 populations with ecological notes (Grozeva and Cvetanova 2011) and distribution in the country (Grozeva 2011), *C. pratericola* (Grozeva 2012a), the genus *Dysphania* (Grozeva and Cvetanova 2013), *C. probstii* and *C. missouriense* (Grozeva 2014), *Blitum virgatum* (Grozeva and Cvetanova 2016). Further taxa studies were *Bassia hirsuta* (Grozeva and Todorova 2014) and *Petrosimonia brachiata* (Grozeva et al. 2019a).

Karyological studies on Chenopodiaceae in Bulgaria

The first karyological data about Chenopodiaceae in Bulgaria was published by Markova (1968) on *Dysphania multifida* (population from the Danubian plain) resulting in a tetraploid chromosome number $2n = 36$. These data was later confirmed by Grozeva and Stoeva (2006) on populations of the species from Sredna Gora Mountain, the Eastern Rhodopes and the Thracian lowland and by Grozeva and Cvetanova (2013) on populations from the Central Stara planina, the Danubian plain and the Thracian lowland.

Kožuharov and Kuzmanov (1969) specified for *Suaeda altissima* diploid chromosome number $2n = 18$ for populations from the Southern Black Sea coast and these data were confirmed by Grozeva (2010a, 2015a, 2015b).

Cheshmedzhiev (1976) published for *Beta trigyna* populations from Eastern Stara planina hexaploid chromosome number $2n = 54$.

Popova and Ceschmedjiev (1978) reported for *Kochia scoparia* population from the experimental field of Agricultural University of Plovdiv diploid chromosome number $2n = 18$. These data were confirmed by Grozeva (2015a, 2015b) for a population of the species from the Thracian lowland.

Table 1. List of members belonging to the family Chenopodiaceae, according to literature dates.

Genus	Species	References for nomenclature
1. ***Beta***	***Beta trigyna*** Waldst. & Kit., ***Beta vulgaris*** L. subsp. ***maritima*** (L.) Arcang.	Iamonico (2019)
2. ***Bassia***	***Bassia hirsuta*** (L.) Asch., ***Bassia laniflora*** (S.G.Gmel) A. J. Scott. (≡ *Salsola laniflora* S.G.Gmel), ***Bassia prostrata*** (L.) Beck (= Kochia prostrata (L.) Schrad.), ***Bassia scoparia*** (L.) A. J. Scott (= Kochia scoparia (L.) Schrad.)	Uotila (2011)
3. ***Camphorosma***	***Camphorosma annua*** Pall., ***Camphorosma monspeliaca*** L. subsp. ***monspeliaca***	Uotila (2011)
4. ***Atriplex***	***Atriplex prostrata*** DC. (= A. hastata L.), ***A. micrantha*** Lebed. (= A. heterosperma Bunge) subsp. ***micrantha***, ***A. hortensis*** L., ***A. sagittata*** Borkh. (= A. nitens Schkuhr), ***A. oblongifolia*** Walds. & Kit., ***A. patula*** L., ***A. rosea*** L., ***A. tatarica*** L.	Kadereit et al. (2010), Uotila (2011)
5. ***Blitum***	***Blitum bonus-henricus*** (L.) Rchb. (= Chenopodium bonus-henricus), ***Blitum virgatum*** L. (= Chenopodium foliosum (Moench) Asch.)	Fuentes-Bazan et al. (2012)
6. ***Ceratocarpus***	***Ceratocarpus arenarius*** L.	Uotila (2011)
7. ***Chenopodiastrum***	***Chenopodiastrum murale*** (L.) S.Fuentes, Uotila & Borsch (= Chenopodium murale), ***Chenopodiastrum hybridum*** (L.) S. Fuentes, Uotila & Borsch. (= Chenopodium hybridum L.)	Fuentes-Bazan et al. (2012)
8. ***Chenopodium***	***Chenopodium vulvaria*** L., ***Chenopodium ficifolium*** Sm., ***Chenopodium pratericola*** Rydb., ***Chenopodium betaceum*** Andrz. (= ***C. strictum*** Roth s.lat.), ***Chenopodium opulifolium*** Schrad. ex W.D.J.Koch & Ziz, ***Chenopodium missouriense*** Aellen, ***Chenopodium probstii*** Aellen, ***Chenopodium album*** L., ***Chenopodium album subsp. pedunculare*** (Bertol.) Arcang. (= C. pedunculare)	Fuentes-Bazan et al. (2012) Mosyakin (2018, for *C. Betaceum*) Iamonico & Mosyakin (2018, for *C. album* subsp. *pedunculare*)
9. ***Corispermum***	***Corispermum nitidum*** Kit. Ex Schult.	
10. ***Dysphania***	***Dysphania ambrosioides*** (L.) Mosyakin et Clements L. (= *Chenopodium ambrosioides* L.), ***Dysphania botrys*** (L.) Mosyakin et Clements (= *C. botrys* L.), ***Dysphania multifida*** (L.) Mosyakin et Clements (= *C. multifidum* L.), ***Dysphania pumilio*** (R. Br.) Mosyakin et Clements (= *C. pumilio* R. Br.), ***Dysphania schraderiana*** (Schult.) Mosyakin et Clements (= *C. schraderianum* Schult.)	Fuentes-Bazan et al. (2012)
11. ***Halimione***	***Halimione pedunculata*** (L.) Aellen (basionym?), ***Halimione portulacoides*** (L.) Aellen (basionym?)	Kadereit et al. (2010)
12. ***Lipandra***	***Lipandra polysperma*** (L.) S. Fuentes, Uotila & Borsch (=Chenopodium polyspermum L.)	
13. ***Oxybasis***	***Oxybasis chenopodioides*** (L.) S. Fuentes, Uotila & Borsch (= *Chenopodium chenopodioides* L.), ***Oxybasis glauca*** (L.) S.Fuentes , Uotila & Borsch (= *C. glaucum* L.), ***Oxybasis rubra*** (L.) S.Fuentes, Uotila & Borsch (= *C. rubrum* L.), ***Oxybasis urbica*** (L.) S.Fuentes , Uotila & Borsch (= *C, urbicum* L.)	Fuentes-Bazan et al. (2012)
14. ***Salicornia***	***Salicornia europaea*** L. subsp. ***europaea***, ***Salicornia perennans*** Willd. subsp. ***perennans***	Kadereit et al. (2012)
15. ***Petrosimonia***	***Petrosimonia brachiata*** Bunge	Uotila (2011)
16. ***Salsola***	***Salsola tragus*** L. (= S. ruthenica Iljin), ***Salsola soda*** L.	Akhani et al. (2007)
17. ***Suaeda***	***Suaeda altissima*** (L.) Pall., ***Suaeda maritima*** (L.) Dumort., ***Suaeda heterophylla*** Bunge	Uotila (2011)
18. ***Polycnemum***	***Polycnemum arvense*** L., ***Polycnemum heuffelii*** Lang., ***Polycnemum majus*** A.Braun	Masson & Kadereit (2013)
19. ***Spinacia***	***Spinacia oleracea*** L.	

Van Loon and Van Setten (1982) reported for *Blitum bonus-henricus* population from Rila mountain tetraploid chromosome number $2n = 36$. These data were confirmed by Grozeva and Stoeva (2006) for populations from the Western Rhodopes, Pirin and Central Stara planina and by Grozeva and Cvetanova (2011) for populations from the Central Rhodopes, Western Stara planina, Rila, Slavyanka, and Vitosha mountains.

Van Loon and Van Setten (1982) reported for *Blitum virgatum* populations from Shipka, Central Stara planina diploid chromosome number $2n = 18$. These data were

confirmed by Grozeva and Stoeva (2006) for other populations of the species from Central Stara planina, Western Rhodopes and Tundzha hilly country by Grozeva and Cvetanova (2016) as well as for populations from Rila, Western and Central Rhodopes, Belasitsa, Tundzha hilly country.

Grozeva and Stoeva (2006) published for the first time chromosome numbers for 4 species from the family Chenopodiaceae, as follows: diploid chromosome number 2*n* = 18 for *Bassia hirsuta* and *Corispermum nitidum* for populations from the Southern Black Sea coast and for *Dysphania botrys* from the Danubian plain, North-Eastern Bulgaria and Central Stara planina; tetraploid chromosome number 2*n* = 32 for *Dysphania ambrosioides* populations from the Danubian plain and the Thracian lowland.

Grozeva (2007b) reported for the first time diploid chromosome number 2*n* = 18 from the Bulgarian populations of 8 species: *Oxybasis chenopodioides* from the Northern Black Sea coast; *Chenopodiastrum hybridum* from the Southern Black Sea coast; Danubian plain and the Eastern Rhodopes; *O. glauca* from the Northern Black Sea coast and the Danubian plain; *C. murale* from Central and Eastern Stara planina; *O. rubra* from North-Eastern Bulgaria; *Lipandra polysperma* from Eastern Sredna gora, Strandzha and Thracian lowland; *C. ficifolium* from the Northern Black Sea coast, North-Eastern Bulgaria and Thracian lowland; *Atriplex tatarica* from the Southern Black Sea coast (Grozeva 2007b). For the newly established species *Dysphania pumilio* diploid chromosome number 2*n* = 18 was published (Grozeva 2007b) and for the 2 new for the country North American species *Chenopodium missouriense* and *C. probstii* – hexaploid chromosome number 2*n* = 54 (Grozeva 2010a). The chromosome number for 3 species was reported for the first time: *A.hastata* 2*n* = 18 from the Danubian plain and the Thracian lowland, *A. patula* 2*n* = 36 from the Eastern Rhodopes and Eastern Sredna Gora, *Suaeda maritima* 2*n* = 36 from the Southern Black Sea coast (Grozeva 2010a).

Grozeva (2010b) published for the first time data about the chromosome number of 7 species from the genera: *Atriplex* (*A. nitens*, *A. rosea*, *A. hortensis*, *A. oblongifolia*), *Chenopodium* (*C. opulifolium*, *C. urbicum*, *C. vulvaria*) and *Oxybaisis* (*O. urbica*). Diploid chromosome number 2*n* = 18 was established for populations of: *A. nitens* from the Eastern Rhodopes; *A. rosea* from the Southern Black Sea coast and the Thracian lowland; *A. hortensis* from the Danubian plain and the Thracian lowland; *O. urbica* from North-East Bulgaria; *C. vulvaria* from the Eastern Rhodopes. Tetraploid chromosome number 2*n* = 36 was registered for populations of *A. oblongifolia* from the Thracian lowland and hexaploid chromosome number 2*n* = 54 for *C. opulifolium* populations from North-Eastern Bulgaria and the Thracian lowland.

For the newly established for the Bulgarian flora species *Chenopodium pratericola* diploid chromosome number 2*n* = 18 was reported (Grozeva 2012a).

Grozeva (2012b) reported for the first time data about the chromosome number of *Chenopodium album subsp. album*, *C. album* subsp. *pedunculare*, *C. betaceum* (sub. *C. striatiforme* and *C. strictum*), and *Suaeda heterophylla*. For *C. album* populations from the Northern Black Sea coast, Eastern Rhodopes and the Thracian lowland and for *C. album* subsp. *pedunculare* from the Northern Black Sea coast hexaploid

chromosome number 2*n* = 54 was reported. For *C. betauceum* populations from the Southern Black Sea coast, Danubian plain and the Eastern Rhodopes tetraploid chromosome number 2*n* = 36 was established. For *S. heterophylla* population from the Southern Black Sea coast diploid chromosome number 2*n* = 18 was reported.

Grozeva and Cvetanova (2013) registered for the first time diploid chromosome number 2*n* = 18 for *Dysphania schraderiana* population from the Eastern Sredna gora mountain. Data about the karyotype of 27 populations of the species from genus *Dysphania* (*D. ambrosioides*, *D. botrys*, *D. multifida*, *D. pumilio* and *D. schraderiana*) was published. Polyploidy and disploidy are cited as basic evolutionary mechanisms in the genus.

Grozeva (2013) reported karyological data about 14 Chenopodiaceae species from their Bulgarian populations. For the first time the chromosome number of the species *Bassia laniflora*, *Salsola tragus* and *Salicornia europaea* subsp. *europaea* was reported for their populations from the Southern Black Sea coast. For *S. tragus* tetraploid chromosome number 2*n* = 36 was registered and for *B. laniflora* and *S. europaea* diploid chromosome number 2*n* = 18. The chromosome numbers known from literature data about 11 species (*Atriplex oblongifolia*, *A. tatarica*, *Bassia hirsuta*, *Chenopodium album subsp. album*, *C. betaceum* (*sub. C. Strictum*), *Corispermum nitidum*, *Dysphania pumilio*, *Lipandra polysperma*, *Oxybasis chenopodioides*, *O. rubra*, *O. urbica*) were confirmed (Grozeva 2013).

Grozeva (2015a) reported for the first time data about the chromosome number from the Bulgarian populations of 4 species (*Atriplex heterosperma*, *Bassia prostrata*, *Salicornia perennans*, *and Salsola soda*). For *A. heterosperma* population from the Southern Black Sea coast chromosome number 2*n* = 36 was registered. For *B. prostrata* population from the Thracian lowland and for the *S. perennans* and *S. soda* populations from the Southern Black Sea coast diploid chromosome number 2*n* = 18 was reported. The chromosome numbers known from literature data from the Bulgarian populations of two species (*Suaeda heterophylla* and *S. maritima*) were confirmed.

Grozeva (2015b) reported for the first time diploid chromosome number 2*n* = 16 for a *Petrosimonia brachiata* population from the Southern Black Sea coast and confirmed the chromosome number known from Bulgarian populations of *Blitum virgatum*, *Chenopodium album subsp. pedunculare*, *C. probstii*, *C. pratericola*, *Salicornia europaea* subsp. *europaea*, *Suaeda altissima*, *S. maritima*. Data about the karyotype of the species from genus *Bassia* (*B. hirsuta*, *B. laniflora*, *B. prostrata*, and *B. scoparia*) was published (Grozeva and Gospodinova 2016).

The karyological variability was traced and the karyotype of *Blitum virgatum* (Grozeva and Cvetanova 2016), of the species from genus *Salsola* (Grozeva et al. 2018) and genus *Atriplex* (Grozeva 2018a) was established.

Grozeva and Atanassova (2019) studied the karyotype of *Chenopodiastrum murale* and *Ch. hybridum* from their Bulgarian populations. Grozeva et al. (2019b) established diploid chromosome number 2*n* = 16 and described the karyotype of *Petrosimonia brachiata* from populations of the species from the Southern Black Sea coast. Diploid chromosome number 2*n* = 18 and data about the karyotype of *Oxybasis chenopodioides*, *O. glauca* and *O. urbica* were reported (Grozeva et al. 2019b).

For the members of family Chenopodiaceae from their Bulgarian populations diploid ($2n$ = 16, 18), tetraploid ($2n$ = 32, 36) and hexaploid ($2n$ = 54) chromosome numbers and two types of chromosomes – metacentric and submetacentric – were found (Grozeva 2018b). Basic chromosome numbers x = 9 and x = 8 were registered with the diploid ones being the dominant, followed by tetraploid and hexaploid species (Grozeva 2018b). According to data by Petrova and Vladimirov (2020), 80.4% of the Chenopodiaceae species have been studied karyologically. The data about the chromosome number of the studied species has been systematized in Chromosome atlas of the Bulgarian vascular plants (Petrova and Vladimirov 2020).

The karyological review showed that until 2021 data about the chromosome number and the karyotype of *Beta vulgaris* subsp. *maritima*, *Camphorosma annua*, *C. monspeliaca*, *Ceratocarpus arenarius*, *Halimione pedunculata*, *H. portucaloides*, *Polycnemum arvense*, *P. heuffelii*, *P. majus*, and *Spinacia oleracea* from their Bulgarian populations was lacking.

Phytochemical studies of Chenopodiaceae in Bulgaria

According to the Medicinal Plants Act (2000), 11 species of Chenopodiaceae are considered as medicinal plants: *Atriplex rosea*, *Blitum bonus-henricus*, *B. virgatum*, *Camphorosma monspeliaca*, *Chenopodium album* subsp. *album*, *C. vulvaria*, *Dysphania botrys*, *Lipandra polysperma*, *Oxybasis rubra*, *Salicornia europaea*, *Salsola tragus*.

Data on the phytochemical composition of medicinal plants of the family Chenopodiaceae so far are known from the Bulgarian populations of two species, i.e. *B. bonus-henricus* and *B. virgatum*.

The phytochemical investigations of genus *Chenopodium* revealed many compounds with a vast variety of structural patterns. The chenopods contained minerals, primary metabolites- carbohydrates, amino acids, nonpolar constituents, proteins, aromatic cytokinins, hormones and secondary metabolites – flavonoids, saponins, terpenes, sterols, alkaloids and vitamins (Nedialkov and Kokanova-Nedialkova 2020).

The aerial parts of *Blitum*. *bonus-henricus* are a rich source of bioactive compounds. Among them thirty-six compounds were distinguished including twenty-two saponins of eight sapogenins (phytolaccagenin, bayogenin, medicagenic acid, 2β-hydroxygypsogenin, 2β-hydroxyoleanoic acid, 2-hydroxy-30-nor-gypsogenin, 2-hydroxyakebonic acid and akebonic acid), twelve flavonoid glycosides of 6-methoxykaempferol, isorhamnetin, patuletin, spinacetin and two ecdysteroids (20-hydroxyecdysone and polypodine B). It was reported that glycosides of spinacetin and patulenin were the predominant compounds in the aerial parts of *C. bonus-henricus* (Kokanova-Nedialkova et al. 2020; Kokanova-Nedialkova and Nedialkov 2021). The occurrence of sapogenins 2-hydroxy-30-nor-gypsogenin, 2-hydroxyakebonic acid, and akebonic acids was also detected. The flavonoid and saponin-rich fractions showed in vitro hepatoprotective and antioxidant activity comparable to those of flavonoid complex silymarin (60 μg/mL) in a model of metabolic bioactivation, induced by CCl4. (Kokanova-Nedialkova et al. 2020). Nine

flavonol glycosides of patuletin, 6-methoxykaempferol and spinacetin were reported to reduce lipid damage, showed antioxidant activity, neuroprotective, anti-α-glucosidase, and lipase activities and possessed no toxic on the HepG2 cell line (Kokanova-Nedialkova and Nedialkov 2021). *B. bonus-henricus* possessed emollient, laxative, anthelmintic, antianemic and vermifuge properties. It is used also as expectorant and for the treatment of inflammated wounds (Kokanova-Nedialkova et al. 2016; Kokanova-Nedialkova et al. 2009). The MeOH extract (60 μg/ml) of the aerial parts of *C. bonus-henricus* showed hepatoprotective and antioxidant activities comparable to those of flavonoid complex silymarin in an in vitro model of metabolic bioactivation, induced by tetrachloromethane. Along with the decreased MDA quantity and increased level of GSH, seven days pre-treatment of rats with the MeOH extract (100 mg/kg/daily) also prevented the tetrachloromethane-caused oxidative damage by increasing antioxidant enzyme activities (CAT, SOD, GPx, GR and GST) (Kokanova-Nedialkova et al. 2016). Extracts from roots of *C. bonus-henricus* L. radix showed radical scavenging activity evaluated by DPPH assay as IC50 was above 200 μg/ml (Nikolova et al. 2011).Moreover, ecdysteroids (especially 20-hydroxyecdysone, derivatives of makisterone A and polypodine B), triterpene saponins (3-O-**β-D**-glucopyranosyl-phytolaccagenin-28-**α-L**-arabinopyranosyl ester, 3-O-**β**-glucuronopyranosyl-bayogenin-28-O-**β**-glucopyranosyl ester, 3-O-**β**-glucopyranosyl-bayogenin-28-**α-L**-arabinopyranosyl ester, 3-O-**β**-glucuronopyranosyl-medicagenic acid-28-**β**-xylopyranosyl(1→4)-**α**-rhamnopyranosyl(1→2)-**α**-arabinopyranosyl ester), 6-methoxyflavonol glycosides(6-methoxykaempferol 3-O-[β-apiofuranosyl(1→2)]-β-glucopyranosyl(1→6)-β-glucopyranoside), flavonoid glycosides (spinacetin 3-O-[β-apiofuranosyl(1→2)]-β-glucopyranosyl(1→6)-β-glucopyranoside and spinacetin 3-O-gentiobioside) were found in the roots of *B. bonus-henricus* (Kokanova-Nedialkova et al. 2009; Kokanova-Nedialkova et al. 2013; Kokanova-Nedialkova et al. 2015). Spinacetin 3-O-gentiobioside possessed stronger DPPH and ABTS radical scavenging activity (IC_{50} 0.44± 0.008 mM and 0.089 ± 0.002 mM) (Kokanova-Nedialkova et al. 2015). Fifteen saponins of six sapogenins were identified in roots of this plant, as saponins bonushenricoside A, 3-O-β-D-glucuronopyranosylbayogenin-28-O-β-D-glucopyranosyl ester, 3-O-β-Dglucuronopyranosyl-medicagenic acid-28-O-β-D-xylopyranosyl (1 → 4)-α-L-rhamnopyranosyl(1 → 2)- α-Larabinopyranosyl ester, 3-O-β-D-glucuronopyranosyl2β-hydroxygypsogenin-28-O-β-D-glucopyranosyl ester (4), 3-O-α-L-rabinopyranosyl-bayogenin-28-O-β-Dglucopyranosyl ester and bonushenricoside B deminstrateds possessed antioxidant and hepatoprotective effect (Kokanova-Nedialkova et al. 2019). Due to their root bioactive compounds infusions from them were used for the treatment of bronchitis, laryngitis, rheumatism, gout, constipation, dermatitis, eczema (Kokanova-Nedialkova et al. 2013). Moreover, the hepatoprotective activity of MeOH extracts from the roots of *C. bonus-henricus* as reported (Kokanova-Nedialkova et al. 2013). The glycosides of phytolaccagenin, bayogenin, medicagenic acid, 2β-hydroxygypsogenin, 2β-hydroxyoleanoic acid and oleanoic acid are a promising and safe class of hepatoprotective agents (Kokanova-Nedialkova et al. 2019). In plant material of *B. bonus-henricus* also sterols and vitamins were detected, especially vitamin C (Kokanova-Nedialkova et al. 2009).

Preliminary phytochemical screening of the aerial parts of *Blitum virgatum* shows the presence of carbohydrates, flavonoids, phytosterols, saponins and alkaloids/amins. Moisture content (6.05%) and total ash (12.19%) of aerial parts were also determined (Kokanova-Nedialkova et al. 2014a). The main secondary metabolites found in *B.virgatum* were terpenes (Kokanova-Nedialkova et al. 2009). This group of monocyclic hydrocarbon monoterpenoids includes limonene, α-terpinene and its γ-isomer, α-terpinolen, β-phellandrene and three related derivatives that were found in this plant. It contains also aromatic monoterpenoid p-cymene, carvacrol, tymol, α-pinene and β-pinene, camphor and camphene, monocyclic sesquiterpenoids as β-caryophyllene (Kokanova-Nedialkova et al. 2009) and the oleanane triterpene 30-normedicagenic acid (Kokanova-Nedialkova et al. 2014b). The aerial parts of this plant also contain phenolic compounds. New flavonol glycosides were detected as 6-methoxy kaempferol-3-O-β-gentiobioside, gomphrenol-3-O-β-gentiobioside and gomphrenol-3-O-[6-O-(β-Dglucopyranosyl)-β-D-glucopyranoside], as well as the already known compounds patuletin-3-O-β-gentiobioside and spinacetin-3-O-β-gentiobioside. The decoction prepared from *C. foliosum* was evaluated as a potential source of flavonoids with a radical-scavenging activity. The highest radical-scavenging activity evaluated by DPPH and ABTS methods were patuletin-3-O-β-gentiobioside and 6-methoxykaempferol-3-O-βgentiobioside, which were comparable with those of classic antioxidant ascorbic acid (Kokanova-Nedialkova et al. 2014a). The new acylated flavonol triglycoside namely gomphrenol-3-O-(5'''-O-E-feruloyl)-β-D-apiofuranosyl-(1→2)[β-D-glucopyranosyl-(1→6)]-β-D-glucopyranoside was also identified in the aerial parts of the plant collected from Beglika, Western Rhodopes, Bulgaria. This compound demonstrated low activity radical scavenging activity evaluated by DPPH and ABTS radicals and lack of antioxidant activity evaluated FRAP assay and inhibition of lipid peroxidation (LP) in the linoleic acid system by the ferric thiocyanate method. However, in combination with CCl4, gomphrenol-3-O-(5'''-O-E-feruloyl)-β-D-apiofuranosyl-(1→2)[β-D-glucopyranosyl-(1→6)]-β-D-glucopyranoside reduced the damage caused by the hepatotoxic agent and preserved cell viability and GSH level, decreased LDH leakage and reduced lipid damage at the highest concentration (100 μg/mL) (Kokanova-Nedialkova et al. 2014b).

References

Act MP (2000) Darzhaven vestnik, 29/07.04, 2000. [in Bulgarian]

Akhani H, Edwards G, Roalson EH (2007) Diversification of the Old World Salsoleae s.l. (Chenopodiaceae): Molecular phylogenetic analysis of nuclear and chloroplast data sets and a revised classification. International Journal of Plant Sciences, 168(6): 931–956. https://doi.org/10.1086/518263

Andreev N (1992) Chenopodiaceae. In: Kozhuharov S (Ed.) Field Guide to the vascular plants in Bulgaria. Naouka & Izkoustvo, Sofia, 326–335. [in Bulgarian]

Assyov B, Petrova A, Dimitrov D, Vassilev R (2012) Conspectus of the Bulgarian vascular flora. Distribution maps and floristic elements. Sofia. Bulgarian Biodiversity Foundation.

Assyov B, Petrova A [Eds] (2006) Conspectus of the Bulgarian vascular flora. Distribution maps and floristic elements. Bulgarian Biodiversity Foundation, Sofia.

Baev S (1947) Botanical Outings. Bulgarian Academy Press. [in Bulgarian]

Biological diversity act (2007) SG issue 77/2002; SG Issue No. 2001/200 94/2007. http://chm.moew.government.bg/

Bornmüller JFN (1888) Beiträge zur Kenntnis der Flora des bulgarischen Küstenlandes. Botanisches Centralblatt 36: 152–153.

Cheshmedzhiev IV (1976) Reports. In: Löve Á (Ed.) IOPB chromosome number reports LIV. Taxon 25(5/6): 642–643 (631–649). https://doi.org/10.1002/j.1996-8175.1976.tb03496.x

Cheshmedzhiev I (1988) New materials and chorological data for the flora of Bulgaria. Fitologiya 35: 58–63. [in Bulgarian]

Davidov B (1904) Contribution of the investigation to the Shumen district. Sborn. Nar. Umotv. Nauka Knizhn. 20: 1–54 (in Bulgarian).

Davidov B (1905) Contribution to the investigation of the flora of Varna district. Sborn. Nar. Umotv. Nauka Knizhn. 21: 1–73. [in Bulgarian]

Davidov B (1905) Contribution to the study of the flora of Varna county. Compendium of Folk Minds, Science and Paper 21: 1–73.

Delipavlov DD, Cheshmedzhiev IV (1984) New data and critical notes on the Bulgarian flora. Fitologiia 26: 60–68. https://agris.fao.org/agris-search/search.do?recordID=US201302011527

Delipavlov D, Cheshmedzhiev I (2011) Key to the Plants in Bulgaria. Agrarian University Academy Press, Plovdiv. [in Bulgarian]

Delipavlov D, Dimitrov S (1973) Beitrag zum Studium der Flora Bulgariens. Feddes Repertorium 83(7-8): 489–493. https://doi.org/10.1002/fedr.19730830704

Directive 92/43/EEC (1992) Directive 92/43/EEC. http://www.biodiversity.bg/

Fuentes-Bazan S, Uotila P, Borsch T (2012) A novel phylogeny-based generic classification for Chenopodium sensu lato, and a tribal rearrangement of Chenopodioideae (Chenopodiaceae). Willdenowia 42: 5–24. https://doi.org/10.3372/wi.42.42101

Georgiev S (1889) Materials for the flora of south Bulgaria (Trakia). Sborn Nar Umotv Naouka Knizhn 1: 22–24. [in Bulgarian]

Grozeva N (2004) Family Chenopodiaceae plants with conservation value. Journal of Balkan Ecology 7(2): 125–134.

Grozeva N (2005) The Flora of Atanasovsko Lake Natural Reserve. In: Gruev P, Nikolova M, Donev A (Eds) Proceedings of the Balkan scientific conference of biology, Plovdiv, Bulgaria, 19–21 May 2005: 381–396. [CD-format]

Grozeva N (2007a) *Chenopodium pumilio* (Chenopodiaceae): A new species to the Bulgarian flora. Phytologia Balcanica 13(3): 331–334.

Grozeva N (2007b) Reports (1623–1630) In: Kamari G, Felber F, Garbari F (Eds) Mediterranean chromosome number reports –17, Flora Mediterranea 17: 299–307.

Grozeva N (2009) Variation and evolutionary trends of genus *Chenopodium* L. (Goosefoots) in Bulgaria. Ph.D. thesis, Institute of Botany, BAS, Bulgaria.

Grozeva N (2010a) Reports (1709–1714) In: Kamari G, Blanché C, Siljak-Yakovlev S (Eds) Mediterranean chromosome number reports –20. Flora Mediterranea 20: 260–265.

Grozeva N (2010b) Reports (1715–1721) In: Kamari G, Blanché C, Siljak-Yakovlev S (Eds) Mediterranean chromosome number reports –20. Flora Mediterranea 20: 266–272.

Grozeva N (2011) *Chenopodium bonus-henricus* L. (Perennial Goosegoot) in Bulgaria: II. Morphology, chorology and ecology. Trakia Journal of Sciences 9(3): 8–12.

Grozeva N (2012a) *Chenopodium pratericola* (Chenopodiaceae): A new alien species for the Bulgarian flora. Phytologia Balcanica 18(2): 121–126.

Grozeva N (2012b) Reports (1763–1758). In: Kamari G, Blanché C, Siljak-Yakovlev S (Eds) Mediterranean chromosome number reports –22. Flora Mediterranea 22: 226–231. https://doi.org/10.7320/FlMedit22.211

Grozeva N (2013) IAOP/IOPB Chromosome data 16. In: Marhold K (Ed.) IAOP/IOPB column. Taxon 62(3): 1356, E2–E4. https://doi.org/10.12705/626.41

Grozeva N (2014) A comparative morphological characteristics of *Chenopodium album* L., *C. missouriense* Aellen and *C. probstii* Aellen. Turkish Journal of Agricultural and Natural Sciences 2: 1949–1954.

Grozeva N (2015a) Reports (1852–1858). In: Kamari G, Blanche C, Siljak-Yakovlev S (Eds) Mediterranean chromosome number reports – 25. Flora Mediterranea 25: 150–156. https://doi.org/10.7320/FlMedit25.143

Grozeva N (2015b) Reports. In: Marhold K (Ed.) IAPT/IOPB chromosome data 19. Taxon 64(5): 1071, E1–E21. https://doi.org/10.12705/645.34

Grozeva NH (2018a) Karyological study of genus *Atriplex* L. in Bulgaria. Bulgarian Journal of Agricultural Science 24(1): 52–58.

Grozeva NH (2018b) Karyological and morphological studies of Chenopodiaceae family in Bulgaria. DSc thesis. Trakia University (Bulgaria).

Grozeva N, Atanassova S (2019) Karyology of the *Chenopodiastrum* s. Fuentes et al. (Amaranthaceae) from Bulgaria. Bulgarian Journal of Agricultural Science 25(Suppl 3): 131–135.

Grozeva N, Cvetanova Y (2008) Variability among the populations of two *Chenopodium* genus species. Proceedings 7 Scientific Conference of Ekology and Health, Academic Publishing House of Agrarian University. Plovdiv (Vol. 135140). Bulgaria.

Grozeva N, Cvetanova Y (2011) *Chenopodium bonus-henricus* L. (Perennial Goosefoot) in Bulgaria: I. Population variability. Trakia Journal of Sciences 9(3): 1–7.

Grozeva N, Cvetanova Y (2013) Karyological and morphological variations within the genus *Dysphania* (Chenopodiaceae) in Bulgaria. Acta Botanica Croatica 72(1): 49–69. https://doi.org/10.2478/v10184–012-0017-5

Grozeva N, Cvetanova Y (2016) Karyological and morphological variations within *Blitum virgatum* L. Trakia Journal of Sciences 1(1): 16–23. https://doi.org/10.15547/tjs.2016.01.002

Grozeva N, Gospodinova S (2016) Karyological study of genus *Bassia* All. in Bulgaria. Trakia Journal of Sciences 2(2): 158–162. https://doi.org/10.15547/tjs.2016.02.007

Grozeva N, Stoeva M (2006) Reports (1456–1462) In: Kamari G, Felber F, Garbari F (Eds) Mediterranean chromosome number reports – 16. Flora Mediterranea 16: 400–408.

Grozeva N, Todorova M (2014) Karyological and morphological variations within *Bassia hirsuta* (L.) Asch. in Bulgaria. Trakya University Journal of Natural Sciences 15(1): 17–23. https://dergipark.org.tr/en/pub/trkjnat/issue/25382/267872

Grozeva N, Miteva Ch, Ivanov P, Videv V (2004) Flora of Atanasovsko Lake Natural Reserve presented through Web-based information system. Journal of Balkan Ecology 7(4): 362–373.

Grozeva N, Terzieva S, Gerdzhikova M, Pavlov D (2018) Chromosome and pollen morphology of *Salsola soda* L. and *Salsola tragus* L. in Bulgaria. Bulgarian Journal of Agricultural Science 24(1): 59–67.

Grozeva N, Todorova M, Pavlov D (2019a) Karyological and morphological variation within *Petrosimonia brachiata* Bunge in Bulgaria. Botanica Serbica 43(1): 13–21. https://doi.org/10.2298/BOTSERB1901013G

Grozeva N, Atanassova S, Terzieva S (2019b) Karyological study of genus *Oxybasis* Kar. & Kir. in Bulgaria. Bulgarian Journal of Agricultural Science 25(Suppl. 3): 124–130.

Iamonico D (2014) Taxonomical, morphological, ecological and chorological notes on *Oxybasis chenopodioides* and *O. rubra* (Chenopodiaceae) in Italy. Hacquetia 13(2): 297–302. https://doi.org/10.2478/hacq-2014-0005

Iamonico D (2019) Remarks on the subfam. Betoideae (Chenopodiaceae/Amaranthaceae sensu APGIV). Phytotaxa 400(3): 145–164. https://doi.org/10.11646/phytotaxa.400.3.3

Ilyin MM (1936) Chenopodiaceae. In: Komarova VL (Ed.) Flora USSR. USSR, 2–354.

Kadereit G, Borsch T, Weising K, Freitag H (2003) Phylogeny of Amaranthaceae and Chenopodiaceae and the evolution of C4 photosynthesis. International Journal of Plant Sciences 164(6): 959–986. https://doi.org/10.1086/378649

Kadereit G, Mavrodiev EV, Zacharias EH, Sukhorukov AP (2010) Molecular phylogeny of Atripliceae (Chenopodioideae, Chenopodiaceae): Implications for systematics, biogeography, flower and fruit evolution, and the origin of C4 photosynthesis. American Journal of Botany 97(10): 1664–1687. https://doi.org/10.3732/ajb.1000169

Kadereit G, Piirainen M, Lambinon J, Vanderpoorten A (2018) Cryptic taxa should have names: Reflections in the glasswort genus Salicornia (Amaranthaceae), TAXON International Journal of Taxonomy, Phylogeny and Evolution, Taxon 61: 1227–1239. https://doi.org/10.1002/tax.616005

Kiryakov K, Dimitrov S, Delipavlov D (1951) Contribution to the investigation of the medicinal vegetation of the Central Stara Planina Mt (Boroushtitsa – peak Balvan). Godishnik na Darzavnia Univeristet v Plovdiv, Agronomicheski Fakultet 5: 1949–1950, 295–326. [in Bulgarian]

Kokanova-Nedialkova Z, Nedialkov PT, Nikolov SD (2009) The genus *Chenopodium*: Phytochemistry, ethnopharmacology, and pharmacology. Pharmacognosy Reviews 3: 280–306.

Kokanova-Nedialkova Z, Simeonova R, Kondeva-Burdina M, Nikolov S, Heilmann J, Nedialkov P (2013) Triterpene saponins from *Chenopodium bonus-henricus* roots. Planta Medica 79(13): PI57. https://doi.org/10.1055/s-0033-1352146

Kokanova-Nedialkova Z, Nedialkov PT, Nikolov SD (2014a) Pharmacognostic investigations of the aerial parts of *Chenopodium foliosum* Asch. and radical-scavenging activities of five flavonoids isolated from methanol extract of the plant. Pharmacognosy Journal 6(4): 43–48. https://doi.org/10.5530/pj.2014.4.6

Kokanova-Nedialkova Z, Kondeva-Burdina M, Zheleva-Dimitrova D, Bücherl D, Nikolov S, Heilmann J, Nedialkov PT (2014b) A new acylated flavonol glycoside from *Chenopodium foliosum*. Records of Natural Products 8(4): 401–406.

Kokanova-Nedialkova Z, Kondeva-Burdina M, Zheleva-Dimitrova D, Tzankova V, Nikolov S, Heilmann J, Nedialkov PT (2015) 6-Methoxyflavonol glycosides with in vitro hepatoprotective activity from *Chenopodium bonus-henricus* roots. Natural product communications 10(8): e1934578X1501000816. https://doi.org/10.1055/s-0035-1565573

Kokanova-Nedialkova Z, Nedialkov P, Kondeva-Burdina M, Simenova R, Tsankova V, Nikolov S (2016) Good king-henry (*Chenopodium bonus-henricus* L.) – a source of hepatoprotective flavonoids. Planta Medica 82(S01): P840. https://doi.org/10.1055/s-0036-1596856

Kokanova-Nedialkova Z, Nedialkov PT, Momekov G (2019) Saponins from the roots of *Chenopodium bonus-henricus* L. Natural Product Research 33(14): 2024–2031. https://doi.org/10.1080/14786419.2018.1483928

Kokanova-Nedialkova Z, Kondeva-Burdina M, Nedialkov PT (2020) Neuroprotective, anti-α-glucosidase and prolipase active flavonoids from Good King Henry (*Chenopodium bonus-henricus* L.). Natural Product Research: 1–5. https://doi.org/10.1080/14786419.2020.1784172

Kokanova-Nedialkova Z, Nedialkov P (2021) Validated UHPLC-HRMS method for simultaneous quantification of flavonoid contents in the aerial parts of *Chenopodium bonus-henricus* L. (wild spinach). Pharmacia 68: e597. https://doi.org/10.3897/pharmacia.68.e69781

Kolev ID (1956) Investigation of weed dissemination on the Sofia plain. Vissh Selskostopanski Inst. "Georgi Dimitrov". Agron. Fakul. Nauch. Trudove 3: 139–173. [in Bulgarian]

Kolev I (1959) Floristic notes. Vissh Selskostopanski Inst. "Georgi Dimitrov". Agronomicheski Fakultet Nauchni Trudove 6: 413–421. [in Bulgarian]

Kovachev V (1903) Addition to the Flora of the Region of Rouse. Periodichesko Spisanie na Bulkgarskoto Knizhovno Drouzhestvo v Sofia 63: 721–723.

Kožuharov S, Kuzmanov B (1969) Chromosome numbers of flowering plants in Bulgaria. 2. Izv. Bot. Inst. (Sofia) 19: 109–115.

Kühn U, Bittrich V, Carolin R, Freitag H, Hedge IC, Uotila P, Wilson PG (1993) Chenopodiaceae. In: Kubitzki K, Rohwer JG, Bittrich V (Eds) Flowering Plants Dicotyledons. The Families and Genera of Vascular Plants vol 2. Springer, Berlin, Heidelberg. https://doi.org/10.1007/978-3-662-02899-5_26

Markova M (1968) Karyological study of *Epimedium pubigerum* (DC) Morren and Decne and *Chenopodium multifidum* L. Comptes Rendus de lAcademie Bulgare des Sciences 21: 51–53.

Masson R, Kadereit G (2013) Phylogeny of Polycnemoideae (Amaranthaceae): Implications for biogeography, character evolution and taxonomy. Taxon 62(1): 100–111. https://doi.org/10.1002/tax.621009

Meshinev T, Velchev V, Apostolova I, Vasilev V (1994) Flora and vegetation on the sand dunes in the area of the tourist complex Sunny Beach. Institute of Botany, Sofia, 64 pp. [with map]

Michev T, et al. (2003) Management of the Maintained Reserve "Atanasovsko Lake". BSPOBZ. MOEW, Bulgaria.

Mosyakin SL (2018) Notes on taxonomy and nomenclature of *Chenopodium acerifolium* and *C. betaceum* (*C. strictum* auct.) (Chenopodiaceae). Phytotaxa 324(2): 139–154. https://doi.org/10.11646/phytotaxa.324.2.3

Nedialkov PT, Kokanova-Nedialkova Z (2020) Bioactive Compounds of Goosefoot (Genus *Chenopodium*). In: Murthy HN, Paek KY (Eds) Bioactive Compounds in Underutilized Vegetables and Legumes. Reference Series in Phytochemistry. Springer, Cham, 1–24. https://doi.org/10.1007/978-3-030-44578-2_7-1

Neichev I (1905) About the flora of Sevlievo and Gabrovo. Trav Soc Bulg Sci Nat 4–8: 56–58. [in Bulgarian]

Nikolova M, Evstatieva L, Nguyen TD (2011) Screening of plant extracts for antioxidant properties. Botanica Serbica 35(1): 43–48. https://botanicaserbica.bio.bg.ac.rs/arhiva/pdf/2011_35_1_529_full.pdf

Panov P (1975) Floristic materials and critical notes. iI. Fitologiia 1: 88–96. [in Bulgarian]

Panov P (1987) Newly registered plants for the flora of Bulgaria. In: Kuzmanov B (Ed.) Works of the Fourth National Conference on Botany (Sofia). item 1: 103–107.

Peev D, et al. [Eds] (2015) Red Book of the Republic of Bulgaria. item 1. Plants and Fungi. BAS, Ministry of Environment and Water. Sofia, Bulgaria.

Petkov St (1907) Contribution to the flora of the southern corner of the Bulgarian Black Sea coast. Periodic journal of the Bulgarian Literary Society (Sofia) 17(2): 17–18.

Petrova A, Vladimirov V (2020) Chromosome atlas of the Bulgarian vascular plants. Phytologia Balcanica: International Journal of Balkan Flora and Vegetation 26(2): 217–427.

Philipova-Marinova M, Ivanov D, Dimitrov D (1997) Flora and vegetation in the region of Shabla-Lake Lakes and adjacent territories, BSPB report. Sofia, Bulgaria.

Popova M, Ceschmedjiev I (1978) Reports. In: Löve Å (Ed.) IOPB chromosome number reports LXI. Taxon 27: 375–392. https://doi.org/10.1002/j.1996-8175.1978.tb04261.x

Rechinger K (1933) Ergebnisse einer botanischen Reise nach Bulgarien. Mag. Bot. Lap. 33: e48. https://doi.org/10.1002/fedr.4870332702

Stefanov B (1943) Phyto-geographic elements of Bulgaria. In: Symposium of Bulgarian Academy of Science and art., Branch nature and math N°19: b. XXIX.

Stoyanov D (2009) Integrated management plan for protected area "Pomorie Lake" (Bg0000152) under the Pomorie Protected Area Directive (Bg0000620) under the Habitats Directive "Pomorie Lake" and Ramsarsko Place "Pomorie Lake".

Stoyanov N, Stefanov B (1924) Flora of Bulgaria. Ed. 1., item 1, Science and Art. Sofia, Bulgaria.

Stoyanov N, Stefanov B (1933) Flora of Bulgaria. Ed. 2, Ed. Gutenberg. Sofia, Bulgaria.

Stoyanov N, Stefanov B (1948) Flora of Bulgaria. Ed. 3, Univ. Ed. Sofia, Bulgaria.

Stoyanov N, Kitanov B, Velchev V (1954) Plants fasteners of erosion terrains in the arda river basin. Nature 1: 20–23.

Stoyanov N, Stefanov B, Kitanov B (1966) Flora of Bulgaria. Ed. 4, vol. 1. Nauka & Izkustvo, Sofia. [in Bulgarian]

Stranski I (1921) Contribution à la flore des Rhodopes centrales. Dokladi na Bulgarskata Akademiâ na Naukite 16: 3–147. [in Bulgarian]

Todorova M, Grozeva N, Pleskuza L, Yaneva Z, Gerdgikova M (2014) Relationship between soil salinity and *Bassia hirsuta*, *Salicornia europaea* agg. and *Petrosimonia brachyata* distribution on the territory of Pomorie lake and Atanasovsko lake. Agricultural Science and Technology 6(4): 465–470.

Toshev A (1895) Materials on the flora of Bulgaria. Periodichno spisanie na balgarskoto knizhovno druzhestvo 49–50: 329–356. [In Bulgarian]

Tzonev R, Gussev C (2015) Communities of annual halophytes in coastal salt marshes at the Black Sea. Red data book of the Republic of Bulgaria 3: 49–50.

Tzonev R, Lysenko T, Gussev C, Zhelev P (2008) The halophytic vegetation in South-East Bulgaria and along the Black Sea coast. Bioloski Institut Jovana Hadzija. Hacquetia 7(2): 95–121. https://doi.org/10.2478/v10028-008-0006-3

Uotila P (2011) Chenopodiaceae (pro parte majore). In: Euro+ Med Plantbase-the information resource for Euro-Mediterranean plant diversity. Euro+ med plantbase.

Urumov I (1897) Materials on the flora of Lovech district. Sborn. Nar. Umotv. Naouka Knizhn. 14: 3–85. [in Bulgarian]

Urumov I (1901) A contribution to the Bulgarian flora. Sborn. Nar. Umotv. Naouka Knizhn. 18: 1–124. [in Bulgarian]
Urumov I (1904) Third contribution to the Bulgarian flora. Sborn. Nar. Umotv. Naouka Knizhn. 20: 1–103. [in Bulgarian]
Urumov I (1905) Fifth contribution to the Bulgarian flora. Sborn. Nar. Umotv. Naouka Knizhn. 21: 1–125. [in Bulgarian]
Urumov I (1906) Sixth contribution to the Bulgarian flora. Sborn. Nar. Umotv. Naouka Knizhn. 22: 1–126. [in Bulgarian]
Urumov I (1908a) Seventh contribution to the Bulgarian flora. Sborn. Nar. Umotv. Naouka Knizhn. 24: 1–113. [in Bulgarian]
Urumov I (1908b) Eigth contribution to the Bulgarian flora. Period. Spis. Bulg. Knizh. Druzh. 69: 41–72. [in Bulgarian]
Urumov I (1908c) Ninth contribution to the Bulgarian flora. Sborn. Nar. Umotv. Naouka Knizhn. 24: 1–112. [in Bulgarian]
Urumov I (1909) Tenth contribution to the Bulgarian flora. Sborn. Nar. Umotv. Naouka Knizhn. 25: 1–159. [in Bulgarian]
Urumov I (1913) Twelfth contribution to the Bulgarian flora. Sborn. Bălg. Akad. Nauk. 3: 1–243. [in Bulgarian]
Urumov I (1917) Thirteenth contribution to the Bulgarian flora. Sborn. Bălg. Akad. Nauk. 7: 1–225. [in Bulgarian]
Urumov I (1923) Materials on the flora of the Pirin Mts. Sborn. Bălg. Akad. Nauk. 28: 1–163. [in Bulgarian]
Urumov I (1926) Fifteenth contribution to the Bulgarian flora. Spis. Bălg. Akad. Nauk. 22: 3–128. [in Bulgarian]
Urumov I (1928) Sixteenth contribution to the Bulgarian flora. Sborn. Bălg. Acad. Nauk. 23: 1–128. [in Bulgarian]
Urumov I (1929a) The flora of Mt Ljulin. Spis. Bălg. Akad. Nauk. 15: 1–117. [in Bulgarian]
Urumov I (1929b) List of the plants collected in the district of Karlovo. Sborn. Bălg. Akad. Nauk. 25: 6–135. [in Bulgarian]
Urumov I (1930) The flora of Mt Vitosha. Sborn. Bălg. Akad. Nauk. 26: 1–143. [in Bulgarian]
Urumov I (1935) The flora of Vratsa district. Sborn. Bălg. Akad. Nauk. 29: 1–205. [in Bulgarian]
Van Loon I, Van Setten A (1982) Reports. In: Löve A (Ed.) Chromosome number reports, LIX. Taxon 27: 56–60.
Velenovský J (1891) Flora bulgarica. Pragae.
Velenovský J (1898) Flora bulgarica Supplementum. Pragae.
Yavashev A (1890) Contribution to knowledge of the Bulgarian flora. Periodic journal of the Bulgarian Literary Society 27: 290–311.
Yordanov D (1923–1924) On the phytogeography of western Stara Planina. Yr. Cds. Univ. Fizz. Checkmate. Fak. 1: 71–102.
Yordanov D, Kozhuharov B, Markova M (1966) Chenopodiaceae. In: Yordanov D (Ed.) Flora of the People's Republic of Bulgaria 3: 527–576, Aedibus Academiae Scientiarum Bulgaricae, Serdicae (Bg).

BioRisk 18: 35–55 (2022)
doi: 10.3897/biorisk.18.76997
https://biorisk.pensoft.net

RESEARCH ARTICLE

A peer-reviewed open-access journal
BioRisk

Potential risk resulting from the influence of static magnetic field upon living organisms. Numerically simulated effects of the static magnetic field upon simple alkanols

Wojciech Ciesielski[1], Tomasz Girek[1], Zdzisław Oszczęda[2], Jacek A. Soroka[3], Piotr Tomasik[2]

1 *Institute of Chemistry, Jan Długosz University, 42–201 Częstochowa, Poland* **2** *Nantes Nanotechnological Systems, 59–700 Bolesławiec, Poland* **3** *Scientific Society of Szczecin, 71–481 Szczecin, Poland*

Corresponding author: Wojciech Ciesielski (w.ciesielski@interia.pl)

Academic editor: Josef Settele | Received 24 October 2021 | Accepted 3 April 2022 | Published 13 June 2022

Citation: Ciesielski W, Girek T, Oszczeda Z, Soroka JA, Tomasik P (2022) Potential risk resulting from the influence of static magnetic field upon living organisms. Numerically simulated effects of the static magnetic field upon simple alkanols. BioRisk 18: 35–55. https://doi.org/10.3897/biorisk.18.76997

Abstract

Background: Recognising effects of static magnetic field (SMF) of varying flux density on flora and fauna is attempted. For this purpose, the influence of static magnetic field upon molecules of lower alkanols i.e. methanol, ethanol, propan-1-ol, propan-2-ol, butan-1-ol, *S*-butan-2-ol, isobutanol and *tert*-butanol is studied.

Methods: Computations of the effect of real SMF 0.0, 0.1, 1, 10 and 100 AFU (Arbitrary Field Unit; here 1AFU > 1000 T) flux density were performed in silico (computer vacuum), involving advanced computational methods.

Results: SMF polarises molecules depending on applied flux density, but it neither ionises nor breaks valence bonds. Some irregularities in the changes of positive and negative charge densities and bond lengths provide evidence that molecules slightly change their initially fixed positions with respect to the force lines of the magnetic field. Length of some bonds and bond angles change with an increase in the applied flux density, providing, in some cases, polar interactions between atoms through space.

Conclusions: Since SMF produced and increase in the negative charge density at the oxygen atom of the hydroxyl group and elongated the –O-H bond length, these results show that SMF facilitates metabolism of the alkanols.

Keywords
Butanols, ethanol, methanol, organisms, propanols, static magnetic field

Introduction

Modern technologies and technical solutions in several areas of our everyday life result in considerable environmental pollution with magnetic fields (Hamza et al. 2002; Rankovic and Radulovic 2009; Committee to Assess the Current Status and Future Direction of High Magnetic Field Science in the United States 2013; Bao and Guo 2021; Tang et al. 2021). Recent studies showed an eminent effect of the static magnetic field (SMF) upon various micro-organisms, also on the colonising organisms of flora and fauna (Jaworska et al. 2014; Jaworska et al. 2016; Jaworska et al. 2017; Beretta et al. 2019). Numerous studies of the origin and mechanisms of observed effects pointed to a generation of free radicals which could interact with biological systems (Steiner and Ulrich 1989; Kohno et al. 2000; Woodward 2002; Buchachenko 2009; Buchachenko et al. 2012; Buchachenko 2014). The role of metal ions was also taken under consideration (Andreini et al. 2008; Rittie and Perbal 2008; Buchachenko 2016; Letuta and Berdinskiy 2017). It was found that SMF polarised molecules depending on the applied flux density, but causes neither ionisation nor breaking valence bonds of those molecules (Ciesielski et al. 2021).

Our former preliminary studies on the effect of SMF-treated water upon entomopathogenic organisms (Jaworska et al. 2017) and on functional properties of selected cosmetics (Zamiatała et al. 2013) suggest a necessity of an insight into the role of SMF in a modification of the molecular structure of simple molecules and interaction taking place in their combinations. For that purpose, numerical simulations of the real effect SMF of 0.0, 0.1, 1, 10 and 100 T were performed in a computer vacuum for single and grouped-in-three molecules of oxygen, nitrogen, water, carbon dioxide, ammonia and methane. Additionally, in this paper, T (Tesla) values were employed as commonly accepted units of the SMF flux density. However, since the response of the applied computational programme to the magnitudes of applied flux density remained unknown, the flux densities were expressed in terms of Arbitrary Field Units (AFU).

Organisms belonging to flora and fauna contain, amongst others, compounds bearing the hydroxyl groups bound to the sp^3 carbon atoms. They are alcohols. These in the flora organisms spread into sugar alcohols (Lewis and Smith 1967), fatty alcohols (Rowland and Domerque 2012) and steroid alcohols (Dinan et al. 2001). Similar types of alcohols reside in the fauna including human organisms.

Under normal conditions in the human organism, up to 0.15 ppm of so-called physiological ethanol is formed mainly through fatty acid synthesis, glycerolipid metabolism and bile acid biosynthesis pathways (Woronowicz 2003; Wade 2021).

In this paper, the effect of SMF of flux density from 0 to 100 AFU is recognised upon simple primary, secondary and tertiary C_1 to C_4 alkanols as the model compounds for the alcohols of more complex structure residing in the flora and fauna organisms. For this purpose, advanced numerical simulations of the effect were employed.

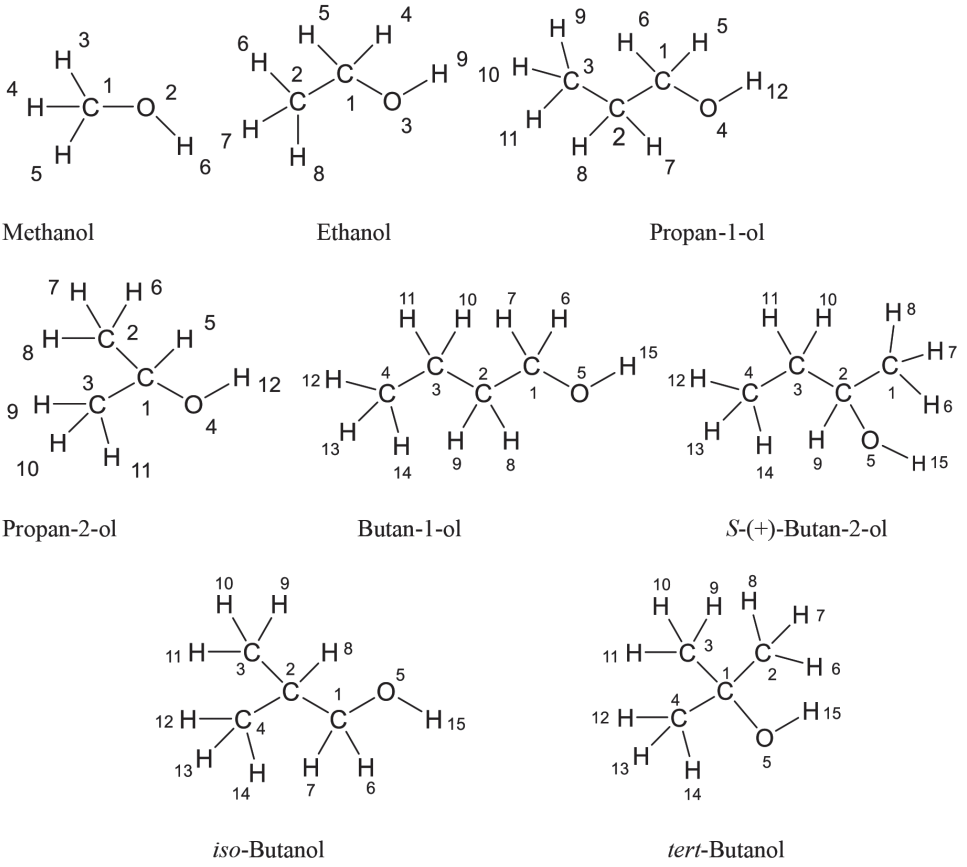

Figure 1. Alkanols under consideration and applied numbering of atoms in particular molecules.

Numerical computations

Molecular structures were drawn using the Fujitsu SCIGRESS 2.0 software (Froimowitz 1993; Marchand et al. 2014,). Their principal symmetry axes were orientated along the x-axis of the Cartesian system. Molecules of alcohols were situated inside of a three-axial elypsoid. The longest axis of that elypsoid was accepted as the x-axis and the shortest quasi-perpendicular axis considered as the z-axis. The magnetic field was fixed in the same direction, along the x-axis with the south pole from the left side. Thus, the methanol molecule was so orientated along its C-O bond and the remaining alcohols along their longest carbon chain. The magnetic field was fixed in the same direction with the south pole from the left side. Subsequently, involving Gaussian 0.9 software equipped with the 6-31G** basis (Frisch et al. 2016), the molecules were optimised and all values of bond length, dipole moment, heath of formation, bond energy and total energy for systems were computed.

In the consecutive steps, the influences of the static magnetic field (SMF) upon optimised molecules were computed with Amsterdam Modelling Suite software (Farberovich

and Mazalova 2016; Charistos and Muñoz-Castro 2019) and the NR_LDOTB (non-relativistically orbital momentum L-dot-B) method (Glendening et al. 1987; Carpenter and Weinhold 1988). Following that step, values of bond length, dipole moment, heath of formation equal to the energy of dissociation and charges at the atoms were calculated using Gaussian 0.9 software equipped with the 6-31G** basis (Marchand et al. 2014).

Results

Numerical simulations were performed for alkanols presented in Fig. 1.

Table 1 presents values of heat of formation and dipole moments for those alkanols placed in the SMF of flux density ranging from 0 (control sample) to 100 AFU.

Subsequent Tables contain computed values of charge density at particular atoms and bond lengths between atoms in methanol (Tables 2, 3), in ethanol (Tables 4, 5), in propan-1-ol (Tables 6, 7).

Table 1. Effect of SMF of increasing flux density upon heat of formation and dipole moment of alcohols.

Alcohol	Heat of formation [kJ·mol^{-1}] at SMF flux density [AFU]					Dipole moment [D] at SMF flux density [AFU]				
	0	0.1	1.0	10	100[a]	0	0.1	1.0	10	100[a]
Methanol	-201.8	-195.3	-158.2	-114.2	-103.5 (49%)	1.94	2.03	2.15	2.36	3.01 (55%)
Ethanol	-238.8	-230.5	-219.8	-203.5	-151.1 (37%)	1.81	1.83	1.90	2.11	2.68 (42%)
Propan-1-ol	-251.7	-248.6	-231.2	-205.6	-171.6 (32%)	1.87	1.89	1.99	2.18	2.38 (27%)
Propan-2-ol	-271.5	-270.6	-263.8	-249.2	-199.3 (27%)	1.92	1.95	1.99	2.08	2.22 (16%)
Butan-1-ol	-276.1	-271.1	-253.6	-214.3	-161.1 (42%)	1.79	1.83	1.99	2.07	2.25 (26%)
S-Butan-2-ol	-302.8	-298.5	-278.2	-264.5	-211.6 (30%)	2.10	2.13	2.26	2.48	2.79 (33%)
iso-butanol	-285.1	-283.3	-279.2	-263.4	-183.3 (36%)	1.98	2.03	2.09	2.18	2.32 (17%)
tert-Butanol	-312.7	-310.2	-281.6	-231.6	-184.7 (41%)	1.91	1.93	2.08	2.16	2.37 (25%)

[a]The final increase (in %) in the reported value at applied SMF of 100 AFU is given in parentheses.

Table 2. Distribution of the charge density [a.u.] at particular atoms of the methanol molecule depending on the applied SMF flux density [AFU].

Atom	Charge density [a.u.] at SMF flux density [AFU]					
	Tendency[b]	0	0.1	1.0	10	100
C1	V	-0.127	-0.105	-0.162	-0.137	-0.077
O2	RH	-0.739	-0.737	-0.688	-0.671	-0.610
H(3–5)	**V**	**0.156**	**0.146**	**0.161**	**0.151**	**0.120**
H6	V	0.398	0.404	0.367	0.355	0.326

[a]Data taken for drawing the average value for two or more either atoms or bonds are given in bold. [b]Abbreviations: RH – regularly increasing, RL - regularly decreasing, IH - irregularly increasing, IL - irregularly decreasing, V - lack of any regular tendency.

Table 3. Bond lengths [Å] in the methanol molecule depending on the applied SMF flux density [AFU].

Bond	Bond length [Å] at applied SMF flux density [AFU]					
	Tendency	0	0.1	1.0	10	100
C1-O2	IL	1.430	1.393	1.365	1.353	1.354
C1-H(3–5)	RH	1.090	1.167	1.178	1.213	1.328
O2-H6	IH	0.960	1.055	1.033	1.073	1.137

[a]See Table 2 for notation.

Table 4. Distribution of the charge density [a.u.] at particular atoms of the ethanol molecule depending on the applied SMF flux density [AFU].

Atom	Charge density [a.u.] at SMF flux density [AFU]					
	Tendency	0	0.1	1.0	10	100
C1	H	-0.079	-0.062	-0.024	0.053	0.196
C2	V	-0.662	-0.570	-0.548	-0.587	-0.550
O3	L	-0.684	-0.692	-0.702	-0.725	-0.753
H(4–5)	**L**	**0.181**	**0.176**	**0.158**	**0.120**	**0.051**
H(6–8)	**IL**	**0.210**	**0.197**	**0.190**	**0.187**	**0.190**
H9	H	0.374	0.381	0.390	0.407	0.434

[a]See Table 2 for notation.

Table 5. Bond lengths [Å] in the molecule of ethanol depending on the applied SMF flux density [AFU].

Bond	Bond length [Å] at applied SMF flux density [AFU]					
	Tendency	0	0.1	1.0	10	100
C1-C2	IL	1.540	1.520	1.500	1.495	1.528
C1-O3	L	1.430	1.418	1.394	1.389	1.252
C1-H(4–5)	**H**	**1.090**	**1.098**	**1.142**	**1.222**	**1.352**
C2-H(6–8)	**IH**	**1.090**	**1.143**	**1.171**	**1.178**	**1.155**
O3-H9	H	0.960	0.963	0.986	1.021	1.130

[a]See Table 2 for notation.

Table 6. Distribution of the charge density [a.u.] at particular atoms of the propan-1-ol molecule depending on the applied SMF flux density [AFU].

Atom	Charge density [a.u.] at SMF flux density [AFU]					
	Tendency	0	0.1	1.0	10	100
C1	IH	-0.047	-0.091	-0.015	0.155	0.129
C2	IL	-0.449	-0.441	-0.441	-0.411	-0.467
C3	IH	-0.594	-0.573	-0.567	-0.597	-0.483
O4	L	-0.687	-0.696	-0705	-0.733	-0.785
H(5–6)	**IL**	**0.178**	**0.176**	**0.172**	**0.088**	**0.169**
H(7–8)	**IL**	**0.223**	**0.215**	**0213**	**0.193**	**0.201**
H(9–11)	**L**	**0.201**	**0.192**	**0.191**	**0.183**	**0.159**
H12	H	0.373	0.378	0.386	0.415	0.438

[a]See Table 2 for notation.

Table 7. Bond lengths [Å] in the molecule of propan-1-ol depending on the applied SMF flux density [AFU].

Bond	Bond length [Å] at applied SMF flux density [AFU]					
	Tendency	0	0.1	1.0	10	100
C1-C2	IL	1.540	1.521	1.508	1.517	1.526
C2-C3	L	1.540	1.529	1.518	1.445	1.375
C3-O4	L	1.430	1.418	1.407	1.318	1.290
C1-H(5–6)	**H**	**1.075**	**1.088**	**1.093**	**1.299**	**1.161**
C2-H(7–8)	**IH**	**1.090**	**1.125**	**1.128**	**1.252**	**1.186**
C3-H(9–11)	**H**	**1.090**	**1.127**	**1.140**	**1.216**	**1.286**
O4-H12	H	0.960	0.962	0.968	1.061	1.102

[a]See Table 2 for notation.

In propan-2-ol (Tables 8, 9), in butan-1-ol (Tables 10, 11), in *S*-butan-2-ol (Tables 12, 13), in *iso*-butanol (Tables 14, 15) and in *tert*-butanol (Table 16, 17)

The visualisation of the shapes of those molecules at varying SMF flux density are presented in Figs 2–9.

Table 8. Distribution of the charge density [a.u.] at particular atoms of the propan-2-ol molecule depending on the applied SMF flux density [AFU].

Atom	Charge density [a.u.] at SMF flux density [AFU]					
	Tendency	0	0.1	1.0	10	100
C1	H	0.064	0.077	0.093	0.097	0.136
C(2–3)	**IH**	**-0.584**	**-0.542**	**-0.526**	**-0.537**	**-0.508**
O4	IH	-0.683	-0.686	-0.675	-0.672	-0.523
H5	V	0.191	0.177	0.170	0.182	0.174
H(6–8)	**L**	**0.208**	**0.190**	**0.190**	**0.175**	**0.171**
H(9–11)	**V**	**0.199**	**0.188**	**0.178**	**0.201**	**0.191**
H(6–8)&H(9–11)	**IL**	**0.203**	**0.189**	**0.184**	**0.188**	**0.181**
H12	IL	0.373	0.381	0.365	0.358	0.192

[a]See Table 2 for notation.

Table 9. Bond lengths [Å] in the molecule of propan-2-ol depending on the applied SMF flux density [AFU].

Bond	Bond length [Å] at applied SMF flux density [AFU]					
	Tendency	0	0.1	1.0	10	100
C1-C(2–3)	**V**	**1.540**	**1.577**	**1.514**	**1.518**	**1.391**
C1-O4	L	1.430	1.414	1.379	1.353	1.325
C1-H5	IH	1.090	1.142	1.164	1.152	1.189
C2-H(6–8)	**H**	**1.090**	**1.172**	**1.186**	**1.194**	**1.280**
C3-H(9–11)	**IH**	**1.090**	**1.139**	**1.171**	**1.188**	**1.142**
C2-H(6–8)&C3-H(9–11)	**H**	**1.090**	**1.155**	**1.179**	**1.191**	**1.211**
O4-H12	IH	0.960	0.925	1.045	1.084	1.610

[a]See Table 2 for notation.

Table 10. Distribution of the charge density [a.u.] at particular atoms of the butan-1-ol molecule depending on the applied SMF flux density [AFU].

Atom	Charge density [a.u.] at SMF flux density [AFU]					
	Tendency	0	0.1	1.0	10	100
C1	H	-0.050	-0.007	0.077	0.143	0.200
C2	V	-0.425	-0.399	-0.404	-0.390	-0.405
C3	V	-0.408	-0.396	-0.416	-0.393	-0.317
C4	V	-0.574	-0.500	-0.532	-0.506	-0.521
O5	L	-0.688	-0.699	-0.728	-0.766	-0.705
H(6–7)	**L**	**0.178**	**0.161**	**0.125**	**0.109**	**0.103**
H(8–9)		**0.221**	**0.205**	**0.204**	**0.191**	**0.175**
H(10–11)	**IL**	**0.204**	**0.183**	**0.191**	**0.172**	**0.124**
H(12–14)	**V**	**0.199**	**0.173**	**0.187**	**0.180**	**0.187**
H15	IL	0.372	0.382	0.404	0.427	0.386

[a]See Table 2 for notation.

Table 11. Bond lengths [Å] in the molecule of butan-1-ol depending on the applied SMF flux density [AFU].

Bond	Bond length [Å] at applied SMF flux density [AFU]					
	Tendency	0	0.1	1.0	10	100
C1-C2	V	1.540	1.516	1.512	1.536	1.576
C2-C3	L	1.540	1.529	1.504	1.448	1.378
C3-C4	IL	1.540	1510	1.489	1.486	1.491
C1-O5	L	1.430	1.405	1.344	1.291	1.256
C1-H(6–7)	**H**	**1.090**	**1.129**	**1.206**	**1.234**	**1.267**
C2-H(8–9)	**H**	**1.090**	**1.155**	**1.158**	**1.219**	**1.297**
C3-H(10–11)	**IH**	**1.090**	**1.178**	**1.168**	**1.205**	**1.372**
C4-H(12–14)	**V**	**1.090**	**1.215**	**1.155**	**1.177**	**1.153**
O5-H15	H	0.950	0.983	1.022	1.089	1.486

[a]See Table 2 for notation.

Table 12. Distribution of the charge density [a.u.] at particular atoms of the *S*-butan-2-ol molecule depending on the applied SMF flux density [AFU].

Atom	Charge density [a.u.] at SMF flux density [AFU]					
	Tendency[a]	0	0.1	1.0	10	100
C1	V	-0.575	-0.503	-0.513	-0.517	-0.553
C2	IL	0.086	0.087	0.067	0009	-0.176
C3	V	-0.435	-0.397	-0.428	-0.477	-0.313
C4	V	-0.601	-0.525	-0.545	-0.521	-0.538
O5	RH	-0.689	-0.673	-0.665	-0.627	-0.589
H(6–8)	**V**	**0.207**	**0.183**	**0.188**	**0.186**	**0.217**
H9	V	0.189	0.174	0.188	0.245	0.288
H10	V	0.203	0.183	0.202	0.198	-0.045
H11	V	0.223	0.202	0.212	0.211	0.285
H(12–14)	**V**	**0.198**	**0.190**	**0.179**	**0.189**	**0.207**
H15	IL	0.383	0.383	0.379	0.355	0.366

[a]See Table 2 for notation.

Table 13. Bond lengths [Å] in the molecule of *S*-butan-2-ol depending on the applied SMF flux density [AFU].

Bond	Bond length [Å] at applied SMF flux density [AFU]					
	Tendency[a]	0	0.1	1.0	10	100
C1-C2	IL	1.540	1.521	1.505	1.466	1.494
C2-C3	V	1.540	1.555	1.583	1.569	1.382
C3-C4	V	1.540	1.501	1.478	1.502	1.459
C1-H(6–8)	**IH**	**1.090**	**1.200**	**1.171**	**1.186**	**1.307**
C2-O5	RH	1.430	1.435	1.443	1.522	2.105
C2-H9	V	1.090	1.151	1.134	1.188	1.150
C3-H10	V	1.090	1.188	1.141	1.211	1.861
C3-H11	V	1.090	1.185	1.145	1.193	1.177
C3-H(12–14)	**IL**	**1.090**	**1.200**	**1.190**	**1.177**	**1.157**
O5-H15	IH	0.960	0.968	0.990	1.081	0.933

[a]See Table 2 for notation.

Table 14. Distribution of the charge density [a.u.] at particular atoms of the *iso*-butanol molecule depending on the applied SMF flux density [AFU].

Atom	Charge density [a.u.] at SMF flux density [AFU]					
	Tendency	0	0.1	1.0	10	100
C1	IH	-0.020	0.064	0.083	0.127	0.069
C2	V	-0.345	-0.391	-0.385	-0.374	-0.515
C(3–4)	**IH**	**-0.550**	**-0.504**	**-0.513**	**-0.418**	**-0.251**
O5	RL	-0.688	-0.700	-0.719	-0.738	-0.756
H(6–7)	**V**	**0.178**	**0.132**	**0.133**	**0.140**	**0.203**
H8	V	0.230	0.220	0.221	0.211	0.305
H(9–11)	**RL**	**0.202**	**0.197**	**0.190**	**0.172**	**0.089**
H(12–14)	**RL**	**0.198**	**0.181**	**0.181**	**0.147**	**0.099**
H(9–11)&H(12–14)	**RL**	**0.200**	**0.189**	**0.185**	**0.159**	**0.094**
H15	RH	0.375	0.392	0.397	0.405	0.428

[a]See Table 2 for notation.

Table 15. Bond lengths [Å] in the molecule of *iso*-butanol depending on the applied SMF flux density [AFU].

Bond	**Bond length [Å] at applied SMF flux density [AFU]**					
	Tendency	**0**	**0.1**	**1.0**	**10**	**100**
C1-C2	V	1.540	1.518	1.512	1.538	1.551
C2-C3	V	1.540	1.536	1.534	1.494	1.440
C3-C4	V	1.540	1.532	1.515	1.471	1.500
C1-O5	RL	1.430	1.406	1.366	1.294	1.081
C1-H(6–7)	**IL**	**1.090**	**1.215**	**1.193**	**1.186**	**1.103**
C2-H8	V	1.090	1.155	1.148	1.228	1.171
C3-H(9–11)	**IH**	**1.090**	**1.176**	**1.163**	**1.227**	**1.857**
C4-H(12–14)	**IH**	**1.090**	**1.172**	**1.170**	**1.332**	**2.051**
C3-H(9–11)&C4-H(12–14)	**IH**	**1.090**	**1.174**	**1.167**	**1.279**	**1.954**
O5-H15	V	0.960	0.955	1.018	1.131	1.104

[a]See Table 2 for notation.

Table 16. Distribution of the charge density [a.u.] at particular atoms of the *tert*-butanol molecule depending on the applied SMF flux density [AFU].

Atom	**Charge density [a.u.] at SMF flux density [AFU]**					
	Tendency	**0**	**0.1**	**1.0**	**10**	**100**
C1	V	0.162	0.169	0.172	0.177	0.092
C(2–4)	**IH**	**-0.551**	**-0.502**	**-0.516**	**-0.474**	**-0.373**
O5	V	-0.684	-0.683	-0.694	-0.696	-0.689
H(6–14)	**IL**	**0.200**	**0.183**	**0.189**	**0.174**	**0.100**
H15	H	0.371	0.370	0.375	0.376	0.387

[a]See Table 2 for notation.

Discussion

SMF turned negative values of heat of formation of alcohols less negative. It meant that SMF destabilised these molecules. That effect was accompanied with an increase in dipole moment (Table 1). The length of the carbon chain appeared to be crucial for the magnitude of those effects. Performed numerical simulations revealed that alcohols dis-

Table 17. Bond lengths [Å] in the molecule of *tert*-butanol depending on the applied SMF flux density [AFU].

Bond	Bond length [Å] at applied SMF flux density [AFU]					
	Tendency	0	0.1	1.0	10	100
C-C	**RL**	**1.540**	**1.533**	**1.530**	**1.524**	**1.504**
C-H	**IH**	**1.090**	**1.166**	**1.163**	**1.229**	**1.542**
C1-O5	IL	1.430	1.421	1.411	1.386	1.397
O5-H15	IH	0.960	0.984	0.969	1.006	1.013

[a]See Table 2 for notation.
Methanol Ethanol Propan-1-ol
Propan-2-ol Butan-1-ol *S*-(+)-Butan-2-ol
iso-Butanol *tert*-Butanol

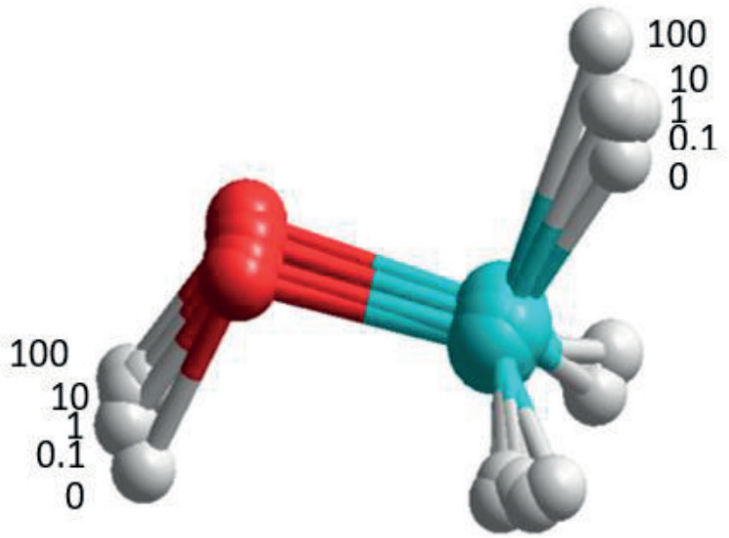

Figure 2. Visualisation of the conformational changes of the methanol molecule structure produced by SMF of increasing flux density.

tinguished from one another in their expressed heat of formation and dipole moment sensitivity to increased SMF flux density. It is shown by corresponding orders of those parameters arranged, based on the effect observed at SMF flux density at 100 AFU.

Order of sensitivity of heat of formation:

Methanol > Butan-1-ol > *tert*-Butanol > Ethanol > *iso*-Butanol > Propan-1-ol > *S*-Butan-2-ol > Propan-2-ol

Order of sensitivity of dipole moment:

Methanol > Ethanol > *S*-Butan-2-ol > Propan-1-ol > Butan-1-ol > *tert*-Butanol > *iso*-Butanol > Propan-2-ol

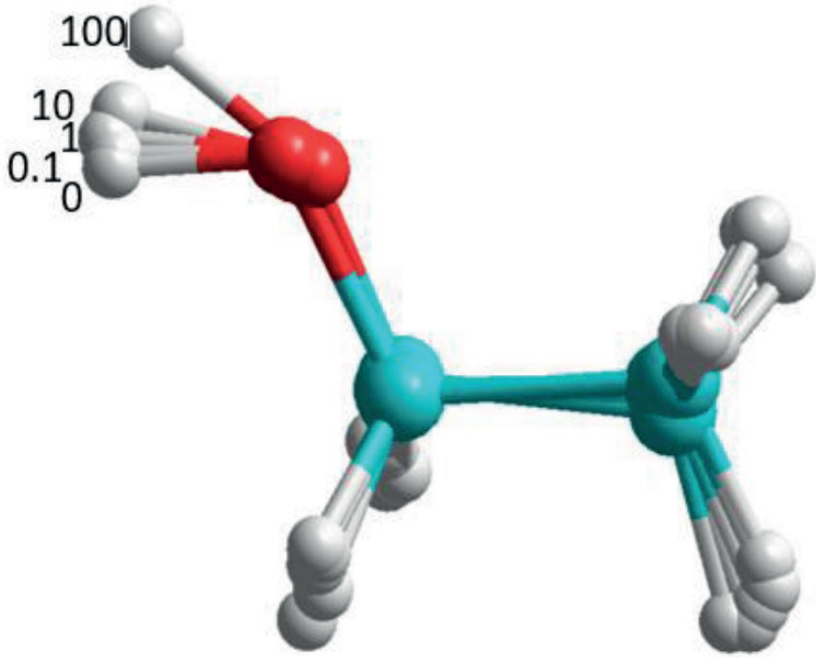

Figure 3. Visualisation of the conformational changes of the ethanol molecule structure produced by SMF of increasing flux density.

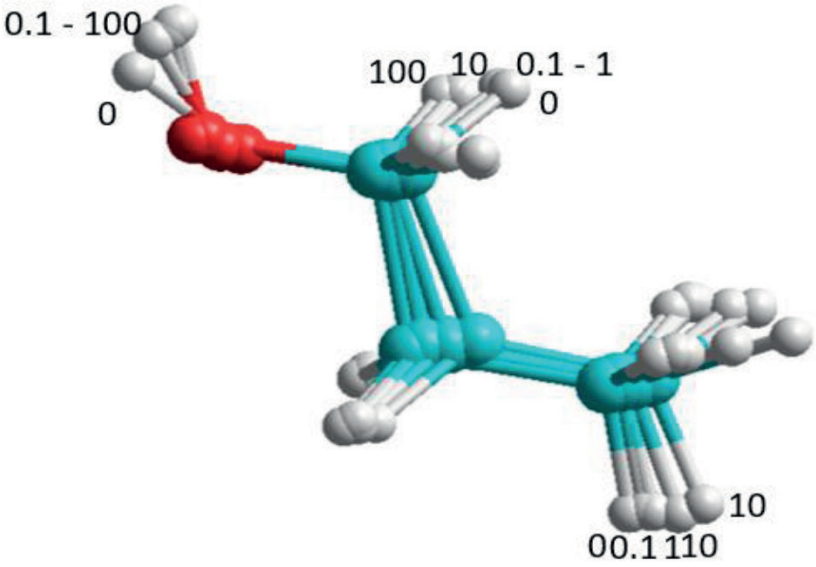

Figure 4. Visualisation of the conformational changes of the propan-1-ol molecule structure produced by SMF of increasing flux density.

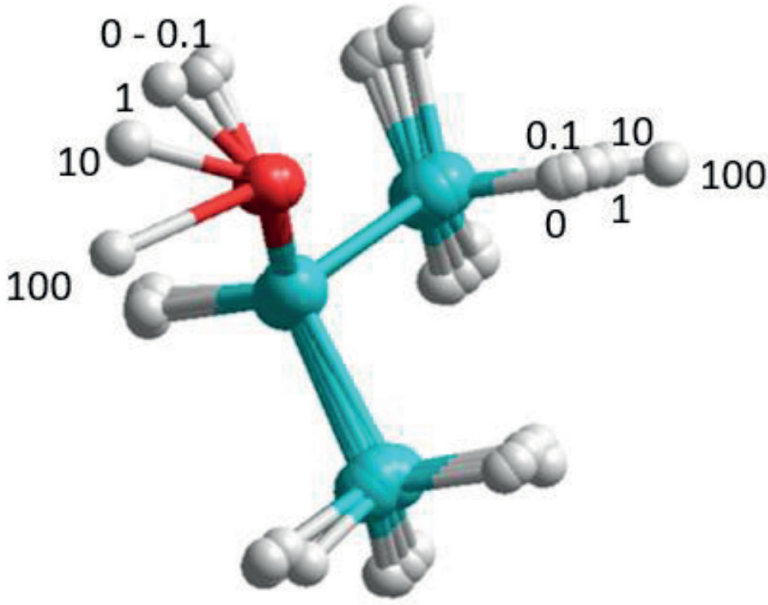

Figure 5. Visualisation of the conformational changes of the propan-2-ol molecule structure produced by SMF of increasing flux density.

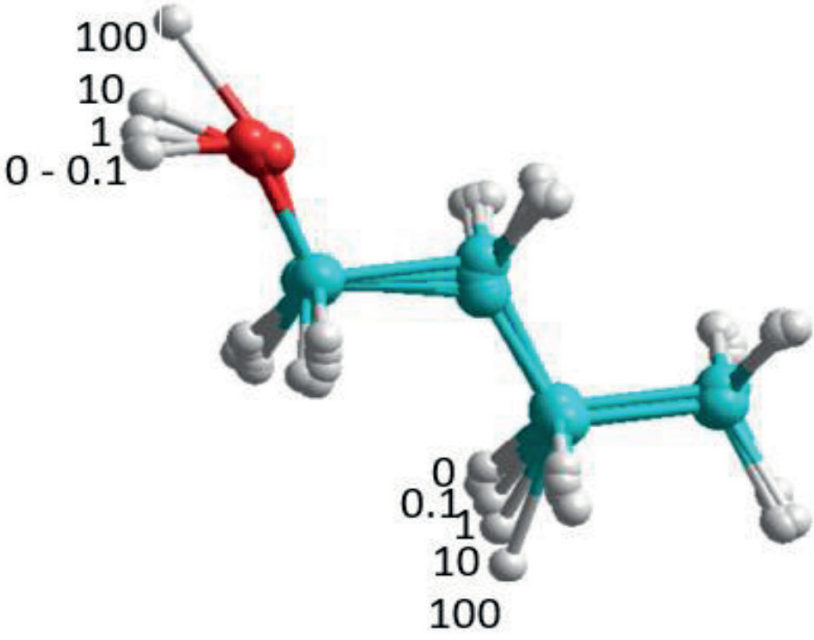

Figure 6. Visualisation of the conformational changes of the butan-1-ol molecule structure produced by SMF of increasing flux density.

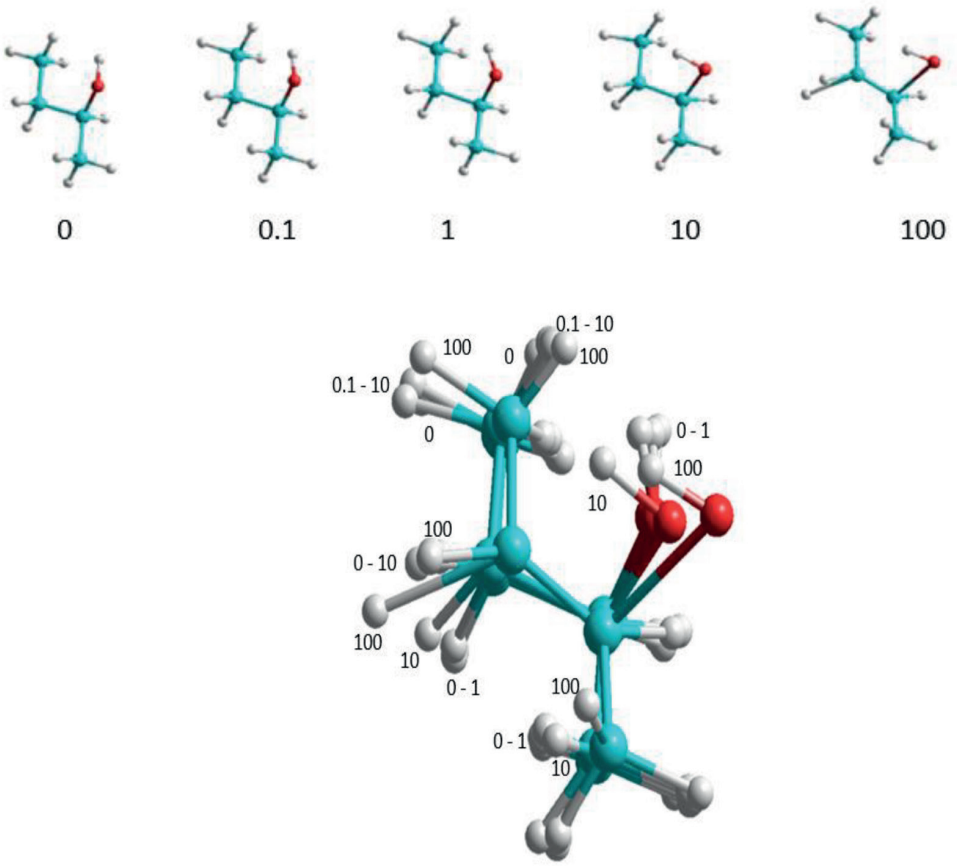

Figure 7. Visualisation of the conformational changes of the structure of *S*-butan-2-ol molecule produced by SMF of increasing flux density.

For instance, at 100 AFU, the heat of formation and dipole moment rose by approximately 49% and 55%, respectively. Under the same accepted conditions, these parameters for butan-1-ol rose by approximately 42% and 26%, respectively. Results of the simulations showed that the sensitivity of the alcohols to the applied SMF changed irregularly against the length of the carbon chain (Table 1). Such behaviour pointed to an involvement of complex factors. It is likely that they included changes in the conformation of the carbon chains, bond lengths and bond angles leading to repulsion of some fragments of the structure of those molecules away from the direction of the applied SMF. Such behaviour could evoke variable electrostatic and polar interactions through space, between particular atoms of the molecules.

These postulates were then recognised separately for particular alcohols under consideration (Fig. 1).

In the methanol molecule, because of the polarisation of the C-H bonds, the C1 atom took the negative charge. Its density changed irregularly with an increase in the

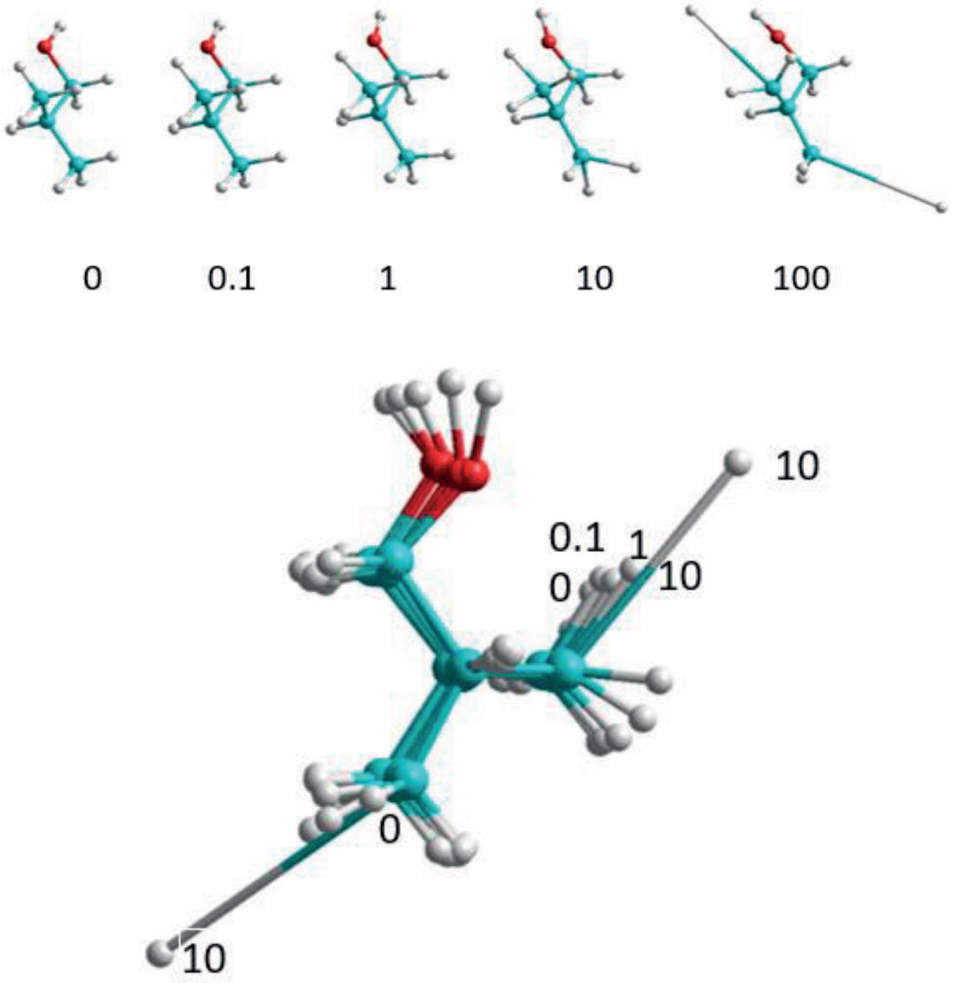

Figure 8. Visualisation of the conformational changes of the structure of *iso*-butanol molecule produced by SMF of increasing flux density.

SMF flux density. Initially, at 0.1 AFU, it decreased possibly due to polarisation of the C-O bond caused by the electron accepting properties of the O2 atom. The highest negative charge density at the C1 atom was noted at 1.0 AFU and substantially declined regularly up to 100 AFU (Table 2). Since the negative charge density at the O2 atom fairly regularly declined with an increase in AFU, the observed regularity should result from the C1-H interactions. Due to free rotation around the C1-O2 bond all three hydrogen atoms (H3, H4 and H5) of the methyl group are, in fact, equivalent to one another. However, the rules accepted in situating that molecule in the magnetic field cancelled that equivalence. Therefore, in Table 2, computed values of the charge density of those atoms were not identical. In order to omit that in consequence, the average of those three parameters was discussed. The average positive charge density

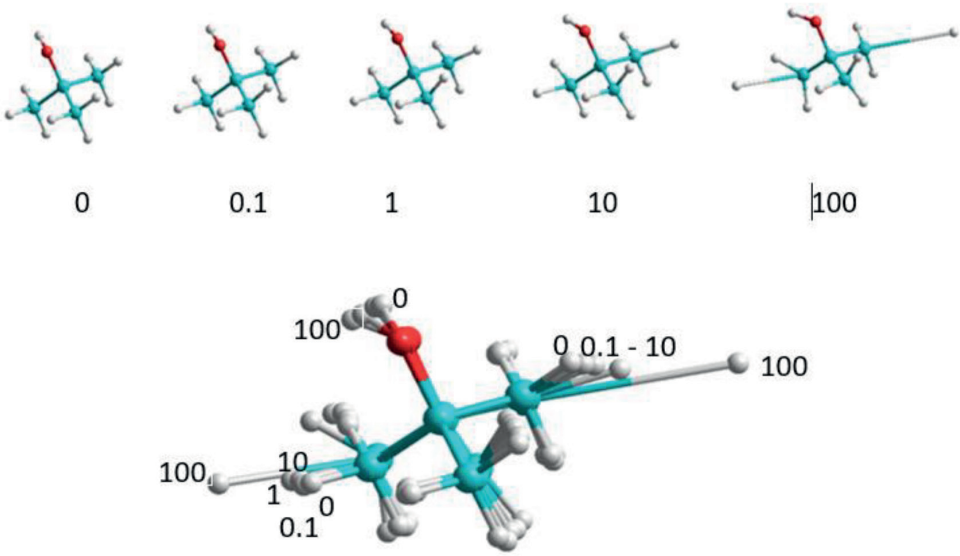

Figure 9. Visualisation of the conformational changes of the structure of the *tert*-butanol molecule produced by SMF of increasing flux density.

at the H3-H5 atoms and at the H6 atom irregularly decreased with an increase in the SMF flux density. These changes could originate from pushing particular hydrogen atoms out of the magnetic field. In Table 3, the bond lengths between particular atoms revealed a general tendency of the shortening the C1-O2 bond with an increase in applied SMF. This behaviour was observed in spite of simultaneous declining of the negative charge at those atoms. The length of the remaining bonds increased although slight irregularities in the case of the C1-(H3-H5) and O2-H6 bonds, in both cases taking place at 1 AFU were noted. The visualisation of the shapes of the molecule at varying SMF flux density (Fig. 2) confirmed that the irregularities could result from slight mobility of the molecule placed in the magnetic field and subtle changes of the bond angles.

In the ethanol molecule without SMF, both the C1 and C2 atoms were negatively charged (Table 4). As the applied SMF flux density increased, the charge density at both atoms declined. That at the C1 atom reached positive charge already at 10 AFU. It could rationalise the increase in the negative charge density at the O3 atom. Under SMF, the latter atom polarised not only the C1-O3, but also the O3-H9 bond. In consequence, the positive charge density at the H9 atom rose with an increase in the flux density. As the result of the decrease in the electronegativity of the C1 atom, the positive charge density at the H4 and H5 atoms declined. Declining with increasing flux density electronegativity of the C2 atom resulted in a gradual decrease of the positive charge density at the H6, H7 and H8 atoms. The latter irregularity was reflected by irregular changes in the C2-H6 bond (Table 5). Under the influence of SMF, the length of the C1-C2 and C1-O3 bonds declined with an increase in the applied flux

density. Simultaneously, the length of all C-H bonds and the O3-H9 bond increased with the flux density applied.

The visualisation of the ethanol molecule placed in SMF with increased flux density (Fig. 3) demonstrated the slight conformational changes in the initial position of the molecule out of the field. The essential change of the position of the H9 atom corresponded to observed irregularity in the C1-C2 bond length at 100 AFU.

In the charge density distribution in the propan-1-ol molecule SMF of increasing flux density generated many more irregularities. They were caused mainly by SMF of 100 AFU although some irregularities were noted also in the charge density at the C1 atom at 0.1 AFU, at the C3 atom at 10 AFU and the H(5–6) atom at 10 AFU (Table 6). All three carbon atoms in this alcohol were negatively charged. In the SMF of increasing flux density, the negative charge density at all carbon atoms declined. The C2 and C3 carbon atoms retained that charge also at 100 AFU, but the C1 atom turned into positively charged already at 10 AFU. Since with an increase in the flux density, the O4 atom turned more electron attracting, this phenomenon could be rationalised in a similar manner as presented for ethanol. The positive charge density at the H12 atom regularly rose, likely as the consequence of increasing electronegativity of the O4 atom. In contrast to that, the positive charge density declined with an increase in the flux density at the H(5–6), H(7–8) and H(9–11) atoms at the flux density up to 100 AFU. In the two first cases, it declined solely up to 10 AFU and at 100 AFU it rose. In the case of the H(9–11) atoms, a possibility of their polar interaction with the O4 atom could eventually be taken into account, but visualisation of the shape of that molecule in the SMF (Fig. 4) did not support that assumption. The length of all C-C bonds, although irregularly in the case of the C1-C2 bond, decreased with an increase in the applied flux density (Table 7). The C3-O4 bond also shortened. All the C1-H(5–6) and C2-H(7–8) bonds regularly expanded up to 10 AFU in order to compress at 100 AFU. The C3-H(9–11) and the O4-H12 were regularly elongated up to 100 AFU.

The visualisation presented in Fig. 4 confirmed that observed effects originated from small movements of the molecule at increasing SMF intensity and associated changes in bond angles.

The carbon chain in the molecule of propan-2-ol was more capable of various conformational transformations involving the methyl groups. On the other hand, intervention of the intramolecular polar interactions was unlikely. It resulted in irregular responses of the charge density (Table 8) and bond lengths (Table 9) to the application of SMF and its increasing flux density. The C1 carbon atom holding the hydroxyl and two methyl groups was positively charged and the charge density regularly increased with an increase in the flux density. The C2 and C3 carbon atoms of both side methyl groups were negatively charged and these charges, even without SMF, were not identical. As the flux density rose, the charge density at both these atoms declined although it proceeded irregularly. This trend was accompanied by a fairly regular decrease of the negative charge density at the O4 atom. The positive charge density at the H5 – H11 atoms generally, although irregularly, decreased with increasing flux density. These rather subtle irregularities were observed at 10 AFU. The charge density at the

H12 atom declined regularly against the increasing flux density. The C1-C(2–3) bond length at 0.1 AFU increased in order to decrease up 100 AFU and, at the same time, the length of the C1-O4 bond decreased regularly. All the C-H bonds [C2-H(6–8) & C3-H(9–11) av.] and O-4-H12 bonds increased their lengths with increasing flux density although the latter bond did it irregularly at 0.1 AFU. Fig. 5 demonstrates the origin of those irregularities. They were changes in bond angles and subtle re-orientations in the original position along the x-axis.

As in case of results of computations for ethanol and propan-1-ol, such computations for normal carbon chain butan-1-ol delivered the scope of data with very few irregularities in the flux density dependent on changes of charge density (Table 10) and bond lengths (Table 11).

Out of SMF, the C1-carbon atom holding the hydroxyl group was weakly negatively charged. As the flux density of the applied SMF increased, the charge of that atom turned to positive and its value increased regularly with increasing flux density. All remaining carbon atoms of the chain were negatively charged and their charge density fairly regularly decreased with an increase in the flux density applied. Amongst them, the C3 atom was the least electronegative and, at 1.0 AFU, its electronegativity jumped considerably. The electronegativity of the O5 atom increased with an increase in the flux density up to 10 AFU and regularly decreased up to 100 AFU. The positive charge density at the H6 – H10 and H14 atoms fairly regularly decreased with an increase in the flux density, whereas the charge density at the H11-H13 atoms irregularly increased. The positive charge density at the H15 atom belonging to the hydroxyl group regularly increased up to 10 AFU and declined regularly up to 100 AFU. The length of the C1-C2 bond, initially at 0.1, 1 and 10 AFU, decreased and then increased regularly up to 100 AFU. The length of C2-C3, C3-C4 and C1-O5 bonds at that time declined. The bond length of all C-H bonds and the O5-H14 group increased with an increase in flux density. That increase became irregular in the case of the terminal methyl group (Table 11). The visualisation of the structural changes in the butan-1-ol molecule evoked by applied SMF (Fig. 6) points to the same factors rationalising the results of computations. Additionally, the polar interactions between the hydrogen atoms of the H10 atom, particularly at 100 AFU, seems to be likely.

Butan-2-ol called also *sec*-butanol exists in two, *R* and *S* enantiomers. The *S* enantiomer is more common. The asymmetry centre at the C2 atom did not influence the results of computations, thus, data collected in Tables 12, 13 were valid for both enantiomers. Due to the asymmetry centre located at the C2 atom, the H10 and H11 atoms and the C3-H10 and C3-H11 were not equivalent to one another, respectively. Therefore, corresponding values were not average. Except for the C2 carbon atom, the remaining carbon atoms in that molecule carried a negative charge density although, at 100 AFU, the C2 atom also took the negative charge density. Increasing flux density decreased that negative charge. Additionally, the negative charge density at the O5 atom behaved similarly. Except for the H10 atom which carried the negative charge density at 100 AFU, all remaining carbon atoms carried the positive charge density. Its value varied highly irregularly with increasing flux density (Table 12). These facts pointed to a considerable role of conformational changes within that molecule and

intramolecular polar interactions. Solely the C2-O5 bond length regularly increased with the flux density. The lengths of the other bonds varied irregularly (Table 13).

The visualisation of the structural changes in the *S*-butan-2-ol molecule evoked by applied SMF (Fig. 7) pointed to the same factors rationalising the results of computations. Additionally, the polar interactions between the hydrogen atoms of the H10 atom, particularly at 100 AFU, seemed to be likely.

For the same reasons as mentioned in case of propanol-2-ol, computed changes in the charge density (Table 14) and bond length in the *iso*-butanol fairly irregularly changed with an increase in the SMF flux density. The residual electronegativity of the C1 atom in the molecule out of SMF ceased already at 0.1 AFU. The positive charge at that atom rose up to 10 AFU and slightly declined regularly up to 100 AFU. The electronegativity of the C2 increased with the flux density in contrast to that of the C3 and C4 atoms whose electronegativity was reduced. Simultaneously, the electronegativity of the O5 atom regularly increased. The flux density of 100 AFU considerably increased the positive charge density at the H8 and H15 atoms. The positive charge density at the remaining H- atoms, except for the H6 and H7 atoms, declined under the influence of lower flux densities (Table 14). There were also numerous irregularities in the influence of increasing flux density upon the bond lengths. The length of the C1-C2 bond initially decreased in order to increase again at 10 AFU and the C2-C3, C3-C4 and C1-O5 bonds were shortened. Simultaneously, all the C-H bonds expanded, some of them irregularly against increasing flux density (Table 15). The visualisation of the effects of SMF upon the structure of the *iso*-butanol molecule (Fig. 8) suggested possible intervention in the structure modification from intramolecular polar interactions involving the H10 hydrogen and O5 atoms.

The highly-branched carbon chain of *tert*-butanol provided three methyl groups. Potentially, they could change their orientation in SMF, controlled by the generated variable positive charge density located at a particular hydrogen atom at a given flux density. That factor could rationalise irregular changes of charge densities at particular atoms (Table 16) and bond lengths (Table 17) on increasing flux density. Thus, for instance, the positive charge density at the C1 atom rose up regularly to decline at 100 AFU. The negative charge density at the equivalent C2, C3 and C4 atoms also declined with an increase in the flux density. Increasing flux density only slightly influenced the negative charge density at the O5 oxygen atom. The positive charge density of the carbon bound hydrogen atoms fairly regularly declined against increasing flux density, whereas the positive charge density located at the O5 atom bound to the hydrogen atom slightly, but regularly increased. These effects contributed to irregular changes of the bond lengths presented in Table 17. The observed irregularities could also result from perturbations in rotation of the vicinal groups caused by electrostatic repulsion of the hydrogen atoms through space. The length of the C-C- and C1-O5 bonds decreased with an increase in the flux density, whereas, simultaneously, the length of the C-H and O5-H15 bonds increased (Table 17). Fig. 9 presents conformational changes evoked by SMF in the molecule of *tert*-butanol.

A rigid molecule situated in respect to the direction of the magnetic field resulted in diamagnetic interactions with electrons of the bonds. Thus, these interactions could

be reflected by elongation of the bonds instead of moving in the space. This is known as a phenomenon of levitating living frogs observed in SMF on the level of 12–20T (Berry 1997) (≈ 0.012–0.02 AFU) and these remaining healthy after experiments.

In performed computations, a decrease in heat of formation of alkanols with an increase in applied SMF flux density accompanied with increase in dipole moments pointed to weakening the bonds and, at the same time, elongation of the bonds. It resulted from the destabilising effect of SMF upon spin-paired electrons. Inspection of the alkanols geometry changing with SMF arranged parallel to the long axis of the molecules showed that, in several cases, the effect of the bond elongation is the strongest when the bond and direction of the field force lines reached approximately the 45° angle. It was noted for the molecules of methanol, butan-1-ol, *S*-butan-2-ol, *iso*-butanol and *tert*-butanol.

Biological function of alcohols in organisms of flora and fauna chiefly involves the hydroxyl group. That group is attacked by various enzymes metabolising alcohols via a complex catabolic and metabolic pathway (US Department of Health & Human Services 2007; Vaswami 2019). In the first step, the hydroxyl group of alcohol plays a role of the Lewis base. Hence the high negative charge density at the oxygen atom of that group favours the initial step of the alcohol metabolism. Simultaneously, elongation of the O-H bond should favour the contact of the alcohol with attacking enzymes. Taking these arguments into account, based on the insight in particular Tables, one could state that SMF declined the Lewis basicity, that is, inhibited reaction with enzymes in methanol, propan-2-ol and S-butan-2-ol. Except for methanol, the alkanols bearing their hydroxyl groups at the terminal CH_2 group of the chain were stimulated by SMF to react with enzymes. Amongst the SMF stimulated alkanols, the *tert*-butanol was least sensitive. The length of the O-H bond increased in all cases.

Taking into account the chemical oxidation of alkanols, attention should be paid to the response of the positive charge density at the hydrogen atom bound to the carbon atom holding also the hydroxyl group to an increase in the applied SMF flux. One could see that, in the molecules of methanol, ethanol, propan-1-ol, propan-2-ol and butan-1-ol, the positive charge density decreased making that hydrogen atom less acidic. Only in S-butan-2-ol and isobutanol, this charge density varied very chimerically. t*ert*-Butanol did not possess such a hydrogen atom. A decrease in the positive charge at the geminal hydrogen atom made it more sensitive to the reactions of the free radical mechanism that is less susceptible to the reactions involving the ionic mechanism.

Conclusions

Static magnetic field of flux density increasing from 0 to 100 AFU destabilised the molecules of alkanol as shown by the increasing heat of formation of those molecules and their dipole moment.

SMF produced an increase in the negative charge density at the oxygen atom of the hydroxyl group and elongated the –O-H bond length. These results show that SMF facilitates metabolism of the alkanols.

Some irregularities in the changes of positive and negative charge densities and bond lengths provide evidence that molecules slightly change their initially fixed positions in respect to the force lines of the magnetic field. Length of some bonds and bond angles change with an increase in the applied flux density providing, in some cases, polar interactions between atoms through the space.

SMF flux density initially defined in T evoked much stronger effects than could be anticipated, based on the comparative analysis with experimental results of flux density. Computations were performed for extremely high intensity of SMF at which almost every molecule and every element of construction could be destroyed. In natural Earth conditions, generated SMF of hardly 2 AFU destroyed electromagnetism within milliseconds. Thus, introduced AFU were at 1000 times higher than T. Hence, results of effects of SMF to humans predicted in this paper are purely theoretical in contrast to effects of alternating electromagnetic fields of much lower intensity.

References

Andreini C, Bertini I, Cavallaro G, Holliday GL, Thornton JM (2008) Metal ions in biological catalysis: From enzyme databases to general principles. Journal of Biological Inorganic Chemistry 13(8): 1205–1218. https://doi.org/10.1007/s00775-008-0404-5

Bao S, Guo W (2021) Transient heat transfer of superfluid $^{4}\mathrm{He}$ in nonhomogeneous geometries: Second sound, rarefaction, and thermal layer. Physical Review B 103(13): e134510. https://doi.org/10.1103/PhysRevB.103.134510

Beretta G, Mastorgio AF, Pedrali L, Saponaro S, Sezenna E (2019) The effects of electric, magnetic and electromagnetic fields on microorganisms in the perspective of bioremediation. Reviews in Environmental Science and Biotechnology 18(1): 29–75. https://doi.org/10.1007/s11157-018-09491-9

Berry MV, Geim AK (1997) Of flying frogs and levitrons. European Journal of Physics 18(4): 307–313. https://doi.org/10.1088/0143-0807/18/4/012

Buchachenko A (2009) Magnetic isotope effect in chemistry and biochemistry. Nova Science Publisher, NY.

Buchachenko LA (2014) Magnetic control of enzymatic phosphorylation. Journal of Physical Chemistry & Biophysics 4: e1000142. https://doi.org/10.4172/2161-0398.1000142

Buchachenko A (2016) Why magnetic and electromagnetic effects in biology are irreproducible and contradictory? Bioelectromagnetics 37(1): 1–13. https://doi.org/10.1002/bem.21947

Buchachenko AL, Kuznetsov DA, Breslavskaya NN (2012) Chemistry of enzymatic ATP synthesis: An insight through the isotope window. Chemical Reviews 112(4): 2042–2058. https://doi.org/10.1021/cr200142a

Carpenter JE, Weinhold F (1988) Analysis of the geometry of the hydroxymethyl radical by the different hybrids for different spins natural bond orbital procedure. Journal of Molecular Structure (Teochem) 139: 41–62. https://doi.org/10.1016/0166-1280(88)80248-3

Charistos ND, Muñoz-Castro A (2019) Double aromaticity of the B-40 fullerene: Induced magnetic field analysis of pi and sigma delocalization in the boron cavernous structure.

Physical Chemistry Chemical Physics 21(36): 20232–20238. https://doi.org/10.1039/C9CP04223G

Ciesielski W, Girek T, Oszczęda Z, Soroka JA, Tomasik P (2021) Towards recognizing mechanisms of effects evoked in living organisms by static magnetic field. Numerically simulated effects of the static magnetic field upon simple inorganic molecules. F1000 Research 10: e611. https://doi.org/10.12688/f1000research.54436.1

Committee to Assess the Current Status and Future Direction of High Magnetic Field Science in the United States (2013) High Magnetic Field Science and Its Application in the United States; Current Status and Future Directions. Natl. Res. Council, National Acad., The National Academies Press, Washington, D.C.

Dinan L, Harmatha J, Lafont R (2001) Chromatography procedures for isolation of plant steroids. Journal of Chromatography A 935(1–2): 105–122. https://doi.org/10.1016/S0021-9673(01)00992-X

Farberovich OV, Mazalova VL (2016) Ultrafast quantum spin-state switching in the Co-octaethylporphyrin molecular magnet with a terahertz pulsed magnetic field. Journal of Magnetism and Magnetic Materials 405: 169–173. https://doi.org/10.1016/j.jmmm.2015.12.038

Frisch MJ, Trucks GW, Schlegel HB, Frisch MJ, Trucks GW, Schlegel HB, Scuseria GE, Robb MA, Cheeseman JR, Scalmani G, Barone V, Mennucci B, Petersson GA (2016) Gaussian 09, Revision A.02, Gaussian, Inc., Wallingford.

Froimowitz M (1993) HyperChem: A software package for computational chemistry and molecular modelling. BioTechniques 14: 1010–1013.

Glendening ED, Reed AE, Carpenter JE (1987) Extension of Lewis structure concepts to open-shell and excited-state molecular species, NBO Version 3.1. Ph.D. thesis, University of Wisconsin, Madison, WI.

Hamza A-SHA, Shaher SA, Mohmoud A, Ghania SM (2002) Environmental pollution by magnetic field associated with power transmission lines. Energy Conversion and Management 43(17): 2442–2452. https://doi.org/10.1016/S0196-8904(01)00173-X

Jaworska M, Domański J, Tomasik P, Znój K (2014) Methods of stimulation of growth and pathogenicity of entomopathogenic fungi for biological plant protection. Polish Patent 223412.

Jaworska M, Domański J, Tomasik P, Znój K (2016) Preliminary studies on stimulation of entomopathogenic fungi with magnetic field. Journal of Plant Diseases and Protection 12: 295–300. https://doi.org/10.1007/s41348-016-0035-y

Jaworska M, Domański J, Tomasik P, Znój K (2017) Preliminary studies on stimulation of entomopathogenic nematodes with magnetic field. Prom. Zdr. Ekol 4(9).

Kohno M, Yamazaki M, Kimura I, Wada M (2000) Effect of static magnetic fields on bacteria: *Streptococcus mutans*, *Staphylococcus aureus*, and *Escherichia coli.* Pathophysiology 7(2): 143–148. https://doi.org/10.1016/S0928-4680(00)00042-0

Letuta UG, Berdinskiy VL (2017) Magnetosensitivity of bacteria *E. coli*: Magnetic isotope and magnetic field effects. Bioelectromagnetics 38(8): 581–591. https://doi.org/10.1002/bem.22073

Lewis DH, Smith DC (1967) Sugar alcohols(polyols) in fungi and green plants. The New Phytologist 66(2): 143–184. https://doi.org/10.1111/j.1469-8137.1967.tb05997.x

Marchand N, Lienard P, Siehl H, Izato H (2014) Applications of molecular simulation software SCIGRESS in industry and university. Fujitsu Scientific and Technical Journal 50(3): 46–51.

Rankovic V, Radulovic J (2009) Environmental pollution by magnetic field around power lines. International Journal of Qualitative Research 3(3): 1–6.

Rittie L, Perbal B (2008) Enzymes used in molecular biology: A useful guide. Journal of Cell Communication and Signaling 2(1–2): 25–45. https://doi.org/10.1007/s12079-008-0026-2

Rowland O, Domerque F (2012) Plant fatty acyl reductases: Enzyme generating fatty alcohols for protective layers with potential for industrial applications. Plant Science 193–194: 28–38. https://doi.org/10.1016/j.plantsci.2012.05.002

Steiner UE, Ulrich T (1989) Magnetic field effects in chemical kinetics and related phenomena. Chemical Reviews 89(1): 51–147. https://doi.org/10.1021/cr00091a003

Tang Y, Guo W, Lvov W, Pomyalov A (2021) Eulerian and Lagrangian second-order statistics of superfluid $^{4}\mathrm{He}$ grid turbulence. Physical Review B 103(14): e144506. https://doi.org/10.1103/PhysRevB.103.144506

US Department of Health & Human Services (2007) Alcohol metabolism: An update. Alcohol alert: 72.

Vaswami M (2019) ADH and ALDH polymorphism in alcoholism and alcohol misuse/dependence. In: Preedy VR (Ed.) Neuroscience of Alcohol: Mechanism and Treatment. Academic Press, London. https://doi.org/10.1016/B978-0-12-813125-1.00004-0

Wade LG (2021) Alcohol chemical compounds. Encyclopedia Britannica. [Accessed 26 June 2021]

Woodward JR (2002) Radical pairs in solution. Progress in Reaction Kinetics and Mechanism 27(3): 165–207. https://doi.org/10.3184/007967402103165388

Woronowicz B (2003) Without Secrets on Addictions and Their Therapy. Ed. Instytut Psychiatrii i Neurologii, Warsaw. [in Polish]

Zamiatała K, Domański J, Krystyjan M, Tomasik P (2013) Effect of magnetic field upon selected cosmetics creams. Polish Journal of Cosmetology 16(2): 144–147.

BioRisk 18: 57–91 (2022)
doi: 10.3897/biorisk.18.77001
https://biorisk.pensoft.net

RESEARCH ARTICLE

A peer-reviewed open-access journal
BioRisk

Potential risk resulting from the influence of static magnetic field upon living organisms. Numerically-simulated effects of the static magnetic field upon carbohydrates

Wojciech Ciesielski[1], Tomasz Girek[1], Henryk Kołoczek[2], Zdzisław Oszczęda[3], Jacek A. Soroka[4], Piotr Tomasik[3]

1 *Institute of Chemistry, Jan Długosz University, 42 201 Częstochowa, Poland* **2** *Institute of Chemistry and Inorganic Technology, Krakow University of Technology, 31155 Krakow, Poland* **3** *Nantes Nanotechnological Systems, 59 700 Bolesławiec, Poland* **4** *Scientific Society of Szczecin, 71-481 Szczecin, Poland*

Corresponding author: Wojciech Ciesielski (w.ciesielski@interia.pl)

Academic editor: Josef Settele | Received 24 October 2021 | Accepted 3 April 2022 | Published 6 June 2022

Citation: Ciesielski W, Girek T, Kołoczek H, Oszczeda Z, Soroka JA, Tomasik P (2022) Potential risk resulting from the influence of static magnetic field upon living organisms. Numerically-simulated effects of the static magnetic field upon carbohydrates. BioRisk 18: 57–91. https://doi.org/10.3897/biorisk.18.77001

Abstract

Background: Recognising effects of static magnetic field (SMF) of varying flux density on flora and fauna is attempted. For this purpose, the influence of SMF upon molecules of *a*- and *β*-D-glucose, *a*- and *β*-D-galactose, *a*- and *β*-fructopyranoses, *a*- and *β*-fructofuranoses and *a*- and *β*-D-xylofuranoses and *a* and *β*-D-xylopyranoses is studied.

Methods: Computations of the effect of static magnetic field (SMF) of 0.0, 0.1, 1, 10 and 100 AFU (1 AFU > 1000 T) flux density were performed in silico for SMF changes distribution of the electron density in these molecules.

Hyper-Chem 8.0 software was used together with the AM1 method for optimisation of the conformation of the molecules of monosaccharides under study. Then polarisability, charge distribution, potential and dipole moment for molecules placed in SMF were calculated involving DFT 3-21G method.

Results: Application of SMF induced polarisability of electrons, atoms and dipoles, the latter resulting in eventual re-orientation of the molecules along the applied field of the molecules and the electron density redistribution at particular atoms. Increase in the field strength generated mostly irregular changes of the electron densities at particular atoms of the molecules as well as polarisabilities. Energy of these molecules and their dipole moments also varied with the SMF flux density applied.

Conclusions: Saccharides present in the living organisms may participate in the response of the living organisms to SMF affecting metabolism of the molecules in the body fluids by fitting molecules to the enzymes. Structural changes of saccharide components of the cell membranes can influence the membrane permeability.

Keywords
D-fructose, D-galactose, D-glucose, D-xylose, organisms, static magnetic field

Introduction

Carbohydrates (mono-, di-, oligo- and polysaccharides) serve several key functions in fauna and flora. Customarily, products of their physical, chemical and biological transformations are also accounted for in this group of compounds. Cellulose, a polysaccharide, is the most abundant carbohydrate all over the world. It is a structural component of the cell walls of plants including aquatic plants like algae. Green plants, which constitute about half of the living matter on the earth, also contain abundant number of mono-, di- and oligosaccharides. Some of them are found also in animals. Metabolism of those oligo- and lower carbohydrates provides energy and nutrients for the plants (Heldt and Piechulla 2010).

In organisms of fauna and their life, the role of carbohydrates is much more complex than in plants. They co-build membranes of body cells and microorganisms colonising the body, enzymes and elements of genetic code. Carbohydrates are present in systems protecting the cells from oxidative stress and participate in several reactions in the body (Maton et al. 1993; Campbell et al. 2006; Reynolds et al. 2019). Carbohydrates in various forms are delivered to the organisms as food components. The latter are either physically, chemically or enzymatically transformed (metabolised) or left intact playing the role of fibre. Fibre promotes a proper functioning of the excretory system and, as an adsorbent, removes toxins concentrated in the intestines. All kinds of physical, chemical and biochemical transformations are controlled by several factors, such as conformations of reacting molecules, equilibria, formation of transition molecule – enzyme transition states and mechanisms of the transformations which can be either reversible or irreversible. Their transformation can proceed following either ionic or radical mechanisms (Tomasik 1997; Tomasik 2007a, 2007b; Keung and Mehta 2015; Churuangsuk et al. 2018).

The effect of increasing environmental pollution with a magnetic field (Hamza et al. 2002; Rankovic and Radulovic 2009) and the role of the magnetic field in current and future technologies (Committee to Assess the Current Status and Future Direction of High Magnetic Field Science in the United States, Board on Physics and Astronomy 2013; Bao and Guo 2021; Tang et al. 2021) evokes certain anxiety. Therefore, recently (Ciesielski et al. 2021) we presented a numerically-simulated effect of static magnetic field (SMF) on the structure and behaviour of simple molecules, that is, triplet and singlet oxygen, nitrogen, water, ammonia, carbon dioxide and methane (Ciesielski et al. 2021) and lower alkanols (Ciesielski et al. 2022). The results prompted us to study the effect of that field upon further molecules important in constituting and functioning organisms of flora and fauna.

This paper presents results of numerical computations applied to selected monosaccharides, that is to *α*- and *β*-D-glucose, *α*- and *β*-D-galactose, *α*- and *β*-fructopyranoses, *α*- and *β*-fructofuranoses, *α*- and *β*-D-xylopyranoses and *α*- and *β*-D-xylofuranoses. They play essential roles in building structure and functioning of organisms of flora and fauna.

Numerical computations

Molecular structures were drawn using the Fujitsu SCIGRESS 2.0 software (Marchand et al. 2014). Their principal symmetry axes were orientated along the x-axis of the Cartesian system. A molecule of saccharide was situated inside of a triaxial elypsoid. The long axis of that ellipsoid was accepted to be the x-axis. The shortest axis quasi-perpendicular to either the pyranose or furanose ring was considered as the z-axis. The y-axis was quasi-parallel to those rings plane. The magnetic field was fixed in the same direction, along the x-axis with the south pole from the left side. Subsequently, involving Gaussian 0.9 software, equipped with the 6-31G** basis (Frisch et al. 2016) i.e. equipped with multiple polarization functions (Frisch et al. 1984), the molecules were optimised and all values of bond length, dipole moment, health of formation, bond energy and total energy for the systems were computed.

In the next step, the tendency of the static magnetic field (SMF) influence, employed as Arbitrary Field Unit (AFU) (1 AFU > 1000 T), upon optimised molecules was computed with Amsterdam Modelling Suite software (Farberovich and Mazalova 2016; Charistos and Muñoz-Castro 2019) and the NR_LDOTB (non-relativistically orbital momentum L-dot-B) method (Glendening et al. 1987; Carpenter and Weinhold 1988). Following that step, values of bond length, dipole moment, health of formation equal to the energy of dissociation and charges at the atoms, were calculated using Gaussian 0.9 software equipped with the 6-31G** basis (Frisch et al. 2016).

Visualisation of molecules in the coordinate system was performed involving the HyperChem 8.0 software (Froimowitz 1993).

Results

Numerical simulations were performed for both anomers of D-glucose (Fig. 1)

Both anomers of D-galactose (Fig. 2)

Both anomers of D-fructopyranoses and both anomers of D-fructofuranoeses (Fig. 3)

Both anomers of D-xylopyranoses and both anomers of D-xylofuranoses (Fig. 4)

Particular structures contain numbering atoms followed in further discussions.

Tables 1–3 provide data illustrating properties of the α- and β-D-glucose molecules situated along the x-axis of the Cartesian system in SMF of the flux density of 0 to 100 AFU, distribution of charge density and bond lengths in those molecules, respectively.

Results of those computations are visualised in Fig. 5.

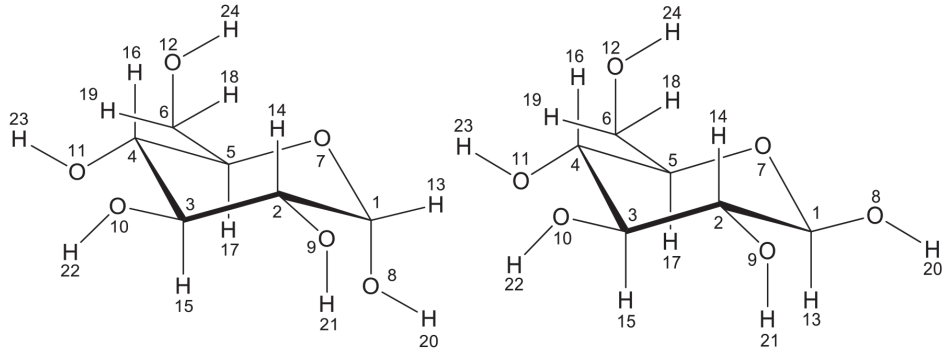

Figure 1. Structure of α- and β-D-glucose (**a** and **b** respectively) and followed by numbering of atoms.

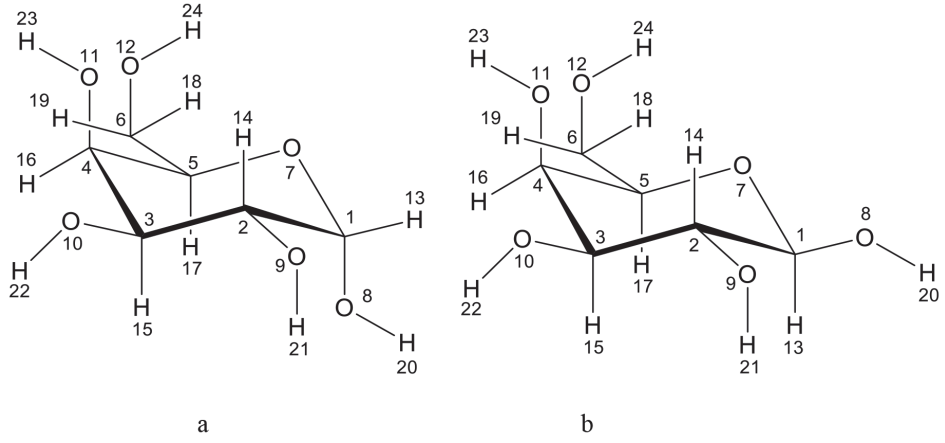

Figure 2. Structure of α- and β-D-galactose (**a** and **b** respectively) and followed by numbering of atoms.

Table 1. Properties of the α- and β-D-glucose molecules situated along the x-axis of the Cartesian system in SMF of the flux density of 0 to 100 AFU.

Property	Anomer	Flux density [AFU]				
		0	**0.1**	**1**	**10**	**100**
Dipole moment [D]	α	8.68	8.69	8.77	8.89	9.06
	β	8.34	8.44	9.75	10.12	14.52
Heat of formation [kcal/mole]	α	-1259.6	-1259.6	-1248.7	-1141.5	-985.8
	β	-1246.6	-1245.8	-1223.5	-1095.3	-912.6

Corresponding data computed for anomers of D-galactose are presented in Tables 4–6. They are visualised in Fig. 6.

Tables 7–9 contain results of analogous computations for anomers of D-fructopyranoses and visualisation of those data are visualised in Fig. 7.

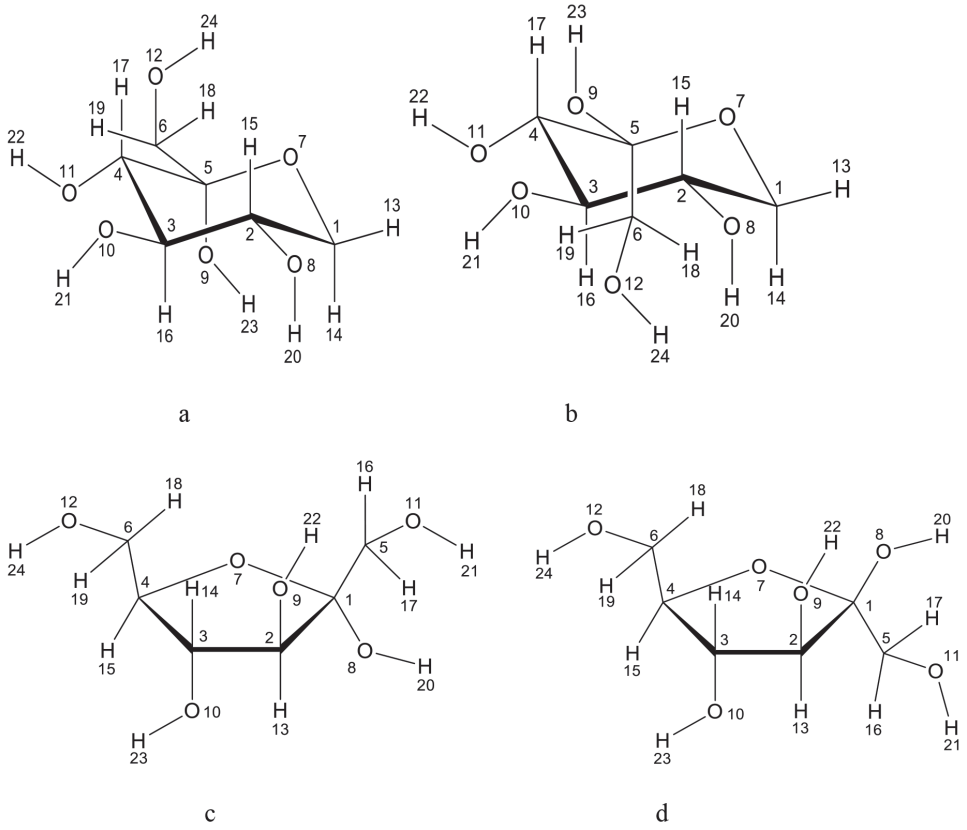

Figure 3. Structure of α- and β-D-fructopyranoses (**a** and **b** respectively) and α- and β-D-fructofuranoses (**c** and **d** respectively) and followed by numbering of atoms.

Properties computed for anomers of D-fructofuranoses are given in Tables 7, 10 and 11 and their visualisation can be seen in Fig. 8.

Corresponding data for D-xylopyranose anomers are provided in Tables 12–14 and visualisation of those data are presented in Fig. 9.

Finally, computations for anomers of D-xylofuranoses are presented in Tables 12, 15 and16. Visualisation of those data is given in Fig. 10.

Discussion

This study focused on recognising effects of SMF upon metabolism of monosaccharides in the organisms of fauna and flora. Particular attention was paid to the effect of SMF of increasing flux density upon the charge density at the atoms being the reaction sites of the selected monosaccharide molecules responsible for initiating the metabolic processes.

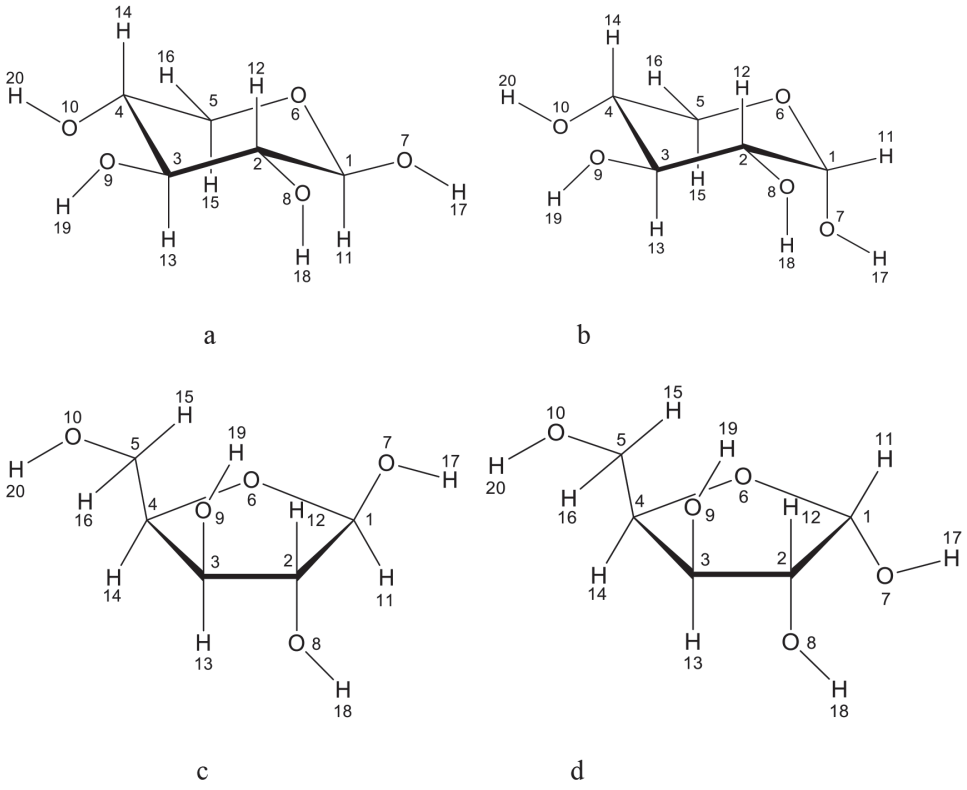

Figure 4. Structure of α- and β-D-xylopyranoses (**a** and **b** respectively) and α- and β-D-xylofuranoses (**c** and **d** respectively) and followed by numbering of atoms.

SMF could perturb the trajectory of bonds forming electrons involving the Lorentz force. Additionally, the stability of the lone and bonding electron pairs resulting from their oppositely-directed magnetic spins could be reduced. Such kind of electron pairs reside in valence bonds and in non-bonding lone electron pairs of the oxygen atoms. One of the two lone electron pairs of the latter atoms should be particularly sensitive to the effect of SMF. SMF could turn hybridisation of that atom from nearly sp^2 to sp^3 proportionally to an increase in the flux density. That effect would influence the electrostatic interactions through space within the molecules.

D-Glucose

This aldohexose resides chiefly in the cyclic form of α- and β-pyranose (Fig. 1). The thermodynamically less stable open-chain molecule spontaneously isomerises into one of two anomeric pyranoses (Tomasik 1997; Tomasik 2007a;, 2007b; Keung and Mehta 2015; Churuangsuk et al. 2018).

Both anomers of D-glucose, that is, α- and β-D-glucose are utilied in organisms of flora and fauna as a main source of energy (Domb et al. 2019). They are directly

Table 2. Charge density [a.u] at particular atoms of the α- and β-D-glucose molecules depending on SMF flux density [AFU].

Atom		Fluxdensity[AFU]				
	Tendency	0	0.1	1.0	10	100
C1	**H1**	**0.421**	**0.428**	**0.430**	**0.435**	**0.434**
	L2	***0.466***	***0.442***	***0.425***	***0.398***	***0.375***
C2	**H3**	**0.094**	**0.108**	**0.126**	**0.148**	**0.156**
	H2	***0.138***	***0.149***	***0.161***	***0.172***	***0.178***
C3	**V**	**0.135**	**0.137**	**0.129**	**0.050**	**0.053**
	V	***0.108***	***0.108***	***0.079***	***0.050***	***0.093***
C4	**V**	**0.176**	**0.179**	**0.181**	**0.153**	**0.164**
	L1	***0.192***	***0.192***	***0.187***	***0.166***	***0.163***
C5	**IL**	**0.121**	**0.121**	**0.124**	**0.076**	**0.067**
	IL	***0.102***	***0.110***	***0.096***	***0.058***	***0.034***
C6	**H3**	**0.004**	**0.010**	**0.036**	**0.371**	**0.427**
	H	***0.009***	***0.027***	***0.139***	***0.374***	***0.460***
O7	**IH**	**-0.639**	**-0.636**	**-0.632**	**-0.620**	**-0.628**
	H2	***-0.631***	***-0.620***	***-0.610***	***-0.598***	***-0.017***
O8	**L2**	**-0.697**	**-0.706**	**-0.715**	**-0.734**	**-0.736**
	H2	***-0.727***	***-0.708***	***-0.702***	**-0.696**	***-0.688***
O9	**IH**	**-0.706**	**-0.708**	**-0.708**	**-0.689**	**-0.683**
	H	***-0.752***	***-0.750***	***-0.740***	***-0.716***	***-0.696***
O10	**IH**	**-0.752**	**-0.745**	**-0.721**	**-0.475**	**-0.551**
	H2	***-0.745***	***-0.712***	***-0.580***	***-0.489***	***-0.634***
O11	**V**	**-0.744**	**-0.741**	**-0.738**	**-0.724**	**-0.740**
	V	***-0.747***	***-0.740***	***-0.735***	***-0.728***	***-0.753***
O12	V	-0.711	-0.715	-0.716	-0.669	-0.651
	H1	*-0.708*	*-0.707*	*-0.702*	*-0.659*	*-0.600*
H13	**V**	**0.174**	**0.173**	**0.172**	**0.184**	**0.187**
	V	***0.150***	***0.147***	***0.155***	***0.169***	***0.172***
H14	**L**	**0.182**	**0.178**	**0.175**	**0.174**	**0.175**
	V	***0.192***	***0.191***	***0.161***	***0.201***	***0.201***
H15	**IH**	**0.200**	**0.201**	**0.204**	**0.241**	**0.240**
	V	***0.155***	***0.153***	***0.164***	***0.172***	***0.134***
H16	**V**	**0.196**	**0.195**	**0.194**	**0.198**	**0.191**
	V	***0.207***	***0.207***	***0.207***	***0.211***	***0.205***
H17	IH	0.186	0.185	0.186	0.228	0.230
	H1	*0.161*	*0.162*	*0.179*	*0.214*	*0.221*
H18	L3	0.155	0.130	0.075	-0.479	-0.493
	L3	*0.156*	*0.093*	*-0.087*	*-0.488*	*-0.434*
H19	IH	0.186	0.183	0.185	0.256	0.278
	H2	*0.186*	*0.183*	*0.197*	*0.257*	*0.513*
H20	H1	0.406	0.409	0.412	0.438	0.439
	V	*0.415*	*0.410*	*0.408*	*0.415*	*0.408*
H21	V	0.395	0.396	0.393	0.393	0.396
	L1	*0.422*	*0.420*	*0.413*	*0.407*	*0.391*
H22	L3	0.405	0.396	0.370	0.120	0.087
	L2	*0.423*	*0.395*	*0.285*	*0.187*	*0.133*
H23	V	0.417	0.417	0.416	0.422	0.433
	V	*0.420*	*0.420*	*0.418*	*0.424*	*0.438*
H24	H2	0.395	0.407	0.421	0.502	0.523
	H2	*0.397*	*0.418*	*0.451*	*0.500*	*0.513*

[a]Data in normal font and in italics are for α- and β-anomers, respectively. Data given in bold are related to the effects at atoms which could be interpreted in details as not perturbed by a free rotation. Notation: H - high, L - low, IH and IL- irregular high and irregular low changes, respectively and V – totally irregular changes of the values. Figures following symbol or L characterise intensity of the change: 1 –weak, 2 – moderate, 3 – very strong.

Table 3. Bond lengths [Å] in the α- and β-D-glucose molecules depending on the applied SMF flux density [AFU][a].

Bond		Flux density [AFU]				
	Tendency	0	0.1	1	10	100
C1-C2	**H1**	**1.530**	**1.536**	**1.554**	**1.579**	**1.587**
	H1	***1.528***	***1.533***	***1.534***	***1.539***	***1.552***
C1-O8	**L1**	**1.413**	**1.413**	**1.408**	**1.389**	**1.394**
	L1	***1.390***	***1.389***	***1.387***	***1.382***	***1.382***
O8-H20	H1	0.972	1.011	1.048	1.041	1.045
	V	*0.972*	*1.058*	*1.020*	*1.062*	*1.028*
C1-H13	**H1**	**1.099**	**1.117**	**1.125**	**1.121**	**1.126**
	H1	***1.100***	***1.194***	***1.169***	***1.164***	***1.156***
C2-C3	**H1**	**1.528**	**1.530**	**1.533**	**1.553**	**1.561**
	H1	***1.526***	***1.532***	***1.545***	***1.552***	***1.547***
C2-O9	**H1**	**1.412**	**1.411**	**1.413**	**1.427**	**1.427**
	H1	***1.412***	***1.416***	***1.417***	***1.424***	***1.431***
O9-H21	V	0.972	1.007	1.004	1.004	0.993
	V	*0.972*	*0.989*	*0.983*	*0.955*	*0.969*
C2-H14	**H1**	**1.099**	**1.147**	**1.153**	**1.155**	**1.149**
	H1	***1.099***	***1.187***	***1.170***	***1.152***	***1.155***
C3-C4	**V**	**1.527**	**1.518**	**1.514**	**1.525**	**1.523**
	V	***1.527***	***1.514***	***1.517***	***1.530***	***1.534***
C3-O10	**V**	**1.412**	**1.416**	**1.423**	**1.381**	**1.397**
	V	***1.412***	***1.419***	***1.3934***	***1.378***	***1.194***
O10-H22	H3	0.972	1.198	1.389	3.084	3.685
	H3	*0.972*	*1.378*	*1.979*	*2.886*	*3.990*
C3-H15	**H1**	**1.099**	**1.115**	**1.132**	**1.127**	**1.134**
	H1	***1.099***	***1.132***	***1.116***	***1.148***	***1.125***
C4-C5	**V**	**1.533**	**1.529**	**1.531**	**1.529**	**1.525**
	V	***1.532***	***1.530***	***1.527***	***1.533***	***1.538***
C4-O11	**H1**	**1.412**	**1.422**	**1.434**	**1.461**	**1.476**
	H1	***1.412***	***1.427***	***1.442***	***1.455***	***1.461***
O11-H23	V	0.972	0.968	0.972	0.964	0.964
	V	*0.972*	*0.969*	*0.957*	*0.977*	*0.970*
C4-H16	**H2**	**1.099**	**1.161**	**1.169**	**1.176**	**1.171**
	H2	***1.099***	***1.187***	***1.168***	***1.140***	***1.153***
C5-C6	H1	1.528	1.531	1.540	1.556	1.570
	H1	*1.528*	*1.532*	*1.538*	*1.553*	*1.559*
C6-O12	IL	1.412	1.392	1.368	1.292	1.298
	IL	*1.412*	*1.375*	*1.328*	*1.287*	*1.309*
O12-H24	H	0.972	0.995	1.011	1.050	1.058
	H	*0.972*	*1.026*	*1.048*	*1.050*	*1.061*
C6-H18	H2	1.099	1.148	1.150	1.168	1.169
	V	*1.099*	*1.184*	*1.204*	*1.175*	*1.189*
C6-H19	H3	1.099	1.262	1.444	2.675	3.259
	H3	*1.099*	*1.410*	*1.771*	*2.656*	*3.742*
C5-O7	**V**	**1.433**	**1.431**	**1.429**	**1.429**	**1.437**
	V	***1.434***	***1.430***	***1.430***	***1.435***	***1.467***
O7-C1	**L1**	**1.433**	**1.414**	**1.392**	**1.387**	**1.375**
	V	***1.432***	***1.402***	***1.3942***	***1.400***	***1.403***

[a]See Table 2 for notation.

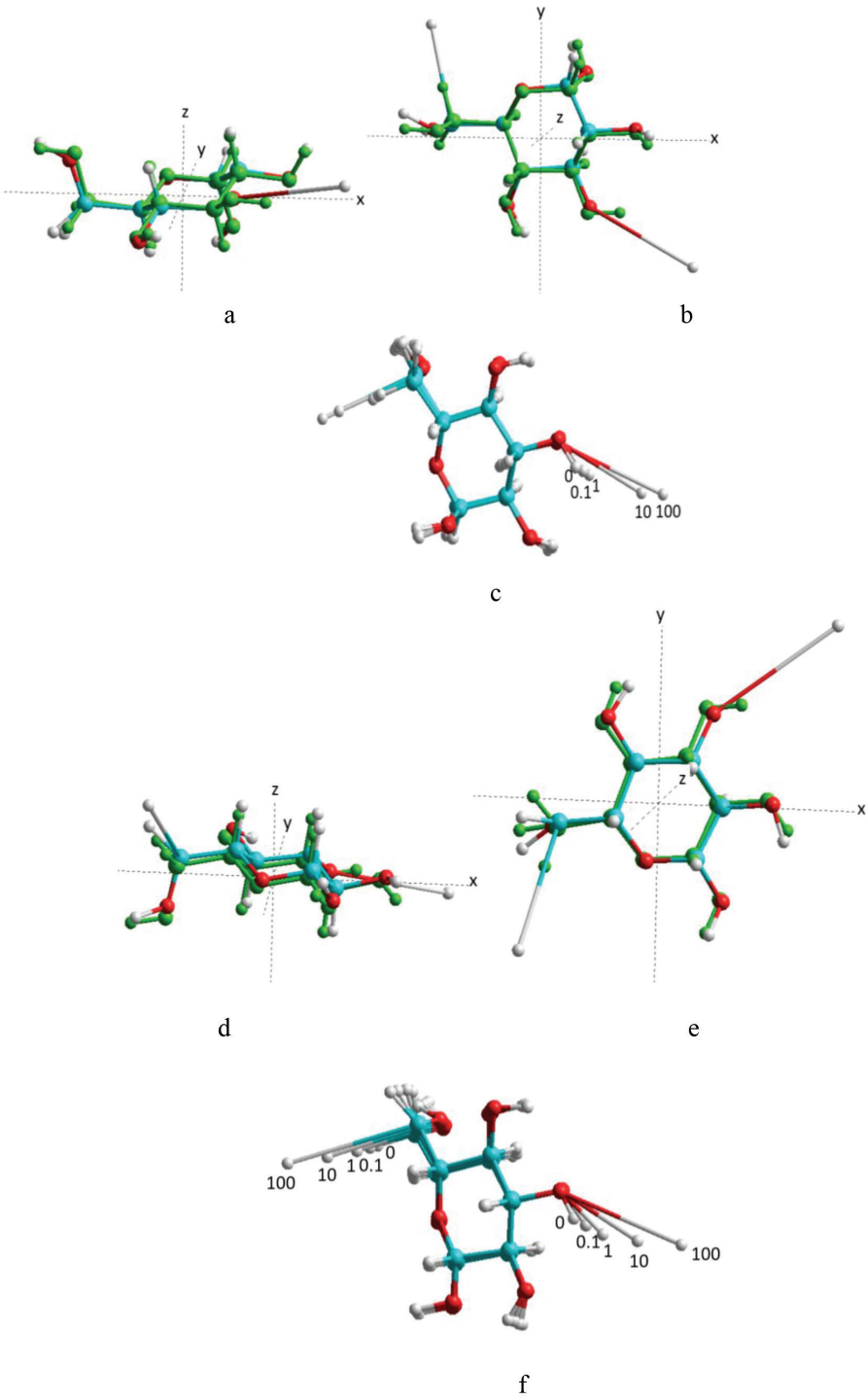

Figure 5. Simplified visualisation of the effect of SMF upon conformation and bond length of α-D- and β-D-glucose anomers (**a–c** and **d–f** respectively), situated in the Cartesian system.

Table 4. Properties of the α- and β-D-galactose molecules situated along the x-axis of the Cartesian system in SMF of the flux density of 0 to 100 AFU.

Property	Anomer	Flux density [AFU]				
		0	0.1	1	10	100
Dipole moment [D]	α	8.63	8.72	8.83	8.93	9.18
	β	8.66	8.72	8.88	8.98	9.32
Heat of formation [kcal/mole]	α	-1286.3	-1285.2	-1267.4	-1206.5	-1128.4
	β	-1252.3	-1251.2	-1247.4	-1198.7	-1111.3

metabolised in the body. In human organisms, that energy is generated chiefly from glycogen stored in the liver. Under specific cases, D-glucose is delivered into organisms as a component of food, for instance, a spice and supplement of diet injected as an additional source of energy (World Health Organization 2019). D-Glucose is metabolised in enzymatic processes. The first step of that process involves its esterification with adenosine-triphosphate (ATP) at the C6-OH group (Heinrich et al. 2014). Within the Entner-Doudoroff pathway operating in Gram-negative bacteria, certain Gram-positive bacteria and archaea begin at the same reaction site engaging the C1 atom (Conway 1992).

One of the important enzymatic reactions of D-glucose, called the Maillard reaction, is known as the enzymatic browning reaction. In the reaction of D-glucose with lysine and arginine, residues of the protein pentosidine are formed (Sell and Monnier 1989). Pentosidine is formed most readily from pentoses, but glucose, fructose and other saccharides may also react in such a manner.

Performed computations showed that, based on the criterion of heat of formation, the α-D-anomer was slightly more stable than the β-D-anomer (Table 1). The stability of both anomers decreased unevenly against the applied SMF flux density. The β-D-anomer reacted more strongly to SMF. It was also associated with a significantly stronger increase in dipole moment. These trends fitted results performed with density functional/*ab initio* computation in silico. The same computations for both anomers of D-glucose in water pointed to the α-D-anomer as more stable than the β-D-anomer (Facundo Ruiz et al. 2005). However, electrochemical oxidation of the α-D-anomer glucose and β-D-anomer on the anode surface showed that the β-D-anomer was much more reactive (Largeaud et al. 1995).

The charge density at particular atoms of both anomers varied irregularly with an increase in the flux density (Table 2). An increase in the SMF flux density produced a more remarkable decrease in the electron density at the 1,2,4,5,6,7,11,12,15 and 20 atoms of the β-anomer than at the same atoms of the α-anomer. Extremely strong, but an opposite effect was noted at the C2 and H21 atoms. Both atoms were bound to one another and the C2 atom was in the vicinity to the endocyclic O7 atom. Thus, observed effects could result from electrostatic interactions through space involving a partially weakened lone electron pair of the oxygen atom. An increase in the electron density produced by SMF was observed at C1β (atom C1, β-anomer), C4β, C5, O8α and H14α atoms, whereas the electron density remarkably decreased at C1α, C2, O7α,

Table 5. Charge density [a.u] at particular atoms of the α- and β-D-glucose molecules depending on SMF flux density [AFU].

Atom		Flux density [AFU]				
	Tendency	0	0.1	1.0	10	100
C1	**V**	**0.447**	**0.456**	**0.452**	**0.439**	**0.399**
	V	***0.448***	***0.436***	***0.426***	***0.431***	***0.398***
C2	**H1**	**0.112**	**0.113**	**0.132**	**0.148**	**0.203**
	IH	***0.191***	***0.197***	***0.200***	***0.185***	***0.210***
C3	**IL**	**0.102**	**0.131**	**0.086**	**0.040**	**0.099**
	L1	***0.112***	***0.111***	***0.090***	***0.045***	***0.077***
C4	**IH**	**0.086**	**0.094**	**0.108**	**0.114**	**0.105**
	V	***0.118***	***0.125***	***0.128***	***0.128***	***0.107***
C5	**L2**	**0.129**	**0.129**	**0.027**	**-0.044**	**-0.112**
	IL	***0.107***	***0.112***	***0.080***	***0.002***	***-0.069***
C6	**H2**	**-0.038**	**-0.043**	**0.212**	**0.310**	**0.483**
	H2	***-0.040***	***-0.062***	***0.001***	***0.249***	***0.476***
O7	**V**	**-0.641**	**-0.641**	**-0.645**	**-0.637**	**-0.641**
	IL	***-0.629***	***-0.626***	***-0.622***	***-0.612***	***-0.623***
O8	**IL**	**-0.714**	**-0.734**	**-0.749**	**-0.749**	**-0.745**
	H1	***-0.698***	***-0.688***	***-0.669***	***-0.668***	***-0.646***
O9	**V**	**-0.747**	**-0.746**	**-0.745**	**-0.742**	**-0.772**
	V	***-0.728***	***-0.721***	***-0.713***	***-0.700***	***-0.733***
O10	**V**	**-0.747**	**-0.758**	**-0.607**	**-0.502**	**-0.712**
	V	***-0.719***	***-0.706***	***-0.665***	***-0.483***	***-0.692***
O11	**H1**	**-0.777**	**-0.769**	**-0.731**	**-0.679**	**-0.608**
	H1	***-0.690***	***-0.685***	***-0.667***	***-0.660***	***-0.617***
O12	H	-0.758	-0.727	-0.677	-0.619	-0.534
	H	*-0.724*	*-0.704*	*-0.674*	*-0.628*	*0.551*
H13	**V**	**0.183**	**0.184**	**0.184**	**0.195**	**0.181**
	V	***0.156***	***0.146***	***0.144***	***0.150***	***0.163***
H14	**V**	**0.190**	**0.181**	**0.182**	**0.190**	**0.183**
	V	***0.220***	***0.219***	***0.218***	***0.228***	***0.210***
H15	**V**	**0.196**	**0.202**	**0.217**	**0.233**	**0.150**
	V	***0.167***	***0.167***	***0.170***	***0.183***	***0.110***
H16	**V**	**0.189**	**0.195**	**0.205**	**0.214**	**0.200**
	H1	***0.185***	***0.186***	***0.192***	***0.205***	***0.209***
H17	**IH**	**0.204**	**0.233**	**0.302**	**0.354**	**0.353**
	H1	***0.174***	***0.179***	***0.195***	***0.236***	***0.267***
H18	H1	0.205	0.204	0.239	0.283	0.301
	IH	*0.182*	*0.166*	*0.169*	*0.214*	*0.283*
H19	L2	0.181	0.093	-0.277	-0.496	-0.315
	L2	*0.163*	*0.158*	*0.040*	*-0.349*	*-0.376*
H20	H1	0.431	0.436	0.443	0.451	0.457
	V	*0.395*	*0.396*	*0.394*	*0.408*	*0.388*
H21	V	0.435	0.433	0.422	0.423	0.434
	H1	*0.411*	*0.412*	*0.412*	*0.413*	*0.420*
H22	IL	0.445	0.449	0.443	0.209	0.078
	IL	*0.394*	*0.379*	*0.339*	*0.179*	*0.105*
H23	L1	0.461	0.446	0.414	0.384	0.325
	L1	*0.398*	*0.394*	*0.382*	*0.374*	*0.339*
H24	H1	0.425	0.438	0.455	0.480	0.487
	H1	*0.409*	*0.411*	*0.427*	*0.472*	*0.524*

[a]See Table 2 for notation.

Table 6. Bond lengths [Å] in the α- and β-D-galactose molecules depending on the applied SMF flux density [AFU][a].

Bond	Tendency	Flux density [AFU]				
		0	0.1	1	10	100
C1-C2	**V**	**1.5120**	**1.528**	**1.551**	**1.542**	**1.551**
	V	***1.540***	***1.543***	***1.560***	***1.556***	***1.551***
C1-O8	**V**	**1.404**	**1.412**	**1.110**	**1.411**	**1.401**
	V	***1.430***	***1.421***	***1.400***	***1.388***	***1.366***
O8-H20	V	0.978	0.974	0.962	0.974	0.966
	IH	*0.960*	*1.011*	*1.071*	*1.026*	*1.096*
C1-H13	**V**	**1.100**	**1.141**	**1.103**	**1.149**	**1.116**
	V	***1.090***	***1.179***	***1.168***	***1.172***	***1.092***
C2-C3	**V**	**1.515**	**1.497**	**1.504**	**1.576**	**1.536**
	V	***1.537***	***1.520***	***1.505***	***1.510***	***1.543***
C2-O9	**V**	**1.408**	**1.390**	**1.386**	**1.390**	**1.410**
	IL	***1.430***	***1.416***	***1.394***	***1.386***	***1.424***
O9-H21	V	0.979	1.003	0.962	0.991	0.955
	V	*0.960*	*1.013*	*1.014*	*0.998*	*0.972*
C2-H14	**V**	**1.100**	**1.189**	**1.171**	**1.212**	**1.166**
	IH	***1.090***	***1.137***	***1.171***	***1.180***	***1.159***
C3-C4	**V**	**1.512**	**1.509**	**1.515**	**1.519**	**1.513**
	V	***1.537***	***1.532***	***1.522***	***1.532***	***1.528***
C3-O10	**V**	**1.407**	**1.490**	**1.380**	**1.364**	**1.381**
	L1	***1.430***	***1.429***	***1.427***	***1.374***	***1.370***
O10-H22	H3	0.922	1.345	2.062	2.947	4.432
	H3	*0.960*	*1.191*	*1.439*	*2.279*	*3.963*
C3-H15	**V**	**1.100**	**1.145**	**1.140**	**1.143**	**1.154**
	IH	***1.090***	***1.117***	***1.139***	***1.121***	***1.144***
C4-C5	**L1**	**1.539**	**1.525**	**1.521**	**1.512**	**1.509**
	IL	***1.540***	***1.535***	***1.534***	***1.532***	***1.533***
C4-O11	**V**	**1.412**	**1.432**	**1.153**	**1.158**	**1.475**
	H1	***1.430***	***1.433***	***1.445***	***1.452***	***1.467***
O11-H23	V	0.982	0.932	1.005	0.932	0.972
	V	*0.960*	*0.938*	*0.995*	*0.927*	*0.960*
C4-H16	**V**	**1.101**	**1.137**	**1.121**	**1.141**	**1.135**
	IH	***1.090***	***1.111***	***1.130***	***1.117***	***1.138***
C5-C6	**IL**	**1.534**	**1.489**	**1.448**	**1.437**	**1.479**
	V	***1.540***	***1.516***	***1.439***	***1.477***	***1.529***
C6-O12	V	1.100	1.543	1.099	1.210	1.123
	V	*1.090*	*1.167*	*1.127*	*1.182*	*1.132*
O12-H24	V	0.975	1.013	0.988	1.033	1.000
	V	*0.960*	*1.021*	*1.031*	*1.080*	*1.081*
C6-H18	L2	1.418	1.404	1.380	1.346	1.339
	L2	*1.430*	*1.417*	*1.374*	*1.314*	*1.274*
C6-H19	H3	1.100	1.108	2.360	3.401	5.114
	H3	*1.090*	*1.201*	*1.659*	*2.450*	*4.717*
C5-H17	**V**	**1.100**	**1.227**	**1.222**	**1.260**	**1.235**
	V	***1.090***	***1.158***	***1.177***	***1.434***	***1.152***
C5-O7	**V**	**1.432**	**1.437**	**1.440**	**1.439**	**1.432**
	V	***1.433***	***1.434***	***1.437***	***1.434***	***1.429***
O7-C1	**V**	**1.431**	**1.420**	**1.419**	**1.428**	**1.430**
	V	***1.433***	***1.430***	***1.427***	***1.442***	***1.456***

[a]See Table 2 for notation.

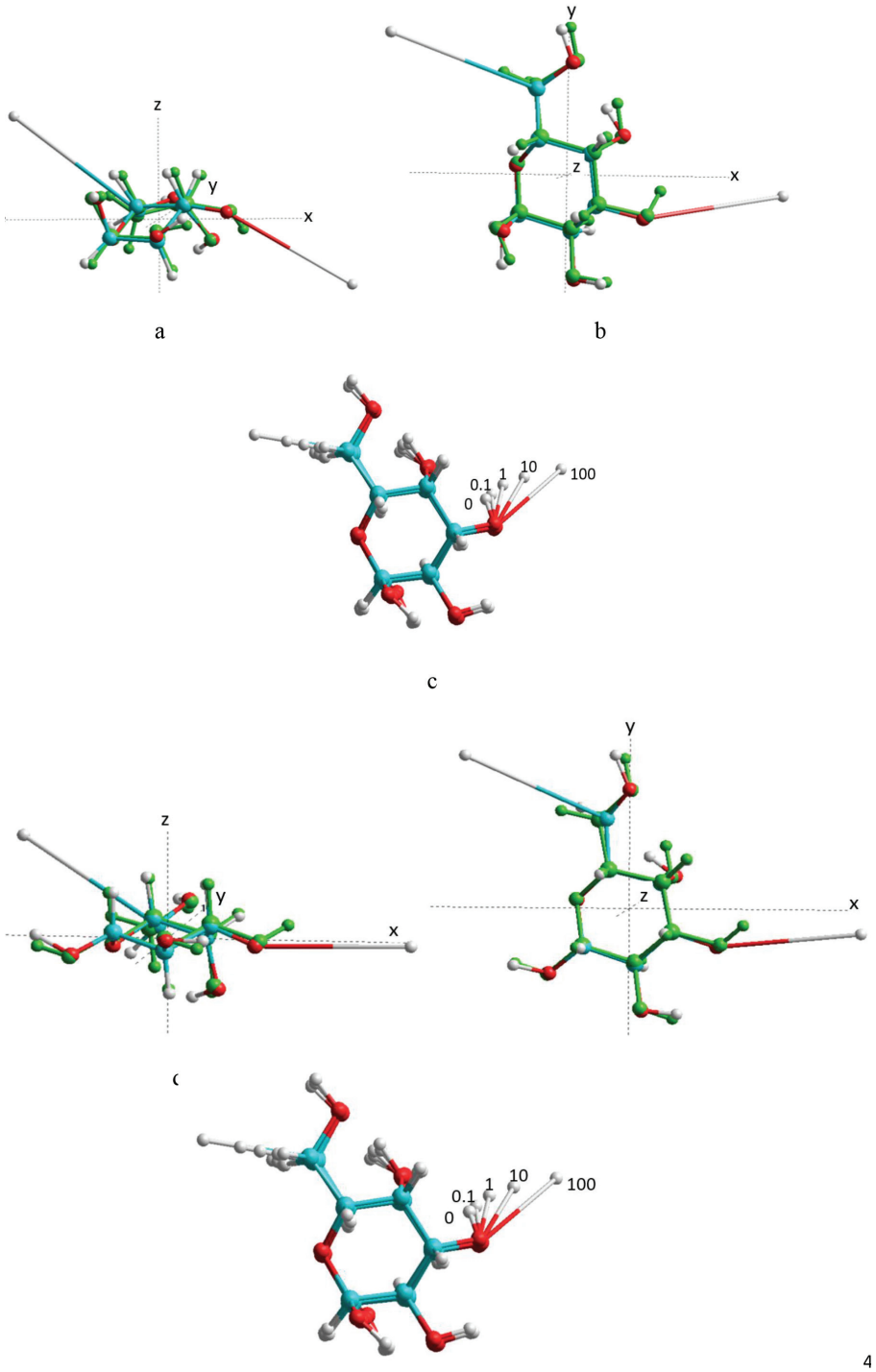

Figure 6. Simplified visualisation of the effect of SMF upon conformation and bond length of α-D- and β-D-galactose anomers (**a–c** and **d–f** respectively), situated in the Cartesian system. (see Fig. 2 for notation).

Table 7. Properties of the α- and β-D-fructopyranose and corresponding α- and β-D-fructofuranose molecules situated along the x-axis of the Cartesian system in SMF of the flux density of 0 to 100 AFU[a].

Property	Anomer	Flux density [AFU]				
		0	0.1	1	10	100
Dipole moment [D]	α-D-Fru*p*	3.63	3.67	3.76	3.93	4.24
	β-D-Fru*p*	3.60	3.61	3.69	3.86	4.16
	α-D-Fru*f*	3.68	3.69	3.87	3.92	4.16
	β-D-Fru*f*	3.66	3.71	3.85	3.90	4.09
Heat of formation [kcal/mole]	α-D-Fru*p*	-1193.2	-1190.4	-1153.8	-1140.6	-1096.5
	β-D-Fru*p*	-1205.5	-1203.2	-1199.9	-1156.7	-1026.5
	α-D-Fru*f*	-1255.6	-1253.5	-1231.5	-1231.5	-1201.8
	β-D-Fru*f*	-1245.6	-1243.5	-1238.6	-1221.4	-1198.5

[a]Upper and lower values (in italics) are for α- and β-isomers, respectively.

O7β, O8β, O9, O10 and H15α atoms. Small and irregular changes of electron density could be observed at C3, C4α, O11, H13, H14β, H15β and H16 atoms. Remarkable changes were noted at the C1, C5 and C2 atoms.

In fact, in a real molecule, all hydrogen atoms of the OH groups changed their positions by free rotation because of the practically identical energy between particular rotamers of those groups. This problem was well illustrated by the results of computation for the twin hydrogen H18 and H19 atoms. Due to accepted computation methodology, the free rotation around the C5-C6 bond was eliminated. In consequence, the H18 atom holds a considerable negative charge, whereas the H19 atom took increased positive charge density. As a result, results of the computations for particular rotamers could not be interpreted in detail in this case as well as in the cases of subsequently discussed carbohydrates. For D-glucose, these restrictions were also valid for the H20, H21, H22, H23, H24 and O12 atoms. Results of detailed analysis of the remaining O7, O8, O9, O10, O11, C1, C2, C3, C4, C5, C6, H13, H14, H15 and H16 atoms are identified in Table 2.

Generally, atoms of the pyranose skeleton were moderately sensitive to SMF, although increasing SMF flux density considerably decreased basicity of the ring O5 atom in the β-anomer. The O and H atoms were the most and least sensitive, respectively, to the effect of SMF. In the group bound to the C3 atom perpendicularly to the field, an increase in the flux density decreased the negative charge density at the O10 atom and the positive charge density at the H22 atom. It suggested a decrease in the acidity of that group. In the quasi-parallel orientated O8-H20 group, SMF evoked the opposite effect. Thus, the accepted orientation of the molecule under consideration appeared very essential. One of the biochemically most important OH group at the C6 atom turned more acidic and that effect could noticeably influence the biochemistry of D-glucose.

Review of Table 2 also identified that increased positive charge density at the C1 in the α-anomer favoured attacks of various Lewis bases at this position. Such reactions were also important from the biochemical point of view. Simultaneously, the reactivity of the β-anomer involving this position was partly inhibited as the positive

Table 8. Charge density [a.u] at particular atoms of the α- and β-D-glucose molecules depending on SMF flux density [AFU].

Atom		Flux density [AFU]				
	Tendency	0	0.1	1.0	10	100
C1	**H3**	**-0.049**	**-0.068**	**0.048**	**0.147**	**0.275**
	H3	***-0.027***	***-0.036***	***-0.018***	***0.131***	***0.493***
C2	**H2**	**0.118**	**0.159**	**0.166**	**0.169**	**0.173**
	L2	***0.103***	***0.098***	***0.098***	***0.062***	***-0.027***
C3	**V**	**0.098**	**0.051**	**0.052**	**0.050**	**0.052**
	V	***0.130***	***0.145***	***0.146***	***0.131***	***0.089***
C4	**IL**	**0.160**	**0.084**	**0.076**	**0.071**	**0.096**
	V	***0.175***	***0.185***	***0.144***	***0.117***	***0.179***
C5	**V**	**0.541**	**0.576**	**0.552**	**0.552**	**0.487**
	V	***0.522***	***0.547***	***0.550***	***0.525***	***0.481***
C6	**IL**	**0.015**	**-0.068**	**-0.044**	**-0.046**	**-0.002**
	H1	***-0.025***	***-0.021***	***0.015***	***0.027***	***0.032***
O7	**V**	**-0.578**	**-0.578**	**-0.570**	**-0.561**	**-0.540**
	V	***-0.598***	***-0.598***	***-0.607***	***-0.586***	***-0.568***
O8	**L**	**-0.699**	**-0.709**	**-0.733**	**-0.741**	**-0.758**
	IH	***-0.705***	***-0.701***	***-0.700***	***-0.691***	***-0.661***
O9	**H1**	**-0.751**	**-0.709**	**-0.688**	**-0.688**	**-0.683**
	H1	***-0.748***	***-0.743***	***-0.715***	***-0.693***	***-0.668***
O10	**V**	**-0.734**	**-0.463**	**-0.453**	**-0.472**	**-0.586**
	IH	***-0.752***	***-0.709***	***-0.563***	***-0.434***	***-0.572***
O11	**V**	**-0.676**	**-0.635**	**-0.631**	**-0.643**	**-0.639**
	V	***-0.728***	***-0.744***	***-0.751***	***-0.740***	***-0.754***
O12	H2	-0.691	-0.660	-0.662	-0.657	-0.540
	IL	*-0.694*	*-0.697*	*-0.690*	*-0.713*	*-0.725*
H13	**H2**	**0.180**	**0.210**	**0.245**	**0.260**	**0.289**
	V	***0.212***	***0.210***	***0.202***	***0.222***	***0.272***
H14	**L1**	**0.208**	**0.171**	**-0.048**	**-0.175**	**-0.260**
	IL	***0.192***	***0.194***	***0.188***	***-0.011***	***-0.329***
H15	**H1**	**0.171**	**0.178**	**0.196**	**0.201**	**0.206**
	IH	***0.169***	***0.161***	***0.162***	***0.184***	***0.212***
H16	**V**	**0.166**	**0.194**	**0.194**	**0.193**	**0.191**
	V	***0.176***	***0.172***	***0.171***	***0.185***	***0.187***
H17	**V**	**0.228**	**0.234**	**0.235**	**0.240**	**0.229**
	IH	***0.239***	***0.234***	***0.248***	***0.261***	***0.281***
H18	V	0.165	0.157	0.149	0.146	0.179
	V	*0.121*	*0.094*	*0.089*	*0.133*	*0.174*
H19	V	0.159	0.200	0.202	0.212	0.142
	V	*0.198*	*0.196*	*0.198*	*0.184*	*0.180*
H20	H2	0.360	0.422	0.434	0.446	0.467
	V	*0.413*	*0.413*	*0.408*	*0.414*	*0.424*
H21	V	0.386	0.413	0.411	0.423	0.420
	V	*0.415*	*0.421*	*0.415*	*0.417*	*0.428*
H22	V	0.418	0.116	0.099	0.110	0.130
	L2	*0.405*	*0.359*	*0.195*	*0.045*	*0.024*
H23	V	0.416	0.316	0.358	0.372	0.387
	V	*0.407*	*0.412*	*0.402*	*0.406*	*0.430*
H24	V	0.390	0.363	0.372	0.372	0.375
	H2	*0.198*	*0.408*	*0.411*	*0.418*	*0.427*

aSee Table 2 for notation.

Table 9. Bond lengths [Å] in the α- and β-D-fructopyranose molecules depending on the applied SMF flux density [AFU][a].

Bond	Flux density [AFU]					
	Tendency	0	0.1	1	10	100
C1-C2	**V**	**1.540**	**1.575**	**1.561**	**1.563**	**1.571**
	V	***1.540***	***1.537***	***1.545***	***1.530***	***1.516***
C1-H13	**H3**	**1.090**	**1.562**	**2.053**	**2.481**	**3.678**
	H3	***1.090***	***1.240***	***1.323***	***1.936***	***3.435***
C1-H14	**V**	**1.090**	**1.091**	**1.145**	**1.006**	**1.172**
	V	***1.090***	***1.102***	***1.116***	***1.126***	***1.100***
C2-C3	**V**	**1.537**	**1.559**	**1.544**	**1.568**	**1.519**
	V	***1.537***	***1.531***	***1.546***	***1.544***	***1.541***
C2-O8	**H1**	**1.430**	**1.433**	**1.437**	**1.437**	**1.439**
	H1	***1.430***	***1.435***	***1.435***	***1.445***	***1.473***
O8-H20	V	0.960	1.026	0.968	1.026	1.017
	V	*0.960*	*0.952*	*1.050*	*0.985*	*1.030*
C2-H15	**V**	**1.090**	**1.252**	**1.190**	**1.217**	**1.234**
	V	***1.090***	***1.217***	***1.178***	***1.215***	***1.198***
C3-C4	**V**	**1.537**	**1.562**	**1.570**	**1.568**	**1.566**
	IH	***1.537***	***1.546***	***1.564***	***1.571***	***1.524***
C3-O10	**V**	**1.430**	**1.470**	**1.415**	**1.394**	**1.389**
	IL	***1.430***	***1.396***	***1.370***	***1.371***	***1.368***
O10-H21	V	0.960	0.986	0.916	1.017	0.907
	V	*0.960*	*0.971*	*0.929*	*0.954*	*0.993*
C3-H16	**V**	**1.090**	**1.193**	**1.137**	**1.202**	**1.173**
	V	***1.090***	***1.127***	***1.113***	***1.122***	***1.1103***
C4-C5	**H1**	**1.540**	**1.621**	**1.622**	**1.627**	**1.628**
	H1	***1.540***	***1.547***	***1.560***	***1.575***	***1.598***
C4-O11	**V**	**1.430**	**1.547**	**1.527**	**1.522**	**1.517**
	V	***1.430***	***1.447***	***1.446***	***1.427***	***1.444***
O11-H22	H3	0.960	2.268	2.928	3.341	3.781
	H3	*0.960*	*1.333*	*1.972*	*2.847*	*4.491*
C4-H17	**V**	**1.090**	**1.137**	**1.110**	**1.137**	**1.116**
	V	***1.090***	***1.099***	***1.410***	***1.087***	***1.083***
C5-C6	**V**	**1.540**	**1.638**	**1.596**	**1.580**	**1.526**
	IH	***1.540***	***1.516***	***1.560***	***1.567***	***1.570***
C5-O9	**IL**	**1.430**	**1.374**	**1.364**	**1.354**	**1.356**
	V	***1.090***	***1.430***	***1.458***	***1.456***	***1.445***
O9-H23	V	0.960	1.035	0.910	1.016	0.897
	V	*0.960*	*1.013*	*0.913*	*0.982*	*1.022*
C6-O12	V	1.430	1.556	1.471	1.435	1.423
	IL	*1.430*	*1.413*	*1.378*	*1.388*	*1.375*
O12-H24	V	0.960	0.963	0.932	0.974	0.928
	V	*0.960*	*0.906*	*0.988*	*0.967*	*0.912*
C6-H18	V	0.960	1.101	1.119	1.080	1.111
	IL	*1.960*	*1.134*	*1.083*	*1.163*	*1.167*
C6-H19	H2	1.090	1.128	1.154	1.157	1.569
	V	*1.090*	*1.184*	*1.205*	*1.107*	*1.170*
C5-O7	**V**	**1.433**	**1.387**	**1.397**	**1.393**	**1.416**
	V	***1.432***	***1.417***	***1.392***	***1.402***	***1.400***
O7-C1	**IH**	**1.433**	**1.467**	**1.477**	**1.485**	**1.462**
	V	***1.433***	***1.454***	***1.481***	***1.470***	***1.470***

[a]See Table 2 for notation.

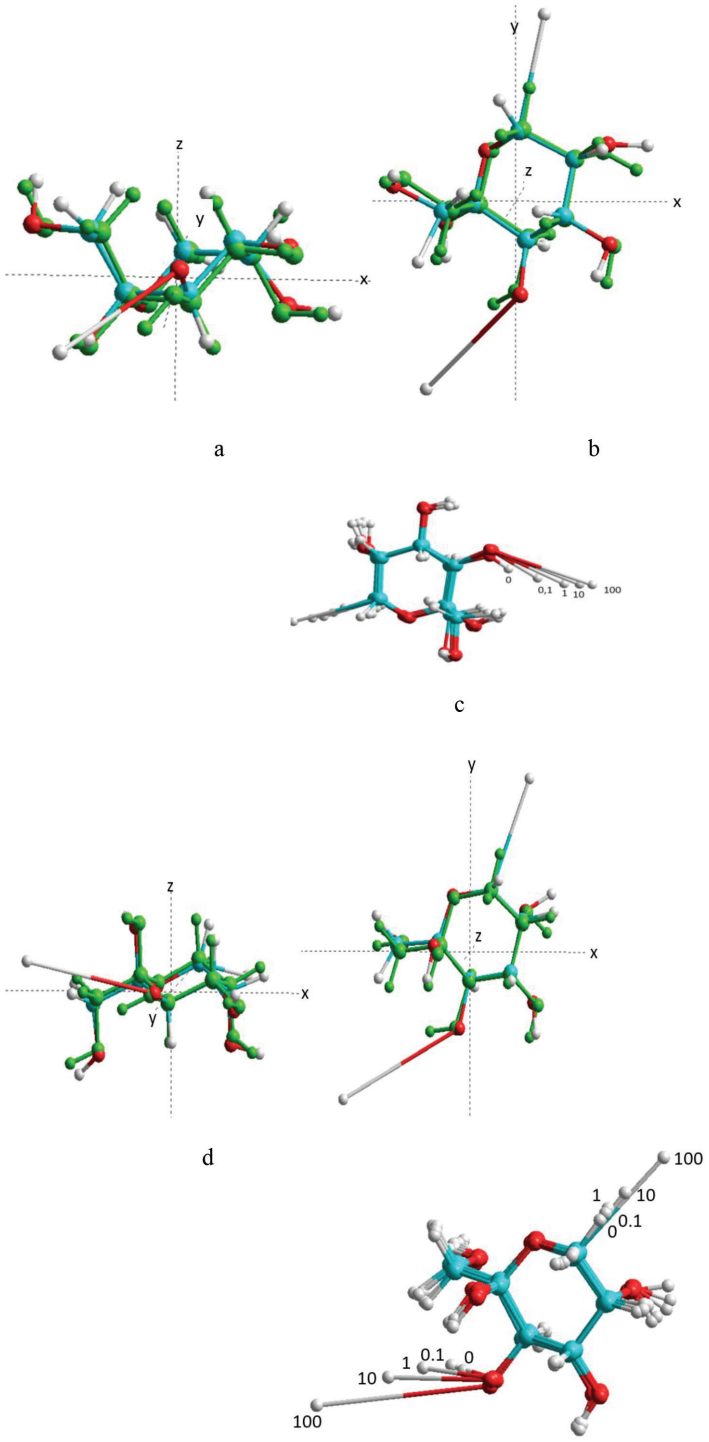

Figure 7. Simplified visualisation of the effect of SMF upon conformation and bond length of α-D- and β-D-fructopyranose anomers (**a–c** and **d–f** respectively), situated in the Cartesian system (see Fig. 2 for notation).

Table 10. Charge density [a.u] at particular atoms of the α- and β-D-glucose molecules depending on SMF flux density [AFU].

Atom	Flux density [AFU]					
	Tendency	0	0.1	1.0	10	100
C1	**IL**	**0.521**	**0.528**	**0.523**	**0.499**	**0.464**
	H2	***0.508***	***0.561***	***0.581***	***0.617***	***0.714***
C2	**L2**	**0.020**	**0.002**	**-0.012**	**-0.022**	**-0.037**
	IL	***0.155***	***0.118***	***0.080***	***0.058***	***0.059***
C3	**V**	**0.129**	**0.129**	**0.124**	**0.121**	**0.189**
	IL	***0.116***	***0.104***	***0.111***	***0.086***	***-0.005***
C4	**H1**	**0.115**	**0.122**	**0.128**	**0.130**	**0.140**
	L1	***0.092***	***0.080***	***0.079***	***0.071***	***0.032***
C5	**IH**	**0.097**	**0.086**	**0.109**	**0.206**	**0.405**
	L2	***0.034***	***0.015***	***-0.002***	***-0.023***	***-0.143***
C6	**IL**	**0.035**	**0.035**	**0.027**	**-0.016**	**-0.063**
	IL	***-0.006***	***-0.019***	***-0.038***	***-0.023***	***-0.038***
O7	**V**	**-0.589**	**-0.597**	**-0.604**	**-0.511**	**-0.620**
	V	***-0.625***	***-0.634***	***-0.676***	***-0.658***	***-0.642***
O8	**H1**	**-0.656**	**-0.639**	**-0.628**	**-0.625**	**-0.560**
	V	***-0.711***	***-0.718***	***-0.665***	***-0.686***	***-0.469***
O9	**IL**	**-0.712**	**-0.696**	**-0.670**	**-0.641**	**-0.680**
	H2	***-0.741***	***-0.714***	***-0.686***	***-0.588***	***-0.380***
O10	**IH**	**-0.711**	**-0.691**	**-0.677**	**-0.670**	**-0.680**
	IH	***-0.734***	***-0.712***	***-0.714***	***-0.699***	***-0.667***
O11	H1	-0.674	-0.641	-0.620	-0.605	-0.580
	H1	*-0.700*	*-0.702*	*-0.690*	*-0.675*	*-0.607*
O12	H2	-0.696	-0.682	-0.644	-0.500	-0.359
	IH	*-0.743*	*-0.724*	*-0.709*	*-0.722*	*-0.699*
H13	**H1**	**0.217**	**0.219**	**0.222**	**0.228**	**0.245**
	IL	***0.235***	***0.228***	***0.205***	***0.221***	***-0.218***
H14	**H1**	**0.180**	**0.182**	**0.184**	**0.188**	**0.189**
	IH	***0.184***	***0.182***	***0.192***	***0.198***	***0.259***
H15	**H1**	**0.205**	**0.205**	**0.207**	**0.212**	**0.225**
	V	***0.196***	***0.202***	***0.187***	***0.200***	***0.202***
H16	H1	0.167	0.170	0.178	0.196	0.244
	V	*0.173*	*0.164*	*0.139*	*0.076*	*0.190*
H17	L2	0.104	0.064	-0.004	-0.148	-0.470
	H1	*0.182*	*0.183*	*0.196*	*0.200*	*0.212*
H18	VI	0.169	0.161	0.159	0.175	0.248
	H	*0.173*	*0.176*	*0.202*	*0.194*	*0.217*
H19	V	0.148	0.142	0.143	0.154	0.171
	V	*0.173*	*0.159*	*0.174*	*0.162*	*0.179*
H20	V	0.365	0.364	0.366	0.374	0.388
	V	*0.415*	*0.433*	*0.451*	*0.408*	*0.124*
H21	H2	0.389	0.395	0.402	0.419	0.454
	V	*0.397*	*0.405*	*0.396*	*0.416*	*0.419*
H22	L2	0.387	0.373	0.355	0.341	0.295
	L2	*0.401*	*0.394*	*0.385*	*0.304*	*0.244*
H23	V	0.403	0.400	0.397	0.398	0.407
	V	*0.414*	*0.410*	*0.398*	*0.397*	*0.401*
H24	L3	0.388	0.373	0.335	0.198	0.005
	V	*0.412*	*0.411*	*0.404*	*0.410*	*0.416*

[a]See Table 2 for notation.

Table 11. Bond lengths [Å] in the α- and β-D-fructofuranose molecules depending on the applied SMF flux density [AFU][a].

Bond		Flux density [AFU]				
	tendency	0	0.1	1	10	100
C1-C2	**H1**	**1.540**	**1.549**	**1.559**	**1.570**	**1.592**
	H3	***1.539***	***1.624***	***1.847***	***2.084***	***2.422***
C1-O8	**V**	**1.413**	**1.408**	**1.406**	**1.406**	**1.409**
	V	***1.430***	***1.365***	***1.273***	***1.304***	***1.225***
O8-H20	H1	0.960	0.955	0.970	0.978	0.985
	H3	*0.960*	*0.994*	*1.155*	*1.183*	*1.783*
C1-C5	**L1**	**1.535**	**1.521**	**1.511**	**1.502**	**1.495**
	IL	***1.540***	***1.527***	***1.509***	***1.473***	***1.485***
C5-O11	IH	1.412	1.389	1.586	1.376	1.848
	V	*1.430*	*1.439*	*1.442*	*1.421*	*1.370*
O11-H21	V	0.960	0.960	0.970	0.978	0.995
	V	*0.960*	*0.992*	*0.982*	*0.961*	*1.001*
C5-H16	V	1.091	1.151	1.150	1.121	1.112
	V	*1.090*	*1.145*	*1.132*	*1.128*	*1.132*
C5-H17	H3	1.091	1.365	1.586	1.936	2.922
	V	*1.090*	*1.337*	*1.242*	*1.358*	*1.255*
C2-C3	**V**	**1.523**	**1.514**	**1.513**	**1.519**	**1.541**
	IL	***1.539***	***1.536***	***1.497***	***1.477***	***1.522***
C2-O9	**V**	**1.412**	**1.422**	**1.427**	**1.426**	**1.395**
	V	***1.430***	***1.398***	***1.327***	***1.298***	***1.177***
O9-H22	H3	0.959	1.173	1.322	1.487	2.036
	H3	*0.960*	*1.063*	*1.069*	*1.322*	*3.213*
C2-H13	H1	1.092	1.109	1.120	1.124	1.153
	V	*1.090*	*1.172*	*1.142*	*1.131*	*1.153*
C3-C4	**IL**	**1.524**	**1.517**	**1.514**	**1.511**	**1.515**
	H1	***1.540***	***1.544***	***1.596***	***1.601***	***1.610***
C3-O10	**IL**	**1.412**	**1.398**	**1.390**	**1.386**	**1.399**
	H2	***1.430***	***1.945***	***1.533***	***1.577***	***1.614***
O10-H23	V	0.960	1.000	1.000	0.983	0.946
	V	*0.960*	*0.971*	*0.986*	*1.001*	*0.995*
C3-H14	**H1**	**1.091**	**1.103**	**1.131**	**1.146**	**1.178**
	V	***1.090***	***1.453***	***1.119***	***1.132***	***1.106***
C4-O7	**H1**	**1.414**	**1.416**	**1.425**	**1.441**	**1.465**
	V	***1.431***	***1.421***	***1.420***	***1.420***	***1.432***
C4-C6	**IH**	**1.531**	**1.532**	**1.536**	**1.540**	**1.5397**
	V	***1.540***	***1.558***	***1.539***	***1.561***	***1.557***
C4-H15	**H1**	**1.092**	**1.142**	**1.166**	**1.172**	**1.198**
	V	***1.090***	***1.207***	***1.079***	***1.069***	***1.036***
C6-O12	IL	1.411	1.417	1.410	1.391	1.360
	V	*1.430*	*1.450*	*1.580*	*1.499*	*1.505*
O12-H24	H3	0.960	1.166	1.378	1.902	3.080
	V	*0.960*	*0.990*	*0.961*	*0.927*	*0.958*
C6-H18	V	1.090	1.134	1.132	1.122	1.122
	V	*1.090*	*1.273*	*1.143*	*1.233*	*1.201*
C6-H19	H2	1.098	1.190	1.246	1.257	1.290
	IH	*1.090*	*1.139*	*1.147*	*1.139*	*1.155*
O7-C1	**L1**	**1.421**	**1.420**	**1.420**	**1.417**	**1.409**
	V1	***1.431***	***1.457***	***1.437***	***1.402***	***1.412***

[a]See Table 2 for notation.

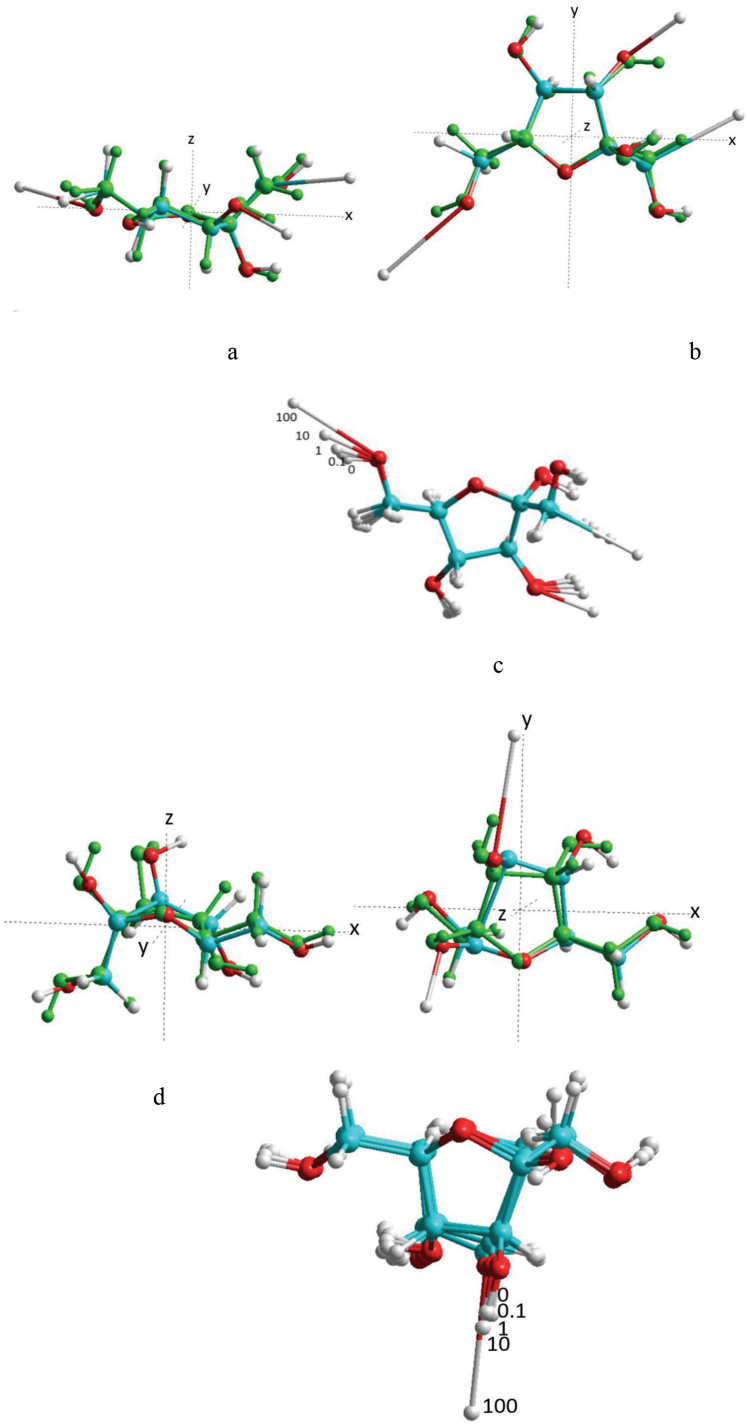

Figure 8. Simplified visualisation of the effect of SMF upon conformation and bond length of α-D- and β-D-fructofuranose anomers (**a–c** and **d–f** respectively), situated in the Cartesian system (see Fig. 2 for notation).

Table 12. Properties of the α- and β-D-xylose molecules situated along the x-axis of the Cartesian system in SMF of the flux density of 0 to 100 AFU[a].

Property	Anomer	Flux density [AFU]				
		0	**0.1**	**1**	**10**	**100**
Dipole moment [D]	α-D-Xyl*p*	4.22	4.24	4.31	4.67	4.73
	β-D-Xyl*p*	1.22	1.23	1.29	1.37	1.47
	α-D-Xyl*f*	4.85	4.89	4.94.	5.15	5.69
	β-D-Xyl*f*	4.87	4.89	4.95	5.01	5.19
Heat of formation [kcal/mole]	α-D-Xyl*p*	-1143.2	-1127.4	-1089.6	-1061.2	-1005.4
	β-D-Xyl*p*	-1154.2	1147.3	-1110.3	-1089.5	-1021.8
	α-D-Xyl*f*	-1076.2	—1075.4	-1069.4	-1041.3	-995.6
	β-D-Xyl*f*	-1051.2	-1049.5	-1036.4	-1004.4	-952.3

[a]Upper and lower values (in italics) are for α- and β-isomers, respectively.

charge density at this atom declined under the influence of SMF. The SMF induced an increase in the positive charge density at the C6 atom. It was non-beneficial for enzymatic processes starting from esterification with adenosine-triphosphate (ATP) at C6-O24 and the functioning of the Entner-Doudorff metabolic pathway (Conway 1992).

An insight into the effect of SMF upon the length of bonds in the molecules of both anomers (Table 3) suggested that these changes resulted from a deformation of the molecules and their deviation from the initially-established location of the molecules along the x-axis. Tendencies of the changes of computed values with an increase in the flux density (Table 3) pointed to a uniform increase in the length of the valence bonds, that is, to weakening their energy. Simultaneously, strongly polarised bonds, with participation of the C1 atom, were regularly shortened, whereas the length of the C3-C4, C3-O10, C3-C5 and C5-O7 bonds varied irregularly. Generally, in the 28 analysed bonds in each anomer, 16 bonds were elongated, four bonds were shortened and the length of eight bonds varied irregularly against increased SMF flux density. These results supported the hypothesis on the weakening of the bonding electron pair. The SMF generated shortening of the C1-O8 bond and elongation of the O8-H20 bond seemed to be the most important. This effect implied the increased susceptibility of the hemi-acetal ring to its opening. Hence, SMF should favour a shift of the mutarotation equilibrium towards the open chain form of D-glucose. This fact could promote the Maillard reaction which proceeds on the open chain forms of saccharides (Grandhee and Monnier 1991).

Visualisation of the data from Table 3 (Fig. 5) also includes non-analysable bonds. The conformation of particular anomers is presented in the form of superposition of the molecules without SMF (green colour) and molecules in the SMF of 100 AFU (blue colour). The oxygen atoms are marked red. Structures *a* and *d* are given as the projection along the *y*-axis, whereas the *b* and *e* structures are projections along the *z*-axis. Structures *c* and *f* are superpositions of the same molecules demonstrating the SMF flux density-dependent change in the bond lengths in the molecules under consideration. Structures in Fig. 5 demonstrate a small effect of SMF upon the conformation of both anomers and a significant effect upon the bond lengths of some peripheral

Table 13. Charge density [a.u] at particular atoms of the α- and β-D-glucose molecules depending on SMF flux density [AFU].

Atom		Flux density [AFU]				
	Tendency	0	0.1	1.0	10	100
C1	**H2**	**0.388**	**0.400**	**0.424**	**0.450**	**0.460**
	V	***0.474***	***0.476***	***0.460***	***0.478***	***0.492***
C2	**L2**	**0.093**	**0.085**	**0.035**	**-0.039**	**-0.059**
	L2	***0.087***	***0.058***	***0.057***	***-0.032***	***-0.055***
C3	**V**	**0.191**	**0.191**	**0.130**	**0.142**	**0.134**
	V	***0.119***	***0.117***	***0.108***	***0.110***	***0.109***
C4	**IH**	**0.142**	**0.145**	**0.161**	**0.172**	**0.167**
	IH	***0.163***	***0.179***	***0.195***	***0.215***	***0.196***
C5	**H2**	**-0.042**	**-0.038**	**-0.029**	**0.010**	**0.125**
	H2	***-0.059***	***-0.048***	***-0.058***	***-0.040***	***0.066***
O6	**V**	**-0.602**	**-0.603**	**-0.568**	**-0.560**	**-0.605**
	V	***-0.590***	***-0.590***	***-0.585***	***-0.569***	***-0.577***
O7	**V**	**-0.695**	**-0.697**	**-0.749**	**-0.682**	**-0.704**
	V	***-0.683***	***-0.665***	***-0.661***	***-0.653***	***-0.674***
O8	**H2**	**-0.735**	**-0.730**	**-0.649**	**-0.522**	**-0.508**
	H2	***-0.726***	***-0.703***	***-0.684***	***-0.494***	***-0.485***
O9	**H1**	**-0.751**	**-0.745**	**-0.719**	**-0.717**	**-0.714**
	H1	***-0.743***	***-0.727***	***-0.721***	***-0.706***	***-0.706***
O10	**V**	**-0.728**	**-0.726**	**-0.725**	**-0.748**	**-0.768**
	V	***-0.730***	***-0.729***	***-0.731***	***-0.748***	***-0.765***
H11	**IH**	**0.160**	**0.161**	**0.166**	**0.193**	**0.190**
	V	***0.160***	***0.160***	***0.156***	***0.166***	***0.172***
H12	**V**	**0.188**	**0.187**	**0.185**	**0.200**	**0.200**
	V	***0.197***	***0.196***	***0.195***	***0.201***	***0.202***
H13	**V**	**0.191**	**0.191**	**0.194**	**0.206**	**0.201**
	V	***0.176***	***0.175***	***0.173***	***0.186***	***0.190***
H14	**V**	**0.169**	**0.164**	**0.161**	**0.182**	**0.205**
	V	***0.180***	***0.173***	***0.176***	***0.183***	***0.196***
H15	**V**	**0.228**	**0.224**	**0.234**	**0.071**	**0.258**
	V	***0.208***	***0.206***	***0.208***	***0.194***	***0.239***
H16	**V**	**0.194**	**0.193**	**0.201**	**0.188**	**-0.062**
	V	***0.181***	***0.168***	***0.177***	***0.105***	***-0.037***
H17	V	0.410	0.405	0.373	0.386	0.396
	V	*0.367*	*0.355*	*0.345*	*0.353*	*0.369*
H18	IL	0.398	0.392	0.335	0.238	0.230
	L1	*0.383*	*0.366*	*0.353*	*0.203*	*0.202*
H19	V	0.415	0.415	0.413	0.407	0.412
	V	*0.419*	*0.416*	*0.414*	*0.411*	*0.413*
H 20	IH	0.414	0.414	0.426	0.423	0.443
	IH	*0.417*	*0.415*	*0.420*	*0.435*	*0.445*

[a]See Table 2 for notation.

C-H bonds. They are the C6-H19 and O10-H22 bonds. An increasing flux density generated a considerable negative charge density at the H18 atom. It made the O12-H24 bond relatively slightly polarised, that is, capable of interaction of electrons of that bond with SMF.

Table 14. Bond lengths [Á] in the α- and β-D-xylopyranose molecules depending on the applied SMF flux density [AFU][a].

Bond		Flux density [AFU]				
	Tendency	0	0.1	1	10	100
C1-C2	**V**	**1.540**	**1.559**	**1.553**	**1.538**	**1.573**
	V	***1.540***	***1.555***	***1.535***	***1.567***	***1.562***
C1-O7	**V**	**1.430**	**1.476**	**1.603**	**1.523**	**1.497**
	V	***1.430***	***1.433***	***1.430***	***1.409***	***1.416***
O7-H17	V	0.960	0.965	0.952	0.956	0.953
	V	*0.960*	*0.971*	*0.968*	*0.964*	*0.951*
C1-H11	**V**	**1.090**	**1.119**	**1.149**	**1.097**	**1.124**
	V	***1.090***	***1.146***	***1.160***	***1.149***	***1.153***
C2-O8	**V**	**1.430**	**1.500**	**1.516**	**1.388**	**1.425**
	V	***1.430***	***1.504***	***1.523***	***1.403***	***1.431***
O8-H18	H3	0.960	1.226	1.565	2.366	3.116
	H3	*0.960*	*1.220*	*1.358*	*2.532*	*3.116*
C2-H12	**V**	**1.090**	**1.128**	**1.159**	**1.124**	**1.139**
	H1	***1.090***	***1.128***	***1.135***	***1.135***	***1.136***
C2-C3	**IH**	**1.538**	**1.542**	**1.580**	**1.511**	**1.584**
	IH	***1.537***	***1.567***	***1.583***	***1.602***	***1.597***
C3-O9	**V**	**1.430**	**1.404**	**1.379**	**1.407**	**1.393**
	V	***1.430***	***1.398***	***1.394***	***1.397***	***1.393***
O9-H19	V	0.960	0.957	0.952	0.953	0.953
	V	*0.960*	*0.958*	*0.958*	*0.958*	*0.952*
C3-H13	**V**	**1.090**	**1.127**	**1.152**	**1.125**	**1.145**
	V	***1.090***	***1.132***	***1.135***	***1.144***	***1.140***
C3-C4	**V**	**1.537**	**1.609**	**1.652**	**1.622**	**1.630**
	V	***1.537***	***1.614***	***1.640***	***1.603***	***1.624***
C4-O10	V	1.430	1.408	1.367	1.412	1.373
	L1	*1.430*	*1.418*	*1.392*	*1.380*	*1.366*
O10-H20	H1	0.960	0.973	0.988	0.989	1.002
	H1	*0.960*	*0.977*	*0.978*	*0.997*	*1.002*
C4-H14	**H2**	**1.090**	**1.166**	**1.240**	**1.270**	**1.293**
	H2	***1.090***	***1.169***	***1.189***	***1.295***	***1.309***
C4-C5	**V**	**1.540**	**1.553**	**1.555**	**1.498**	**1.519**
	V	***1.540***	***1.563***	***1.568***	***1.492***	***1.513***
C5-H15	**H2**	**1.090**	**1.184**	**1.283**	**1.589**	**1.878**
	H2	***1.090***	***1.188***	***1.221***	***1.637***	***1.897***
C5-H16	**V**	**1.090**	**1.110**	**1.108**	**1.180**	**1.085**
	V	***1.090***	***1.118***	***1.115***	***1.162***	***1.104***
C5-O6	**V**	**1.432**	**1.559**	**1.482**	**1.233**	**1.394**
	V	***1.432***	***1.372***	***1.446***	***1.371***	***1.390***
C1-O6	**V**	**1.432**	**1.385**	**1.233**	**1.439**	**1.369**
	V	***1.432***	***1.414***	***1.392***	***1.419***	***1.403***

[a]See Table 2 for notation.

D-Galactose

This aldohexose resides in two anomeric pyranose forms (Fig. 2) interconverting through an open-chain thermodynamically unstable structure. α-D-Galactopyranose (α-D-Gal*p*) can be found in oligo- and polysaccharides, plant mucous and gums and plant glycosides (Maton et al. 1993; Tomasik 1997; Campbell et al. 2006; Tomasik

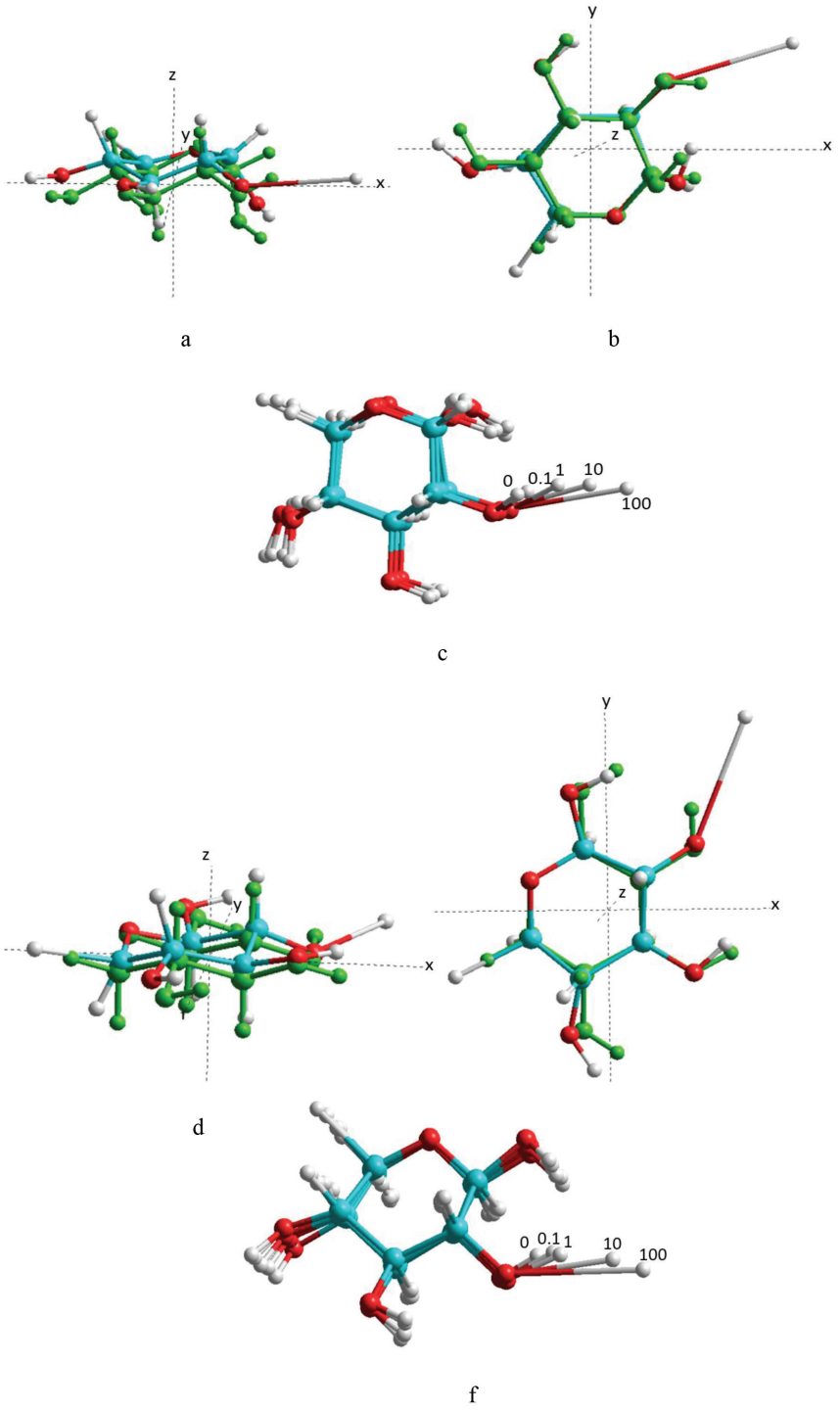

Figure 9. Simplified visualisation of the effect of SMF upon conformation and bond length of α-D- and β-D-xylopyranose anomers (**a–c** and **d–f** respectively) situated in the Cartesian system (see Fig. 2 for notation).

Table 15. Charge density [a.u] at particular atoms of the α- and β-D-glucose molecules depending on SMF flux density [AFU].

Atom		Flux density [AFU]				
	Tendency	0	0.1	1.0	10	100
C1	**V**	**0.350**	**0.348**	**0.353**	**0.353**	**0.343**
	V	***0.433***	***0.431***	***0.441***	***0.451***	***0.451***
C2	**H1**	**0.171**	**0.171**	**0.180**	**0.187**	**0.207**
	V	***0.093***	***0.092***	***0.080***	***0.095***	***0.068***
C3	**IL**	**0.080**	**0.046**	**0.029**	**0.018**	**0.022**
	V	***0.111***	***0.098***	***0.073***	***0.089***	***0.077***
C4	**V**	**0.152**	**0.178**	**0.158**	**0.115**	**0.029**
	L2	***0.123***	***0.181***	***0.153***	***0.097***	***0.007***
C5	**H2**	**-0.018**	**-0.010**	**0.084**	**0.219**	**0.409**
	IH	***-0.044***	***-0.046***	***-0.026***	***0.092***	***0.342***
O6	**V**	**-0.622**	**-0.627**	**-0.627**	**-0.618**	**-0.591**
	V	***-0.606***	***-0.609***	***-0.615***	***-0.600***	***-0.560***
O7	**H1**	**-0.680**	**-0.670**	**-0.670**	**-0.669**	**-0.669**
	IH	***-0.675***	***-0.673***	***-0.661***	***-0.647***	***-0.649***
O8	**IH**	**-0.694**	**-0.671**	**-0.670**	**-0.665**	**-0.670**
	IH	***-0.705***	***-0.699***	***-0.668***	***-0.687***	***-0.634***
O9	**H2**	**-0.743**	**-0.721**	**-0.698**	**-0.675**	**-0.568**
	H2	***-0.735***	***-0.729***	***-0.709***	***-0.681***	***-0.652***
O10	H2	-0.742	-0.733	-0.717	-0.695	-0.527
	H1	*-0.736*	*-0.735*	*-0.726*	*-0.700*	*-0.661*
H11	**H2**	**0.183**	**0.182**	**0.184**	**0.187**	**0.201**
	V	***0.201***	***0.200***	***0.195***	***0.192***	***0.199***
H12	**L1**	**0.193**	**0.185**	**0.176**	**0.176**	**0.170**
	V	***0.192***	***0.191***	***0.172***	***0.150***	***0.164***
H13	**IH**	**0.199**	**0.191**	**0.195**	**0.205**	**0.219**
	V	***0.187***	***0.185***	***0.184***	***0.195***	***0.205***
H14	**IH**	**0.193**	**0.190**	**0.198**	**0.205**	**0.238**
	V	***0.180***	***0.181***	***0.178***	***0.185***	***0.214***
H15	H2	0.177	0.170	0.179	0.190	0.237
	V	*0.183*	*0.181*	*0.176*	*0.205*	*0.227*
H16	L3	0.172	0.145	0.021	-0.145	-0.506
	L3	*0.181*	*0.178*	*0.140*	*-0.037*	*-0.369*
H17	V	0.399	0.396	0.397	0.398	0.411
	V	*0.387*	*0.388*	*0.387*	*0.376*	*0.384*
H18	V	0.397	0.387	0.393	0.391	0.399
	V	*0.398*	*0.396*	*0.385*	*0.398*	*0.356*
H19	L2	0.423	0.427	0.414	0.396	0.291
	V	*0.418*	*0.420*	*0.422*	*0.399*	*0.393*
H20	H1	0.412	0.415	0.421	0.429	0.456
	H1	*0.400*	*0.413*	*0.419*	*0.428*	*0.439*

[a]See Table 2 for notation.

2007a; Tomasik 2007b; Heldt and Piechulla 2010; Keung and Mehta 2015; Churuangsuk et al. 2018; Reynolds et al. 2019). Jointly with α-D-glucose, it constitutes lactose, known as milk sugar. In fauna organisms, it is hydrolytically liberated from lactose. In these organisms, it is converted into galactoso-6-phosphate involving ATP α-D-galactose. The latter reacts with galactoso-1-phosphate uridinyltransferase into UDP-galactose which is subsequently transformed with UDP-galactoso-4-epimerase

Table 16. Bond lengths [Å] in the α- and β-D-xylofuranose molecules depending on the applied SMF flux density [AFU][a].

Bond	Flux density [AFU]					
	Tendency	0	0.1	1	10	100
C1-C2	**H1**	**1.525**	**1.555**	**1.593**	**1.619**	**1.666**
	H1	***1.528***	***1.534***	***1.562***	***1.603***	***1.606***
C1-O7	**L1**	**1.420**	**1.404**	**1.398**	**1.391**	**1.374**
	V	***1.411***	***1.404***	***1.395***	***1.429***	***1.424***
O7-H17	V	0.960	1.037	0.966	1.031	0.972
	V	*0.960*	*0.954*	*0.979*	*1.010*	*0.975*
C1-H11	**V**	**1.090**	**1.143**	**1.123**	**1.143**	**1.178**
	V	***1.091***	***1.103***	***1.137***	***1.106***	***1.124***
C2-C3	**V**	**1.528**	**1.530**	**1.530**	**1.536**	**1.555**
	V	***1.532***	***1.531***	***1.536***	***1.548***	***1.599***
C2-O8	**L1**	**1.412**	**1.382**	**1.342**	**1.323**	**1.292**
	IL	***1.412***	***1.408***	***1.369***	***1.319***	***1.330***
O8-H18	V	0.960	1.101	1.080	1.185	1.187
	IH	*0.960*	*0.981*	*1.142*	*1.111*	*1.341*
C2-H12	**V**	**1.091**	**1.110**	**1.126**	**1.113**	**1.179**
	V	***1.091***	***1.082***	***1.153***	***1.166***	***1.128***
C3-C4	**V**	**1.540**	**1.568**	**1.567**	**1.569**	**1.558**
	H1	***1.537***	***1.542***	***1.581***	***1.676***	***1.659***
C3-O9	**V**	**1.413**	**1.372**	**1.370**	**1.375**	**1.391**
	V	***1.413***	***1.405***	***1.359***	***1.397***	***1.307***
O9-H19	H2	0.960	1.053	1.171	1.246	1.579
	IH	*0.960*	*0.981*	*1.047*	*1.321*	*1.267*
C3-H13	**V**	**1.091**	**1.222**	**1.225**	**1.200**	**1.121**
	V	***1.091***	***1.111***	***1.231***	***1.100***	***1.231***
C4-C5	**IL**	**1.533**	**1.494**	**1.463**	**1.448**	**1.461**
	IL	***1.533***	***1.523***	***1.475***	***1.434***	***1.449***
C5-O10	IL	1.411	1.401	1.401	1.385	1.339
	V	*1.412*	*1.410*	*1.221*	*1.336*	*1.355*
O10-H20	V	0.960	0.953	0.967	0.957	1.004
	V	*0.960*	*0.948*	*1.189*	*1.017*	*0.984*
C5-H15	H3	1.090	1.284	1.681	2.068	3.362
	H3	*1.098*	*1.418*	*1.390*	*1.708*	*2.636*
C5-H16	V	1.091	1.154	1.112	1.123	1.088
	V	*1.092*	*1.121*	*1.151*	*1.096*	*1.108*
C4-H14	**H2**	**1.091**	**1.115**	**1.119**	**1.123**	**1.153**
	V	***1.092***	***1.085***	***1.142***	***1.142***	***1.128***
C4-O6	**H1**	**1.417**	**1.438**	**1.464**	**1.469**	**1.472**
	H1	***1.414***	***1.416***	***1.454***	***1.485***	***1.473***
O6-C1	**V**	**1.413**	**1.418**	**1.417**	**1.414**	**1.421**
	V	***1.412***	***1.412***	***1.428***	***1.447***	***1.417***

[a]See Table 2 for notation.

into UDP-glucose (Candy 1980). Microbiological oxidation of the CH_2OH group of α-D-galactose provides galacturonic acid which essentially inhibits progress of atherosclerosis (Parikka et al. 2015).

Based on computed values of heat of formation, one could note that the α-anomer was more stable than the β-anomer independently of applied SMF flux density. However, as shown by changes of dipole moment (Table 4), the β-anomer was more po-

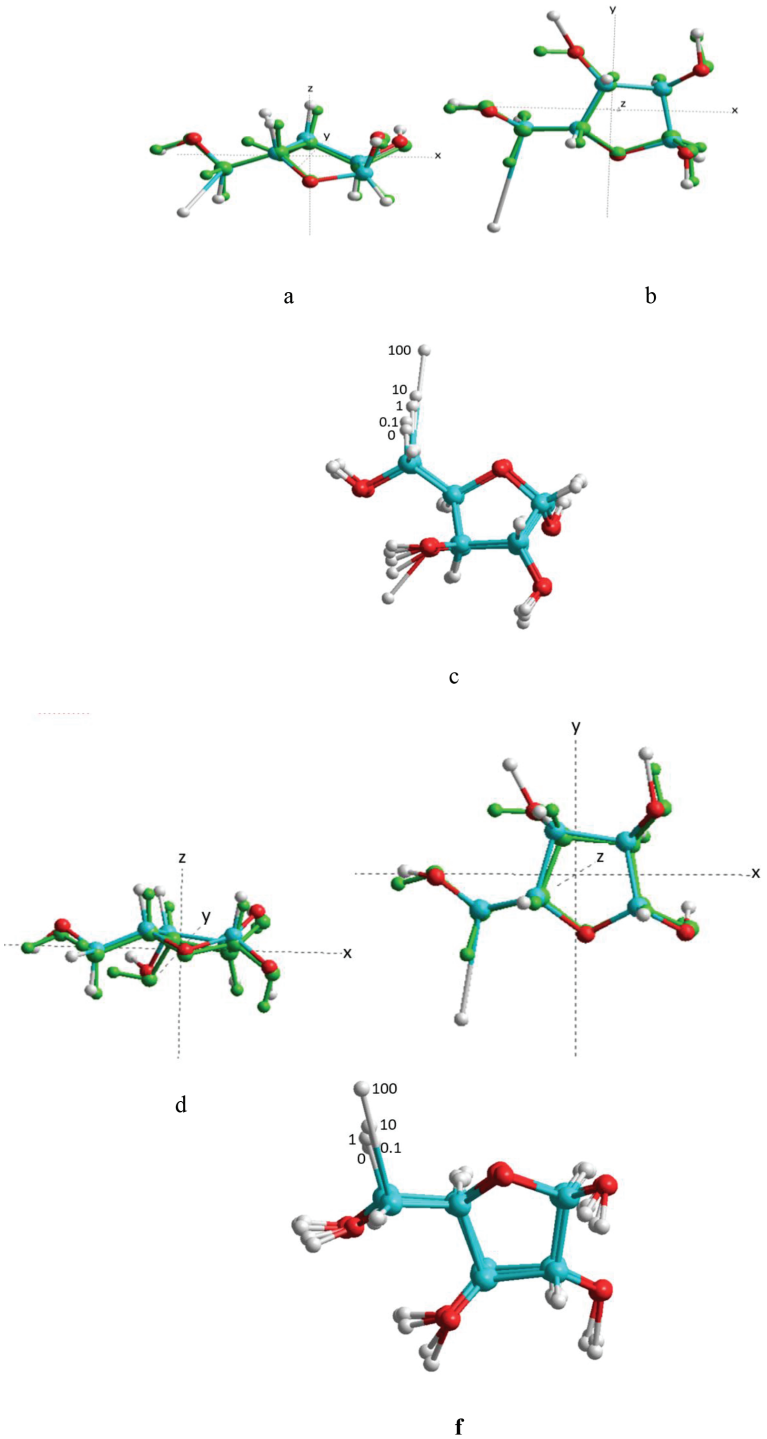

Figure. 10. Simplified visualisation of the effect of SMF upon conformation and bond length of α-D- and β-D-xylofuranose anomers (**a–c** and **d–f** respectively), situated in the Cartesian system (see Fig. 2 for notation).

larised with an increase in the flux density. As in anomers of D-glucose, the charge density at particular atoms irregularly varied with increasing flux density. In contrast to anomers of D-glucose, in anomers of D-galactose, the negative charge concentrated at the O7, C5 and C4 atoms and SMF flux density turned it more negative. The negative charge also concentrated at the C2-H14 atom bound to it (Table 5). The positive charge density was noted at the C3 and C1 atoms, as well as the H15 and H13 atoms bound to them, respectively. These effects generated an increase in the corresponding bond lengths (Table 5).

Due to an increase in the positive charge at the anomeric C6 atom, one could assume a facilitating role of SMF in formation of galactoso-1- phosphate. In addition, the effect of SMF upon the charge density suggested favouring oxidation of D-galactose into galacturonic acid.

Particular attention should be paid to the C5, C6 and H19 atoms. SMF remarkably changed their charge distribution. The negative charge shifted to the C5 and H19 atoms, whereas the C6 atom lost this charge to a considerable extent. The strongest influence was evoked by SMF upon the bonds orientated under 45° to the field strength lines, that is, to the x-axis. Extremal elongation was observed for the C6-H19 and O10-H22 bonds (Table 6). Simultaneously, the C6-H18 bond distinctly shortened. It should be underlined that both H18 and H19 were twin atoms bound to the C6 atom. Thus, observed differences could not originate from different intramolecular electronic interactions and completely different situations by those atoms with respect to the SMF line should be responsible for it.

Unlike in D-glucose, the positive charge density at the C1 atom decreased with an increase in the flux density. Thus, reactions with any Lewis base would be obstructed. Simultaneously, the flux density up to 0.1 AFU increased the negative charge density at the C6 atom. It would favour phosphorylation at the vicinal hydroxyl group. However, higher flux densities turned the charge density at that atom to positive. Thus, the increase in the charge density with the flux density inhibited that reaction.

The susceptibility of D-galactose to the ring opening and to the Maillard reaction depended on its anomer. The C1-O8 bond in the α-anomer varied irregularly with the flux density but, generally, the susceptibility of that anomer to the ring opening was low. That bond in the β-anomer regularly decreased with an increase in the applied flux density. Simultaneously, the O8-H20 bond was shortened in the α-anomer and elongated in the β-anomer (Table 6).

Data shown in Table 6 allowed the visualisation of the effect of SMF upon anomers of D-galactose. Structures in Fig. 6 demonstrate a slight effect of SMF upon the conformation of both anomers and significant effect upon the bond lengths of some peripheral C-H bonds. They were the C6-H18 and O10-H22 bonds. An increasing flux density generated a considerable negative charge density at the H22 atom making the C6-H18 bond relatively slightly polarised. Therefore, that bond was capable of interaction with the electrons of that bond with SMF. In the O10-H22 bond, both its partners carried negative charge. This effect and its origin was the same as that observed in D-glucose anomers.

D-Fructose

D-Fructose, a ketohexose, is a typical monosaccharide of a floral provenance. In the free form, it resides in fruits, honey and flower nectar. In a bound form, it can be found in several di-, oligo- and polysaccharides, for instance, sucrose, raffinose and inulin, respectively. Its presence in the organisms of fauna is a consequence of consumption of plant food. In mammals, free fructose is found in their semen (Maton et al. 1993; Tomasik 1997; Campbell et al. 2006; Tomasik 2007a; Tomasik 2007b; Heldt and Piechulla 2010; Keung and Mehta 2015; Churuangsuk et al. 2018; Reynolds et al. 2019). Humans metabolise D-fructose almost entirely in the liver, where it is directed towards replenishment of liver glycogen and triglyceride synthesis. In muscles and fat tissues, D-fructose metabolism is initiated by phosphorylation with hexokinase at the O11 atom, turning it into fructose-1-phosphate. The latter enters the glycolysis pathway. In the liver, the metabolism of D-fructose is initiated by fructokinase which forms fructose-1-phosphtate engaging the O10 atoms, respectively (Maton et al. 1993; Tomasik 1997; Hames and Hooper 2004; Campbell et al. 2006; ; Tomasik 2007a; Tomasik 2007b; Heldt and Piechulla 2010; Keung and Mehta 2015; Churuangsuk et al. 2018; Reynolds et al. 2019).

Alcohol fermentation and the Maillard browning reaction are other enzymatic processes common for D-fructose. In the Maillard reaction, the anomeric C1 carbon atom is first engaged (Grandhee and Monnier 1991).

D-Fructose resides in four mutually fast interconverting structures, including α-D-fructopyranose (α-Fru*p*), β-D-fructopyranose (β-Fru*p*), α-D-fructofuranose (α-Fru*f*) and β- D-fructofuranose (β-D-Fru*f*) (Fig. 3). Computations of the heat formation (Table 7) pointed to α-D-Fru*f* and α-D-Fru*p* being the most and least stable, respectively, amongst the four anomers taken into account (Fig. 3). Applying SMF of 0.1 AFU, the flux density did not change their positions in this group. At 1 AFU, based on that criterion, β-D-Fru*f* became the most stable, but a further increase in the flux density returned α-D-Fru*f* to the position of the most stable anomer. α-D-Fru*p* holds the position of the least stable anomer at SMF up to 10 AFU. At 100 AFU, β-D-Fru*p* became the least stable. The dipole moment of particular anomers also changed with an increase in the applied flux density. However, these changes were in no simple relationship to the stability of particular anomers. It suggested deformation of their initial structure by polarisation of particular bonds. They could also result from departure from their initial situation in the Cartesian system. This was confirmed by computed changes of charge density and bond lengths (Tables 8–11). Inspection of Table 8 showed that, in α- and β-D-fructopyranoses, the negative charge density essential for the phosphorylation reaction at the O12 atom was lower in the α-anomer and it fairly linearly decreased against increasing flux density. Thus, that anomer should be more reactive than the β-anomer. The Maillard reaction required the positive charge density at the C1 atom. Without SMF, the β-anomer showed a more positive charge at that atom. It decreased against increasing flux density. The α-anomer carried considerably lower positive charge density which additionally decreased against the flux density up to 10 AFU and then increased regularly up to over twice at 100 AFU.

The strongest changes in the electron density occurred at the C1, O12α, H13α, H22β and H24β atoms. Thus, both anomers are clearly distinguished from one another.

Structural deformations of the α- and β-D-fructopyranose molecules in SMF (Table 9 and Fig. 6) resembled those observed for D-glucose and D-galactose anomers. Considerable elongations were observed for the C1-H13, O11-H22 bonds and C6-H19α bonds, whereas the twin C6-H18 bond was only slightly shortened. It was another illustration of the importance of the position of the bonds with respect to the SMF field.

In the case of D-fructofuranoses, comparison of the negative charge density (Table 10) at the O12 and O11 atoms being potentially the reaction sites for the phosphorylation suggested that the β-anomer should react more readily than the α-anomer. An increase in the SMF flux density was not beneficial for this reaction as the value of the charge density at these atoms turned less negative. The positive charge density at the C4 and C1 atoms, being the potential reaction site for the Maillard reaction, were higher in the β-anomer and only slightly decreased with increasing AFU. SMF at 100 AFU generated an essential increase in the positive charge density at the C1β, O9β, O12α and H21α atoms. At the same time, that charge decreased at the C2α, C5β, H17α, H24α and particularly at the H20β atom.

Anomers of D-fructofuranoses were less susceptible to structural deformations evoked by SMF (Table 11 and Fig. 8). In the α-anomer, the O12-H24, O9-H22 and C5-H17 bonds were longer and that effect was noticeable just at 100 AFU. The β-anomer was deformed chiefly by elongation of the O9-H22, C1-C2 and O8-H20β bonds. Untypically, the ring was also deformed by the elongation of the C2-C1 bond.

D-Xylose

D-xylose, aldopentose, is a mono-sugar residing almost exclusively in plants. As a component of hemicelluloses, it constitutes biomass. In the sphere of fauna, D-xylose was also found in some species of Chrysolinina beetles. It co-constituted cardiac glycosides of their defensive glands (David Morgan 2004).

Organisms of fauna receive xylose from their diet. Eukaryotic micro-organisms employ the oxidato-reductase pathway to metabolize D-xylose (Gabaldon et al. 2005). D-xylose is metabolised by humans involving protein xylosyltransferases (XYLT1, XYLT2) which transfer xylose from UDP to a serine in the core protein of proteoglycans (Stoolmiller et al. 1972; Gotting et al. 2000). Mammals metabolise D-xylose with D-xyloisomerase (Ding et al. 2009; Huntley and Patience 2018). Recently, a highly efficient low-temperature, atmospheric-pressure enzymatic process of the hydrogen production from D-xylose was presented. It involved thirteen enzymes, including a novel polyphosphate xylulokinase (Del Campo et al. 2013). In another technically important reaction, D-xylose is used for production of furfural, a precursor for synthetic polymers and to tetrahydrofuran (Hoydonckx et al. 2007). In the initial step, hemicellulose is hydrolysed in an acid-catalysed process (Binder et al. 2010; Millán et al. 2019). That process starts from the protonation of the D-xylopyranose molecule at the O8 atom.

It was also found that D-xylose could be useful in therapy of COVID-19 (Cheudjeu 2020). The latter interacts with D-xylose significantly stimulating the biosynthesis of sulphated glycosylamineglycans (GAGs), particularly heparan sulphate (HS). GAGs, especially HS and D-xylose interact with oral non-steroidal anti-inflammatory drugs, active in lung infections.

D-Xylose resides in the form of α- and β-xylopyranoses (Xyl*p*) (a and b), as well as α- and β-xylofuranoses (Xyl*f*) (c and d) (Fig.4).

The heat of formation criterion pointed to β-D-xylopyranose as the most stable amongst four anomers of D-xylose (Table 12). It is distinguished from other anomers with a considerably low dipole moment. The increase in the SMF flux density regularly increased the dipole moment of all anomers and, at the same time, destabilised them in terms of their heat of formation values. In both D-xylopyranoses, the metabolic reactions should be promoted by the high positive charge density at the O6 atom and low negative charge density at the O8 and O9 atoms. Data in Table 13 showed that the influence of SMF upon the O6, O9 and O8 atoms was negligible, noticeable and strong, respectively. A considerable increase in the positive charge density took place at the C1α, C5 and O8 atoms, whereas its decrease was observed at the C2 and H18β atoms. The SMF flux density promoted reactivity at the C1, especially the C1α atom, slightly promoted reactions at the O9 atom and strongly increased the reactivity of the O8 atom. Taking these arguments under consideration, the α-anomer was more reactive at the C1 atom when residing without SMF and, in SMF, the β-anomer reacted more readily. The reactivity at the O8 atom in the β-anomer was slightly higher when SMF was applied and the reactivity at the O7 atom in the α-anomer was definitely higher.

As shown in Table 14 and Fig. 9, only the O8-H18 bond suffered considerable elongation in SMF. Less intense elongation was observed at the C4-H14 and C5-H15 bonds in both anomers. That effect was in line with the preference for the elongation of the bonds orientated under approximately 45° with respect to the x-axis.

Metabolic processes in D-xylofuranose molecules involved the C1 and O10 atoms. The highly positive and highly negative charge densities, respectively, were beneficial for those reactions. Data in Table 13 showed that, in both anomers, SMF did not influence charge density at the C1 atom. SMF generated a decrease in the negative charge density at the O10 atom. It was particularly noticeable in the α-anomer. It pointed to an inhibition of the reactivity with Lewis acids in these centres. An increase in the positive charge density at the C5α, O9, O10α, H11, H15α and H19 atoms and its decrease at the C4β and H16 atoms confirmed the rule of the importance of 45° orientation of the bonds with respect to the SMF field. Data in Table 16 and Fig. 10 showed that, in both anomers, the C5-H15 bond reacted intensively to an increase in the flux density and the response from the C4-H14 and O9-H19α bonds was weaker.

Comparison of the relevant data for D-xylopyranoses and D-xylofuranoses revealed that pyranose anomers metabolise more readily.

The SMF flux densities ranging from 100 to 10 000 T (0.1 to 100 AFU) employed in performed computations were very high. Experiments performed by Nakamura et al. Takeyama (Nakamura et al. 2018) with SMF of 1200 T (1.2 AFU) resulted in a

destruction of the generators within few microseconds. The pulse electromagnet constructed in 2012 at Los Alamos Laboratories remained stable, but producing a field with an intensity of only 100.75 T (approx. 0.1 AFU) (Nguyen et al. 2016). Therefore, only insignificant effects evoked by SMF of flux density of 0.1–100T (0.0001–0.1 AFU) upon carbohydrates could be anticipated in a real life.

Conclusions

Performed numerical simulations showed the specific influence of static magnetic field (SMF) upon equilibrium constants between particular anomers of the saccharides under study. Their susceptibility to such enzymatic reactions essential for their metabolism as phosphorylation with ATP at the CH_2OH group, the Entner-Duodoroff metabolic pathway and the Maillard reaction, both also engaging the C1 ring carbon atom in reaction with enzymes and amino acids, is also controlled by SMF.

D-Glucose in SMF takes preferably the α-anomeric form. SMF stimulated its reactivity involving the CH_2OH group and the C1-atom.

D-Galactose in SMF takes preferably the α-anomeric form. The reactivity at the CH_2OH group and C1 atom vary irregularly with an increase of the applied flux density.

D-Fructose in SMF takes preferably the α-D-Fru*f* form and D-xylose under such conditions takes preferably the β-D-Xyl*p* form. Their susceptibility to the reactions important for their metabolism irregularly vary with the applied flux density.

Only insignificant effects evoked by SMF of flux density of 0.1–100T upon carbohydrates could be anticipated in a real life.

References

Bao S, Guo W (2021) Transient heat transfer of superfluid He in nonhomogeneous geometries: Second sound, rarefaction, and thermal layer. Physical Review B 103(13): e134510. https://doi.org/10.1103/PhysRevB.103.134510

Binder JB, Blank JJ, Cefali AV, Raines RT (2010) Synthesis of furfural from xylose and xylan. ChemSusChem 22(11): 1268–1272. https://doi.org/10.1002/cssc.201000181

Campbell NA, Williamson B, Heyden RJ (2006) Biology: Exploring Life. Pearson Prentice Hall, Boston.

Candy DJ (1980) The Biochemistry of Plants. Academic Press, New York.

Carpenter JE, Weinhold F (1988) Analysis of the geometry of the hydroxymethyl radical by the different hybrids for different spins natural bond orbital procedure. Journal of Molecular Structure (Teochem) 139: 41–62. https://doi.org/10.1016/0166-1280(88)80248-3

Charistos ND, Muñoz-Castro A (2019) Double aromaticity of the B-40 fullerene: Induced magnetic field analysis of pi and sigma delocalization in the boron cavernous structure. Physical Chemistry Chemical Physics 21(36): 20232–20238. https://doi.org/10.1039/C9CP04223G

Cheudjeu A (2020) Correlation of D-xylose with severity and morbidity-related factors of COVID-19 and possible therapeutic use of D-xylose and antibiotics for COVID-19. Life Sciences 260: e118335. https://doi.org/10.1016/j.lfs.2020.118335

Churuangsuk C, Kherouf M, Combet E, Lean M (2018) Low-carbohydrate diets for overweight and obesity: A systematic review of the systematic reviews. Obesity Revs. Systematic Reviews 19: 1700–1718. https://doi.org/10.1111/obr.12744

Ciesielski W, Girek T, Oszczęda Z, Soroka JA, Tomasik P (2021) Towards recognizing mechanisms of effects evoked in living organisms by static magnetic field. Numerically simulated effects of the static magnetic field upon simple inorganic molecules. F1000 Research 10: e611. https://doi.org/10.12688/f1000research.54436.1

Ciesielski W, Girek T, Oszczeda Z, Soroka JA, Tomasik P (2022) Potential risk resulting from the influence of static magnetic field upon living organisms. Numerically simulated effects of the static magnetic field upon simple alkanols. BioRisk 18: 35–55. https://doi.org/10.3897/biorisk.18.76997

Committee to Assess the Current Status and Future Direction of High Magnetic Field Science in the United States, Board on Physics and Astronomy (2013) High Magnetic Field Science and Its Application in the United States; Current Status and Future Directions. Natl. Res. Council, National Acad., Washington, D.C.

Conway T (1992) The Entner-Doudoroff pathway: History, physiology and molecular biology. Microbiological Reviews 103: 1–28. https://doi.org/10.1111/j.1574-6968.1992.tb05822.x

David Morgan E (2004) Biosynthesis in Insects. Royal Society of Chemistry Publ, London, 112 pp.

Del Campo JSM, Rollin J, Myung S, Chun Y, Chandrayan S, Patino R, Adams MWW, Zhang PY-H (2013) High-yield production of dihydrogen from xylose by using a synthetic enzyme cascade in a cell-free system. Angewandte Chemie International Edition 52(17): 4587–4590. https://doi.org/10.1002/anie.201300766

Ding M, Teng Y, Yin Q, Chen W, Zhao F (2009) Identification, expression, and characterization of the highly conserved D-xyloseisomerase in animals. Acta Biochimica et Biophysica Sinica 41(2): 116–122. https://doi.org/10.1093/abbs/gmn013

Domb AJ, Kost J, Wiseman D (2019) Handbook of Biodegradable Polymers. CRC Press, Boca Raton.

Facundo Ruiz CA-A, Martínez-Mendoza JR, Terrones H (2005) Infrared and Raman spectra, conformational stability, *ab initio* calculations of structure, and vibrational assignment of α and β glucose. Journal of Molecular Structure (Teochem) 714(2–3): 143–146. https://doi.org/10.1016/j.theochem.2004.09.041

Farberovich OV, Mazalova VL (2016) Ultrafast quantum spin-state switching in the Co-ctaethylporphyrin molecular magnet with a terahertz pulsed magnetic field. Journal of Magnetism and Magnetic Materials 405: 169–173. https://doi.org/10.1016/j.jmmm.2015.12.038

Frisch MJ, Pople JA, Binkley JS (1984) Self-consistent molecular orbital methods. 25. Supplementary functions for Gaussian basis sets. The Journal of Chemical Physics 80(7): 3265–3269. https://doi.org/10.1063/1.447079

Frisch MJ, Trucks GW, Schlegel HB, et al. (2016) Gaussian 09, Revision A.02, Wallingford CT, Gaussian Inc.

Froimowitz M (1993) HyperChem: A software package for computational chemistry and molecular modeling. BioTechniques 14: 1010–1013.

Gabaldon T, Rainey D, Huynen MA (2005) Tracing the evolution of a large protein complex in the eukaryotes, NADH: Ubiquinone oxidoreductase (Complex I). Journal of Molecular Biology 348(4): 857–870. https://doi.org/10.1016/j.jmb.2005.02.067

Glendening ED, Reed AE, Carpenter JE (1987) Extension of Lewis structure concepts to open-shell and excited-state molecular species, NBO Version 3.1, Ph.D. thesis, University of Wisconsin, Madison.

Gotting C, Kuhn J, Zahn R, Brinkmann T, Kleesiek K (2000) Molecular cloning and expression of human UDP-d-Xylose: Proteoglycan core protein beta-d-xylosyltransferase and its first isoform XT-II. Journal of Molecular Biology 304(4): 517–528. https://doi.org/10.1006/jmbi.2000.4261

Grandhee SK, Monnier VM (1991) Mechanism of formation of the Maillard protein cross-link pentosidine. The Journal of Biological Chemistry 266(18): 11649–11653. https://doi.org/10.1016/S0021-9258(18)99006-X

Hames BD, Hooper NM (2004) Short lectures, Biochemistry. PWN Scientific Editorial Board, Warsaw. [in Polish]

Hamza A-SHA, Shaher SA, Mohmoud A, Ghania SM (2002) Environmental pollution by magnetic field associated with power transmission lines. Energy Conversion and Management 43(17): 2443–2452. https://doi.org/10.1016/S0196-8904(01)00173-X

Heinrich PC, Mueller M, Graeve L (2014) Löffler/Petrides Biochemie und Pathobiochemie. Springer-Verlag, Berlin. https://doi.org/10.1007/978-3-642-17972-3

Heldt H-W, Piechulla B (2010) Plant Biochemistry, 4th edn. Academic Press, Cambridge MA, US.

Hoydonckx HE, Van Rhijn WM, Van Rhijn W, De Vos DE, Jacobs PA (2007) Furfural and its derivatives. Ullmann's Encyclopaedia of Industrial Chemistry. Wiley-VCH, Weinheim. https://doi.org/10.1002/14356007.a12_119.pub2

Huntley NF, Patience JF (2018) Xylose: Absorption, fermentation, and post-absorptive metabolism in the pig. Journal of Animal Science and Biotechnology 9(1): e4. https://doi.org/10.1186/s40104-017-0226-9

Keung PC, Mehta CBM (2015) Handbook of Food Chemistry. Springer, Berlin/Heidelberg. https://doi.org/10.1007/978-3-642-36605-5_34

Largeaud F, Kokoh KB, Beden B, Lamy C (1995) On the electrochemical reactivity of anomers: Electrocatalytic oxidation of α- and β-D-glucose on platinum electrodes in acid and basic media. Journal of Electroanalytical Chemistry (Lausanne, Switzerland) 397(1–2): 261–269. https://doi.org/10.1016/0022-0728(95)04139-8

Marchand N, Lienard P, Siehl H, Izato H (2014) Applications of molecular simulation software SCIGRESS in industry and university. Fujitsu Scientific and Technical Journal 50(3): 46–51.

Maton A, Hopkins J, McLaughlin CW, Johnson S, Warner MQ, LaHart D, Wright JD (1993) Human Biology and Health. Prentice Hall, New Jersey.

Millán GG, Hellsten S, King AWT, Pokki J-P, Llorca J, Sixta H (2019) A comparative study of water-immiscible organic solvents in the production of furfural from xylose and birch

hydrolysate. Journal of Industrial and Engineering Chemistry 72: 354–363. https://doi.org/10.1016/j.jiec.2018.12.037

Nakamura D, Ikeda A, Sawabe H, Matsuda YH, Sakeyama S (2018) Record indoor magnetic field of 1200 T generated by electromagnetic flux-compression. The Review of Scientific Instruments 89(9): e095106. https://doi.org/10.1063/1.5044557

Nguyen DN, Michel J, Mielke CH (2016) Status and development of pulse magnets at the NHMFL pulsed field facility. IEEE Transactions on Applied Superconductivity 26(4): e1. https://doi.org/10.1109/TASC.2016.2515982

Parikka K, Master E, Tenkanen M (2015) Oxidation with galactose oxidase: Multifunctional enzymatic catalysis. Journal of Molecular Catalysis. B, Enzymatic 120: 47–59. https://doi.org/10.1016/j.molcatb.2015.06.006

Rankovic V, Radulovic J (2009) Environmental pollution by magnetic field around power lines. International Journal of Qualitative Research 3(3): 1–6.

Reynolds A, Mann J, Cummings J, Winter N, Mete E, Morenga L (2019) Carbohydrate quality and human health: A series of systematic reviews and meta-analyses. Lancet (Review) 393(10170): 434–445. https://doi.org/10.1016/S0140-6736(18)31809-9

Sell DR, Monnier VM (1989) Structure elucidation of a senescence cross-link from human extracellular matrix. Implication of pentoses in the aging process. The Journal of Biological Chemistry 264(36): 21597–21602. https://doi.org/10.1016/S0021-9258(20)88225-8

Stoolmiller AC, Horwitz AL, Dorfman A, Kennedy Jr JP (1972) Biosynthesis of the chondroitin sulfate proteoglycan. Purification and properties of xylosyltransferase. The Journal of Biological Chemistry 247(11): 3525–3532. https://doi.org/10.1016/S0021-9258(19)45172-7

Tang Y, Guo W, Lvov W, Pomyalov A (2021) Eulerian and Lagrangian second-order statistics of superfluid He grid turbulence. Physical Review B 103(14): e144506. https://doi.org/10.1103/PhysRevB.103.144506

Tomasik P (1997) Saccharides. In: Sikorski ZE (Ed.) Chemical and Functional Properties of Food Components, Ch. 4. Technomic Publ. Co. Inc., Lancaster – Basil.

Tomasik P (2007) Saccharides in food, Structure and transformations. In: Sikorski ZR (Ed.) Food Chemistry, Ch. 1. WNT, Warsaw.

Tomasik P (2007) Functional properties of saccharides. In: Sikorski ZR (Ed.) Food Chemistry, Ch. 2. WNT, Warsaw.

World Health Organization (2019) Model list of essential medicines: 21st list. Geneva, hdl:10665/325771

BioRisk 18: 93–104 (2022)
doi: 10.3897/biorisk.18.80607
https://biorisk.pensoft.net

RESEARCH ARTICLE

A peer-reviewed open-access journal
BioRisk

Potential risk resulting from the influence of static magnetic field upon living organisms. Numerically simulated effects of the static magnetic field upon porphine

Wojciech Ciesielski[1], Tomasz Girek[1], Zdzisław Oszczęda[2], Jacek A. Soroka[3], Piotr Tomasik[2]

1 *Institute of Chemistry, Jan Długosz University, 42 201 Częstochowa, Poland* **2** *Nantes Nanotechnological Systems, 59 700 Bolesławiec, Poland* **3** *Scientific Society of Szczecin, 71-481 Szczecin, Poland*

Corresponding author: Wojciech Ciesielski (w.ciesielski@interia.pl)

Academic editor: Josef Settele | Received 16 January 2022 | Accepted 9 May 2022 | Published 30 June 2022

Citation: Ciesielski W, Girek T, Oszczeda Z, Soroka JA, Tomasik P (2022) Potential risk resulting from the influence of static magnetic field upon living organisms. Numerically simulated effects of the static magnetic field upon porphine. BioRisk 18: 93–104. https://doi.org/10.3897/biorisk.18.80607

Abstract

Background: Recognizing effects of static magnetic field (SMF) of varying flux density on flora and fauna is attempted. For this purpose the influence of SMF upon the porphine molecule is studied.

Methods: Computations of the effect of static magnetic field (SMF) of 0.0, 0.1, 1, 10 and 100 AFU (1 AFU > 1000 T) flux density were performed in silico for SMF changes distribution of the electron density in that molecule. HyperChem 8.0 software was used together with the AM1 method for optimization of the conformation of the molecule of porphine. The computations of polarizability, charge distribution, potential and dipole moment for molecules placed in SMF were performed for molecule situated subsequently in the x-y, y-z and x-z planes of the Cartesian system. The computations involved the DFT 3-21G method.

Results: Static magnetic field (SMF) decreased stability of the porphine molecule. This effect depended on the situating the molecule in respect to the direction of SMF of the Cartesian system. An increase in the value of heat of formation was accompanied by an increase in dipole moment.

Conclusions: Observed effects resulted from deformations of the molecule which involved pyrrole rings holding the hydrogen atoms at the ring nitrogen atoms and the length of the C–H and N–H bonds. In a consequence that macrocyclic ring lost its planarity.

Keywords

dipole moment, heat of formation, structure deformation

Introduction

Although porphine itself (Fig. 1) does not occur in nature, numerous porphine derivatives play an essential role in functioning in living organisms of flora and fauna.

Porphine is a macrocyclic compound of an aromatic character. It is formed of four pyrrole rings bound with four methine (-CH=) bridges. The macrocyclic ring is planar and only the N–H bonds are bent in opposite (*trans*) directions (Caughey and Ibers 1977; Kadish et al. 2000; Ortiz de Montellano 2008). Involving numerous biosynthetic ways (Elder 1994; Aylward and Bofinger 2005), many porphine derivatives are naturally formed from protoporhyrin IX, it being a precursor of several biologically important compounds. A biological activity of porphine derivatives is achieved when metal ions are coordinated within the macrocyclic ring (Caughey and Ibers 1977; Kadish et al. 2000; Ortiz de Montellano 2008). This course of study was developed as a consequence of considerable environmental pollution with magnetic fields generated by modern technologies and technical solutions in several areas of human everyday life (Hamza et al. 2002; Rankovic and Radulovic 2009; Committee to Assess the Current Status and Future Direction of High Magnetic Field Science in the United States 2013; Magnet Science and Technology 2021; Magnetism in real life 2021). This paper follows a series of three recent papers of ours in which the effect of static magnetic field (SMF) upon small inorganic molecules (Ciesielski et al. 2021), lower alkanols (Ciesielski et al. 2022a) and monosaccharides (Ciesielski et al. 2022b) was recognized. In order to recognize the effect of SMF upon biologically important

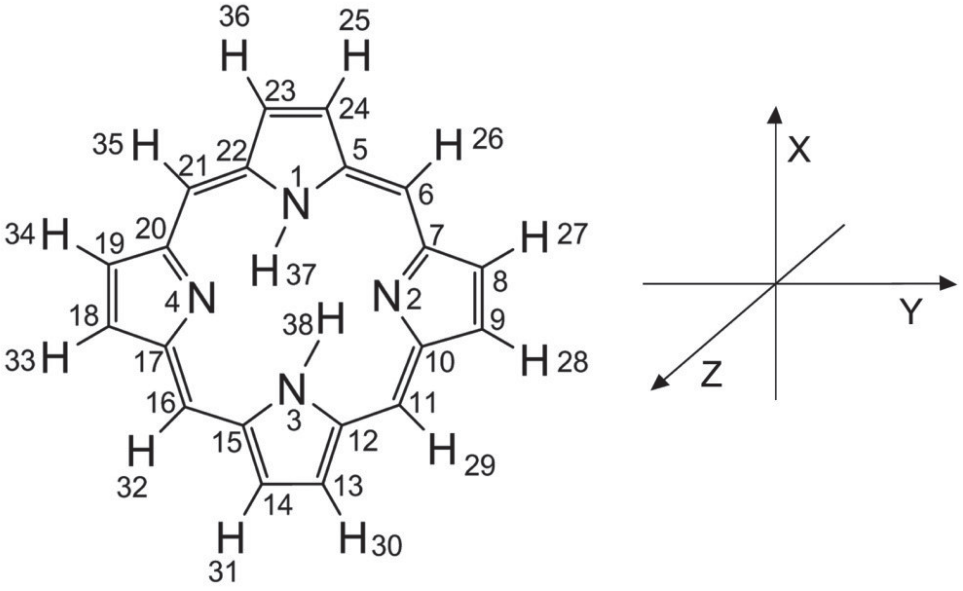

Figure 1. Structure of the porphine molecule with the system of numbering of the atoms followed throughout the discussion and situating axes of the Cartesian system.

metalloporphyrines, in the present study we focused on the effect of SMF upon their free ligand, i.e. porphine itself.

As in our former papers (Ciesielski et al. 2021; Ciesielski et al. 2022a, b) the effect of SMF of flux density varying from 0 to 100 AFU was simulated with advanced numerical computations involving the in silico approach.

Numerical computations

DFT Molecular structures were drawn using the Fujitsu Scigress 2.0 software (Marchand et al. 2014). Their principal symmetry axes were oriented along the x-, y and z-axes of the Cartesian system. The magnetic field was fixed in the same direction with the south pole from the left side. Z axis is directed perpendicularly to the porphine plane, the x and y axes are in the plane of the system, each of them along two nitrogen atoms. In the case of full mesomerism, because of the quaternary symmetry of z axis, the last two axes were undistinguished. When the nitrogen atoms differ from one another, the x axis crossed two nitrogen atoms substituted by hydrogen atoms and y axis crossed remained two unsubstituted nitrogen atoms. Thus, both x and y axes were distinguishable.

Subsequently, utilizing Gaussian 0.9 software equipped with the 6-31G** basis (Frisch et al. 2016), the molecules were optimized and all values of bond length, dipole moment, heath of formation, bond energy, HOMO/LUMO energy level for single molecules as well as HOMO/LUMO energy level and total energy for systems built of three molecules, were computed.

In the consecutive step, the influence of the static magnetic field (SMF) upon optimized molecules was computed with Amsterdam Modelling Suite software (Farberovich and Mazalova 2016; Charistos and Muñoz-Castro 2019) and the NR_LDOTB (non-relativistic orbital momentum L-dot-B) method (Glendening et al. 1987; Carpenter and Weinhold 1988). Following that step, using Gaussian 0.9 software equipped with the DFT with functional B3LYP 6-31G** basis (Frisch et al. 2016) the values of bond length, dipole moment, heath of formation equal to the energy of dissociation, bond energy HOMO/LUMO energy level for single molecules, were again computed using the single-point energy option key word.

Visualization of the HOMO/LUMO orbitals and changes of the electron density for particular molecules and their three molecule systems was performed involving the HyperChem 8.0 software (Froimowitz 1993; Mazurkiewicz and Tomasik 2013).

Results and discussion

Generally, SMF decreased stability of the poprhine molecule (Table 1). Heat of formation increased with an increase in applied flux density. This effect depended on the positioning of the molecule in respect to the direction of SMF defined in terms

of the Cartesian system. The response of the molecule in the x-y, y-z and x-z planes did not parallel one another. An increase in the value of heat of formation was accompanied by an increase in dipole moment. Again, these changes did not parallel one another.

Thus, SMF destabilized porphine, increasing interatomic distances and separating their charges.

Heat of formation and dipole moments regularly, although to a different extent, increased with an increase in the applied SMF flux density. This effect was common for porphine molecule, regardless whether it was located in either the x-y, y-z or x-z plane. However, in terms of dipole moment, the strongest reaction to an increase in flux density was noted for the molecule situated in the x-y plane.

These total effects resulted from the distribution of the charge density at particular atoms, bond lengths, the deformation of the molecules and changes of their initial position in selected plane of the Cartesian system. Table 2 shows that, usually, charge density at particular atoms changed irregularly against an increase in the SMF flux density. The irregularity in associated bond lengths is shown in Table 3.

Table 2 revealed that the highest number of irregular changes of the charge distribution against changes of flux density was met in the molecule situated in the x-y and y-z planes, whereas the number of such irregularities in the x-z plane was minute. It should also be noted that several cases of a lack of sensitivity of the charge density to an increase in the flux density were observed when the molecule was oriented in the x-z plane.

The highest number of irregular changes of the bond lengths against an increase in flux density was observed for the molecule situated in the x-y plane.

Fig. 2 presents deformation of this molecule situated in the x-y, y-z and x-z planes of the Cartesian system.

One might see that, first of all, regardless of the positioning of the molecule in the Cartesian system, the deformation involved pyrrole rings holding the hydrogen atoms at the ring nitrogen atoms and the length of the C–H and N–H bonds. The magnitudes of the deformation are well illustrated by a variation of the charge density at particular atoms (Table 2) and corresponding bond lengths (Table 3). Particularly, but not solely, structures of the molecule situated in the y-z plane show that the macrocyclic ring lost its planarity. Porphine treated with external electric field behaved similarly (Mazurkiewicz and Tomasik 2013).

Table 1. Heat of formation [kJ.mol^{-1}] and dipole moment [D] of the porphine molecule depending on its positioning in the Cartesian system and applied SMF flux density [AFU].

Orientation along the axes of the Cartesian System	Heat of formation [kJ·mol^{-1}] at SMF flux density [AFU]					Dipole moment [D] at SMF flux density [AFU]				
	0	**0.1**	**1.0**	**10**	**100**	**0**	**0.1**	**1.0**	**10**	**100**
x-y	-792	-782	-758	-731	-704	2.01	2.12	2.48	2.88	3.09
y-z	-792	-789	-765	-742	-711	2.01	2.03	2.11	2.16	2.63
x-z	-792	-781	-763	-715	-697	2.01	2.06	2.34	2.74	2.89

Table 2. Charge density [a.u] at particular atoms of the porphine molecule depending on SMF flux density [AFU] positioning in the Cartesian system.

Atom	SMF along indicated Cartesian axis	Tendency*	Charge density [a.u] at SMF flux density [AFU]				
			0	0.1	1.0	10	100
N1	X	**RH**	-1.119	-1.045	-0.987	-0.985	-0.937
	Z	**RH**		-1.025	-1.017	-1.012	-0.934
	Y	**IH**		-1.004	-0.789	-0.940	-0.545
N2	X	**IL**	-0.817	-0.807	-0.795	-0.813	-0.855
	Z	**RH**		-0.783	-0.779	-0.772	-0.756
	Y	**V**		-0.750	-0.684	-0.425	-0.725
N3	X	**IH**	-1.089	-1.025	-0.993	-0.948	-0.985
	Z	**IL**		-0.988	-0.986	-0.991	-0.995
	Y	**IH**		-1.035	-0.938	-0.978	-0.789
N4	X	**RH**	-0.817	-0.816	-0.795	-0.762	-0.754
	Z	**IH**		-0.785	-0.779	-0.785	-0.765
	Y	**V**		-0.662	-0.759	-0.503	-0.454
C5	X	**IH**	0.492	0.454	0.359	0.447	0.572
	Z	**IL**		0.450	0.457	0.431	0.391
	Y	**RL**		0.474	0.282	0.152	0.070
C6	X	**IH**	-0.355	-0.351	-0.312	-0.317	-0.283
	Z	**NC**		-0.354	-0.362	-0.350	-0.348
	Y	**IH**		-0.370	-0.148	-0.121	-0.094
C7	X	**IL**	0.393	0.362	0.310	0.354	0.285
	Z	**NC**		0.384	0.380	0.385	0.383
	Y	**RL**		0.332	0.269	0.163	-0.283
C8	X	**IH**	-0.283	-0.251	-0.267	-0.244	-0.197
	Z	**NC**		-0.274	-0.272	-0.278	-0.273
	Y	**IH**		-0.219	-0.077	-0.007	-0.163
C9	X	**RL**	-0.213	-0.214	-0.233	-0.249	-0.257
	Z	**NC**		-0.226	-0.223	-0.221	-0.222
	Y	**V**		-0.150	-0.150	-0.232	-0.059
C10	X	**RH**	0.282	0.285	0.286	0.305	0.353
	Z	**IL**		0.281	0.278	0.254	0.262
	Y	**IL**		0.220	0.105	0.185	-0.088
C11	X	**V**	-0.253	-0.273	-0.227	-0.301	-0.298
	Z	**V**		-0.296	-0.291	-0.273	-0.268
	Y	**V**		-0.116	-0.202	-0.235	-0.001
C12	X	**V**	0.434	0.418	0.330	0.425	0.476
	Z	**V**		0.389	0.392	0.371	0.409
	Y	**IL**		0.339	0.255	0.260	0.226
C13	X	**V**	-0.292	-0.305	0.018	0.338	0.470
	Z	**V**		-0.266	-0.269	-0.241	-0.272
	Y	**V**		-0.353	-0.207	-0.152	0.356
C14	X	**IH**	-0.292	-0.249	-0.309	0.037	0.023
	Z	**V**		-0.269	-0.269	-0.282	-0.268
	Y	**V**		-0.291	-0.372	-0.184	-0.348
C15	X	**V**	0.434	0.354	0.419	0.247	0.209
	Z	**IL**		0.397	0.392	0.418	0.385
	Y	**RL**		0.410	0.389	0.290	0.094
C16	X	**IH**	-0.253	-0.221	-0.322	-0.139	-0.189
	Z	**IL**		-0.295	-0.291	-0.303	-0.311
	Y	**V**		-0.311	-0.073	-0.103	-0.089

Atom	SMF along indicated Cartesian axis	Tendency*	Charge density [a.u] at SMF flux density [AFU]				
			0	0.1	1.0	10	100
C17	X	**V**	0.282	0.281	0.309	0.243	0.256
	Z	**RL**		0.278	0.278	0.277	0.257
	Y	**RL**		0.252	0.230	0.148	-0.051
C18	X	**NC**	-0.213	-0.201	-0.233	-0.206	-0.207
	Z	**NC**		-0.224	-0.223	-0.224	-0.224
	Y	**IH**		-0.197	-0.127	-0.095	-0.067
C19	X	**V**	-0.283	-0.272	-0.249	-0.274	-0.272
	Z	**V**		-0.272	-0.272	-0.265	-0.274
	Y	**IH**		-0.163	-0.183	-0.189	-0.124
C20	X	**RL**	0.393	0.356	0.348	0.288	0.275
	Z	**NC**		0.388	0.379	0.393	0.400
	Y	**V**		0.235	0.243	0.263	0.113
C21	X	**V**	-0.355	-0.352	-0.360	-0.218	-0.095
	Z	**NC**		-0.363	-0.359	-0.349	-0.375
	Y	**IH**		-0.232	-0.238	-0.146	-0.123
C22	X	**RL**	0.492	0.428	0.419	0.292	0.169
	Z	**RL**		0.470	0.456	0.456	0.442
	Y	**IL**		0.367	0.338	0.183	0.276
C23	X	**V**	-0.230	-0.210	-0.052	-0.175	-0.152
	Z	**NC**		-0.241	-0.241	-0.242	-0.240
	Y	**IH**		-0.133	-0.175	-0.129	-0.019
C24	X	**V**	-0.230	-0.160	-0.223	0.026	-0.032
	Z	**NC**		-0.242	-0.241	-0.234	-0.232
	Y	**V**		-0.288	-0.112	-0.140	-0.021
H25	X	**V**	0.267	0.209	0.290	0.258	-0.071
	Z	**NC**		0.265	0.264	0.273	0.270
	Y	**V**		0.269	0.126	0.077	0.127
H26	X	**V**	0.230	0.217	0.234	0.260	0.237
	Z	**NC**		0.239	0.235	0.232	0.233
	Y	**IL**		0.214	0.069	0.077	0.103
H27	X	**V**	0.240	0.235	0.234	0.270	0.268
	Z	**IL**		0.239	0.241	0.235	0.232
	Y	**V**		0.179	0.175	0.179	0.151
H28	X	**NC**	0.250	0.247	0.245	0.250	0.247
	Z	**NC**		0.246	0.246	0.249	0.251
	Y	**IL**		0.192	0.168	0.179	0.166
H29	X	**NC**	0.254	0.248	0.259	0.260	0.258
	Z	**NC**		0.255	0.252	0.251	0.250
	Y	**IL**		0.170	0.197	0.151	0.075
H30	X	**V**	0.237	0.247	0.018	0.234	0.188
	Z	**NC**		0.245	0.244	0.238	0.243
	Y	**V**		0.080	0.220	0.180	0.027
H31	X	**V**	0.237	0.059	0.256	0.060	0.071
	Z	**NC**		0.243	0.244	0.237	0.238
	Y	**IL**		0.245	0.122	0.120	0.061
H32	X	**IL**	0.254	0.242	0.253	0.218	0.206
	Z	**NC**		0.253	0.252	0.256	0.258
	Y	**IL**		0.261	0.149	0.114	0.099
H33	X	**V**	0.250	0.237	0.250	0.233	0.189
	Z	**NC**		0.246	0.246	0.242	0.244
	Y	**RL**		0.216	0.174	0.167	0.132

Atom	SMF along indicated Cartesian axis	Tendency*	Charge density [a.u] at SMF flux density [AFU]				
			0	0.1	1.0	10	100
H34	X	**V**	0.240	0.233	0.252	0.238	0.218
	Z	**NC**		0.241	0.241	0.244	0.247
	Y	**V**		0.159	0.169	0.288	0.179
H35	X	**V**	0.230	0.232	0.248	0.233	0.244
	Z	**NC**		0.236	0.236	0.227	0.234
	Y	**IL**		0.126	0.139	0.099	0.055
H36	X	**V**	0.267	0.257	0.054	0.339	0.244
	Z	**NC**		0.264	0.264	0.256	0.253
	Y	**V**		0.177	0.207	0.165	0.035
H37	X	**NC**	0.474	0.474	0.479	0.481	0.441
	Z	**IL**		0.452	0.446	0.447	0.434
	Y	**V**		0.585	0.402	0.091	0.378
H38	X	**RH**	0.461	0.485	0.489	0.492	0.530
	Z	**RL**		0.454	0.447	0.445	0.442
	Y	**V**		0.484	0.508	0.048	0.594

*Abbreviations used here and in next Tables: RHregularly increasing, IH - irregularly increasing, RL- regularly decreasing, IL - irregularly decreasing, V - lack of any regular tendency, NC - nearly constant.

Table 3. Bond lengths [Å] between particular atoms of the porphine molecule depending on SMF flux density [AFU] positioning in the Cartesian system. See Table 2 for notation.

Bond	SMF along indicated Cartesian axis	Tendency*	Bond length [Å] at flux density [AFU]				
			0	0.1	1.0	10	100
N1-C5	X	**IL**	1.326	1.352	1.409	1.373	1.387
	Z	**IH**		1.385	1.402	1.390	1.463
	Y	**IH**		1.358	1.451	1.640	1.502
N1-C22	X	**RH**	1.340	1.354	1.381	1.434	1.438
	Z	**V**		1.407	1.402	1.405	1.425
	Y	**IH**		1.417	1.430	1.552	1.432
N1-H37	X	**NC**	1.010	1.112	1.040	1.055	1.108
	Z	**V**		0.990	0.990	0.975	0.985
	Y	**IH**		1.052	1.480	1.732	1.727
N2-C7	X	**V**	1.325	1.357	1.392	1.357	1.345
	Z	**V**		1.432	1.337	1.321	1.320
	Y	**IH**		1.422	1.349	1.448	1.552
N2-C10	X	**V**	1.401	1.410	1.374	1.411	1.379
	Z	**V**		1.432	1.425	1.433	1.431
	Y	**IH**		1.458	1.593	1.579	1.676
N3-C12	X	**IH**	1.328	1.358	1.367	1.389	1.370
	Z	**V**		1.384	1.391	1.375	1.368
	Y	**V**		1.303	1.416	1.484	1.226
N3-C15	X	**RH**	1.328	1.347	1.389	1.404	1.435
	Z	**V**		1.394	1.391	1.392	1.395
	Y	**V**		1.359	1.270	1.358	1.277
N3-H38	X	**NC**	1.010	1.104	1.024	1.023	1.101
	Z	**NC**		0.990	0.993	0.987	0.995
	Y	**V**		0.978	0.824	1.494	1.436
N4-C17	X	**IL**	1.401	1.383	1.411	1.371	1.361
	Z	**IH**		1.427	1.425	1.434	1.500
	Y	**IH**		1.486	1.407	1.500	1.896

Bond	SMF along indicated Cartesian axis	Tendency*	Bond length [Å] at flux density [AFU]				
			0	0.1	1.0	10	100
N4-C20	X	**IH**	1.325	1.368	1.383	1.382	1.381
	Z	**V**		1.339	1.337	1.326	1.320
	Y	**IH**		1.480	1.476	1.365	1.772
C5-C6	X	**RH**	1.340	1.336	1.370	1.440	1.480
	Z	**V**		1.364	1.365	1.361	1.344
	Y	**IH**		1.246	1.432	1.457	1.582
C5-C24	X	**V**	1.458	1.472	1.473	1.350	1.375
	Z	**IH**		1.488	1.492	1.499	1.453
	Y	**RH**		1.478	1.597	1.656	1.671
C6-C7	X	**RL**	1.460	1.442	1.412	1.412	1.379
	Z	**V**		1.428	1.435	1.410	1.450
	Y	**V**		1.416	1.546	1.559	1.596
C6-H26	X	**V**	1.080	1.198	1.123	1.107	1.209
	Z	**IH**		1.098	1.100	1.171	1.113
	Y	**RH**		1.262	1.706	1.854	1.891
C7-C8	X	**V**	1.462	1.453	1.425	1.450	1.514
	Z	**IH**		1.490	1.495	1.493	1.500
	Y	**V**		1.568	1.398	1.429	1.671
C8-C9	X	**V**	1.326	1.307	1.398	1.388	1.396
	Z	**V**		1.366	1.365	1.359	1.395
	Y	**IH**		1.459	1.454	1.461	1.696
C8-H27	X	**V**	1.080	1.172	1.098	1.077	1.223
	Z	**RH**		1.084	1.086	1.094	1.124
	Y	**RH**		1.382	1.657	1.730	1.776
C9-C10	X	**RL**	1.456	1.445	1.428	1.424	1.441
	Z	**IH**		1.492	1.491	1.497	1.500
	Y	**IH**		1.562	1.532	1.547	1.802
C9-H28	X	**V**	1.080	1.129	1.094	1.091	1.150
	Z	**IH**		1.082	1.094	1.104	1.085
	Y	**IH**		1.459	1.499	1.408	1.911
C10-C11	X	**IH**	1.340	1.351	1.419	1.364	1.381
	Z	**V**		1.357	1.358	1.348	1.329
	Y	**IH**		1.418	1.418	1.383	1.587
C11-C12	X	**V**	1.460	1.407	1.397	1.428	1.417
	Z	**V**		1.426	1.430	1.433	1.429
	Y	**V**		1.452	1.463	1.341	1.778
C11-H29	X	**V**	1.080	1.160	1.141	1.076	1.179
	Z	**V**		1.104	1.105	1.097	1.103
	Y	**IH**		1.535	1.433	1.604	2.068
C12-C13	X	**RH**	1.337	1.380	1.380	1.382	1.480
	Z	**V**		1.435	1.430	1.426	1.430
	Y	**IH**		1.410	1.464	1.614	1.599
C13-C14	X	**NC**	1.450	1.400	1.395	1.425	1.431
	Z	**IL**		1.483	1.410	1.480	1.401
	Y	**V**		1.418	1.416	1.537	1.070
C13-H30	X	**V**	1.080	1.138	2.265	1.179	1.109
	Z	**V**		1.082	1.085	1.085	1.007
	Y	**V**		1.817	1.338	1.496	2.060

Bond	SMF along indicated Cartesian axis	Tendency*	Bond length [Å] at flux density [AFU]				
			0	0.1	1.0	10	100
C14-C15	X	**V**	1.337	1.342	1.408	1.403	1.401
	Z	**RH**		1.430	1.430	1.442	1.453
	Y	**IH**		1.406	1.392	1.507	1.620
C14-H31	X	**IH**	1.080	1.798	1.120	3.640	6.799
	Z	**IH**		1.083	1.086	1.127	1.079
	Y	**IH**		1.130	1.739	1.860	1.753
C15-C16	X	**V**	1.460	1.414	1.382	1.436	1.452
	Z	**V**		1.434	1.430	1.428	1.442
	Y	**IH**		1.378	1.454	1.495	1.633
C16-C17	X	**RH**	1.340	1.384	1.368	1.428	1.452
	Z	**IH**		1.355	1.358	1.362	1.329
	Y	**V**		1.316	1.428	1.518	1.497
C16-H32	X	**IH**	1.080	1.225	1.084	1.298	1.359
	Z	**NC**		1.104	1.105	1.098	1.103
	Y	**RH**		1.104	1.595	1.778	1.891
C17-C18	X	**V**	1.456	1.435	1.435	1.424	1.445
	Z	**V**		1.493	1.491	1.476	1.500
	Y	**RH**		1.504	1.508	1.560	1.671
C18-C19	X	**V**	1.337	1.357	1.320	1.418	1.417
	Z	**IH**		1.367	1.365	1.374	1.395
	Y	**IH**		1.387	1.527	1.482	1.696
C18-H33	X	**V**	1.080	1.198	1.085	1.200	1.232
	Z	**RH**		1.084	1.086	1.094	1.095
	Y	**RH**		1.276	1.547	1.568	1.776
C19-C20	X	**V**	1.452	1.448	1.453	1.386	1.384
	Z	**RH**		1.485	1.496	1.499	1.516
	Y	**V**		1.517	1.378	1.417	1.802
C19-H34	X	**V**	1.080	1.138	1.077	1.073	1.223
	Z	**RH**		1.083	1.086	1.094	1.971
	Y	**V**		1.521	1.494	1.407	1.911
C21-C22	X	**V**	1.340	1.364	1.389	1.365	1.344
	Z	**IH**		1.354	1.362	1.368	1.344
	Y	**IH**		1.401	1.324	1.656	1.770
C20-C21	X	**V**	1.460	1.418	1.402	1.451	1.472
	Z	**IL**		1.366	1.362	1.358	1.329
	Y	**V**		1.459	1.432	1.457	1.633
C21-H35	X	**V**	1.080	1.997	1.088	1.157	1.056
	Z	**V**		1.102	1.100	1.095	1.113
	Y	**IH**		1.567	1.465	1.614	2.068
C22-C23	X	**V**	1.458	1.441	1.428	1.520	1.584
	Z	**V**		1.485	1.492	1.475	1.453
	Y	**RH**		1.500	1.544	1.656	1.599
C23-C24	X	**V**	1.333	1.277	1.280	1.355	1.329
	Z	**RH**		1.357	1.362	1.368	1.397
	Y	**IH**		1.403	1.484	1.593	1.070
C23-H36	X	**V**	1.080	1.225	1.733	1.082	1.214
	Z	**V**		1.097	1.088	1.073	1.129
	Y	**IH**		1.528	1.445	1.623	2.060
C24-H25	X	**IH**	1.080	1.354	1.064	3.183	6.835
	Z	**NC**		1.084	1.088	1.083	1.096
	Y	**IH**		1.1591	1.689	1.839	1.753

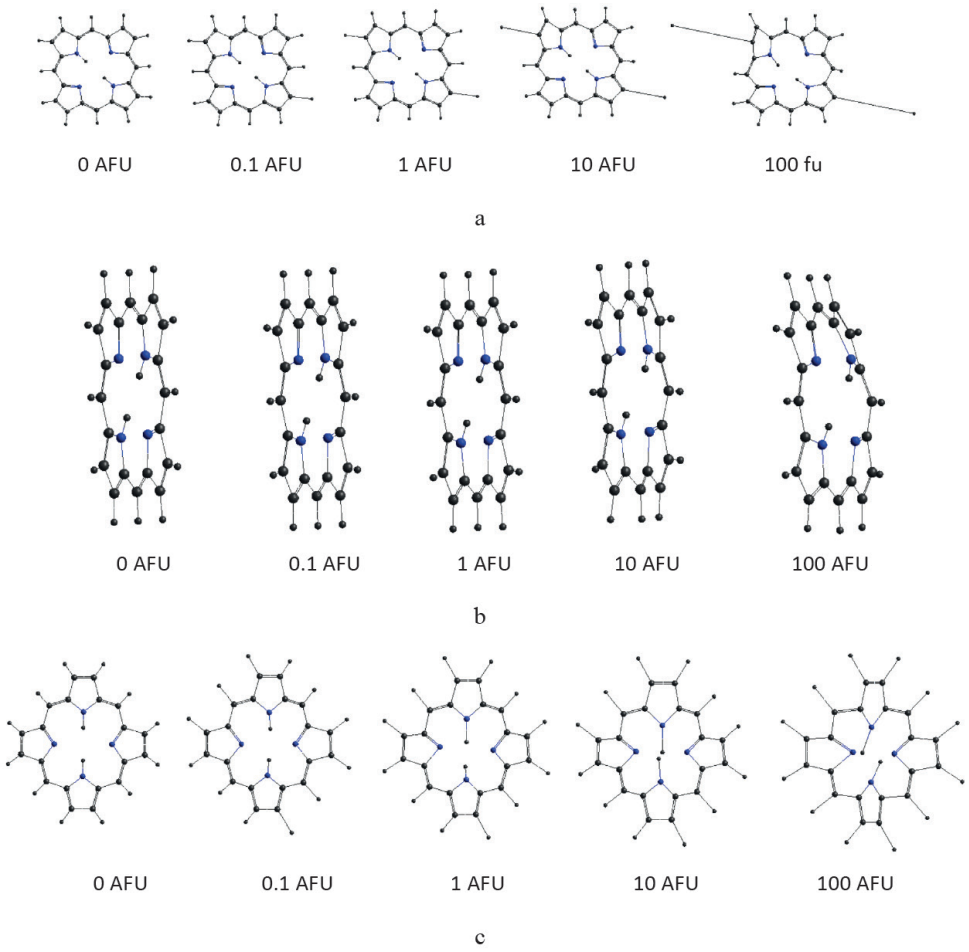

Figure 2. Deformation of the porphine molecule in SMF of flux density increasing from 0 to 100 AFU. The molecule was situated either in the x-y (a), y-z (b) or x-z (c) planes of the Cartesian system. SMF was applied along the x-axis.

Conclusions

The planar molecule of porphine deforms when placed in the static magnetic field. The deformation depends on the situating the molecule against the field. The deformation engages pyrrole rings holding the hydrogen atoms at the ring nitrogen atoms. The length of the C–H and N–H bonds is also an essential factor.

Data availability

All data underlying the results are available as part of the article and no additional source data are required.

References

Aylward N, Bofinger N (2005) Possible origin for porphin derivatives in prebiotic chemistry - a computational study. Origins of Life and Evolution of the Biosphere 35(4): 345–368. https://doi.org/10.1007/s11084-005-2044-x

Carpenter JE, Weinhold F (1988) Analysis of the geometry of the hydroxymethyl radical by the different hybrids for different spins natural bond orbital procedure. Journal of Molecular Structure (Teochem) 139: 41–62. https://doi.org/10.1016/0166-1280(88)80248-3

Caughey WS, Ibers JA (1977) Crystal and molecular structure of the free base porphyrin, protoporphyrin IX dimethyl ester. Journal of the American Chemical Society 99(20): 6639–6645. https://doi.org/10.1021/ja00462a027

Charistos ND, Muñoz-Castro A (2019) Double aromaticity of the B-40 fullerene: Induced magnetic field analysis of pi and sigma delocalization in the boron cavernous structure. Physical Chemistry Chemical Physics 21(36): 20232–20238. https://doi.org/10.1039/C9CP04223G

Ciesielski W, Girek T, Oszczęda Z, Soroka JA, Tomasik P (2021) Towards recognizing mechanisms of effects evoked in living organisms by static magnetic field. Numerically simulated effects of the static magnetic field upon simple inorganic molecules. F1000 Research 10: e611. https://doi.org/10.12688/f1000research.54436.1

Ciesielski W, Girek T, Oszczęda Z, Soroka JA, Tomasik P (2022a) Potential risk resulting from the influence of static magnetic field upon living organisms. Numerically simulated effects of the static magnetic field upon simple alkanols. BioRisk [in press].

Ciesielski W, Girek T, Kołoczek H, Oszczęda Z, Soroka JA, Tomasik P (2022b) Potential risk resulting from the influence of static magnetic field upon living organisms. Numerically simulated effects of the static magnetic field upon carbohydrates. BioRisk [in press].

Committee to Assess the Current Status and Future Direction of High Magnetic Field Science in the United States (2013) High Magnetic Field Science and Its Application in the United States; Current Status and Future Directions. Natl. Res. Council, National Acad., The National Academies Press, Washington, D.C.

Elder GH (1994) Haem synthesis and the porphyrias. In *Scientific Foundations of Biochemistry in Clinical Practice* (2nd Edn.). Williams DL, Marks V. (Eds), Imprint: Butterworth-Heinemann, Oxford, UK. https://doi.org/10.1016/B978-0-7506-0167-2.50029-7

Farberovich OV, Mazalova VL (2016) Ultrafast quantum spin-state switching in the Co-octaethylporphyrin molecular magnet with a terahertz pulsed magnetic field. Journal of Magnetism and Magnetic Materials 405: 169–173. https://doi.org/10.1016/j.jmmm.2015.12.038

Frisch MJ, Trucks GW, Schlegel HB, Frisch MJ, Trucks GW, Schlegel HB, Scuseria GE, Robb MA, Cheeseman JR, Scalmani G, Barone V, Mennucci B, Petersson GA (2016) Gaussian 09, Revision A.02, Gaussian, Inc., Wallingford.

Froimowitz M (1993) HyperChem: A software package for computational chemistry and molecular modelling. BioTechniques 14: 1010–1013.

Glendening ED, Reed AE, Carpenter JE (1987) Extension of Lewis structure concepts to open-shell and excited-state molecular species, NBO Version 3.1. Ph.D. thesis, University of Wisconsin, Madison, WI.

Hamza A-SHA, Shaher SA, Mohmoud A, Ghania SM (2002) Environmental pollution by magnetic field associated with power transmission lines. Energy Conversion and Management 43(17): 2442–2452. https://doi.org/10.1016/S0196-8904(01)00173-X

Kadish KM, Smith KM, Guilard R (Eds) (2000) Porphyrin Handbook, Academic Press, San Diego.

Magnet Science and Technology (2021) Magnet Science & Technology. https://nationalmaglab.org/magnet-development/magnet-science-technology [Retrieved 4th Jan. 2021]

Magnetism in real life (2021) http://www.scienceclarified.com/everyday/Real-Life-Physics-Vol-3-Biology-Vol-1/Magnetism-Real-life-applications.html [Retrieved 4th Jan. 2021]

Marchand N, Lienard P, Siehl H, Izato H (2014) Applications of molecular simulation software SCIGRESS in industry and university. Fujitsu Scientific and Technical Journal 50(3): 46–51.

Mazurkiewicz J, Tomasik P (2013) Effect of external electric field to porphine and selected metalloporphin systems. Journal of Alternative and Complementary Medicine (New York, N.Y.) 1: 13–21.

Ortiz de Montellano PR (2008) Hemes in Biology. Wiley Encyclopedia of Chemical Biology. John Wiley & Sons. https://doi.org/10.1002/9780470048672.wecb221

Rankovic V, Radulovic J (2009) Environmental pollution by magnetic field around power lines. International Journal of Qualitative Research 3(3): 1–6.

BioRisk 18: 105–113 (2022)
doi: 10.3897/biorisk.18.80357
https://biorisk.pensoft.net

DATA PAPER

A peer-reviewed open-access journal
BioRisk

A study of the microbiology of the intestinal tract in different species of Teleost fish from the Black Sea

Sevginar Ibryamova[1], Stephany Toschkova[1], Borislava Pavlova[1], Elitca Stanachkova[1], Radoslav Ivanov[1], Nikolay Natchev[1], Nesho Chipev[2], Tsveteslava Ignatova-Ivanova[1]

1 *Department of Biology, Shumen University, Shumen, Bulgaria, Shumen University "Konstantin Preslavski" Department of Biology 115 Universitetska Str., Shumen, Bulgaria* **2** *Laboratory of Free Radical Processes, Institute of Neurobiology, Bulgarian Academy of Sciences, Acad. G. Bonchev Str. 23, Sofia, Bulgaria*

Corresponding author: Tsveteslava Ignatova-Ivanova (ts.ignatovaivanova@shu.bg)

Academic editor: Josef Settele | Received 10 January 2022 | Accepted 15 July 2022 | Published 4 August 2022

Citation: Ibryamova S, Toschkova S, Pavlova B, Stanachkova E, Ivanov R, Natchev N, Chipev N, Ignatova-Ivanova T (2022) A study of the microbiology of the intestinal tract in different species of Teleost fish from the Black Sea. BioRisk 18: 105–113. https://doi.org/10.3897/biorisk.18.80357

Abstract

This paper presents a study on the microbial status of different fish species and their habitats in the Bulgarian Black Sea area. The samples were collected in the period of January 2021 until March 2021. The fish species we used in this study were Black Sea turbot (*Scophthalmus maximus*), round goby (*Neogobius melanostomus*), shore rockling (*Gaidropsarus mediterraneus*) and European anchovy (*Engraulis encrasicolus*). The BIOLOG system was used for microbiological determination. From the different fish species, different species of microorganisms were isolated (using selective nutrient media). From the torbut, we isolated species *Enterococcus villorum* with 24 × 10^3 cells in 1 ml, *Moraxella nonliquefaciens* with 70 × 10^3 cells in 1 ml and *Pseudomonas synxantha* with 123 × 10^3 cells. *Pseudomonas putida* was isolated from the round goby with 20 × 10^3 cells in 1 ml. The species *Streptococcus entericus* with 123 × 10^3 cells in 1 ml was isolated from the shore rockling. Pseudomonas fulva with 60 × 10^3 cells in 1 ml was isolated from the *European anchovy*. A total of 223 × 10^3 cells in 1 ml of *Pseudomonas agarici* were isolated from *Trachinus draco*. *Pseudomonas tolaasii* with 145 × 10^3 cells in 1 ml were isolated from *Merlangius merlangus*. A different species of bacteria of the genus *Pseudomonas* was found for each of the investigated species of Black Sea fish. Apparently, the species *Pseudomonas* is characteristic of marine Teleostei and is important for the life and metabolism of these vertebrates. These microorganisms probably are resident species and developed not as result of pollution or environmental change.

Keywords

marine fish, microbial status, intestinal tract

Introduction

Fish are consumed in large quantities throughout the world and are considered one of the main sources of protein. According to FAO (2007), fish are the most important single source of high quality protein providing about 16% of the animal protein consumed by the world's human population. Fish have high nutritional values and are a good source of saturated fats, omega-3 fatty acids that cannot be synthesised by the human body. Fish are known to be low in fat and cholesterol and are easily digested and suitable for infants, children and the elderly. Unlike other local products, the price of fish is much lower and more affordable for most people. The microbiology of fish is closely related to human health because it can represent a risk depository, as fish carry inside and on their surface different types of microorganisms. On the other hand, the microbiology of fish is closely dependent on the state of the environment and can be used as an indicator of the water quality. Several bacterial genera, such as *Escherichia*, *Listeria*, *Pseudomonas*, *Klebsiella* and *Salmonella* were isolated from fish and can indicate multisource pollution (Sichewo et al. 2014; Manhondo et al. 2018). Banquero et al. (2008) described aquatic systems as genetic reactors or hotspots for AMR genes where significant genetic exchange and recombination can occur and can shape the evolution of future resistance profiles. Bacteria very quickly acquire resistance either through gene transfer or through mutations. In this way, antibiotic resistance genes can also be passed on. These processes occur mainly in the intestinal tract of fish (Levy and Marshall 2004). Random use of antimicrobials is associated with increased selection pressure on bacterial populations and favours the survival and reproduction of resistant bacteria. In Bulgaria, Stratev et al. (2015) conducted a study of 161 samples of frozen fish products collected from retail markets. High numbers of total viable counts (TVCs) were found in Black Sea roach (7.28 log cfu/g) and horse mackerel (5.90 log cfu/g). High amounts of *Aeromonas spp*. were found in the Black Sea horse mackerel (2.68 log cfu/g). *Aeromonas spp.* was not found in the Black Sea roach.

After their death, fish undergo rapid bacterial and microbiological changes, which are determining factors in their consumption by humans (Stratevaa et al. 2021). The expiry period of fish is determined by the content of protein, fat, water (Velioğlu et al. 2015) and the amount of microorganisms (Fengou et al. 2019). Fresh fish have a high water quantity and this may be the reason for their rapid spoilage (Zotta et al. 2019).

To date, data on the microbiota of fish in the Black Sea are very limited. Gaining information in this field is important as the sea can be a source of species of bacteria that are potentially dangerous to human health. The main goal of the present work was to study the microbiological composition of the intestinal tract in different species of Teleost fish from the Black Sea.

Place and duration of the study

The study was conducted at the Department of Biology, University of Shumen, Bulgaria, January 2021 until March 2021. The samples were collected from the regions of Varna: 43.18 N, 27.91 E and Sozopol: 42.4317N, 27.70 E (Datum WGS 84) (Fig. 1).

Collection of the samples

The fish individuals were randomly sampled from trawl catches using pelagic Midwater otter trawl (7 × 7 mm mesh size of the codend) from two localities of the Bulgarian Black Sea aquatory (Fig. 1). On board, the fish samples were shock frozen for best preservation and transported to the laboratory for further analyses.

Microbiological analysis

The fish were scrubbed free of dirt, washed in hypochlorite solution (20 mg/l), rinsed with sterile distilled water and shucked with a sterile knife. Tissue liquor samples (about 100 g) were homogenised (Maffei et al. 2009). Faecal coliforms (FC) were enumerated through a five tubes per dilution most probable number (MPN) series (Ignatova-Ivanova et al. 2018). After 3 h at 37 °C plus 21 h at 44 °C, gas positive tubes were recorded for FC. From each FC gas positive tube, 0.1 ml were transferred in tubes with 10 ml of Tryptone Water (Oxoid, Basingstoke, UK) and then incubated for 24 h at 44 °C. E. coli were enumerated by MacConkey agar (Merck, Darmstadt, Germany). The plates very incubated aerobically at 35–37 °C for 18–24 hours. E. coli developed matte dark pink to tile red, surrounded by an opaque area due to the precipitation of bile salts in this environment. Pseudomonas sp. were enumerated by Cetrimide Agar (Merck KGaA, 64271 Darmstadt, Germany).

Figure 1. Sampling locations at the Black sea coast.

Microbial Identification Databases for the "BIOLOG" System

The microbial identification was performed by the BIOLOG Microbial Identification System VIO45101AM. The isolated strains were screened on BL4021502 Tryptic Soy Agar (TCA), cultured for 24 hours at 37 °C and then subjected to Gen III plaque identification to identify Gram positive and Gram negative aerobic bacteria. The microscopic pictures were performed using the stereomicroscope OPTIKA (Italy) with a DinoEye, Eyepiece camera with 5 megapixels. The photographs were taken by using a Canon EOS 60D camera. The GEN III MicroPlate test panel provides a standardised micromethod using 94 biochemical tests to profile and identify a broad range of Gram-negative and Gram-positive bacteria. BIOLOG's Microbial Identification Systems software (e.g. OmniLog Data Collection) is used to identify the bacterium from its phenotypic pattern in the GEN III MicroPlate. The BIOLOG system allows us to quickly and accurately identify more than 2900 species of aerobic and anaerobic bacteria, yeasts and fungi. BIOLOG's advanced phenotypic technology provides valuable information on the properties of the strains, in addition to species-level identification. BIOLOG's carbon technology identifies the environment and pathogenic microorganisms by producing a characteristic pattern or "metabolic fingerprint" of discrete test reactions performed in a 96-well microplate. The culture suspensions are tested with a panel of pre-selected assays, then incubated, read and compared with extensive data-bases. https://www.biolog.com/productsportfolio-overview/microbial-identification.

Results

Using some classical microbiological methods, we investigated probes from the gastrointestinal tract of different species of fish from the Bulgarian Black Sea aquatory. After 24 h of cultivation on different media, the number of cells in 1 ml were obtained. The species of microorganisms were confirmed not only on selective media, but also by the results of the BIOLOG system. Data are represented in Table 1 and Fig. 2.

For the present study, fresh Black Sea fish were used, which were dissected in laboratory conditions. The intestinal tract was used for microbiological analysis. Different species of microorganisms were isolated from the fish species using selective nutrient media (Table 1) – *E. villorum* species (Fig. 2a) were isolated from *S. maximus* with 24×10^3 cells in 1 ml, *M. nonliquefaciens* with 70×10^3 cells in 1 ml and *P. synxantha* with 123×10^3 cells in 1 ml. The species *P. putida* was isolated from the Round goby with 20×10^3 cells in 1 ml. The species S. entericus with 123×10^3 cells in 1 ml was isolated from P. flesus. P. fulva with 60×10^3 cells in 1 ml was isolated from Sardine. A total of 223×10^3 cells in 1 ml of *P. agarici* (Fig. 2b) were isolated from *T. draco* and *P. tolaasii* with 145×10^3 cells in 1 ml were isolated from *M. merlangus*.

Table 1. Number of cells in 1 ml on the different media.

Media/ fish	Pseudomonas agar	Streptococcus selective agar	Chromokult agar	MacConkey agar	strain BIOLOG
T26F1 *Scophthalmus maximus* – turbot–Varna				24.10^3	*Enterococcus villorum*
Scophthalmus maximus – turbot – Varna		70.10^3			*Moraxella nonliquefaciens*
Scophthalmus maximus – turbot – Varna				123.10^3	*Pseudomonas synxantha*
T26F3 *Neogobius melanostomus* – round goby – Varna				20.10^3	*Pseudomonas putida*
20T29-30F7 *Platichthys flesus* – shore rockling – Varna				123.10^3	*Streptococcus entericus*
Engraulis encrasicolus – European anchovy Sozopol				60.10^3	*Pseudomonas fulva*
20T10-11F2 *Trachinus draco* – greater wever – Varna	223.10^3				*Pseudomonas agarici*
20T10-11F3 *Merlangius merlangus* – whiting–Varna	145.10^3				*Pseudomonas tolaasii*

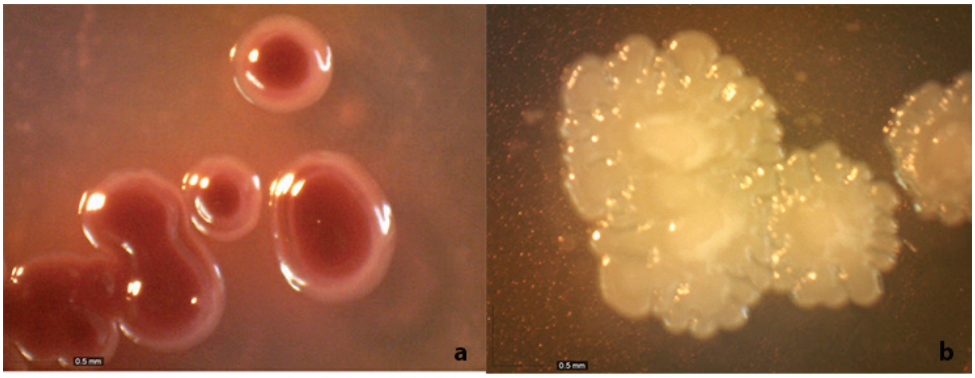

Figure 2. Stereomicroscope picture of the colonies of the isolated species in this case **a** *E. villorum* on media Chromocult agar and **b** *P. agarici* on media Pseudomonas agar. The picture was taken using the stereomicroscope OPTIKA (Italy) and DinoEye, Eyepiece camera, USB, 1.3 megapixsel, up to 5 megapixels.

Discussion

The probable explanation for the difference in the species of microorganisms that were isolated from the intestine of the different fish species indicated that this may be due to the different habitats of fishes and their diet. In the winter months, the round goby lives at a depth of less than 60 m. The turbot is a predator and is found at a depth of 80 m buried in the sand. The flounder inhabits thin bottom layers at a depth of 50 m and feeds on crustaceans, worms and molluscs. The shore rockling feeds on "worms" and crustaceans, while the anchovy feed on plankton. According to Jorquera et al. (2001), some of the bacterial populations that inhabit the intestinal tract of fish include species

such as *Vibrio*, *Pseudomonas*, *Acinetobacter*, *Photobacterium*, *Moraxella*, *Aeromonas*, *Micrococcus* and *Bacillus*. The bacterial species that are part of the intestinal tract of fish depend, on the one hand, on the diet of the fish and, on the other hand, on the state of the marine environment. The microbiota found in marine organisms can be considered in two aspects – the so-called "resident" microbiota, which is stable and unaffected by the environment and the "transitional" microbiota, which depend on environmental conditions. There are very little data in literature on the microbiological composition of the intestine of Black Sea fish. Some data were recently published (Orozova et al. 2010; Stratev et al. 2015; Stratevaa et al. 2021) and showed that these are mainly representatives of *Aeromonas* spp., which cause fish diseases, such as haemorrhagic septicaemia and ulcers. This may lead to large economic losses in fish farms. To date, mostly freshwater fish were studied, such as carp, trout and silver carp. A study on turbot conducted in Turkey showed that the total number of microorganisms isolated on day 0 was 3.3 log cfu/g, but no concrete species were identified (Özogul et al. 2006). There are no data on the exact species composition of microorganisms in the intestinal tract of Black Sea fish to date.

The microbiota of fish may be influenced by many factors, both endogenous and exogenous. Endogenous factors include the origin of the fish host (Miyake et al. 2015), genotype and diet (Wu et al. 2012), parasitic load (Llewellyn et al. 2017), immunological condition (Pérez et al. 2010), but also lifestyle (Stephens et al. 2016). Exogenous factors are habitat specific and include: environment condition, physicochemical parameters of water (Llewellyn et al. 2016; Sylvain et al. 2016) and bacterioplankton composition (Sylvain et al. 2017). Usually in fish intestines, microorganisms play a key role in nutrition, facilitating the breakdown and absorption of specific compounds present in the diet of the host fish.

According to data published very recently (Sylvain et al. 2020), the diverse microbiota community in fish skin mucus is suitable for the development of microbial biomarkers indicating the conditions of the environment, while the more stable and persistent intestinal microbiome is more suitable for studying long-term host-microbial interactions. The different fish species and their habitats showed differences in the taxonomic structure of the microbial community and this was confirmed for all studied species.

Conclusion

The question whether host-related microbiomes are primarily species-specific or depend on environmental factors still remains open. Our study is one of the few to focus on the intestinal microbiome of Black Sea fish species. It is interesting to note that the phylogenetic structure of the microbial communities of different fish is formed by species and habitat-specific factors. A different species of bacteria of the genus *Pseudomonas* was found for each of the investigated species of Black Sea fish. Apparently, *Pseudomonas* species are characteristic of marine Teleostei and are important for the

life and metabolism of these vertebrates. These microorganisms are probably resident species and have developed not as result of pollution or environmental change. The presence of the species *Enterococcus villorum* and *Moraxella nonliquefaciens*, which are pathogenic species, may be due to pollutants of seawater, which settled in the sediment and infested the turbot in its natural habitat.

Acknowledgements

This study was financially supported by the National Research Fund of the Bulgarian Ministry of Education and Science (Grant – KP-06-PH41/2 28.09.2020) and the project by Shumen University project 08-80 / 09.02.2022 Department of Biology.

References

Banquero F, Mart'ınez JL, Canton R (2008) Antibiotics and antibiotic resistance in water environments. Current Opinion in Biotechnology 19(3): 260–265. https://doi.org/10.1016/j.copbio.2008.05.006

FAO (2007) Social issues in small-scale fisheries: how a human rights perspective can contribute to respective fisheries in Proceedings of the Presentation to FAO Committee of Fisheries No 27, Rome, Italy.

Fengou LC, Lianou A, Tsakanikas P, Gkana EN, Panagou EZ, Nychas GJE (2019) Evaluation of Fourier transform infrared spectroscopy and multispectral imaging as means of estimating the microbiological spoilage of farmed sea bream. Food Microbiology 79: 27–34. https://doi.org/10.1016/j.fm.2018.10.020

Ignatova-Ivanova TS, Ibrjmova S, Stanachkova E, Ivanov R (2018) Microbiological characteristic of microflora of (*Mytilus galloprovincialis* Lam.) in the Bulgarian Black Sea aquatory. Research Journal of Pharmaceutical, Biological and Chemical Sciences 9(1): 199–205. https://www.rjpbcs.com/pdf/2018_9(1)/[29].pdf

Jorquera MA, Silva FR, Riquelme CE (2001) Bacteria in the culture of the scallop *Argopecten purpuratus* (Lamarck, 1819). Aquaculture International 9(4): 285–303. https://doi.org/10.1023/A:1020449324456

Levy SB, Marshall B (2004) Antibacterial resistance worldwide: Causes, challenges and responses. Nature Medicine 10(S12): S122–S129. https://doi.org/10.1038/nm1145

Llewellyn MS, McGinnity P, Dionne M, Letourneau J, Thonier F, Carvalho GR, Creer S, Derome N (2016) The biogeography of the Atlantic salmon (*Salmo salar*) gut microbiota. The ISME Journal 10(5): 1280–1284. https://doi.org/10.1038/ismej.2015.189

Llewellyn MS, Leadbeater S, Garcia C, Sylvain FE, Custodio M, Ang KP, Powell F, Carvalho GR, Creer S, Elliot J, Derome N (2017) Parasitism perturbs the mucosal microbiome of Atlantic Salmon. Scientific Reports 7(1): 43465. https://doi.org/10.1038/srep43465

Maffei M, Vernocchi P, Lanciotti R, Guerzoni ME, Belletti N, Gardini F (2009) Depuration of Striped Venus Clam (*Chamelea gallina* L.): Effects on microorganisms. sand content

and mortality. Journal of Food Science 74(1): M1–M7. https://doi.org/10.1111/j.1750-3841.2008.00971.x

Manhondo P, Gono RK, Muzondiwa J, Mafa B (2018) Isolation and identification of pathogenic bacteria in edible fish: A case study of bacterial resistance to antibiotics at Lake Chivero, Zimbabwe. African Journal of Agricultural Research.

Miyake S, Ngugi DK, Stingl U (2015) Diet strongly influences the gut microbiota of surgeonfishes. Molecular Ecology 24(3): 656–672. https://doi.org/10.1111/mec.13050

Orozova P, Chikova V, Najdenski H (2010) Antibiotic resistance of pathogenic for fish isolates of *Aeromonas* spp. Bulgarian Journal of Agricultural Science 16(3): 376–386. https://www.agrojournal.org/16/03-17-10.pdf

Özogul Y, Özogul F, Kuley E, Özkutuk AS, Gökbulut C, Köse S (2006) Biochemical, sensory and microbiological attributes of wild turbot (*Scophthalmus maximus*), from the Black Sea, during chilled storage 2006. Food Chemistry 99(4): 752–758. https://doi.org/10.1016/j.foodchem.2005.08.053

Pérez T, Balcázar JL, Ruiz-Zarzuela I, Halaihel N, Vendrell D, de Blas I, Múzquiz JL (2010) Host-microbiota interactions within the fish intestinal ecosystem. Mucosal Immunology 3(4): 355–360. https://doi.org/10.1038/mi.2010.12

Sichewo PR, Gono RK, Muzondiwa J, Mungwadzi W (2014) Isolation and identification of pathogenic bacteria in edible fish: A case study of rural aquaculture projects feeding livestock manure to fish in Zimbabwe. International Journal of Current Microbiology and Applied Sciences 3(11): 897–904. https://citeseerx.ist.psu.edu/viewdoc/download?doi=10.1.1.680.9981&rep=rep1&type [=pdf]

Stephens WZ, Burns AR, Stagaman K, Wong S, Rawls JF, Guillemin K, Bohannan BJ (2016) The composition of the zebrafish intestinal microbial community varies across development. The ISME Journal 10(3): 644–654. https://doi.org/10.1038/ismej.2015.140

Stratev D, Vashin I, Daskalov H (2015) Microbiological status of fish products on retail markets in the Republic of Bulgaria. International Food Research Journal 22(1): 64–69.

Stratevaa M, Pencheva G, Stratev D (2021) Histological, physicochemical and microbiological changes in the carp (Cyprinus carpio) muscles after freezing. Journal of Aquatic Food Product Technology 30(3): 323–337. https://doi.org/10.1080/10498850.2021.1882633

Sylvain FE, Derome N (2017) Vertically and horizontally transmitted microbial symbionts shape the gut microbiota ontogenesis of a skin-mucus feeding discus 646 fish progeny. Scientific Reports 7(1): 14. https://doi.org/10.1038/s41598-017-05662-w

Sylvain FÉ, Cheaib B, Llewellyn M, Gabriel Correia T, Barros Fagundes D, Luis Val A, Derome N (2016) pH drop impacts differentially skin and gut microbiota of the Amazonian fish tambaqui (*Colossoma macropomum*). Scientific Reports 6: 64310. https://doi.org/10.1038/srep32032

Sylvain FÉ, Holland A, Bouslama S, Audet-Gilbert É, Lavoie C, Val AL, Derome N (2020) Fish skin and gut microbiomes show contrasting signatures of host species and habitat. Applied and Environmental Microbiology 86(16): e00789–e20. https://doi.org/10.1128/AEM.00789-20

Velioğlu HM, Temiz HT, Boyaci IH (2015) Differentiation of fresh and frozen-thawed fish samples using Raman spectroscopy coupled with chemometric analysis. Food Chemistry 172: 283–290. https://doi.org/10.1016/j.foodchem.2014.09.073

Wu S, Wang G, Angert ER, Wang W, Li W, Zou H (2012) Composition, diversity and origin of the bacterial community in Grass Carp intestine. PLoS ONE 7(2): e30440. https://doi.org/10.1371/journal.pone.0030440

Zotta T, Parente E, Ianniello RG, De Filippis F, Ricciardi A (2019) Dynamics of bacterial communities and interaction networks in thawed fish fillets during chilled storage in air. International Journal of Food Microbiology 293: 102–113. https://doi.org/10.1016/j.ijfoodmicro.2019.01.008

BioRisk 18: 115–132 (2022)
doi: 10.3897/biorisk.18.86616
https://biorisk.pensoft.net

RESEARCH ARTICLE

A peer-reviewed open-access journal
BioRisk

Potential risk resulting from the influence of static magnetic field upon living organisms. Numerically simulated effects of the static magnetic field upon metalloporphyrines

Wojciech Ciesielski[1], Tomasz Girek[1], Zdzisław Oszczęda[2], Jacek A. Soroka[3], Piotr Tomasik[2]

1 *Institute of Chemistry, Jan Długosz University, 42 201 Częstochowa, Poland* **2** *Nantes Nanotechnological Systems, 59 700 Bolesławiec, Poland* **3** *Scientific Society of Szczecin, 71-481 Szczecin, Poland*

Corresponding author: Wojciech Ciesielski (w.ciesielski@interia.pl)

Academic editor: Josef Settele | Received 16 May 2022 | Accepted 31 July 2022 | Published 23 August 2022

Citation: Ciesielski W, Girek T, Oszczęda Z, Soroka JA, Tomasik P (2022) Potential risk resulting from the influence of static magnetic field upon living organisms. Numerically simulated effects of the static magnetic field upon metalloporphyrines. BioRisk 18: 115–132. https://doi.org/10.3897/biorisk.18.86616

Abstract

Background: An attempt to recognize the effects of a static magnetic field (SMF) of varying flux density on flora and fauna.. For this purpose the influence of static magnetic field upon molecules of Mg(II), Fe(II), Fe(III), Co(II), Co(III) and Cu(II) metalloporphyrins is studied.

Methods: Computations of the effect of real SMF 0.0, 0.1, 1, 10 and 100 AFU (Arbitrary Magnetic Field Unit; here 1AMFU > 1000 T) flux density were performed in silico (computer vacuum) involving advanced computational methods.

Results: The static magnetic field (SMF) decreased the stability of the metalloporphyrine molecules. This effect depended on the situation of the molecule in respect to the direction of the SMF of the Cartesian system. An increase in the value of heat of formation was accompanied by an increase in the dipole moment. It was an effect of deformations of the molecule which involved pyrrole rings holding the hydrogen atoms at the ring nitrogen atoms and the length of the C-H and N-H bonds. As a consequence, that macrocyclic ring lost its planarity.

Conclusions: SMF even of the lowest, 0.1 AMFU flux density influences the biological role of metalloporphyrines associated with their central metal atoms. This effect is generated by changes in the electron density at these atoms, its steric hindering and polarization of particular bonds from pure valence bonds possibly into ionic bonds.

Keywords
Co(II)porphyrine, Co(III)porphyrine, Cu(II)porphyrine, Fe(II)porphyrine, Fe(III)porphyrine, Mg(II) porphyrine

Introduction

Our previous paper (Ciesielski et al. 2022) described the effect of Static Magnetic Field (SMF) of 0.1 to 100 AMFU (Arbitrary Magnetic Field Unit. 1 AMFU > 1000 T) upon porphine. Porphine and its derivatives are precursors of several biologically important compounds. They are derivatives of protoporphyrine IX. (Kadish et al. 2000; Ortiz de Montellano 2008). A biological activity of porphine results from two ways of its modification. One of them is binding various functional groups as external substituents of protoporphyrin IX. For instance, in such a way proteins like cysteine which are bound via thioether bonds form *C*-type cytochromes essential for the life of virtually all organisms (Stevens et al. 2004). The second way of modification involves coordination of metal ions inside the porphine ring to form metalloporphyrines. One of the most common representatives of metalloporphyrines are chlorophylls containing Mg atom inside the porphine ring. In chlorophylls, its presence is responsible for the green color of those compounds. Chlorophyll is a group of 6 compounds which differ from one another with substituents of the macrocyclic ring. Two of them (chlorophylls *a* and *b*) exist in the photosystem (chloroplasts) of green plants and algae. They absorb sunlight, employing its energy to synthesize carbohydrates from CO_2 and water. It is so-called photosynthesis. Several green chlorophyll pigments reside also in mesosomes of cyanobacteria. Animals and humans obtain chlorophyll as the component of their diet. During photosynthesis, plants take in carbon dioxide (CO_2) and water (H_2O) from the air and soil. Within the plant cell, the water is oxidized, meaning it loses electrons, while the carbon dioxide is reduced, meaning it gains electrons. This transforms the water into oxygen and the carbon dioxide into glucose. Magnesium in chlorophylls provides absorption of the blue and red potion of the electromagnetic spectrum, leaving the green portion of that spectrum non-absorbed. It does not constitute any particular reaction site for water and carbon dioxide (Kadish et al. 2000; Ortiz de Montellano 2008).

In metalloporphyrines holding either Fe(II), Fe(III), Co(II), Co(III) or Cu(II) these central atoms of the complexes act as coordination sites. Porphine derivatives with Fe(II) and Fe(III) ions coordinated and chemically bound within the macrocyclic ring are called hem and hemin, respectively. They are red-coloured compounds constituting the animal and human blood. Ferrous cation in heme can coordinate such as molecular oxygen, carbon monoxide, cyanide anion and other ligands. In hemin Fe(III) atom utilizes one of its valence bonds for binding chlorine atom. It is formed from a hem group, such as hem B found in the hemoglobin of human blood (Kadish et al. 2000; Ortiz de Montellano 2008).

Porphine derivatives coordinated to the Co(II) and Co(III) ions are known as vitamin B_{12}, (cobalamin). It is a cofactor in DNA synthesis, in both fatty acid and amino

acid metabolism. It is essential for the normal functioning of the nervous system and the maturation of red blood cells in the bone marrow (Kadish et al. 2000; Ortiz de Montellano 2008).

In the organisms of some invertebrates such as snails, lobsters and spiders, oxygen is transported by hemicyanines containing Cu(II) atom instead of Fe(II)/Fe(III) ions. Such hemocyanines (hemolymph) carrying coordinated oxygen are blue colored. Hence these invertebrates have blue blood (Walter et al. 2010).

Recently, numerous synthetic derivatives of the parent porphine in the form of metalloporhyrines have found their application in the material sciences of engineering, chemistry, physics, biology, and medicine (Anderson et al. 1995; Kadish et al. 2000; Yella et al. 2011; Ptaszek 2013 Huang et al. 2015), particularly in anticancer photodynamic therapy (Hodak and Pavlovsky 2015).

The subject of this paper focuses on the effect of SMF of 0.1 to 100 AMFU (Arbitrary Magnetic Field Unit) upon Mg (II), Fe(II), Fe(III), Co(II), Co(III), and Cu(II) porphyrines as the most essential and most common in functioning organisms of flora and fauna. The target is achieved involving in silico (computer vacuum) advanced computational methods.

Numerical computations

DFT (Density Functional Theory) Molecular structures were drawn using the Fujitsu Scigress 2.0 software (Marchand et al. 2014). Their principal symmetry axes were oriented along the x, y and z-axes of the Cartesian system. The magnetic field was fixed in the same direction, with the south pole from the left side.

Z axis is perpendicular to the porphine plane, the x and y axes are in the plane of the system, each of them along two nitrogen atoms. Because of mesomerism only, due to quaternary symmetry z axis the last two axes are undistinguished and symmetry D_{4h} is observed (Scheidt and Lee 1987). Since pairs of the nitrogen atoms differ from one another, the x axis cross two nitrogen atoms substituted by hydrogen atoms and y axis cross remains two unsubstituted nitrogen atoms and itself both axis x,y are distinguished.

Subsequently, involving Gaussian 0.9 software equipped with the 6–31G** basis (Frisch et al. 2016), the molecules were optimized and all values of bond length, dipole moment, total energy, heath of formation, bond energy and HOMO/LUMO energy level for single molecules.

In the consecutive step, influence of static magnetic field (SMF) upon optimized molecules were computed with Amsterdam Modelling Suite software (Farberovich and Mazalova 2016; Charistos and Munoz-Castro 2019) and the NR_LDOTB (non-relativistic orbital momentum L-dot-B) method (Glendening et al. 1987; Carpenter and Weinhold 1988). Following that step, using Gaussian 0.9 software equipped with the DFT with functional B3LYP 6–31G** basis (Charistos and Munoz-Castro 2019) values of bond length, dipole moment, heath of formation equal to the energy

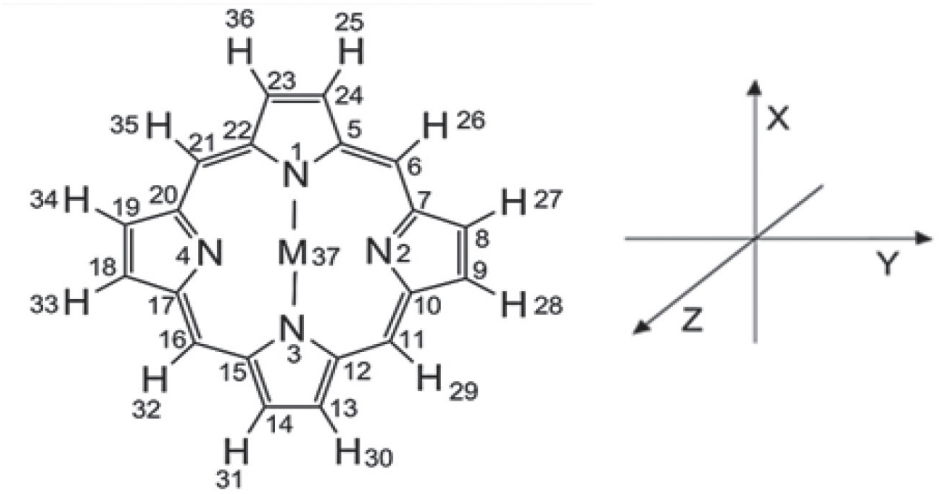

Figure 1. Structure of a metallporphine molecule with the system of numbering of the atoms followed throughout the discussion. M symbolizes any metal.

of dissociation, bond energy HOMO/LUMO energy level for single molecules were again computed using the single-point energy option key word.

Visualization of the HOMO/LUMO orbitals and changes of the electron density for particular molecules and their three molecule systems were performed involving the HyperChem 8.0 software (Froimowitz 1993).

Fig. 1 presents notation of particular atoms in metalloporphyrins.

Results and discussion

Based on the criterion of values of heat of formation (the stability of the system increases with declining negative value) (Table 1) the stability of metalloporphyrines under consideration declined in the order:

$$Fe(III)^{+} > Co(III)^{+} > Fe(II) > Co(II) > Cu(II) > Mg(II)$$

SMF destabilized the Mg(II)porphyrine. The value of heat formation gradually turned into less negative against an increase in applied flux density (Table 1). In every case the magnitude of the changes depended on the orientation of the molecule in the Cartesian system. The strongest destabilization was noted in the molecule oriented along the X-axis followed by its orientations along Y- and Z-axes, respectively. The changes in the heat of formation were accompanied by an increase in the values of dipole moment of the molecule. It rose depending in the same manner on the orientation of the molecule in the Cartesian system. Deformed porphyrin skeleton could take one of four conformations, that is, saddle (B_{2u}), ruffle (B_{1u}), dome (A_{2u}) or wave ($E_{gx,y}$) (Kingsbury and Senge 2021).

Table 1. Heat of formation [kJ.mol^{-1}] and dipole moment [D] of the metalloporphyrine molecules depending on applied SMF flux density [AMFU] and their situating in the Cartesian system.

SMF along indicated Cartesian axis	Heat of formation [kJ·mol^{-1}] at SMF flux density [AMFU]					Dipole moment [D] at SMF flux density [AMFU]				
	0	0.1	1.0	10	100	0	0.1	1.0	10	100
					Mg(II)					
X	-803	-781	-772	-731	-698	2.06	2.10	2.15	2.19	2.31
Z		-799	-794	-771	-726		2.09	2.10	2.11	2.18
Y		-796	-781	-762	-716		2.10	2.14	2.20	2.29
					Fe(II)					
X	-982	-972	-953	-911	-875	1.99	2.03	2.10	2.24	2.41
Z		-979	-967	-932	-904		2.01	2.06	2.11	2.24
Y		-979	-964	-936	-906		2.03	2.11	2.16	2.34
					Fe(III)+					
X	-1125	-1038	-987	-894	-815	2.06	2.11	2.19	2.35	2.62
Z		-1097	-1005	-974	-897		2.09	2.15	2.19	2.31
Y		-1023	-1000	-971	-902		2.11	2.24	2.32	2.62
					Co(II)					
X	-969	-942	-918	-781	-743	2.03	2.09	2.22	2.38	3.24
Z		-952	-947	-932	-918		2.06	2.15	2.21	2.38
Y		-946	-923	-761	-694		2.09	2.23	2.59	3.48
					Co(III)+					
X	-1021	-1014	-997	-876	-831	2.03	2.09	2.22	2.38	3.04
Z		-1006	-985	-934	-858		2.06	2.13	2.25	2.32
Y		-1015	-995	-968	-885		2.08	2.23	2.42	2.97
					Cu(II)					
X	-921	-892	-871	-811	-752	2.01	2.06	2.15	2.39	2.68
Z		-918	-906	-893	-812		2.03	2.06	2.09	1.98
Y		-885	-872	-803	-711		2.06	2.17	2.51	3.69

In Mg(II)porphyrine (Fig. 2), considered as very simplified model of chlorophyll, the central metal atom was not coordinated to the N2 and N4 ring nitrogen atoms. Planar structures (a) and (c) showed that one Mg-bound and one non-bound pyrrole rings were mostly responsible for the deformation of the molecule. Structures (b) revealed that the deformation led to bending of the molecule.

The shape of the porphyrin skeleton differed from the flat one characterized by the point group D_{4h}. It took the shape of a dome typical for the point group A_{2u}. The increase in SMF ejected the magnesium atom from the center of the molecule because of increasing lengths of the Mg-N bonds.

Corresponding variations of the charge density on the N- and Mg(II) atoms and the Mg(II)-N bond lengths are reported in Tables 2 and 3, respectively.

Data in Table 2 indicate irregular changes of the charge density at the N1 and N3 magnesium-bound atoms. Independently of the situating of the molecule against SMF, the charge at the N1 atom always remained negative. However, the charge density at the N3 magnesium bound atom situated along the Z-axis turned positive and also changed irregularly against applied flux density. The central Mg atom invariantly hold the positive charge density which irregularly rose with an increase in the flux density.

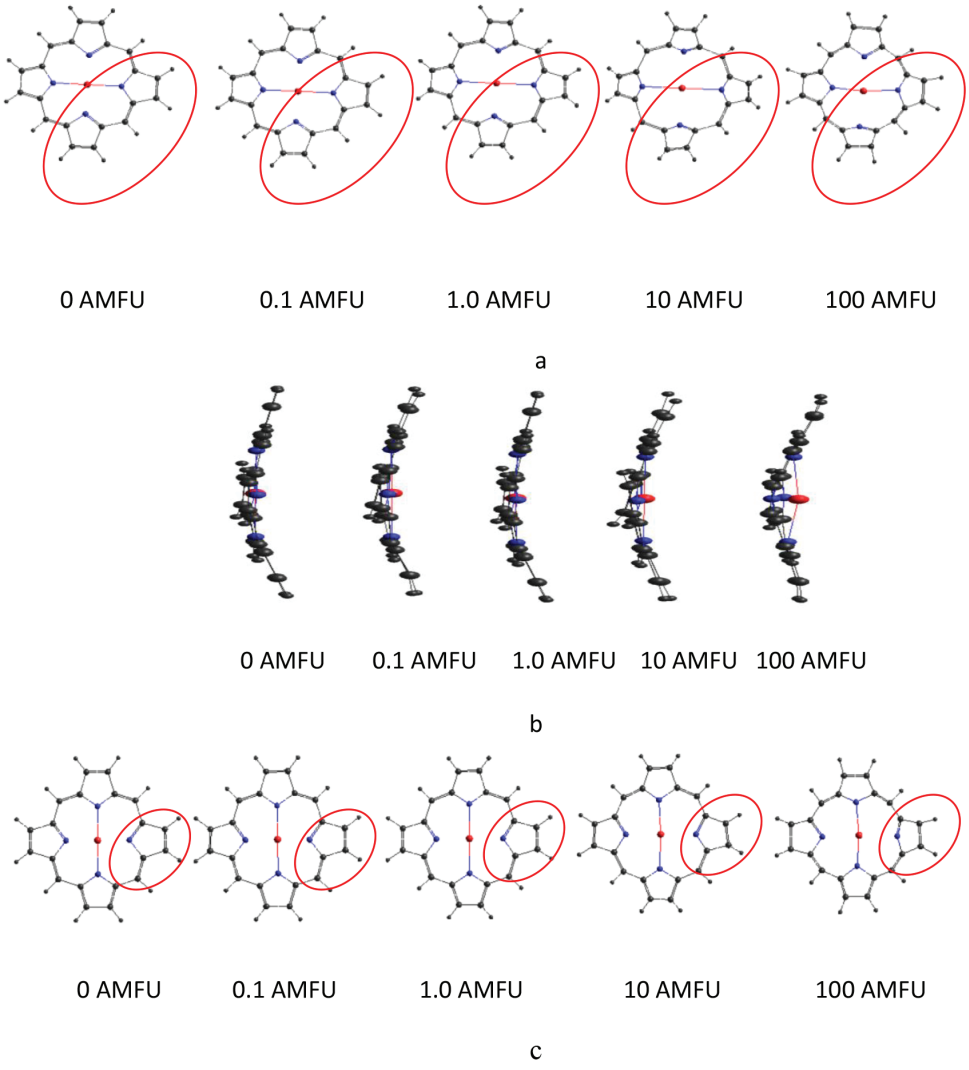

Figure 2. Deformation of Mg(II) porphyrine in SMF of 0 – 100 AMFU when the SMF direction is in (**a–c**) along X, Z and Y axes, respectively.

The smallest changes were noted in the molecule oriented along the Z-axis. Increasing charge density at the Mg atom should be beneficial for bonding Lewis bases. That is, it should promote photosynthesis provided the reaction site is not obscured by steric hindrances.

In their character the Mg-N bonds were intermediate between ionic and atomic, making the binding electron pair essential. Under the influence of a high external SMF, the durability of such a pair, maintained by magnetic forces, decreased. Thus, the bond become weaker and longer (Table 3).

Table 2. Charge density [a.u] at particular atoms of the Mg(II)porphyrine molecule depending on SMF flux density [AMFU] situating in the Cartesian system.

Atom	SMF along indicated Cartesian axis	Charge density [a.u] at SMF flux density [AMFU]				
		0	0.1	1.0	10	100
N1	X	-0.219	-0.095	-0.045	-0.297	-0.021
	Z		-0.212	-0.122	-0.118	-0.083
	Y		-0.067	-0.135	-0.249	-0.153
N3	X	-0.197	-0.192	-0.122	-0.255	-0.037
	Z		0.051	0.179	0.167	0.172
	Y		-0.167	-0.174	-0.218	-0.136
Mg37	X	0.387	0.637	0.638	0.538	0.532
	Z		0.521	0.546	0.556	0.577
	Y		0.626	0.640	0.567	0.646

Table 3. Bond lengths [Å] between particular atoms of the Mg(II)porphyrine molecule depending on SMF flux density [AMFU] situating in the Cartesian system.

Bond	SMF along indicated Cartesian axis	Bond length [Å] at flux density [AMFU]				
		0	0.1	1.0	10	100
N1-Mg37	X	1.917	2.161	2.286	2.125	2.438
	Z		2.111	2.045	2.077	2.156
	Y		2.096	2.140	2.066	2.136
N3-Mg37	X	1.898	2.169	2.298	1.944	2.459
	Z		2.109	2.061	2.090	2.126
	Y		2.106	2.126	1.910	1.155

The criterion of the heat of formation of Fe(II)porphyrine and Fe(III)porphyrine indicated that SMF destabilized these molecules.

The Fe(II) atom in Fe(II)porhyrine was tetracoordinated (Fig. 3).

Already out of SMF the molecule was non-planar and SMF considerably contributed to its deformation. In the molecule situated in the X-Y plane, particularly at 10 and 100 AMFU, remarkable charge density (Table 4) and elongation of some C-H bonds (Table 5) could be observed. The positive charge density at the Fe(II) atom slightly decreased with an increase in the applied flux density when the molecule was oriented along the X axis but, simultaneously increased in the molecules oriented along the Z and Y axes. Such response of the molecule to SMF was beneficial for the accepting Lewis bases, for instance, CO.

An elongation of the Fe-N was much less remarkable than that observed in Mg(II)porphyrine (Table 5). The mean value of the Fe-N bond length for all metalloporphyrines orientations along the SMF directions remained approximately constant. As with magnesium, electron density decreased on the atoms of nitrogen bound to iron, as well as on the iron itself, so the growing SMF caused the electrons to move to the periphery of the molecule.

The Fe(III) atom of Fe(III)porhyrine cation was also tetra-coordinated. Deformations of the molecules by increasing flux density are presented in Fig. 4.

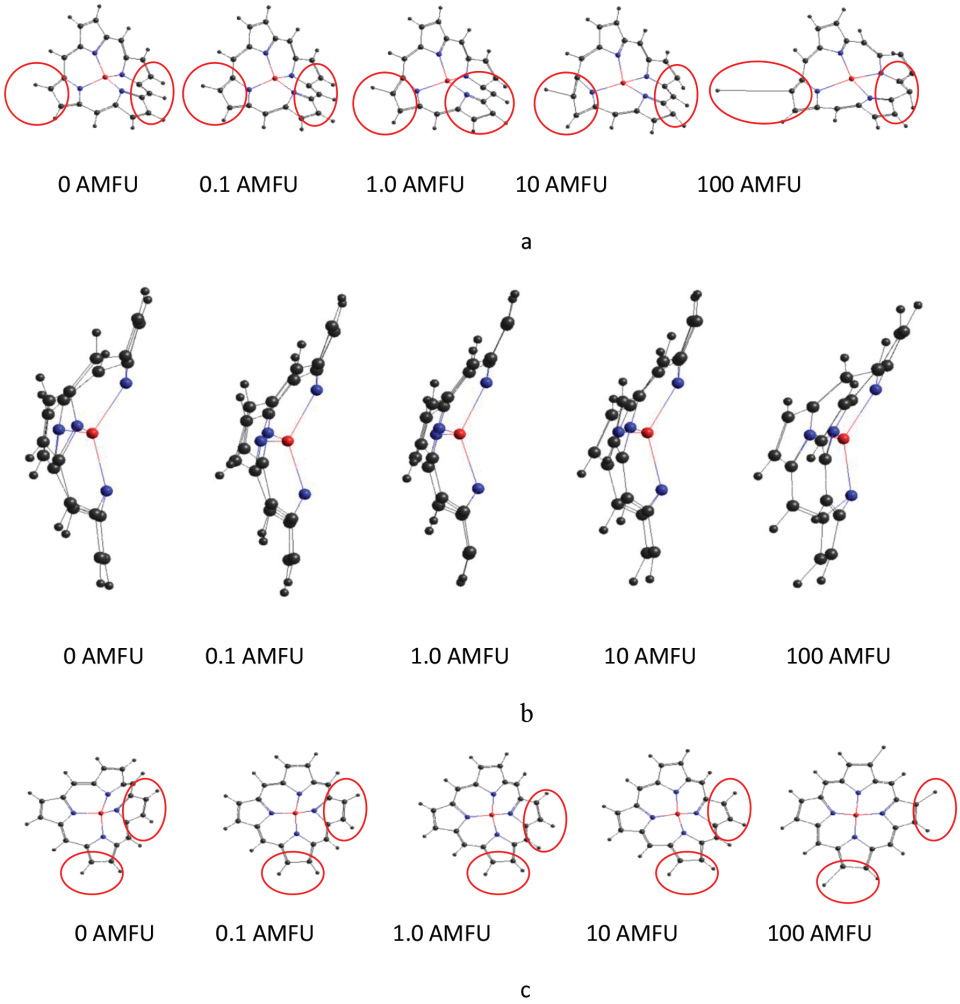

Figure 3. Deformation of Fe(II)porphyrine in SMF of 0 – 100 AMFU when SMF direction is in (**a–c**) along X, Z and Y axes, respectively.

Table 4. Charge density [a.u.] at particular atoms of the Fe(II)porphyrine molecule depending on SMF flux density [AMFU] situating in the Cartesian system.

Atom	SMF along indicated Cartesian axis	Charge density [a.u] at SMF flux density [AMFU]				
		0	0.1	1.0	10	100
N1	X	-0.408	-0.379	-0.425	-0.252	-0.123
	Z		-0.384	-0.385	-0.375	0.004
	Y		-0.408	-0.425	-0.488	-0.439
N3	X	-0.346	-0.397	-0.315	-0.249	-0.199
	Z		-0.350	-0.325	-0.336	0.165
	Y		-0.501	-0.503	-0.438	-0.497
Fe37	X	1.651	1.602	1.473	1.212	1.039
	Z		1.734	1.685	1.661	1.019
	Y		1.845	1.823	1.822	1.769

Table 5. Bond lengths [Å] between particular atoms of the Fe(II)porphyrine molecule depending on SMF flux density [AMFU] situating in the Cartesian system.

Bond	SMF along indicated Cartesian axis	Bond length [Å] at flux density [AMFU]				
		0	0.1	1.0	10	100
N2-Fe37	X	1.893	1.994	2.170	2.047	2.109
	Z		1.730	1.794	1.770	1.787
	Y		1.782	1.658	1.763	1.801
N3-Fe37	X	1.898	1.926	2.170	2.214	2.644
	Z		1.855	1.840	1.860	1.885
	Y		1.689	1.692	1.738	1.772

Compared to Fe(II)porphirine the porphine skeleton localized along X and Z axes faced only slight deformation evoked by SMF.

Relevant charge density at particular atoms and bond lengths are collected in Tables 6 and 7, respectively.

An increase in applied SMF resulted in an irregular change of the positive charge density of the Fe atom. A general tendency in decrease of that charge was perturbed mainly in the molecules oriented against SMF along Z-axis. The same effect could be observed for negative charge density at the N1 and N3 atoms which, generally, decreased with an increase in applied SMF (Table 6). Thus, the flux density of 0.1 and 1.0 AMFU should facilitate reactions of the Fe(III) atom with Lewis bases.

Such irregularities were accompanied with irregular changes of the N-Fe bond lengths. These bonds generally were elongated with an increase in applied SMF (Table 7).

An insight in Table 1 showed that SMF destabilized Co(II) and Co(III)porphyrines and negatively influenced their biological functions.

The Co(II) atom in Co(II)porphyrine remained bidentate. Its presence inhibited to a great extent the deformation of the molecule involving bending molecule typical for formerly mentioned metalloporphyrines (Fig. 5). Instead, a local deformation within the macrocyclic took place. Corresponding charge density and bond lengths computed for these molecule are presented in Tables 12 and 13, respectively.

The SMF acting along the Z- axis flatted the molecule. The increase in SMF changed the conformations in the order: dome-flat-flat-dome with simultaneous distancing of the cobalt atom from the plane of the molecule.

The action of SMF along the X or Y axis evoked a wave mode deformation, with a point group $E_{gx,y}$ (Kingsbury and Senge 2021).

The applied SMF atom always affected the negative charge density at the N-atoms and positive charge density at the Co-atom. These changes were chimerically dependent on the orientation of the molecules against SMF (Table 8). However, always resulting charge density at the Co(II) atom increased in respect to that in the molecule out of SMF. Thus, the ability of the Co(II) atom to bind Lewis bases increased. Molecules oriented against SMF along the Y axis should react with Lewis bases the most readily.

The SMF also influenced and extended the length of both N-Co bonds and that effect was strongly dependent on the orientation of the molecule against the SMF (Table 9).

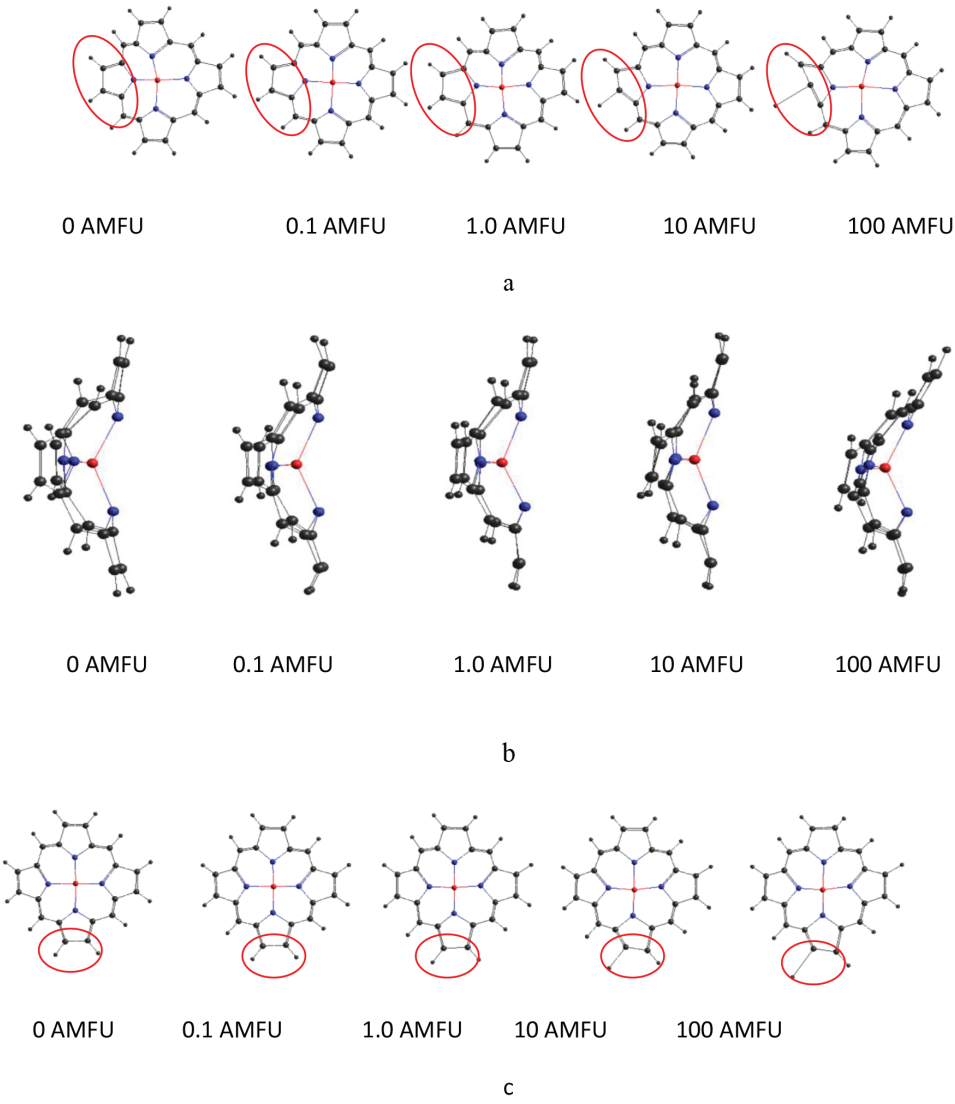

Figure 4. Deformation of Fe(III)porphyrine in SMF of 0 – 100 AMFU when the SMF direction is in (**a–c**) along X, Z and Y axes, respectively.

The Co(III) atom in Co(III)porphyrine cation also remained bidentate and, principally, it also inhibited deformation of the molecule by bending. In comparison to Co(II) atom its presence in the macrocyclic ring favoured elongation of some C-H bonds to the extent suggesting their dissociation (Fig. 6).

The action of the SMF along each axis causes deformation of the flat system to corrugated, wave mode $E_{gx,y}$ (Kingsbury and Senge 2021).

The relevant changes of the charge density at Co and N atoms and the Co-N atom bonds are reported in Tables 10 and 11, respectively. As in the case of formerly presented

Table 6. Charge density [a.u.] at particular atoms of the Fe(III)porphyrine molecule cation depending on SMF flux density [AMFU] situating in the Cartesian system.

Atom	SMF along indicated Cartesian axis	Charge density [a.u] at SMF flux density [AMFU]				
		0	0.1	1.0	10	100
N1	X	-0.354	-0.457	-0.465	-0.437	-0.065
	Z		-0.430	-0.382	-0.403	-0.423
	Y		-0.455	-0.452	-0.057	-0.082
N3	X	-0.363	-0.400	-0.395	-0.329	-0.073
	Z		-0.352	-0.385	-0.396	-0.414
	Y		-0.451	-0.441	-0.149	-0.121
Fe37	X	1.696	1.767	1.765	1.429	0.928
	Z		1.654	1.726	1.765	1.807
	Y		1.787	1.797	1.154	1.199

Table 7. Bond lengths [Å] between particular atoms of the Fe(III)porphyrine molecule cation depending on SMF flux density [AMFU] situating in the Cartesian system.

Bond	SMF along indicated Cartesian axis	Bond length [Å] at flux density [AMFU				
		0	0.1	1.0	10	100
N1-Fe37	X	1.917	1.802	1.820	1.997	2.173
	Z		1.905	1.828	1.886	1.803
	Y		1.822	1.835	1.912	1.945
N3-Fe37	X	1.873	1.823	1.809	2.140	2.126
	Z		1.950	1.807	1.796	1.723
	Y		1.897	1.798	1.863	1.835

metalloporphyrines, these changes with an increase in applied flux density were irregular and strongly dependent on the orientation of the molecules against SMF. In contrast to Co(II)porphyrine where SMF facilitated reaction of the central metal atom with Lewis bases, SMF flux density decreased the ability of the Co(III) to bind Lewis bases.

SMF negatively perturbs biological functions of Cu(II)porphyrine as it increased its heat of formation (Table 1).

Inserting the Cu(II) atom into the porphine ring produced its deformation by bending already out of SMF.

An increase in SMF caused a change in conformation from the dome to the flat one. It distinguished Cu(II)porphyrine from those discussed above. The presence of the Cu(II) atom favored considerable elongation of the C-H bonds.

Charge density distribution in this molecule and relevant bond lengths are grouped in Tables 12 and 13, respectively.

Performed computations presented fairly unusual effects of insertion of Cu(II) atom into porphine. Thus, already in the molecule out of SMF both nitrogen atoms bound to the Cu(II) atom hold the positive charge density. Already SMF of flux density of 0.1 AMFU turned the charge density at the N1 atom into negative when the molecule was oriented along either X or Z axis. In the molecule oriented along the Y axis just the flux density of 100 AMFU developed negative charge density at that atom.

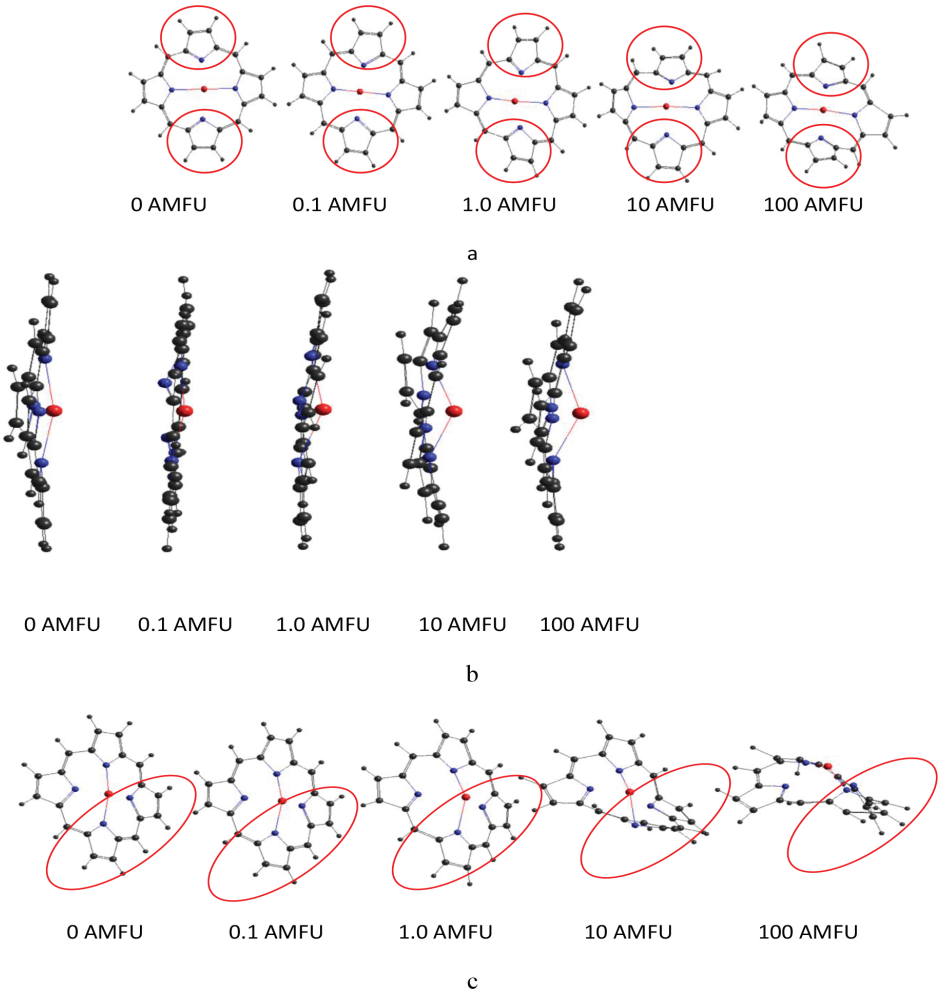

Figure 5. Deformation of Co(II) porphyrine in SMF of 0 – 100 AMFU when the SMF direction is in (**a–c**) along X, Z and Y axes, respectively.

Table 8. Charge density [a.u] at particular atoms of the Co(II)porphyrine molecule depending on SMF flux density [AMFU] situating in the Cartesian system.

Atom	SMF along indicated Cartesian axis	Charge density [a.u] at SMF flux density [AMFU]				
		0	0.1	1.0	10	100
N1	X	-0.218	-0.094	-0.247	-0.149	-0.059
	Z		-0.226	-0.118	-0.144	0.085
	Y		-0.214	-0.281	-0.190	-0.129
N3	X	-0.220	-0.149	-0.164	-0.259	-0.288
	Z		-0.034	-0.160	-0.126	-0.227
	Y		-0.201	-0.254	-0.094	0.131
Co37	X	0.509	0.584	0.705	0.611	0.878
	Z		0.587	0.596	0.574	0.467
	Y		0.605	0.754	0.596	0.971

Table 9. Bond lengths [Å] between particular atoms of the Co(II)porphyrine molecule depending on SMF flux density [AMFU] situating in the Cartesian system.

Bond	SMF along indicated Cartesian axis	Bond length [Å] at flux density [AMFU]				
		0	0.1	1.0	10	100
N1-Co37	X	1.958	2.054	2.138	2.224	2.202
	Z		2.011	2.064	1.889	1.925
	Y		2.113	2.323	2.450	2.406
N3-Co37	X	1.945	2.036	2.123	2.142	2.394
	Z		2.139	2.052	1.090	1.892
	Y		1.862	2.230	1.926	2.745

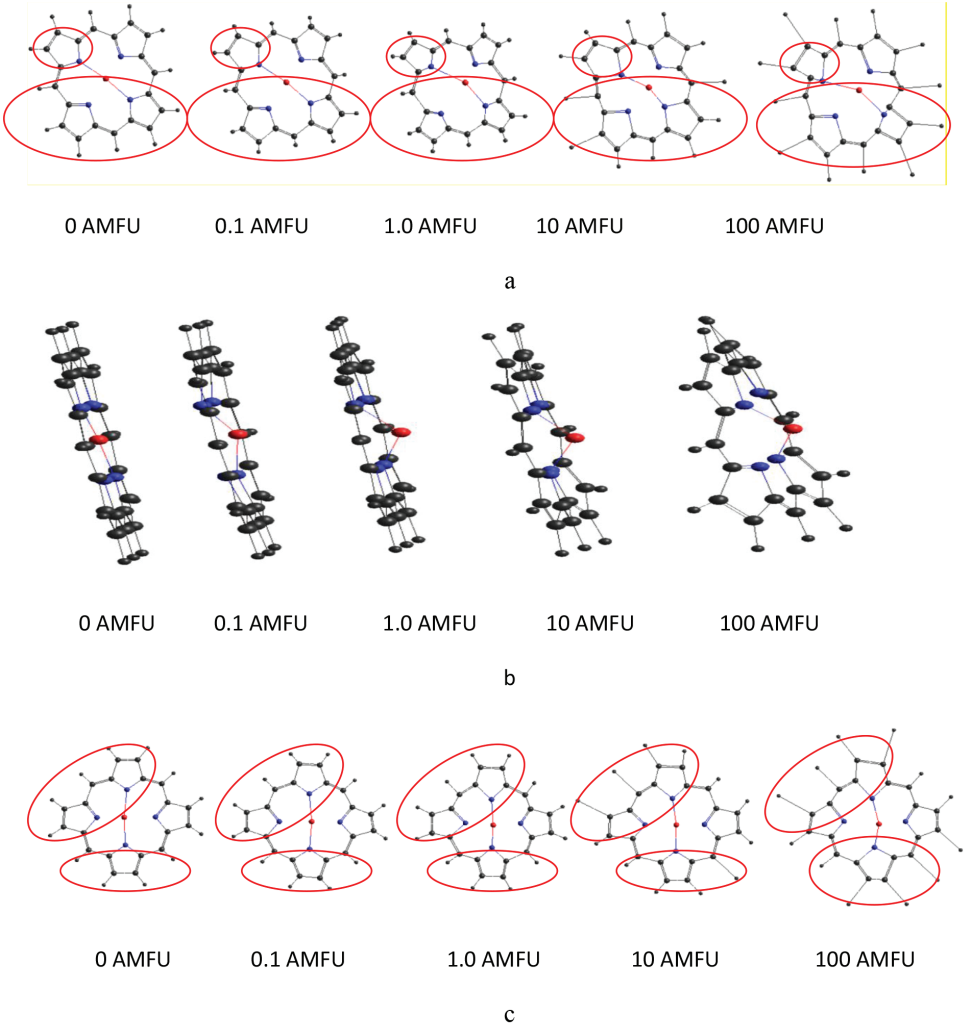

Figure 6. Deformation of Co(III)porphyrine in SMF of 0 – 100 AMFU when the SMF direction is in (**a–c**) along X, Z and Y axes, respectively.

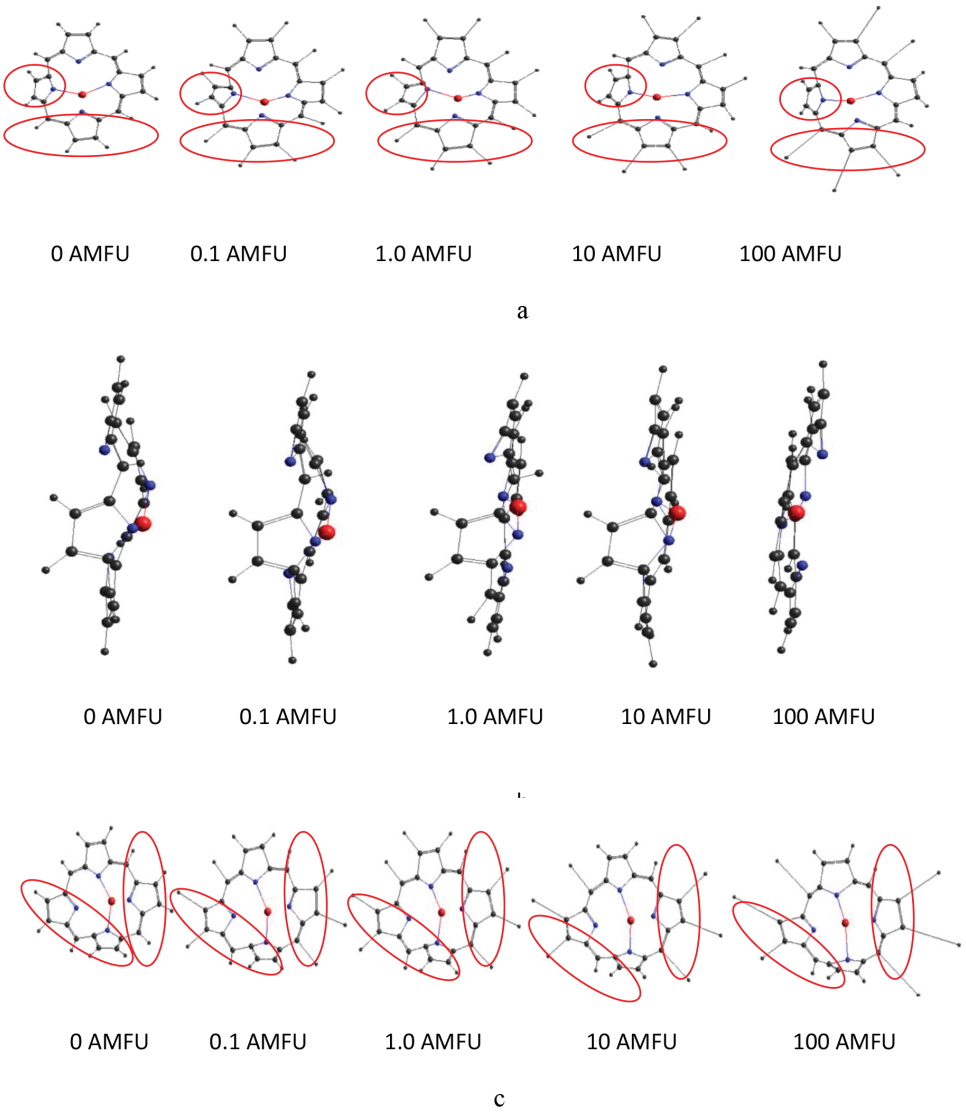

Figure 7. Deformation of Cu(II)porphyrine in SMF of 0 – 100 AMFU when the SMF direction is in (**a–c**) along X, Z and Y axes, respectively.

The N3 atom appeared to be more susceptible to the conversion of its initial positive charge density into negative. In the molecule located along the X axis solely flux density of 0.1 AMFU could not convert that charge density into negative. In all remained cases the charge density at that atom readily converted into negative.

Applied SMF invariantly increased positive charge density at the Cu atom (Table 12) what should facilitate coordination of Lewis bases. The length of both N-Cu bonds varied irregularly with an increase in the applied flux density and orientation against

Table 10. Charge density [a.u] at particular atoms of the Co(III)porphyrine molecule cation depending on SMF flux density [AMFU] situating in the Cartesian system.

Atom	SMF along indicated Cartesian axis	Charge density [a.u] at SMF flux density [AMFU]				
		0	0.1	1.0	10	100
N1	X	-0.243	-0.205	-0.048	-0.052	-0.017
	Z		-0.223	-0.200	-0.200	0.034
	Y		-0.303	-0.378	-0.303	-0.252
N3	X	-0.304	-0.270	-0.004	-0.365	0.516
	Z		-0.258	-0.161	-0.147	0.134
	Y		-0.358	-0.312	-0.186	-0.337
Co37	X	1.223	1.247	1.220	1.018	0.651
	Z		1.158	1.175	1.155	0.864
	Y		1.206	1.110	1.188	0.946

Table 11. Bond lengths [Å] between particular atoms of the Co(III)porphyrine molecule cation depending on SMF flux density [AMFU] situating in the Cartesian system.

Bond	SMF along indicated Cartesian axis	Bond length [Å] at flux density [AMFU]				
		0	0.1	1.0	10	100
N1-Co37	X	2.052	2.181	2.471	1.979	2.497
	Z		2.053	1.899	1.859	1.867
	Y		2.049	1.892	1.967	1.930
N3-Co37	X	2.064	2.069	1.972	1.588	2.221
	Z		2.106	1.910	1.921	1.956
	Y		2.027	1.646	1.961	1.779

Table 12. Charge density [a.u] at particular atoms of the Cu(II)porphyrine molecule depending on SMF flux density [T] situating in the Cartesian system.

Atom	SMF along indicated Cartesian axis	Charge density [a.u] at SMF flux density [AMFU]				
		0	0.1	1.0	10	100
N1	X	0.202	-0.237	-0.259	-0.534	-0.473
	Z		-0.235	-0.260	-0.248	-0.202
	Y		0.109	0.054	0.012	-0.241
N3	X	0.040	0.061	-0.227	-0.465	-0.413
	Z		-0.137	-0.258	-0.165	-0.124
	Y		-0.160	-0.084	-0.120	-0.302
Cu37	X	0.726	0.907	0.814	0.962	0.942
	Z		0.967	1.003	1.076	0.911
	Y		0.847	0.790	0.882	0.993

SMF. The N-Cu bonds were the least sensitive to elongation when the molecule was oriented along the Z- axis (Table 13).

Thus, in summary, static magnetic field (SMF) decreased stability of the metalloporphyrine molecules. This effect depended on the situating of the molecule in respect to the direction of SMF of the Cartesian system. An increase in the value of heat

Table 13. Bond lengths [Å] between particular atoms of the Cu(II)porphyrine molecule depending on SMF flux density [AMFU] situating in the Cartesian system.

Bond	SMF along indicated Cartesian axis	Bond length [Å] at flux density [AMFU]				
		0	0.1	1.0	10	100
N1-Cu37	X	1.964	1.649	1.437	2.046	1.991
	Z		1.962	1.975	2.058	1.947
	Y		2.213	1.932	2.243	2.884
N3-Cu37	X	1.966	2.166	2.172	1.836	1.860
	Z		1.956	1.961	2.045	2.032
	Y		2.044	2.060	2.132	2.483

of formation was accompanied by an increase in dipole moment. It was an effect of deformations of the molecule which involved pyrrole rings holding the hydrogen atoms at the ring nitrogen atoms and the length of the C-H and N-H bonds. As a consequence that macrocyclic ring lost its planarity. Recently, (Kong et al. 2022) discovered in the Milky Way the Highest-energy CRSF from the First Galactic Ultraluminous X-Ray Pulsar Swift J0243.6+6124. It reached over 1.6 billion Tesla. The presence of multipole field components close to the surface of the neutron star confirms deteriorating effect of SMF of high density upon metalloporphyrines suggested by performed in silico computations described in this paper.

Conclusions

SMF even of the lowest, 0.1 AMFU flux density influences the biological role of metalloporphyrines associated with their central metal atoms. This effect is generated by changes in the electron density at these atoms, its steric hindering and polarization of particular bonds from pure valence bonds possibly into ionic bonds. Regardless of its situation along x, y and z axis, SMF always destabilized the metalloporphyrine molecules. Evoked deformation of particular molecules facilitated additional ligation of the central metal atom. Potentially, this effect could be used in synthetic modifications of metalloporphyrines.

References

Anderson S, Anderson HL, Bashall A, McPartlin M, Sanders JKM (1995) Assembly and crystal structure of a photoactive array of five porphyrins. Angewandte Chemie 34(10): 1096–1099. https://doi.org/10.1002/anie.199510961

Carpenter JE, Weinhold F (1988) Analysis of the geometry of the hydroxymethyl radical by the different hybrids for different spins natural bond orbital procedure Journal of Molecular Structure (Teochem) 139: 41–62. https://doi.org/10.1016/0166-1280(88)80248-3

Charistos ND, Munoz-Castro A (2019) Double aromaticity of the B-40 fullerene: Induced magnetic field analysis of pi and sigma delocalization in the boron cavernous structure.

Physical Chemistry Chemical Physics 21(36): 20232–20238. https://doi.org/10.1039/C9CP04223G

Ciesielski W, Girek T, Oszczęda Z, Soroka JA, Tomasik P (2022) Potential risk resulting from the influence of static magnetic field upon living organisms. Numerically simulated effects of the static magnetic field upon porphine. BioRisk 18: 93–104. https://doi.org/10.3897/biorisk.18.80607

Farberovich OV, Mazalova VL (2016) Ultrafast quantum spin-state switching in the Co-octaethylporphyrin molecular magnet with a terahertz pulsed magnetic field. Journal of Magnetism and Magnetic Materials 405: 169–173. https://doi.org/10.1016/j.jmmm.2015.12.038

Frisch MJ, Trucks GW, Schlegel HB, Scuseria GE, Robb MA, Cheeseman JR, Scalmani G, Barone V, Mennucci B, Petersson GA (2016) Gaussian 09, Revision A.02, Gaussian, Inc., Wallingford CT.

Froimowitz M (1993) HyperChem: A software package for computational chemistry and molecular modelling. BioTechniques 14: 1010–1013.

Glendening ED, Reed AE, Carpenter JE, Weinhold F (1987) Extension of Lewis structure concepts to open-shell and excited-state molecular species, NBO Version 3.1, PhD thesis, University of Wisconsin, Madison, WI.

Hodak E, Pavlovsky L (2015) Phototherapy of mycosis fungoides. Dermatologic Clinics 33(4): 697–702. https://doi.org/10.1016/j.det.2015.05.005

Huang H, Song W, Rieffel J, Lovell JF (2015) Emerging applications of porphyrins in photomedicine. Frontiers in Physics 3: e23. [1–15] https://doi.org/10.3389/fphy.2015.00023

Kadish KM, Smith KM, Guilard R [Eds] (2000) Porphyrin Handbook. Academic Press, San Diego.

Kingsbury JC, Senge MO (2021) The shape of porphyrins. Coordination Chemistry Reviews 431: 213760. https://doi.org/10.1016/j.ccr.2020.213760

Kong L-D, Zhang S, Zhang S-N, Ji L, Doroshenko V, Santangelo A, Chen Y-P, Lu F-J, Ge M-Y, Wang P-J, Tao L, Qu J-L, Li T-P, Liu C-Z, Liao J-Y, Chang Z, Peng J-Q, Shui Q-C (2022) Insight-HXMT discovery of the highest-energy CRSF from the first galactic ultraluminous X-ray pulsar swift J0243.6+6124. The Astrophysical Journal. Letters 933(1): L3. https://doi.org/10.3847/2041-8213/ac7711

Marchand N, Lienard P, Siehl H, Harunobu I (2014) Applications of molecular simulation software SCIGRESS in industry and university. Fujitsu Scientific and Technical Journal 50(3): 46–51.

Ortiz de Montellano PR (2008) Hemes in Biology. Wiley Encyclopedia of Chemical Biology. John Wiley & Sons. https://doi.org/10.1002/9780470048672.wecb221.

Ptaszek M (2013) Rational design in fluorophores for *in vitro* applications. In: Morris MC (Ed.) Progress in Molecular Biology and Translational Science, vol. 113 Fluorescence – based Biosensors, from Concepts to Applications, Fluorescence-Based Biosensors in Progress in Molecular Biology and Translational Science. Academic Press, Oxford. https://doi.org/10.1016/B978-0-12-386932-6.00003-X

Scheidt WR, Lee YJ (1987) Recent advances in the stereochemistry of metallotetrapyrroles. In: Buchler JW (Ed.) Metal Complexes with Tetrapyrrole Ligands I. Structure and Bonding, vol 64. Springer, Berlin, Heidelberg. https://doi.org/10.1007/BFb0036789.

Stevens JM, Daltrop O, Allen JWA, Fergusson SJ (2004) C-type cytochrome formation: Chemical and biological enigmas. Accounts of Chemical Research 37(12): 999–1007. https://doi.org/10.1021/ar030266l

Walter MG, Rudine AB, Wamser CC (2010) Porphyrins and phthalocyanines in solar photovoltaic cells. Journal of Porphyrins and Phthalocyanines 14(09): 759–792. https://doi.org/10.1142/S1088424610002689

Yella A, Lee HW, Tsao HN, Yi C, Chandiran AK, Nazeeruddin MK, Diau EW-G, Yeh C-Y, Zakeeruddin SM, Grätzel M (2011) Chandiran AK, Nazeeruddin K et al. Porphyrin-sensitized solar cells with cobalt (II/III)–based redox electrolyte exceed 12 percent efficiency. Science 334(6056): 629–634. https://doi.org/10.1126/science.1209688

BioRisk 18: 133–143 (2022)
doi: 10.3897/biorisk.18.87433
https://biorisk.pensoft.net

SHORT COMMUNICATIONS

A peer-reviewed open-access journal
BioRisk

The first evidence of microplastics in plant-formed fresh-water micro-ecosystems: *Dipsacus* teasel phytotelmata in Slovakia contaminated with MPs

Katarína Fogašová[1], Peter Manko[1], Jozef Oboňa[1]

1 *Department of Ecology, Faculty of Humanities and Natural Sciences, University of Prešov, 17. novembra 1, SK – 081 16 Prešov, Slovakia*

Corresponding author: Katarína Fogašová (katarina.fogasova@smail.unipo.sk)

Academic editor: Josef Settele | Received 25 June 2022 | Accepted 17 August 2022 | Published 30 August 2022

Citation: Fogašová K, Manko P, Oboňa J (2022) The first evidence of microplastics in plant-formed fresh-water micro-ecosystems: *Dipsacus* teasel phytotelmata in Slovakia contaminated with MPs. BioRisk 18: 133–143. https://doi.org/10.3897/biorisk.18.87433

Abstract

Tiny pieces of plastic, or microplastics, are one of the emerging pollutants in a wide range of different ecosystems. However, they have, thus far, not been confirmed from phytotelmata – specific small water-filled cavities provided by terrestrial plants. The authors confirmed microplastics (141 μm – 2.4 mm long fibres of several colour and blue and orange fragments with diameters of 9–81 μm) in quantities from 101 to 409 per ml in *Dipsacus* telmata from two different periods. The phytotelmata, therefore, appear to be possible indicators of current and future microplastic pollution of the environment. However, further research is needed to obtain accurate information and verify the methodology for possible assessment of the local environmental burden of microplastics.

Keywords

plants, plastics, transport, telmata

Introduction

Microplastics (MPs) are becoming an important problem (e.g. Andrady 2011; Cole et al. 2011; Weber et al. 2021 etc.). They have been recorded in a wide range of different ecosystems, from terrestrial to aquatic (e.g. de Souza Machado et al. 2018; Weber et al. 2021; Yang et al. 2021) and even in food, bottled drinking water and the organs of various organisms, including humans (e.g. Carbery et al. 2018; Jin et al. 2021;

Ragusa et al. 2021). Most studies of MPs, or SAMPs (atmospheric MPs), are more focused on the marine and freshwater ecosystems (e.g. Panebianco et al. 2019; Weber et al. 2021; Yang et al. 2021) and we still do not have enough information about their impact on organisms (e.g. Al-Jaibachi et al. 2019).

To the authors' knowledge, the presence of MPs has not yet been confirmed in phytotelmata, a wide range of generally non-permanent aquatic microecosystems in plants (e.g. Kitching 2000; Kanašová et al. 2020). Amongst the few phytotelmata in the temperate zone of Europe are dendrotelmata and phytotelmata provided by the teasel *Dipsacus* (e.g. Williams 1996, 2006; Kitching 2000; Oboňa et al. 2011; Oboňa and Svitok 2012; Kanašová 2017; Kanašová et al. 2020). Teasel phytotelmata (Fig. 1) are a relatively common, but overlooked aquatic microcosm with a very short-term occurrence of only 3 to 4 months (Kanašová et al. 2020). *Dipsacus* teasel has characteristic opposite leaves that grow on the stem above each other in several levels (the oldest near the soil surface and the youngest are the highest), clasping the stem and forming cup-like structures that collect water (water axil or telmata).

The main purpose of the sampling was to describe the seasonal dynamics of organisms living in teasel telmata. The detection of MPs in these samples was accidental and unexpected. The objective of this paper is to describe the first documented evidence of MPs in phytotelmata.

Materials and methods

Water samples with sediment from phytotelmata on teasel *Dipsacus* came from two areas of eastern Slovakia (see Map. 1) near the villages of Demjata (49°6'58.578231"N, 21°18'47.3838982"E, Fig. 2) and Kapušany (49°3'12.6212568"N, 21°20'16.680325"E).

The samples were obtained from five plants at each of two sampling localities at the end of each of five 14-day long collection periods from all levels of leaf axils at examined plants. The collection was carried out using standard methods (see Kanašová et al. 2020) using sterile containers. Therefore, contamination of the samples from another source is clearly excluded. These 50 sampled *Dipsacus* individuals provided 171 functioning phytotelmata. Altogether, 4596 ml of water and sediments were analysed (see Table 1).

In the laboratory, the samples were examined using a microscope method after transfer to a sterile Petri dish. After first MP evidence, the examination was conducted following the microscopic method (see Yang et al. 2021). Positive samples were separated and MPs photographed and measured. From positive samples, we analysed 3 ml of the total sample volume. For the greatest possible accuracy, we analysed this volume in increments of 0.5 ml, always after thorough mixing of the liquid. Quantitative data were then converted to 1 ml of sample. These examinations and measurements were conducted using a Leica M205MC stereomicroscope (magnification of 7.8–160×), equipped with a Leica DFC295 digital camera. The minimal size of particles captured and measured by this method and equipment used is 1 μm.

Table 1. Overview of sample volumes of individual phytotelmata.

Date	Plant number	Locality	total levels on the plant	level 1		level 2		level 3		level 4		level 5		level 6		level 7		level 8		level 9		level 10	
				sample number	volume (ml)	sample number	volume (ml)	sample number	volume (ml)	sample number	volume (ml)	sample number	volume (ml)	sample number	volume (ml)	sample number	volume (ml)	sample number	volume (ml)	sample number	volume (ml)	sample number	volume (ml)
6/14/2021	1	Demjata	6	damaged		damaged		1	38	2	29	3	17	empty									
	2	Demjata	6	1	12	2	14	3	21	empty		empty		empty									
	3	Demjata	6	damaged		1	70	2	37	3	13	empty		empty									
	4	Demjata	7	damaged		1	37	2	85	3	17	empty		empty		empty							
	5	Demjata	7	1	15	2	8	3	16	4	35	5	10	empty		empty							
	1	Kapušany	6	1	12.5	2	44	3	42	4	49	empty		empty									
	2	Kapušany	7	1	17	2	16	3	26	4	6	empty		empty		empty							
	3	Kapušany	6	1	15	2	31	3	10	empty		empty		empty									
	4	Kapušany	6	damaged		1	4	2	16	3	7.5	4	3	empty									
	5	Kapušany	7	damaged		damaged		1	35	2	4	empty		empty		empty							
6/28/2021	1	Demjata	8	damaged		damaged		damaged		1	35	2	18	3	14	4	3	empty					
	2	Demjata	9	damaged		1	20	2	73	3	61	4	49	5	27	empty		empty		empty			
	3	Demjata	9	damaged		damaged		1	6	2	76	3	61	4	47	5	11	empty		empty			
	4	Demjata	9	damaged		damaged		1	10	2	106	3	92	4	43	empty		empty		empty			
	5	Demjata	9	damaged		1	5	damaged		2	41	3	20	4	12	empty		empty		empty			
	1	Kapušany	8	damaged		1	5	2	51	3	41	4	60	5	45	6	20	7	15				
	2	Kapušany	9	damaged		damaged		damaged		1	42	2	37	3	26	4	25	5	5	empty			
	3	Kapušany	8	damaged		damaged		1	29	2	42	3	80	4	34	5	29	6	6				
	4	Kapušany	8	damaged		damaged		1	51	2	92	3	45	4	45	5	36	6	17				
	5	Kapušany	9	damaged		damaged		damaged		1	5	2	85	3	70	4	15	5	16	6	8		
7/12/2021	1	Demjata	9	damaged		damaged		1	50	2	36	3	20	4	10	empty		damaged		damaged			
	2	Demjata	9	damaged		damaged		1	9	2	6	3	17	4	29	5	12	damaged		damaged			
	3	Demjata	8	damaged		damaged		1	7	2	10	3*	11*	empty		empty		damaged					
	4	Demjata	8	damaged		damaged		1	20	2	16	3	17	4	5	damaged		damaged					
	5	Demjata	9	damaged		damaged		1	20	2	60	3	25	4	14	5*	6*	empty		damaged			
	1	Kapušany	8	damaged		1*	9*	2	76	3	95	4	83	damaged		5	12	6	3				
	2	Kapušany	7	damaged		1	12	2	17	3	7	empty		empty		empty							
	3	Kapušany	7	damaged		damaged		damaged		1	7	2	5	empty		empty							
	4	Kapušany	8	damaged		damaged		1	32	2	47	3	24	damaged		empty		damaged					
	5	Kapušany	8	damaged		1	2	2	18	damaged		3	41	4	49	5	15	empty					

Date	Plant number	Locality	total levels on the plant	level 1		level 2		level 3		level 4		level 5		level 6		level 7		level 8		level 9		level 10	
				sample number	volume (ml)	sample number	volume (ml)	sample number	volume (ml)	sample number	volume (ml)	sample number	volume (ml)	sample number	volume (ml)	sample number	volume (ml)	sample number	volume (ml)	sample number	volume (ml)	sample number	volume (ml)
7/26/ 2021	1	Demjata	7	damaged		damaged		1*	8*	empty		empty		damaged		damaged							
	2	Demjata	8	damaged		empty		1	9	2	2	empty		empty		empty		damaged					
	3	Demjata	8	damaged		damaged		empty		1	10	empty		empty		empty		damaged					
	4	Demjata	8	damaged		damaged		damaged		1	12	2	5	damaged		damaged		damaged					
	5	Demjata	8	damaged		damaged		1	11	empty		empty		empty		damaged		damaged					
	1	Kapušany	8	damaged		damaged		1	10	damaged		2*	40*	empty		3	5	empty					
	2	Kapušany	9	damaged		damaged		1	6	2	41	3	110	4	58	5	12	6	6	damaged			
	3	Kapušany	10	damaged		damaged		damaged		damaged		1	15	2	12	empty		empty		damaged		damaged	
	4	Kapušany	9	damaged		damaged		1	5	2	55	3	55	4*	75*	5	11	empty		damaged			
	5	Kapušany	8	damaged		damaged		damaged		damaged		1	90	empty		2	9	empty					
8/9/ 2021	1	Demjata	8	damaged		damaged		damaged		1	5	2	6	empty		empty		empty					
	2	Demjata	7	damaged		damaged		1	8	2	5	3	3	empty		empty							
	3	Demjata	8	damaged		damaged		damaged		damaged		1	3	empty		empty		empty					
	4	Demjata	7	damaged		damaged		damaged		1	3	2	2	empty		empty							
	5	Demjata	8	damaged		damaged		damaged		damaged		1	5	empty		empty		empty					
	1	Kapušany	8	damaged		damaged		damaged		damaged		damaged		damaged		1	15	empty					
	2	Kapušany	8	damaged		damaged		damaged		1	47	2	6	3	14	4	2	empty					
	3	Kapušany	8	damaged		damaged		damaged		damaged		1	24	2	45	3	12	empty					
	4	Kapušany	7	damaged		damaged		damaged		damaged		1	10	empty		empty							
	5	Kapušany	7	damaged		damaged		damaged		1	36	empty		empty		empty							

Table legend: Plant number represent the serial number of the plant at the location (5 plants were examined at each location); levels on the plant represents a number of oppositely growing leaves that are able to retain rainwater; volume (ml) means the total volume of water that was captured by the opposite leaves; sample number - sample designation, * positive sample; empty cells - undeveloped phytotelma

Figure 1. Phytotelmata in the teasel *Dipsacus*.

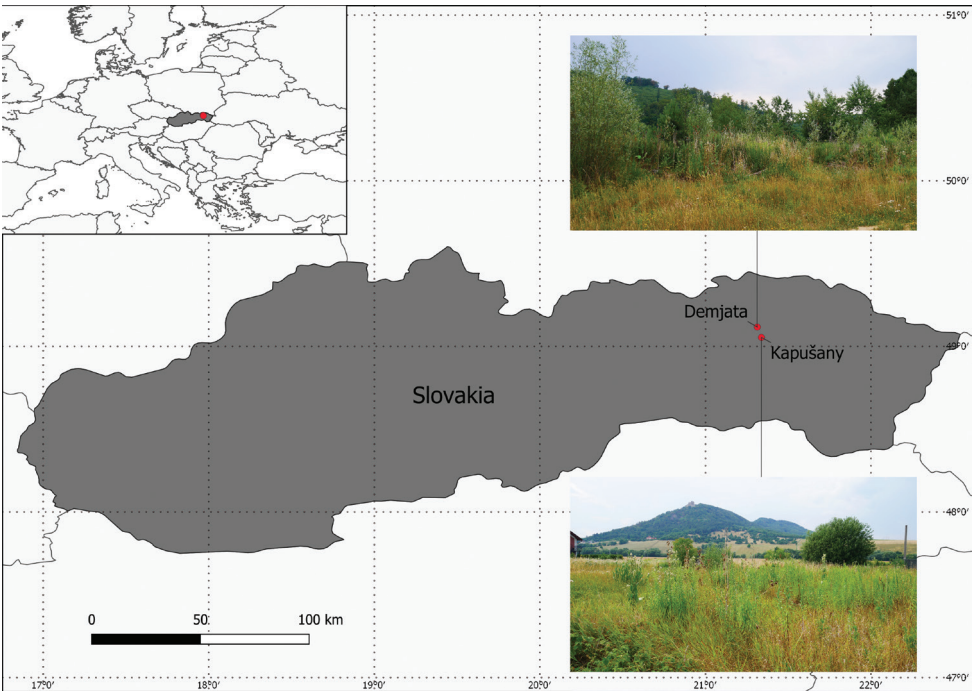

Map 1. Location of the study areas.

Results and discussion

Overall, MPs were detected in only in 6 of 171 examined samples (incidence 3.5%). MPs consisted, in particular, of blue, black, red and white 141 μm to 2.4 mm long fibres and blue and orange fragments with diameters of 9 to 81 μm. There were 101 to 409 MPs in each positive sample (Table 2). Positive telmata were recorded only during two sampling periods (29.6.–12.7.2021 and 13.–26.7.2021) at different levels and always at both locations. These results are the first confirmation of evidence of MPs in phytotelmata on *Dipsacus* teasel (see Fig. 3).

These phytotelmata are very small and have a short lifespan (e.g. Kanašová et al. 2020). The question is, therefore, how were they polluted with MPs? The most probable contamination source is suspended atmospheric SAMPs. Fibres (Liu et al. 2019; Wright et al. 2020) and fragments (Allen et al. 2019) are the most prevalent shapes in SAMPs samples and they also dominated in phytotelmata. Our findings also support the idea that SAMPs could have an MP pollution source (Alfonso et al. 2021), whereas other paths for the spread of fibres and fragments into above-ground phytotelmata are unlikely to be possible. In the case of SAMPs' contamination, the low number of positive phytotelmata may be explained by the density of the surrounding vegetation and by the position and orientation of the water-filled cavities on *Dipsacus*.

Figure 2. Locality of the teasels in Demjata.

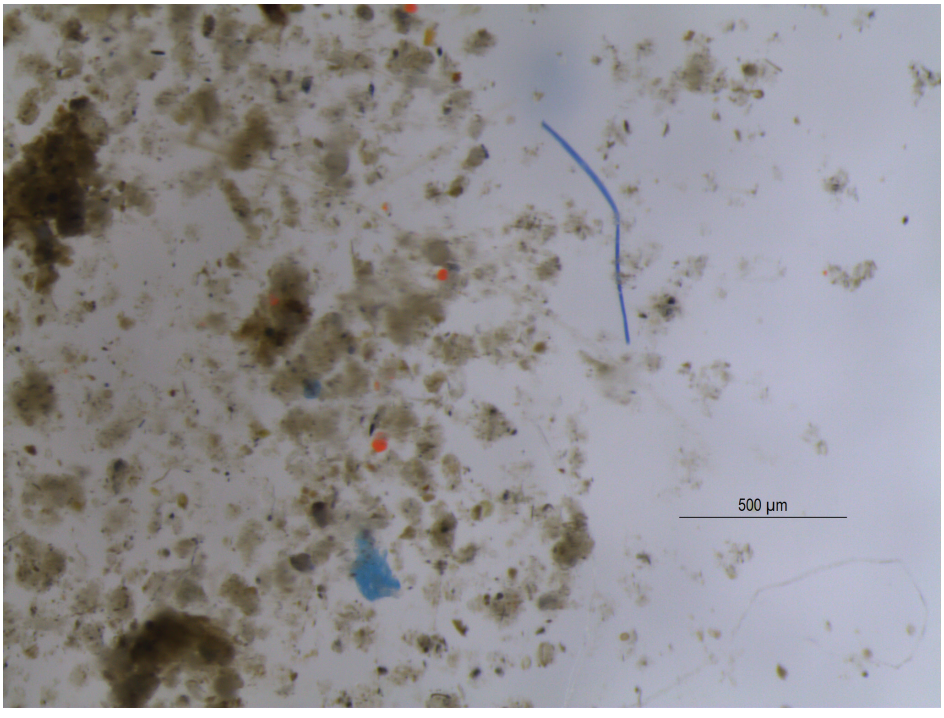

Figure 3. Microplastic fibre and fragments from a phytotelmata sample.

Table 2. The detailed information about MPs in positive phytotelmata.

Date	Plant number	Locality	Total levels on the plant	Level	Sample number	Volume (ml)	Fibers							Fragments					Average amount of MPs per 1 ml		
							Total Number (3 ml)	Colour				Min. length (mm)	Max. length (mm)	Total Number (3 ml)	Colour		Min. size (mm)	Max. size (mm)			
								Blue	Black	Red	White				Blue	Orange			Fibres	Fragments	Total
7/12/2021	3	Demjata	8	5	3	11	8	3	3	1	0	0.2051	1.5790	98	58	40	0.0107	0.0718	2.7	32.7	275.19
7/12/2021	5	Demjata	9	7	5	6	4	2	2	0	0	0.1558	1.3092	159	45	114	0.0096	0.0695	1.3	53.0	408.87
7/12/2021	1	Kapušany	8	2	1	9	12	6	3	0	3	0.1955	2.1730	22	15	7	0.0122	0.0420	4.0	7.3	101.75
7/26/2021	1	Demjata	7	3	1	8	3	3	0	0	0	0.1414	0.8832	142	28	114	0.0096	0.0528	1.0	47.3	358.42
7/26/2021	1	Kapušany	8	5	2	40	13	8	2	3	0	0.1663	2.3937	59	33	26	0.0115	0.0808	4.3	19.7	225.65
7/26/2021	4	Kapušany	9	6	4	75	0	0	0	0	0	0	0	56	18	38	0.0088	0.0551	0.0	18.7	224.73

Figure 4. The presence of snail (*Cepaea*) on teasel leaves.

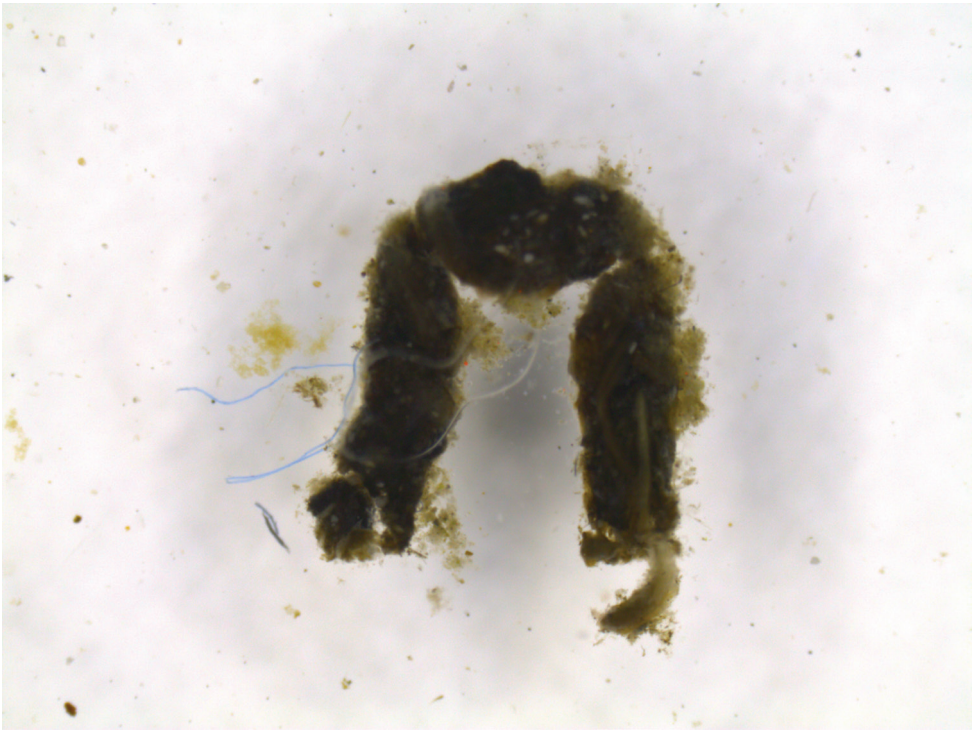

Figure 5. Microparticles in snail excrement.

The second possible pathway of contamination is zoonotic transport (active or passive) through snails (Fig. 4). Snails could transfer particles of MPs on or in their bodies (e.g. Panebianco et al. 2019). This theory can be supported by the frequent presence of living or drowned snails and their excrements in teasel phytotelma (see Fig. 5). Transmission by molluscs from soil and plant surfaces would indicate pollution from the earth's surface. In any case, the surface of the landscape, soil and vegetation could only be contaminated by the atmosphere (SAMPs) at the sites examined in this study, as no other sources of contamination are present at the localities or in their immediate surroundings.

Based on these results, aims in our future research will be: (1) to find out whether the pathway of pollution (i.e. wind transport, active zoonotic transport, passive zoonotic transport) would influence the utility of phytotelmata as indicators of microplastic pollution and (2) to test the hypothesis that the amount of microplastics in phytotelmata reflects their amount in the environment (i.e. more MPs in the environment mean more MPs in phytotelmata). Teasel phytotelmata are a relatively common, but overlooked aquatic microcosms (Kanašová et al. 2020). Due to their abundance and theoretical ability to capture MPs in several ways from the environment, they could be a good indicator of MPs occurrence (rather than directly measuring the environment). Moreover, the temporal character of phytotelmata and the succession of individual levels serves as a natural "time-lapse" sampling with the possibility of identifying temporal differences in the intensity of contamination during the growing season.

MPs have become one of the emerging pollutants in a wide range of different ecosystems (e.g. de Souza Machado et al. 2018; Carbery et al. 2018; Yang et al. 2021; Weber et al. 2021; Jin et al. 2021; Ragusa et al. 2021). The occurrence of MPs has continued to expand on a global scale and has attracted widespread attention from scientists, policy-makers and the public (e.g. Jin et al. 2021). One of the basic prerequisites for a solution and remediation is an understanding of the external forces that drive the transport and diffusion of these pollutants. Our findings point to the possibility of using phytotelmata (and/or artificial telmata) to determine the contamination of the environment by MPs and the relatively simple detection of seasonal/temporal changes in the atmospheric load of the studied sites by SAMPs. In any case, this topic and the bio-indicative potential of telmata in the environmental burden of MP assessment deserve further research and more attention.

Acknowledgements

We thank the editor and all anonymous reviewers for their valuable and constructive comments on the first versions of the manuscript. We also thank the kind and helpful Nathalie Yonow for the thorough proofreading of the second version of the manuscript, her important questions, comments and suggestions. This work was supported by the Slovak Scientific Grant Agency, contract No. VEGA-1/0012/20 and by the Grant Agency of University Prešov in Prešov under contract No. GaPU 6/2021.

References

Al-Jaibachi R, Cuthbert RN, Callaghan A (2019) Examining the effects of ontogenic microplastic transference on *Culex* mosquito mortality and adult weight. The Science of the Total Environment 651(1): 871–876. https://doi.org/10.1016/j.scitotenv.2018.09.236

Alfonso MB, Arias AH, Ronda AC, Piccolo MC (2021) Continental microplastics: Presence, features, and environmental transport pathways. The Science of the Total Environment 799: 149447. https://doi.org/10.1016/j.scitotenv.2021.149447

Allen S, Allen D, Phoenix VR, Le Roux G, Durántez Jiménez P, Simonneau A, Binet S, Galop D (2019) Atmospheric transport and deposition of microplastics in a remote mountain catchment. Nature Geoscience 12(5): 339–344. https://doi.org/10.1038/s41561-019-0335-5

Andrady AL (2011) Microplastics in the marine environment. Marine Pollution Bulletin 62(8): 1596–1605. https://doi.org/10.1016/j.marpolbul.2011.05.030

Carbery M, O'Connor W, Palanisami T (2018) Trophic transfer of microplastics and mixed contaminants in the marine food web and implications for human health. Environment International 115: 400–409. https://doi.org/10.1016/j.envint.2018.03.007

Cole M, Lindeque P, Halsband C, Galloway TS (2011) Microplastics as contaminants in the marine environment: A review. Marine Pollution Bulletin 62(12): 2588–2597. https://doi.org/10.1016/j.marpolbul.2011.09.025

de Souza Machado AA, Kloas W, Zarfl C, Hempel S, Rillig MC (2018) Microplastics as an emerging threat to terrestrial ecosystems. Global Change Biology 24(4): 1405–1416. https://doi.org/10.1111/gcb.14020

Jin M, Wang X, Ren T, Wang J, Shan J (2021) Microplastics contamination in food and beverages: Direct exposure to humans. Journal of Food Science 86(7): 2816–2837. https://doi.org/10.1111/1750-3841.15802

Kanašová K (2017) Vodné bezstavovce fytoteliem na rastlinách rodu Dipsacus. Bakalárska práca, Prešovská univerzita, 48 pp.

Kanašová K, Manko P, Svitok M, Svitková I, Oboňa J (2020) Svet vo svete – od mikrokozmov k ekosystémom. Limnologický spravodajca 14: 14–18.

Kitching RL (2000) Food webs and container habitats: The natural history and ecology of phytotelmata. Cambridge University Press, 431 pp. https://doi.org/10.1017/CBO9780511542107

Liu K, Wu T, Wang X, Song Z, Zong C, Wei N, Li D (2019) Consistent transport of terrestrial microplastics to the ocean through atmosphere. Environmental Science & Technology 53(18): 10612–10619. https://doi.org/10.1021/acs.est.9b03427

Oboňa J, Svitok M (2012) Pilotný výskum fytoteliem Slovenska. Limnologický spravodajca 6: 48–50.

Oboňa J, Svitok M, Čiamporová-Zaťovičová Z, Bitušík P (2011) Vodné bezstavovce fytoteliem a ich prostredie. In: Marušková A, Vanek M (Eds) Ekológia a environmentalistika – zborník príspevkov doktorandov z 8. ročníka Študentskej vedeckej konferencie, FEE TU vo Zvolene, 63–70.

Panebianco A, Nalbone L, Giarratana F, Ziino G (2019) First discoveries of microplastics in terrestrial snails. Food Control 106: 106722. https://doi.org/10.1016/j.foodcont.2019.106722

Ragusa A, Svelato A, Santacroce C, Catalano P, Notarstefano V, Carnevali O, Papa F, Rongioletti MCA, Baiocco F, Draghi S, D'Amore E, Rinaldo D, Matta M, Giorgini E (2021) Plasticenta: First evidence of microplastics in human placenta. Environment International 146: 106274. https://doi.org/10.1016/j.envint.2020.106274

Weber F, Kerpen J, Wolff S, Langer R, Eschweiler V (2021) Investigation of microplastics contamination in drinking water of a German city. The Science of the Total Environment 755: 143421. https://doi.org/10.1016/j.scitotenv.2020.143421

Williams DD (1996) Environmental constraints in temporary fresh waters and their consequences for the insect fauna. Journal of the North American Benthological Society 15(4): 634–650. https://doi.org/10.2307/1467813

Williams DD (2006) The biology of temporary waters. Oxford University Press, 348 pp. https://doi.org/10.1093/acprof:oso/9780198528128.001.0001

Wright SL, Ulke J, Font A, Chan KLA, Kelly FJ (2020) Atmospheric microplastic deposition in an urban environment and an evaluation of transport. Environment International 136: 105411. https://doi.org/10.1016/j.envint.2019.105411

Yang L, Zhang Y, Kang S, Wang Z, Wu C (2021) Microplastics in freshwater sediment: A review on methods, occurrence, and sources. The Science of the Total Environment 754: 141948. https://doi.org/10.1016/j.scitotenv.2020.141948